2016

Transcription factor LSF: a mitotic regulator in hepatocellular carcinoma cells

BOSTON UNIVERSITY

GRADUATE SCHOOL OF ARTS AND SCIENCES

Dissertation

TRANSCRIPTION FACTOR LSF: A MITOTIC REGULATOR IN HEPATOCELLULAR CARCINOMA CELLS

by

JENNIFER LYNN SHERMAN WILLOUGHBY

B.A., Roger Williams University, 2003

Submitted in partial fulfillment of the

requirements for the degree of

Doctor of Philosophy

2016

Approved by

First Reader

Ulla Hansen, Ph.D.
Professor of Biology

Second Reader

Kevin Fitzgerald, Ph.D.
Vice President of Research, Alnylam Pharmaceuticals

“The most exciting phrase to hear in science, the one that heralds the most discoveries, is not “Eureka!” but “That’s funny…..” –Isaac Asimov

DEDICATION

I would like to dedicate this work to my parents, Carolyn M. Sherman and Roy B. Sherman, my patient husband, my son, Jasper, to Wadsworth William Willoughby and to all those who have supported me. I am truly blessed. Special thanks to my parents for their delight in each and every accomplishment, regardless of its magnitude, as well as their unwavering and absolute encouragement for my lofty aspirations. I carry you each with me, always.

ACKNOWLEDGMENTS

To those in my committee, I would like to thank each for their continued and unwavering support. To Kevin for his closing remark to my annual reviews, "When are you going to graduate school?" Many thanks to Kim for alerting me to the existence of the BU program allowing students with full time positions to attend the university and her support in all circumstances. To Cyndi, many thanks for her guidance, encouragement, and engaging course curriculums. I would like to thank Frank for his contribution to my development and for the opportunity to lead his molecular biology discussion section. Finally, I would like to thank Ulla for her many years of endorsement and her willingness to always provide feedback, both solicited and unsolicited!

TRANSCRIPTION FACTOR LSF: A MITOTIC REGULATOR IN HEPATOCELLULAR CARCINOMA CELLS

JENNIFER LYNN SHERMAN WILLOUGHBY
Boston University Graduate School of Arts and Sciences, 2016
Major Professor: Ulla Hansen, Professor of Biology

ABSTRACT

Hepatocellular carcinoma (HCC) is the third leading cause of cancer mortality worldwide. Current treatments are subpar, with late stage diagnosis and poor prognosis contributing to limited treatment options. The evolutionarily conserved, ubiquitously expressed transcription factor LSF is overexpressed in HCC, and its expression is positively correlated with disease severity. Certain small molecules, known as Factor Quinolinone Inhibitors (FQIs), specifically inhibit LSF DNA-binding activity, inhibit HCC cell proliferation *in vitro* and prevent tumor growth in an endogenous mouse liver cancer model without apparent toxicity. The targeting of transcription factors by small molecule inhibitors has been historically difficult, warranting further molecular investigation into the requirement for LSF in HCC to confirm that the anti-tumor effects of FQIs are the consequence of LSF inhibition.

This body of work investigates a dual approach for inhibiting LSF function in order to determine the molecular consequences for HCC cells. To identify the specific point of the cell cycle where LSF is required for HCC proliferation, synchronous HCC cells were treated with FQI or with short interfering RNA to reduce levels of LSF. The results indicate that LSF is required for proper mitotic progression in HCC cells.

Specifically, these data show a reduction of key mitotic regulators Aurora Kinase B and Cdc20, at the level of mRNA and protein expression. Time-lapse microscopy also demonstrated an increase in the time for progression through mitosis, with a prometaphase/metaphase delay. Immunofluorescence analysis revealed a prometaphase delay plus aberrant cell division and generation of multi-nucleated cells. These findings were consistent with both FQI1 treatment and RNA interference. Additionally, shorter incubation with FQI1 surprisingly revealed a distinct, non-transcriptional regulation of mitosis in HCC cells, suggesting that mitotic regulation by LSF is multi-faceted.

As a targeted therapy for use in the clinic, the *in vivo* toxicity of FQIs is critical to investigate. Whole blood provides populations of rapidly dividing normal cells that can test susceptibility to anti-mitotic compounds. When mice were treated with FQI1, the blood analysis showed no toxicity. Taken together, these findings indicate that LSF is a mitotic regulator in HCC, further supporting the therapeutic promise of molecular therapies targeting LSF.

TABLE OF CONTENTS

LIST OF TABLES

LIST OF FIGURES

LIST OF ILLUSTRATIONS

LIST OF ABBREVIATIONS

AEG ..... Astrocyte elevated gene-1

ALB ..... Albumin

ALT ..... Alanine Aminotransferase

APC/C ..... Anaphase promoting complex/cyclosome

AST ..... Aspartate Aminotransferase

AurkB ..... Aurora Kinase B

BASO ..... Basophil

BASO ABS ..... Basophil count

bp ..... base pairs

BSA ..... Bovine Serum Albumin

Cdc20 ..... Cell Division Cycle 20

Cdk(s) ..... Cyclin Dependent Kinase(s)

c-myc ..... Cellular myelocytomatosis viral oncogene

CPC ..... Chromosomal Passenger Complex

DEN ..... N-nitrosodiethylamine

DMEM ..... Dulbecco's Modified Eagle Medium

DMSO ..... Dimethyl Sulfoxide

ECM ..... Extracellular Matrix

EDTA ..... Ethylenediaminetetraacetic acid

EMSA ..... Electrophoretic mobility shift assay

EMT ..... Epithelial to Mesenchymal Transition

EOS ..... Eosinophil

EOS ABS ..... Eosinophil count

FBS ..... Fetal bovine serum

FQI1 ..... Factor Quinolinone Inhibitor 1

FQI2 ..... Factor Quinolinone Inhibitor 2

G0 ..... Non-dividing/quiescent phase

G1 ..... First gap phase

G2 ..... Second gap phase

GI50 ..... Concentration that induces 50% Growth Inhibition

H&E ..... Hematoxylin and Eosin Staining

Hc3716-hTert ..... Immortalized human hepatocytes

HBV ..... Hepatitis B Virus

HCC ..... Hepatocellular Carcinoma

HCT ..... Hematocrit

HCV ..... Hepatitis C Virus

Hep3b ..... Hepatoblastoma cells

HepG3 ..... Hepatocellular carcinoma cells

HeLa ..... Cervical carcinoma cells

HGB ..... Hemoglobin

IC_{50} ..... Concentration that induces 50% activity inhibition

IF ..... Immunofluorescence

INCENP ..... Inner Centromere Protein

K_D ..... Binding affinity

LSF ..... Late Simian Virus 40 factor

LSFdn ..... Dominant Negative LSF

LUC ..... Large Unstained Cells

LUC ABS ..... Large Unstained Cell Count

LYM ..... Lymphocyte

LYM ABS ..... Lymphocyte count

MBA ..... Microtubule Binding Agent

MCH ..... Mean Corpuscular Hemoglobin

MCHC ..... Mean Corpuscular Hemoglobin Count

MCV ..... Mean Corpuscular Volume

MGB ..... Minor Grove Binder

M ..... Mitosis

min ..... minute

MMP9 ..... Matrix metallopeptidase 9

MONO ..... Monocyte

MONO ABS ..... Monocyte Count

NAFLD ..... Non-Alcoholic Fatty Liver Disease

NASH ..... Non-Alcoholic Steatohepatitis

NEUT ..... Neutrophil

NEUT ABS ..... Neutrophil count

NFQ ..... Non-Fluorescent Quencher

OPN.....Osteopontin

PBS .....Phosphate Buffered Saline

PI..... Propidium Iodide

PLT .....Platelet

Raf/Raf1 .....Raf proto-oncogene serine/threonine kinase

RBC..... Red Blood Cells

RETIC ..... Reticulocyte

RETIC ABS ..... Reticulocyte count

RIPA .....Radioimmunoprecipitation assay buffer

RT-qPCR.....Reverse Transcription-quantitative polymerase chain reaction

S ..... DNA Synthesis Phase

SAC.....Spindle Assembly Checkpoint

SAR.....Structure Activity Relationship

Ser ..... Serine

siRNA .....Short interfering RNA

SHARP..... Sorafenib Hepatocellular Carcinoma Assessment Randomized Protocol

TF .....Transcription Factor

TFCP2 ..... LSF gene name

Thr..... Threonine

TUNEL .....Terminal dexoynucleotidyl transferase dUTP end labeling

Tyms .....Thymidylate Synthase

Tyr..... Tyrosine

VEGF ..... Vascular Endothelial Growth Factor

WBC ..... White Blood Cells

YFP ..... Yellow Fluorescent Protein

CHAPTER ONE

INTRODUCTION

The following is a collection of work probing the requirement for Late SV40 Transcription Factor (LSF) function in Hepatocellular Carcinoma (HCC) cells. Reports have shown that small molecules targeting LSF, Factor Quinolinone Inhibitors (FQIs), have successfully reduced and/or prevented tumor growth in both a mouse HCC xenograft model and an endogenous liver model (Grant et al., 2012; Rajasekaran et al., 2015). Using a dual approach to interrogate the functionality of LSF in HCC cells, a role in mitotic regulation has been identified and will be described in detail. This chapter will provide the necessary background to define both the relevance of this work and to allow proper interpretation of the data to follow.

Hepatocellular Carcinoma

According to the National Cancer Institute, cancer is a collection of related diseases where some cells of the body begin to divide without stopping and spread into or invade surrounding tissues Cancerous cells may form solid tumors which are masses of tissue or manifest as cancers of the blood which are not solid and may be referred to as liquid tumors. Tumors that break off, travel through the blood or lymph and establish themselves at distal sites are called metastatic. Hepatocellular Cancer is a form of solid tumor which arises de novo from hepatocyte cells in the liver; it is the predominant type of primary liver cancer. Unfortunately, the incidence of primary liver cancer is on the rise.

Liver cancer in adult men is the fifth most frequently diagnosed cancer worldwide, and is the second leading cause of cancer-related death in the world. In adult women, it is the seventh most commonly diagnosed cancer and the sixth leading cause of cancer death. Globally, liver cancer rates are 2 to 4 times that for men than women. As of 2008, there were an estimated 748,000 new liver cancer cases and 695,900 cancer deaths worldwide, with half of these cases and deaths occurring in China (Jemal et al., 2011). The histological subtype known as Hepatocellular carcinoma (HCC) dominates those primary liver cancer cases observed with incidence rates reaching 70-80% that of total liver cancer burden worldwide (El-Serag and Kanwal, 2014; Jemal et al., 2011). In the United States (US), the annual incidence of hepatocellular carcinoma was at least 6 per 100,000 in 2010 with men three times more susceptible than women. The majority of cases, ~80%, are thought to be the result of chronic infection with HBV and HCV (Venook et al., 2010).

While new treatments have emerged as curative agents for HCV and others in the works for HBV, the sheer number of infected people worldwide with both viruses indicates that HCC will remain an area of high unmet need for years to come. While viral infections remain the top causative agents for the development of HCC, other factors such as chronic fatty liver and alcoholism also contribute. In western countries, risk factors that dominate besides HCV include both alcohol related cirrhosis and non-alcoholic fatty liver disease (NAFLD), a disease associated with obesity. Other risk factors include aflatoxin B1, a toxin common to parts of Africa and Asia which has been shown to increase HCC incidence in HBV positive patients (Venook et al., 2010).

NAFLD, the hepatic manifestation of metabolic syndrome, affects approximately 1/3 of the US adult population, a population that is on the rise (El-Serag and Kanwal, 2014). Typically, these patients can develop nonalcoholic steatohepatitis (NASH) where inflammation combined with fatty liver can trigger fibrotic development. Epidemiology studies support an association between NAFLD or NASH and HCC. An increasing disease prevalence of (NASH), impacting over 1 million adults and children to date, indicate that a significant increased HCC patient population is on the horizon as NASH fibrosis converts to HCC over time (Marengo et al., 2016).

With HCC incidence rates expected to continue to be on the rise in the West, the introduction of universal HBV vaccinations are expected to continue to reduce incidence in the East. However, the HBV vaccination will not impact those already afflicted with the virus. With the rising epidemic of obesity in the western world the incidence of NASH related HCC is growing and may become the predominant driver for HCC in the developed world in the future (Venook et al., 2010). A recent mathematical model generated using the prevalence and natural history of HCV in the U.S. population indicated that the number of HCC cases increased from 1990 to 1999 from 37,697 to 86, 765 between 2000 and 2009, an increase of 130%, with a projected increase to 130,366 (+50%) by 2019. However, this model simply examines HCV as a risk factor. Even though HCC cases induced by HCV viral infections are projected to be reduced, the overall incidence likely will not decline as NASH related cirrhosis is increasing HCC incidence with metabolic syndrome incidence on the rise.

The risk factors discussed above (mainly liver infections and NASH) operate by promoting development of cirrhosis which exerts a promotional effect via the induction of hepatocyte regeneration (Marquardt et al., 2012; Perz et al., 2006; Zhou et al., 2014). Exceptions are rare in HCV related HCC as most cases documented occur with the concurrence of some type of fibrosis. Whereas most HBV related HCC cases also include cirrhosis, ~85%, there have been cases where HBV can cause HCC in the absence of advanced documented fibrosis or cirrhosis (Perz et al., 2006). Several mechanisms have been proposed for progression of NAFLD to HCC in instances of mild or undetected fibrosis; however, there has not been a systematic analysis to quantify this contention. The risk of developing HCC in patients with cirrhosis varies with the underlying condition (El-Serag and Kanwal, 2014; Perz et al., 2006). Combinations of various risk factors have increased risk of HCC development, for example heavy alcohol intake in HCV afflicted individuals has been documented to increase risk of progression to HCC.

Current therapeutic options for the HCC population are subpar (Bruix and Sherman, 2011). HCC is often diagnosed late in disease as it produces non-specific symptoms, lacks early diagnostic biomarkers, and the option to diagnose by biopsy is not ideal. One third of those diagnosed qualify for invasive treatments including surgical resection or liver transplantation (Kim et al., 2016). However, two thirds of patients do not qualify for such treatments as their disease is too far advanced, leaving only palliative treatment options. Few molecular therapies have shown promise, with Sorafenib currently the only approved treatment. Sorafenib, a molecular inhibitor of vascular

endothelial growth factor receptor (VEGFR) as well as C and B-raf kinase was originally approved for use in kidney cancer patients, but has demonstrated an improvement in overall survival rates of 3 months in clinical trials of HCC (Llovet et al., 2008; Santhekadur et al., 2012b). Bevacizumab, a vascular endothelial growth factor (VEGF) pathway inhibitor, examined alone or in a combinatorial approach with chemotherapy, has also demonstrated limited positive responses (Torrecilla and Llovet, 2015). The recent SHARP clinical trial which re-evaluated Sorafenib efficacy in HCC observed median survival rates of 7 to 11 months, an impact attributed to the improved clinical trial design for the HCC patient population (Llovet et al., 2015; Worns and Galle, 2014). The re-examination of clinical trial design for this patient population paved the way for numerous other molecular targeted therapies to be evaluated as the trial established critical criteria required to determine drug efficacy. Many types of therapies have been examined including anti-angiogenics, epigenetic modulators, pro-apoptotic or DNA damaging agents, immune modulators, and, lastly, cell cycle inhibitors. Unfortunately, of the numerous therapies evaluated to date, not a single agent improved survival or progression free survival rates to a greater degree than Sorafenib (Bruix and Sherman, 2011; Llovet et al., 2015).

Clearly, given the lack of current effective therapies, the unmet need for novel approaches to treat HCC is very high. The lack of clinical translation of therapies showing promise in pre-clinical models has been problematic. It has, however, led to multiple hypotheses as to what types of new or combined therapies might make an impact on this patient population.

A hallmark of cancer is loss of cell cycle and cell division control; whereas normal cell division is tightly regulated with multiple checkpoints to ensure genomic integrity. Targeting oncogenic cell cycle regulators has been a favored hypothesis to preferentially target tumor cell populations in the body. To navigate through the proposed molecular breakthrough therapies for HCC, many that target cell cycle regulators, we must first understand the complexities of cell cycle regulation.

Mammalian Cell Division

Mitosis, the portion of the mammalian cell cycle that results in cell division, comprises a spatiotemporal regulated system reliant on sequential expression/and degradation of key proteins as well as post translational modifications; processes that are tightly regulated to ensure proper cell division following DNA replication (Carmena et al., 2012; Foley and Kapoor, 2013; Guttinger et al., 2009; Hardwick and Shah, 2010). The cell cycle is comprised of Interphase and Mitosis (M), where the former encompasses the following phases: Gap 0 (G0), Gap 1 (G1), DNA synthesis (S), and Gap 2 (G2). External growth factors introduced to G0 cells, which are by definition quiescent or resting, can trigger cell cycle entry. The overall cell cycle is depicted in Illustration 1.1, a depiction which also includes the estimated time spent in each phase.

Illustration 1.1 The Mammalian Cell Cycle

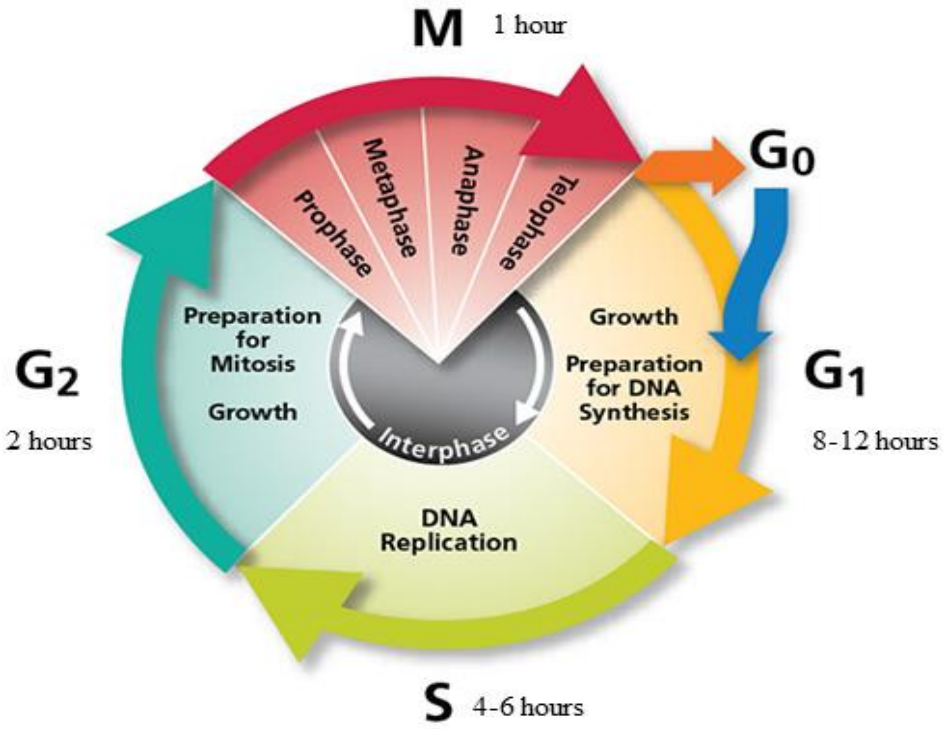

http://www.bdbiosciences.com/anz/research/apoptosis/analysis/index.jsp

Upon entry into the first Gap phase, G1, the cell stimulates production of both key proteins and cytoplasmic organelles in preparation for cellular division, so that the process, once complete, will result in the production of two identical daughter cells. Genome duplication is executed under intense scrutiny in Synthesis, or "S" phase. Completion of DNA synthesis is followed by the second Gap phase, G2, where the cell completes the growth phase and prepares for mitotic entry, a point at which all transcriptional activities will cease until re-entry into G1/G0 (Bertoli and de Bruin, 2014; Bertoli et al., 2013) (Illustration 1.1). Completion of the G2 phase allows a rapid entry into Mitosis where telophase/cytokinesis completes successful cellular division.

Although normal mitotic progression requires the least time of all cell cycle stages, it is the most complicated with multiple sub phases regulated by post translation modifications, both prior expression and degradation of key proteins, cytoskeletal events, and chromatid separation and re-location. Mitosis therefore comprises five sub stages, including prophase, prometaphase, metaphase, anaphase and telophase.

Illustration 1.2 Microtubule Attachment is a Mitotic Requirement

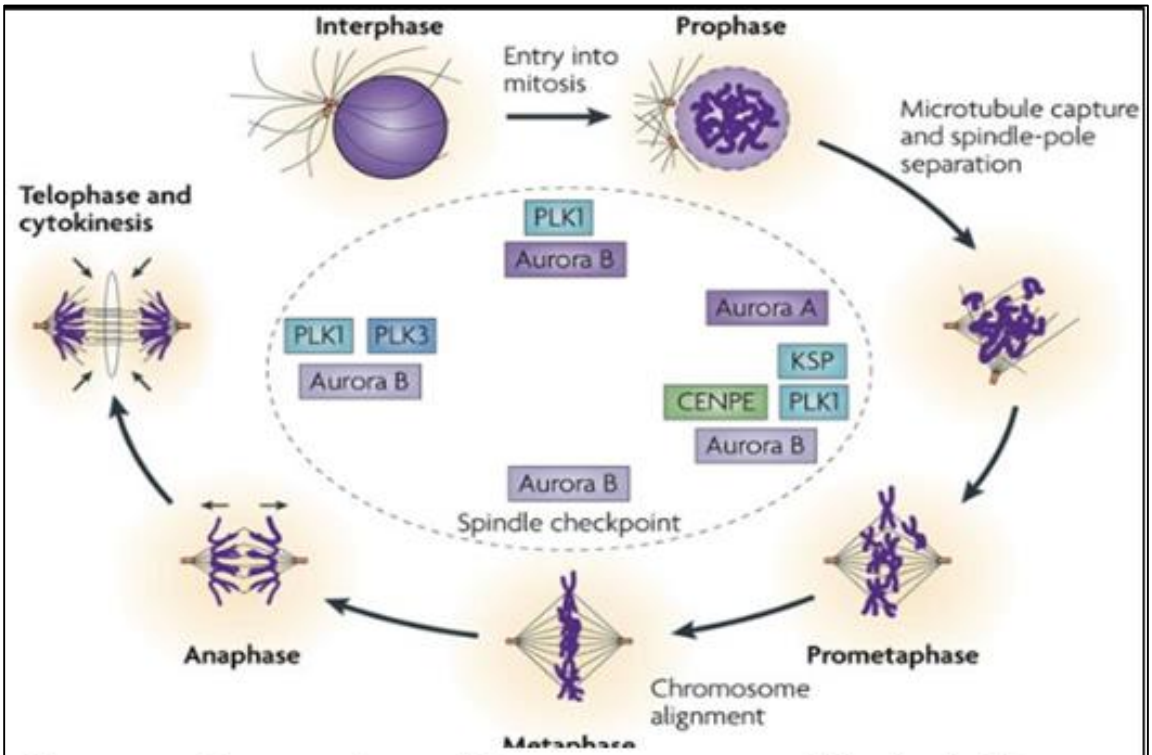

Mitosis is not a key target of microtubule agents in patient tumors. Edina Komlodi-Pasztor, Dan Sackett, Julia Wilkerson & Tito Fojo Nature Reviews Clinical Oncology 8, 244-250 (April 2011)

Illustration 1.2 summarizes the events in each of the mitotic stages as the duplicated chromatids are separated into opposite sides of the cell by microtubules. The microtubules, attached to the centrosomes located at each pole, first attach to the

kinetochore on each sister chromatid. Once all kinetochores have successfully attached, only then can the microtubules facilitate successful separation with a bipolar orientation, pulling each sister chromatid to opposite sides of the cell. The cleavage furrow forms immediately following telophase where cytokinesis permits the separation into two identical daughter cells.

Each cell cycle phase has a surveillance system, or checkpoint, responsible for ensuring successful completion of each stage. Following a successful growth period, the cell arrives at the G1 checkpoint, where a successful growth period and proper DNA integrity is confirmed prior to genome duplication in S phase. The G1 checkpoint, which has been studied extensively, ensures DNA integrity in order to allow proper entry in S phase. If any risk factors identified at this check point cannot be remedied, then pathways may be activated to trigger cellular demise through apoptotic signaling or senescence (a state in which the cell will never divide). A cell that satisfies the G1 checkpoint will duplicate its genome. In mitosis, a distinct type of checkpoint occurs. The proper attachment of microtubules to the kinetochores is closely monitored by the Spindle Assembly Checkpoint (SAC), involving a complex that includes Mad2 and Bub1. The SAC delays or prevents the metaphase to anaphase transition through sequestering of Cdc20, the key member of the Anaphase Promoting Complex (APC/C). Once the SAC has been satisfied through proper attachment of the microtubules to the kinetochores, Cdc20 will be released to associate with APC/C; this allows anaphase onset through degradation of key mitotic proteins. The APC/C coordinates destruction of mitotic proteins including

Cyclin B1, the major mitotic cyclin upregulated prior to mitotic entry (Casimiro et al., 2012; Lim and Kaldis, 2013). Successful anaphase is followed by telophase and cytokinesis. Cancer cells have dysregulated division which can be a direct result of abnormal activity or expression of various factors controlling cellular division, a crucial observation that led to both the identification of dysregulated mitotic proteins and pathways in HCC.

Clinical Targets for Cancer

Given that cancers have dysregulated mitoses, is not a stretch that investigators have been proposing therapies targeting known mitotic regulators required for cell division as a means of exploiting this cancer cell vulnerability. This vulnerability was hypothesized to allow for selective targeting of cancer cells as the majority of normal cells are typically in quiescence, a state in which the cells are not dividing. To date, there have been a large number of small molecules targeting various aspects of mitotic regulation evaluated for anti-tumor activity. Two of different targets that have been extensively evaluated to date are microtubule (MT) binding agents (MBAs) and Aurora Kinase B inhibitors, both of which will be discussed below. A third strategy for targeting mitotic regulation will also be reviewed, which involves inhibiting the Anaphase Promoting Complex (APC/C). This has merely been proposed as advantageous, although not yet clinically evaluated.

Microtubule Dynamics

Microtubules have a critical regulatory function not only for proper mitotic progression, but also for maintenance of cytoskeletal shape, cell motility, and intracellular protein and organelle transport. Composed of α and β tubulin heterodimer subunits, these subunits interact in a dynamic equilibrium allowing tubulin to both polymerize and depolymerize (Foley and Kapoor, 2013). Two fundamental aspects of tubulin dynamics that occur *in vivo* are treadmilling and dynamic instability (Foley and Kapoor, 2013). The first process, dynamic instability, is accelerated during mitosis, as required for spindle formation and attachment of the mitotic spindles to chromosomes. The second process, treadmilling, is defined as the net growth at one end of the microtubule and the net shortening at the opposite end, a process required in the polar movement of the chromosomes during anaphase. These dynamics are regulated by various microtubule associated proteins and other regulatory proteins, variable expression of tubulin isotypes, post translational tubulin modifications and tubulin mutations.

Microtubule binding agents, MBAs, are compounds that disrupt microtubule dynamics involving the mitotic spindle. Suppression of these two key dynamic microtubule functions are the principal means by which MBAs disrupt cellular function and induce cellular death. A large collection of MBAs have been or are currently being evaluated in clinical trials, however few have are being tested in HCC (Loong and Yeo, 2014). Gene expression profiling studies have recently shown that microtubule–related cellular assembly and organization is crucial in HCC development indicating that molecular therapies targeting microtubules could be successful (Loong and Yeo, 2014). Evaluations of MBAs in clinical trials have had mixed results with clinical activity not

translating as well as expected based on preclinical models. Only moderate responses at best were observed in select patients. The lack of efficacy was puzzling in light of the success of early MBA in other cancer settings. For instance, two decades ago paclitaxel treatment achieved clinical response rates for 17-62% in breast cancer, 20-48% in ovarian cancer and 21-41% in lung cancer. Although some individuals had a minimal response, there were positive results. While these agents displayed clinical activity, they were not without side effects as they were unable to distinguish between tumor and normal cells, killing off both. Significant toxicities included neurotoxicity, impacts on movement, sensation, and even organ function failure.

The challenge to identify safe and effective MTAs capable of specifically inhibiting mitosis of cancer cells but not normal cells remains.

Illustration 1.3 The Expression Profile of Mitotic Cyclin

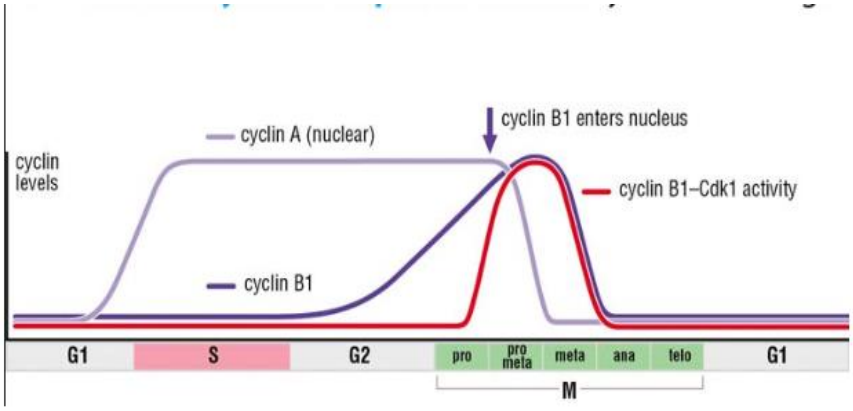

The Cell Cycle, Principles of Control. David O. Morgan. .New Science Press, 2007

Aurora Kinases

Aurora Kinases include three major mitotic kinases required for mitotic entry, progression, and cellular division. These three distinct isoforms were named A, B, and

C. Aurora Kinase A has documented roles in early mitosis through regulation of centrosome maturation and disjunction allowing establishment of the bipolar mitotic spindle. Aurora Kinase B is the key member of the chromosomal passenger complex (CPC) where it associates with survivin, INCENP, and borealin (Ditchfield et al., 2003; Kim et al., 2011; Le et al., 2013; Poon, 2013). The CPC contributes to SAC function at kinetochores by correcting faulty spindle attachments. One key role of Aurora Kinase B is for proper microtubule-kinetochore attachment, through phosphorylation of key mitotic proteins at the kinetochores where Aurora kinase B destabilizes incorrect attachments and stabilizes proper microtubule-kinetochore attachments. Aurora Kinase B regulates modification of other phosphorylated proteins required for mitotic processes, such as Histone 3 on both Serine 10 and 28 as well CENPA; more than 50 targets of Aurora Kinase B have been identified (Carmena et al., 2012; Ditchfield et al., 2003). Another role for such protein modification occurs after anaphase, when Aurora kinase B regulates cytokinesis and localizes to the cleavage furrow (Vader and Lens, 2008).

Abnormal activities of Aurora Kinases are associated with defects in cell division and aneuploidy. Aurora Kinase A is amplified in multiple cancer types including breast, ovary, lung, bladder stomach, and colon whereas Aurora Kinase B is increased in breast cancer, glioblastoma, and prostate cancer (Andrews, 2005). A role for Aurora Kinase C in cancer has not yet been described. Aurora Kinase B is not only upregulated in HCC, but its expression positively correlates with disease severity. It has, therefore, been proposed as a promising therapeutic target for the HCC patient population (Sistayanarain et al., 2006). In fact, Aurora Kinases in general generated great excitement in recent

decades for cancer therapeutics, as promising preclinical anti-tumor activity observed with various small molecules led to 30 entering into clinical trials (Andrews, 2005). However, the clinical translation of these targets has been disheartening.

Danusertib, a pan Aurora Kinase inhibitor, resulted in meager efficacy when tested in chronic lymphocytic leukemia with a 13-22% response. Investigation of Barasertib, an inhibitor specific to Aurora Kinase B (AurkB), resulted in complete response in 25% of the acute myeloid leukemia patients (Bavetsias and Linardopoulos, 2015). However, both therapies resulted in toxicities including myelosuppression and gastrointestinal effects. The observed toxicities are most likely due to the requirement of these mitotic kinases in normal cell division. The surprising lack of efficacy observed has been attributed to dose limitations due to toxic side effects, the low proliferation index in human tumors, as well as pathway redundancy in human cells where the tumor cells are not reliant on Aurora Kinases. The implication of pathway redundancy in ineffective tumor therapies is discussed in greater detail below.

APC/C Proteasome: Cdc20/Cdh1

The Anaphase Promoting Complex (APC), has a key role in mitotic timing through formation of two functionally distinct E3 ubiquitin ligase sub complexes with cofactors, Cdc20 or Cdh1, responsible for targeting key mitotic proteins for ubiquitination resulting in subsequent degradation by the proteasome. Most notably, the APC in complex with Cdc20 targets securin, the inhibitory protein for separase, allowing cleavage of cohesin thereby permitting the sister chromatids to separate and migrate to opposite poles. Other key targets include cyclins, where Cyclin A is degraded in early

mitosis and Cyclin B is degraded prior to mitotic exit. This process is a requirement for mitotic exit in normal cells.

Cdc20, a key cofactor of the APC/C complex, has not yet been targeted for inhibition in clinical trials. However, Cdc20 is overexpressed in some cancers, and in complex with APC degrades p21, a tumor suppressor (Wang et al., 2015; Wu et al., 2013). Further, increased expression of Cdc20 was associated with clinical progression in human tumors. Recently, Cdc20 was proposed as a potential target for tumor therapies (Wang et al., 2013). Additionally, RNAi mediated knockdown of Cdc20 increased mitotic arrest in cancer cells treated with an anti-mitotic, a combinatorial treatment approach that resulted in mitotic death rather than mitotic slippage (Huang et al., 2009).

Clinical Translation

Thus far, large amounts of preclinical data have demonstrated robust anti-tumor responses, however, where explored these agents have not translated into positive tumor response or survival in clinical trials (Wang et al., 2015; Wu et al., 2013). In certain cases it is possible that the lack of efficacy is due to functional redundancy in mammalian cell cycle control with multiple family members possibly covering for or being upregulated under selective pressure (Fernando et al., 2008; Sasai et al., 2004; Slattery et al., 2009). A second hypothesis takes into account the proliferation rate paradox put forth by Tim Mitchison (Mitchison, 2012). He describes an obstacle that anti-mitotic drugs face in general, that they have been chosen based on their cytotoxic properties for rapidly proliferating cells, while HCC and many other tumor types are slow growing. Other key

characteristics include drug retention and the ability to kill quiescent cells (Mitchison, 2012).

Consistent with the family or pathway redundancy hypothesis, tumor escape has been observed in treatments with molecular therapies targeting a single oncogenic factor (Llovet et al., 2015; Torrecilla and Llovet, 2015; Villanueva and Llovet, 2011). This phenomenon led to the hypothesis that targeting oncogenic transcription factors could provide a significant therapeutic benefit, in which inhibition of a broader oncogenic pathway could prevent tumor escape. Additionally, cases of oncogene addiction have been highlighted, where certain tumor types are dependent on single genes that, when removed, result in immediate cancer cell death whereas normal cells with functional redundancy are spared. Ideally if one were to attempt to target a transcription factor for cancer, it would be an oncogenic transcription factor to which cancer cells are addicted.

A therapy targeting an oncogenic transcription factor (TF), a TF that was a proven case of oncogene addiction, would have multiple advantages: (1) In contradiction to the normal human cell that has built in functional redundancy for a complex operating system, the tumor cells are literally addicted to a single factor, incapable of surviving or proliferating without it. (2) Targeting an entire pathway could potentially eliminate tumor cell escape. Exploiting a case of oncogene addiction would theoretically protect normal cells, however, identification of an oncogenic transcription factor that regulates mitotic cells would select for the proliferating tumor cells. LSF has recently been shown to be on oncogenic transcription factor to which HCC tumors are addicted.

The Transcription Factor LSF

LSF, a ubiquitously expressed, evolutionarily conserved transcription factor was first discovered while investigating Simian Virus 40 in HeLa cells, where it was identified as a transcriptional activator of the late promoter (Veljkovic and Hansen, 2004). LSF binds DNA as a homotetramer, targeting a bipartite site with two repeated consensus sequences spaced 10 bp apart (Huang et al., 1990; Veljkovic and Hansen, 2004). An LSF family member, LBP1a, can oligomerize with LSF suggesting that the regulation of key targets and pathways could potentially involve both TFs. LSF is involved in many biological processes including cell growth, cell cycle regulation and development (Hansen et al., 2009; Saxena et al., 2009; Veljkovic and Hansen, 2004). Specifically, LSF binds the thymidylate synthase (Tyms) promoter and activates Tyms expression following cell cycle re-entry of quiescent cells. LSF is essential at the G1/S transition in a mouse fibroblast line as well as a human prostate cancer cell line, as expression of a dominant negative LSF caused apoptosis in S phase (Powell et al., 2000). Apoptosis was a consequence of reduction of Tyms, the rate limiting enzyme required for dTTP production for DNA synthesis, as apoptosis was circumvented with the addition of a low concentration of exogenous thymidine.

Enhanced LSF expression was found in 90% of Hepatocellular Carcinoma patient samples analyzed, and its expression positively correlated with disease severity (Fan et al., 2011b; Yoo et al., 2010). *In vivo* analysis in a mouse xenograft model demonstrated that increased expression resulted in increased tumorigenicity as shown with reduced tumor proliferation in a LSF dominant negative line and overexpression resulted in tumor

formation in a previously non-tumorigenic HCC cell line (Yoo et al., 2010). In addition, expressing a dominant negative LSF in a highly tumorigenic HCC cell line reduced colony formation and tumorigenicity *in vivo*. LSF is also linked to key oncogenic processes including angiogenesis, through regulation of matrix malloproteinase 9 (MMP9)(Santhekadur et al., 2012a) and to the epithelial to mesenchymal transition (EMT) through mediating Snail 1 induced upregulation of fibronectin, an EMT marker (Porta-de-la-Riva et al., 2011). EMT is a key process required for tumor metastasis. Finally, LSF is downstream of Notch 2, where activation of Notch 2 not only led to increased tumorigenicity, but increased LSF expression. These data combined indicated that LSF is an oncogene in hepatocellular carcinoma. Ideally one would be able to identify small molecules capable of inhibiting LSF activity for HCC. Traditionally, however, inhibitors of transcription factors have been difficult to identify. Nonetheless, compounds capable of inhibiting LSF were recently identified.

Factor Quinolinone Inhibitors

A screen of 110,000 compounds identified small molecules that directly inhibited LSF DNA binding activity as ascertained in a fluorescent polarization assay combining fluorescently labelled DNA with purified LSF. Named "Factor quinolinone inhibitors", or FQIs, many of these compounds were synthesized (Grant et al., 2012). The prototypes, FQI1 and FQI2, also inhibited LSF activity in a LSF-dependent luciferase reporter assay, showing their ability to inhibit LSF activity within cells.

Both *in vitro* and *in vivo*, FQIs inhibited LSF DNA binding as detected by the electrophoretic mobility shift assay (EMSA) as well as chromatin immunoprecipitation

(ChIP) in an LSF inducible cell line. Further evidentiary support for LSF specificity emerged when FQIs were found to be incapable of inhibiting the DNA-binding or transcriptional activation mediated by other classes of transcription factors including Sp1, Oct1, E2F3, USF, and p53 (Grant et al., 2012). The three-dimensional structure of the LSF DNA binding region has been predicted to be quite similar to that of p53, a transcription factor that binds DNA in similar fashion as a homo-tetramer (Kokoszynska et al., 2008). This intriguing report prompted the investigation as to whether FQIs could inhibit p53 binding to one of its direct targets, p21. Grant et al. indeed confirmed that FQIs did not impact the ability of p53 to activate p21 gene expression. These data provided confidence that FQI inhibition was specific to LSF.

Evaluation of the FQIs in HCC cells resulted in significant growth inhibition which was translated *in vivo* in a mouse xenograft model (Grant et al., 2012). Particularly compelling data were also generated in an endogenous liver cancer model in transgenic mice that expressed c-Myc downstream of an albumin promoter, which developed cancer when administered a carcinogen N-nitrosodiethylamine (DEN). FQI1 or FQI2 treatment resulted in remarkable prevention or reduction of the endogenous liver cancer (Rajasekaran et al., 2015). In both *in vivo* circumstances, evaluation of normal rapidly dividing cell populations, popular off target activities of the anti-mitotic drug modalities, were unchanged. Evaluation of liver injury markers to identify potential toxic consequences of the FQIs indicated that the liver was not negatively impacted in the subcutaneous mouse xenograft model (Grant et al., 2012; Rajasekaran et al., 2015). These data established a stark contrast to other anti-mitotic compounds evaluated in

preclinical contexts (Chan et al., 2012) as toxicities to the non-tumor cell populations, in the case of FQIs, were undetected. These findings led to speculation that LSF could be the 'Achilles heel' to HCC with a robust anti-tumor activity that was specific to the HCC cell population, a case meeting the requirements of oncogene addiction (Shlomai, 2012; Weinstein, 2008; Weinstein and Joe, 2008). The clean toxicity profile of compounds inhibiting LSF could be due to many reasons. First, LSF may not in fact be required for normal cell division, as it is ubiquitously expressed only at low levels in normal cells. It may also be redundant in normal cells whereas the HCCs are oncogene addicted. Finally, some properties of the compounds themselves may render the exposure of the compounds higher in HCC cells than normal cells thus achieving a high therapeutic index.

Targeting Transcription Factors

Targeting transcription factors regulating pathways implicated in human disease has been an attractive therapeutic goal, especially for cancer. As previously mentioned, tumor cells can escape molecular targeted therapies, resulting in the initial efficacy of a compound to vanish in a patient over time (Llovet et al., 2015; Torrecilla and Llovet, 2015; Villanueva and Llovet, 2011). Targeting an entire pathway could potentially abrogate the tumor cells' ability to adapt and prove more efficacious, as approaches that neutralize pathway redundancy are more difficult for a cancer cell to overcome. However, transcription factors in general have been difficult to target by small molecule inhibitors as they are intrinsically disordered within their protein and DNA binding sites and lack stable tertiary and/or

secondary structure under physiological conditions *in vitro* (Dunker and Uversky, 2010). Further, many human TFs have small DNA binding pockets making them difficult to target. In contrast, LSF has a relatively large DNA binding domain which could provide support for the rationale of why FQIs successfully inhibit LSF DNA binding (Dunker and Uversky, 2010; Yan and Higgins, 2013).

Clearly, anti-tumor activity of FQIs requires further evaluation to understand why LSF is indeed required for hepatocellular carcinoma survival. Early studies expressing a dominant negative LSF in a highly tumorigenic cell line reduced tumor cell growth, however, did not obliterate tumor formation. This could simply be due to the endogenous LSF that remained partially active, or it could be that the dominant negative LSF did not alter LSF protein-protein interactions that could play a role in HCC cell survival, and possibly their proliferation. To confirm that the FQI inhibition of LSF was the sole reason for its anti-tumor activity, and also to understand why HCC cells were dependent on LSF, a dual approach was taken to interrogate the molecular requirement for LSF. These studies led to the following novel results: 1) identification of LSF as a mitotic regulator in HCC cells, 2) demonstration that reducing LSF activity either with FQI1 or RNAi technology resulted in similar mitotic defects, including a prometaphase/metaphase delay, increased time for progression through mitosis, improper cell division, and production of multi-nucleated cells, 3) determination that loss of LSF activity led to a dose dependent reduction of Aurora Kinase B and Cdc20 levels, 4) establishment of an additional, non-transcriptional role for LSF in regulating mitotic progression in HCC cells, and finally, 5) further evidence of the lack of toxicity of FQI1 and FQI2 in mice, by

evaluating hematopoietic cell types in whole blood. In total, the work in this thesis further validates the promise of FQIs, or the targeting of LSF, for treatment of hepatocellular carcinoma patients, as LSF is a required mitotic regulator in this cancer type.

CHAPTER TWO

Materials and Methods

2.1 Cell lines, culturing, and cell cycle synchronization

QGY-7703 cells (obtained from Devanand Sarkar's laboratory, Virginia Commonwealth University) were cultured at 37°C in 10 % CO_2 in DMEM (Dulbecco's Modified Eagle's Medium; Corning Cellgro) supplemented with 10% Fetal Bovine Serum (FBS; Atlanta Biologicals). Cells were propagated in T-75 flasks (Corning). Cells were split 1:10 using 0.25 % Trypsin (Gibco) once cells were at 85 % to 90 % confluence. Cells were frozen in 5 % DMSO (Sigma) in DMEM containing 10% FBS at passage 2 after a thaw. After a thaw, cells were not passaged greater than 10 times to maintain the consistency of the cell line.

QGY-7703 cells were plated at 0.45-0.9 $x10^6$ cells per 35 x 10 mm tissue culture plate in complete medium (DMEM+10% FBS), at 0.250 x 10^6 cells per well in a 6 well plate, and at 5,000 cells per well in a 96 well plate on Day 1 for each experiment. All protocols were initiated 24 hours post plating unless otherwise specified.

For synchronization, cells were then treated with freshly prepared 2 mM thymidine (Sigma) in complete medium for 18 hours, washed twice with 1xPhosphate Buffered Saline (PBS) acquired from ThermoFisher Scientific (1.5 mM Potassium Phosphate monobasic (KH_2PO_4), 137 mM Sodium Chloride (NaCl), 0.9 mM Calcium Chloride ($CaCl_2$), 0.5 mM Magnesium Chloride ($MgCl_2$-$6H_20$), 2.7 mM Potassium Chloride (KCl) and 8.05 mM Sodium phosphate dibasic) and incubated with complete medium for 6 hours. The complete medium was then removed and 2 mM thymidine in

complete medium was added to the cells for second 18-hour incubation. Cells were washed with 1xPBS twice and released from the G1/S block in complete medium. For preparation of the 2 mM thymidine solution, thymidine was measured on an analytical scale, diluted into the appropriate amount of complete medium, and sterile filtered using a Corning vacuum top filter.

For certain assays, the Factor Quinolinone Inhibitors were added after the first incubation with 2 mM thymidine and that concentration was maintained during the first release, the second block, and at the second release. Alternatively, FQI1 was added into complete medium only at the second release. For all siRNA experiments, the thymidine block was started 24 hours post transfection with siRNA. At each release 20 μM of thymidine was added into complete media for certain studies investigating RNAi mediated LSF knockdown or FQI1 treatment.

For all synchronization experiments, cells were then collected either at the final G1/S block, or at times after release from the second block, in order to investigate time points representative of the cell cycle phases: DNA Synthesis (S), Gap 2 (G2), Mitosis (M), and Gap 1 (G1). For most analyses, the following protocol was used in order to ensure that rounded, mitotic cells were included at the point of cell harvest. The media was first transferred into a 50 ml BD Falcon tube, then the cells were washed with 1xPBS which was then transferred into the same 50 ml Falcon tube to include all unattached cells. In order to remove the attached cells, 0.25% trypsin was added to each well/plate and incubated for 5 minutes at 37^{o}C in 10% CO_2. The media/PBS from the BD Falcon tube was added to its designated well to collect the trypsinized cell population and then

transferred back to the BD Falcon tube. The harvested cells were then treated for the appropriate analyses.

2.2 siRNA transfection to achieve specific gene knockdown

Cells were plated either in 100 mm x 20 mm culture dishes, 6 well, or 96 well Costar plates with no coating, or in 6 well glass plates (MatTek Corporation) specifically acquired for time lapse imaging. Cells were plated on Day 0 at cell numbers ensuring that the cells would be between 40-60 % confluent on day 2. The confluence was essential as plating at too low a confluence resulted in toxicity due to the amount of lipid transfection reagent per cell. On Day 1, the cells were transfected using RNAimax (Life Technologies). The Imax reagent was diluted 1:25 into OptiMEM (Gibco) and incubated for 5 minutes at room temperature. The siRNAs were also diluted into OptiMEM (Gibco). All the dilutions were performed in 50 ml BD Falcon Tubes. After 5 minutes, the RNAimax/OptiMEM was carefully added to each siRNA dilution in a 1:1 fashion. The solution was then carefully swirled by hand to ensure that the integrity of the lipoplex was not compromised. Following a 10-minute incubation at room temperature, the lipid formulated siRNA was added to each well/plate according to the instructions provided by Life Technologies. 0.5 ml of siRNA/lipid was added to 2 ml of complete media in a 6 well plate, 2 ml to 8 ml of complete media in 10 mm plates, and 0.05 ml to 0.1 ml in a 96 well plate, respectively. The plates were then placed in the 37°C incubator at 10% CO_2 for the rest of the study. Transfection efficiency was measured by fluorescent microscopy 24 hours post transfection by cellular uptake of the Cy3 labeled siRNA control sequence.

2.3 Preparation of FQIs

FQI1 was synthesized by the Schaus laboratory at Boston University. Solid FQI1 was stored at -20 °C for no more than 5 months. FQI1 was suspended with DMSO (analytical grade from Sigma) and aliquoted for storage at -20 °C for no more than 1 month to a concentration of 20 mM. Aliquots were then diluted to a 2 mM concentration into DMSO immediately before addition to cells in culture. The final DMSO concentration added to the cells in any group was 0.5%.

2.4 Reagents

Table 2.1 Taqman Probes from Life Technologies

Taqman probes were acquired from Life Technologies in order to determine relative gene expression levels.

Human Gene Target	Probe Information	Catalog Number
Aurora Kinase B	HS009645858 M1	4331182
Bub1	HS01557695 M1	4331182
Cyclin A	Hs00171105m1	4331182
Cyclin B	Hs01565448 g1	4331182
Cdc20	HS00426680 M1	4331182
Cdh1/FZZD	HS00393592 M1	4331182
GAPDH	Not provided	4326317E
LBP1a	HS00232691 M1	4331182
LSF	HS00232185 M1	4331182
Mad2	HS00365651 M1	4331182

Table 2.2 Probe Information for Affymetrix Quantigene Kit

The probes included below were acquired from Affymetrix from those currently in stock that successfully targeted the genes of interest in human samples. The probes utilized in this body of work are listed below.

Human Target	NCBI Accession Number (If required)	Catalog number
Aurora Kinase B		SA-10088
Cdc20		SA-11364
GAPDH		SA-10001
TFCP2	NM_005653.3	QG0052
18S		SD-10001

Table 2.3 Reagent and Kit Product Information

The following kits were acquired and utilized to investigate various aspects of the impact of LSF activity reduction in human cells. The manufacturer's protocol was strictly followed unless otherwise specified. All kits were used prior to expiration date and stored according to protocol guidelines.

Reagent/Kit	Company	Catalog Number
Senescence kit	Cell Signaling	9860
FlowCellect™ Bivariate Cell Cycle Kit	EMD Millipore Corporation	FCCH025103
Cell Titer Blue	Promega	G8081
Thymidine	Sigma Aldrich	T1895-10G
γH2AX Kit	EMD Millipore Corporation	FCCH025142
Cell Cycle Kit	EMD Millipore Corporation	4500-0220
Apotoxglo assay	Promega	G6321

Table 2.4 Antibody Information

The following antibodies were acquired and utilized in the experiments conducted in this work. They were chosen based on user ratings and those predicted for success for either immunocytochemistry or western blotting. They all target, or were predicted to target the human protein. The host species in which the antibody was derived was carefully

considered when co-staining was required. Polyclonal antibodies were chosen if that option was available on candidates that fit the previously described criteria.

Antibody	Catalog Number	Company	Dilution	
			Immuno-fluorescence	Western Blot
Alpha tubulin	AB7750	Abcam	50	-
Aurora Kinase B	AB2254	Abcam	-	500
Cyclin A	AB38	Abcam	-	200
Cyclin B1	AB72	Abcam	-	500
Cdc20	AB26483	Abcam	-	500
γH2AX phosphorylated-Histone	9718S	Cell Signalling	50	-
3 (Serine 10) phosphorylated Histone	AB5176	Abcam	-	1000
3 (Serine 28)	AB5169	Abcam	-	1000
LBP1a	ABE181	Abcam	-	500
LSF	ABE180	Abcam	100	1000
Gamma Tubulin	AB11316	Abcam	50	-
α-Tubulin	10002	Sigma	-	1000
Anti-rabbit Alexa 488	AB150069	Abcam	200	-
Anti-mouse Alex 647	AB150111	Abcam	200	-

Donkey anti mouse IR800	926-32212	LI-COR,Inc.	-	5000
Donkey anti rabbit IR800	926-32213	LI-COR,Inc.	-	5000
Goat anti rabbit IR680	926-68073	LI-COR,Inc.	-	5000
Goat anti mouse IR680	926-32214	LI-COR,Inc.	-	5000

2.5 Phase contrast and fluorescent microscopy.

Cells were imaged using an Axiovert 40 CFL (Zeiss) microscope for both phase contrast as well as fluorescent imaging in cultured cells. Paraformaldehyde fixed cells were analyzed using a Zeiss Axioimager M1 microscope utilizing both 63x and 100x magnifications to analyze mitotic progression based on both DNA staining by DAPI (Invitrogen) and actin staining by Alexa Fluor 488 Phalloidin (Thermo Fisher Scientific Inc. product number A12379) or with anti-antibodies detecting Alpha Tubulin or Aurora Kinase B.

2.6 Cell flow cytometry

Attached cells were harvested with 0.25% Trypsin (Gibco) at pre-determined time points and combined with the media supernatant containing non-attached cells. Cells were centrifuged at 23 x g for 5 minutes. They were re-suspended in 1xPBS at a concentration of $1x10^6$ cells per ml and centrifuged at 23 x g for 5 minutes. Cell pellets were re-suspended in 150 µl of 3.33x PBS and 350 µl of 100% ethanol. Cell solutions were fixed overnight at 4°C. Cells were stored no later than one week at 4°C prior to analysis. Cells were centrifuged at 22 x g for 5 minutes. The PBS/ethanol solution was

decanted without compromising the integrity of the cell pellet. Cells were washed with 1xPBS and centrifuged at 23 x g for 5 minutes. 1xPBS was removed and Guava cell cycle reagent (EMD Millipore), which contains propidium iodide to determine the DNA content, was added at a ratio of 200 µl per $2x10^5$ cells. Cells were stained for 30 minutes at room temperature in the dark. Cell solutions were transferred into 50 ml BD Falcon FACS tubes with straining caps (BD Falcon). Samples were stored at 4°C in the dark for no more than 1 week prior to analysis on the BD Dickenson FACS Calibur.

2.7 Immunofluorescence

22 mm x 22 mm non-coated glass coverslips (Fisher Scientific) were placed in sterile 6 well Costar tissue culture plates in a sterile recirculating tissue culture hood. The coverslips were submerged in 70% ethanol for 2 minutes. 70% ethanol was removed by suction and wells/coverslips were allowed to dry in the hood. Once 70% ethanol was fully evaporated, UV light was utilized to sterilize the coverslips and wells for 10 minutes. Cells were plated on the coverslips. For analysis, media was removed and the cells were placed in 2 ml of 4% paraformaldehyde for 10 minutes. Cells were washed twice with 1xPBS. Coverslips with cells were treated with 0.1% Triton X-100 (Thermo Fisher Scientific Inc.) for 10 minutes to permeabilize the cell membrane. Coverslips were then incubated in 1% Bovine Serum Albumin (Sigma Aldrich) freshly prepared in 1xPBS for 1 hour to block nonspecific interactions, followed by incubation with primary antibody alone or in combination with a second primary antibody at the indicated dilution (Table 2.4) containing 1% Bovine Serum Albumin overnight at 4°C. Cells were washed three times with 1xPBS. Secondary antibodies were added at a pre-determined dilution

(Table 2.4) and incubated for 2 hours at room temperature in dark. Cells were washed 3 times with 1xPBS. The corner of the coverslip was blotted on a paper towel to remove excess 1xPBS. Cells were then mounted using Anti-fade DAPI Mounting Medium (Invitrogen) or Permount mounting solution. Cells were dried overnight in the dark. Coverslips were sealed on glass slides with clear nail polish.

2.8 Immunoblotting

Cells were lysed in RIPA buffer (125 mM Tris HCl, 150 mM NaCl, 0.1% NP-40, 1.0% Sodium deoxycholate, 1.0% SDS, pH 7.6) containing ROCHE protease cocktail phosphatase inhibitors (Sigma Aldrich 4693159001) at the manufacturer's recommended concentrations, prepared no greater than 1 week prior to the experimental end. Lysates were placed on ice for 10 minutes then mixed by vortexing for 10 seconds. Protein concentrations were determined by the Pierce BCA protein kit using a BSA standard prepared at concentrations from 25 to 2000 μg/ml. Equivalent protein concentrations were boiled for 10 minutes in 4x SDS Laemmli buffer (277.8 mM Tris-HCL pH 6.8, 44.4% (v/v) glycerol, 4.4% lithium dodecyl sulfate, 0.02% bromophenol blue with 355 nM β-mercaptoethanol; Bio-rad). The final concentration of the SDS Laemmli buffer was 2x. Lysates were loaded onto 10 or 15 well 4-20% Mini-PROTEAN® TGX™ Precast gradient gels (Bio-rad, product number 456-1096). The proteins were transferred to a PVDF membrane using the Bio-rad wet transfer apparatus for 30 minutes at 90 volts or the iblot system from Invitrogen according to the manufacturer's protocol. Ponceau red (Sigma) staining confirmed proper protein transfer. The dual labeled molecular weight ladder (Bio-rad #13-032) with blue and red dye allowing visualization in both 600

and 800 channels available with the Licor odyssey was utilized in each experiment. PDVF membranes were incubated for 1 hour in odyssey blocking buffer (LI-COR Biosciences cat# 927-40000). The odyssey blocking buffer was PBS-based with 0.1% of sodium azide. Primary antibodies were incubated at pre-determined concentrations (see Table 2.4) in PBS/Odyssey Blocking buffer overnight at 4°C. Membranes were washed three times in 1xPBS 0.01% Tween 20 for 20 minute intervals. Membranes were then incubated in a 1/5,000 dilution of appropriate secondary antibody (or antibodies) at room temperature for 2 hours. Membranes were washed three times in 1xPBS in 20 minute increments. PVDF membranes were then imaged using the Licor Odyssey (Boveia and Schutz-Geschwender, 2015). Infrared detection quantitated each band on an individual pixel basis using western analysis tools in the Image Studio program. This system allowed quantitation from each channel separately following the capture of single image, on an individual pixel basis (Boveia and Schutz-Geschwender, 2015). Additionally, the background signal is subtracted from the area immediately surrounding the band being analyzed.

2.9 RNA analysis: bDNA assay from Affymetrix

RNA quantification was executed using a hybridization based assay, Quantigene 1.0 and/or 2.0 systems, available from Affymetrix. Probes were designed by Affymetrix according to NCBI accession numbers, or sequences were used according to previously developed probes for the gene of interest. The probe concentration for the assay was determined using a standard curve for each probe on untreated cell lysates plated at the 10,000 cells per well in at 96 well plate at day 1 with cell lysates harvested 24 hours later.

The cell concentration was kept constant and the probe concentration was chosen based on the standard curve. Media was removed by suction and 100 µl of the Affymetrix lysis buffer with proteinase K (Promega), added to the buffer immediately prior to the lysis step, was then added to each well. Plates were placed on a shaker for 30 minutes at 56°C. Lysates were frozen at -20°C until analysis. The manufacturer's protocol was followed. Fluorescent signal was determined by 30 second reads on each well using the Victor plate reader (PerkinElmer). Each target gene was normalized to a ubiquitous control gene. GAPDH, ACTB, and 18S rRNA were utilized as the ubiquitous control genes (see Table 2.2).

2.10 Measuring Gene Expression with RT-qPCR

RNA isolation using the QIAzol reagent (trizol based chemical from Qiagen) was performed by adding the reagent either to growing cells immediately following a 1xPBS wash, or to frozen cell pellets collected after a 1xPBS wash and snap frozen at -80°C. Alternatively, RNA was isolated from samples using the Qiagen RNAeasy kit following the manufacturer's instructions. RNA concentrations were determined using a Nanodrop spectrophotometer (ThermoFisher Scientific). The RNA concentrations were adjusted to 25 ng/µl where 250 ng was then used to make cDNA using a Reverse Transcription kit from Applied Biosystems (catalogue number 4368814). All probes for RNA quantification were acquired from Taqman gene expression system utilizing dual labeled probes which allowed for analysis of gene expression. TaqMan® gene expression assays consist of a pair of unlabeled PCR primers and a TaqMan® probe with a FAM™ or VIC® dye label on the 5' end, and minor groove binder (MGB) non-fluorescent quencher

(NFQ) on the 3' end. RNA from samples of interest was reverse transcribed into cDNA, and the synthesized cDNA served as a template for real-time PCR. Target gene expression was normalized to the GAPDH ubiquitous control in each well utilizing a dual label system where the control probe targeting GAPDH RNA was labeled with FAM and the probe targeting the gene of interest was labeled with VIC. Ct values were measured using a Roche Light Cycler 480. The following formula was used to determine relative gene expression: $2^{-(C_t \text{ Target})}/2^{-(C_t \text{ Control})}$.

2.11 Caspase activity and viability

Caspase activity, viability, and cytotoxicity were measured using the Apo Tox-Glo™ kit (Promega). The kit measured viability and cytotoxicity using substrates that were cleaved by live cell proteases or dead cell proteases, respectively, resulting in the emission of a fluorescent signal at different wavelengths (Niles et al., 2007). Specifically, the live-cell protease activity is restricted to intact viable cells and is measured using a fluorogenic, cell-permeant, peptide substrate (GF-AFC). The substrate enters intact cells where it is cleaved by the live-cell protease activity to generate a fluorescent signal proportional to the number of living cells. This live-cell protease becomes inactive upon loss of cell membrane integrity and leakage into the surrounding culture medium. A second, fluorogenic cell-impermeant peptide substrate (bis-AAF-R110) is used to measure dead-cell protease activity, which is released from cells that have lost membrane integrity. Because bis-AAF-R110 is not cell-permeant, essentially no signal from this substrate is generated by intact, viable cells. The live- and dead-cell proteases produce different products, AFC and R110, which have different excitation and emission spectra,

allowing them to be detected simultaneously. Additionally, the kit measured the cleavage of Caspase 3/7 substrates by luminescence. Cells were cultured with FQIs or transfected with siRNA following plating of $2x10^5$ cells per well in 96 well pates (Corning), and the Apoptoxglo kit was utilized using manufacturer's instructions. The substrates for both live and dead cell proteases were added to wells with 100 µl of complete media. The plate was mixed on a lab rotator orbital shaker at a speed of 300 units for 1 minute. The plate was incubated for 30 minutes at 37°C 10% CO_2 prior to the measuring the luminescence or fluorescence on the VersaMax™ plate reader (Molecular Devices).

2.12 Viability determined by mitochondrial activity

Cell Titer Blue (Promega) was utilized to measure cell viability via the ability of the cell to convert a redox dye into a fluorescent end product. Cells were plated on day 1 on a 6-well plate with 250,000 cells per well, on day 2 when the cells reached about 40% confluence they were treated with FQIs, vehicle, or transfected with siRNA utilizing RNAiMax transfection reagent (Invitrogen). At selected time points, cell titer blue was added to the experimental wells at a volume of 500 µl into 2 ml of complete media for 6 well costar plate and 20 µl into 100 µl of complete media for a 96 well costar plate. Once the reagent was added, the plates were shaken for 1 min. The cells were then incubated at 37°C with 10% CO_2 for 1 to 4 hours. The fluorescent signal was detected on a VersaMax™ plate reader (Molecular Devices) exciting at 560 nM and measuring fluorescence emission at 590 nM.

2.13 Isolation of primary mouse hepatocytes.

Primary mouse hepatocytes were isolated according to the protocol in Severgini et al. 2012. Once isolated, the hepatocytes were plated in 6 well plates with sterilized coverslips. The cells were allowed to adhere to the coverslips for 4 hours, and then the cells were treated with FQI1 or vehicle. The coverslips were collected at various time points, fixed for 20 min in 4% paraformaldehyde, washed twice with 1xPBS and stored in 1xPBS at 4°C. The cells were either stained with DAPI and Phalloidin or with Hematoxylin and Eosin prior to imaging.

2.14 *Ex vivo* maintenance of primary mouse hepatocytes

Primary hepatocytes isolated according to 2.13 were plated in 6 well plates at 500,000 cells per well and maintained in Williams Media (ThermoFisher Scientific cat#1217901) supplemented with hepatocyte maintenance supplement pack (ThermoFisher Scientific cat#CM4000). Specifically, cell culture plates were coated with 0.1% rat tail collagen (Sigma) 24 h before plating cells. After isolation, cell number and viability were determined. The cell pellet was re-suspended by gently pipetting up and down in the appropriate volume of 37 °C plating medium [Dulbecco's Modified Eagle's Medium, 2% bovine serum albumin (BSA, Sigma-Aldrich), Hepatocyte Plating/Thawing and Maintenance Supplement (ThermoFisher Scientific cat#C3000), 0.1% rat tail collagen (Sigma-Aldrich)]. Cells were seeded gently and incubated in a tissue culture incubator set at 37 °C, 5% CO_2. After 4.5–5 h, cells were washed once with 1xPBS and 2 ml of maintenance medium was added to each well. At this time FQI1 or vehicle control was

added to the media at a final concentration of 5 μM. Phase-contrast pictures were taken with an Axiovert 40 CFL (Zeiss) microscope.

2.15 Generation and LSF knockdown of QGY-7703 mEmerald Alpha-Tubulin and QGY-7703 YFP Histone H2B cell lines

Calcium Phosphate Transfection of HEK-293

Packaging Cells (GP2-293 packaging cells; Clontech) were cultured at 37°C in 5% CO_2 in DMEM (Dulbecco's modification of Eagle's Medium (Corning Cellgro) supplemented with 10% FBS (Atlanta Biologicals), 6 mM L-Glutamine (Cellgro), and 1 mM sodium pyruvate (Cellgro). Since L-Glutamine degrades over time at 4°C, the media was re-supplemented with L-glutamine when the cells began to exhibit slow growth. Cells were grown on 10 cm tissue culture plates coated with 0.1% collagen (extracted from rat tails; gift from the Bradham laboratory) for 30 minutes at 37°C and washed twice with PBS. To begin, $5x10^6$ GP2-293 cells were plated on a 10 cm collagen coated tissue culture plate. The next day, the cells were transfected with 10 μg of pVSV-G expression plasmid (Clontech) and 10 μg of a pBABE vector containing a gene for YFP-tagged histone H2B protein and a gene encoding G418 resistance (gift from Jagesh Shah laboratory, Harvard Medical School) via calcium phosphate method (Kingston, et al., 2003). Five hours post transfection, the DNA-containing media was removed, and the plates were washed once with 1x PBS. Then, 10% sterile glycerol in DMEM was added to the plate and left to incubate at room temperature for 1.5 minutes. The glycerol/DMEM was then removed, the plate was washed once more with 1x PBS, and 10 mL of the supplemented DMEM

was added to the plate. [Performed by Mark Roberto of the Hansen laboratory at Boston University.]

Preparation of virus-containing media and Infection of QGY-7703 cells

Two days after transfection of the packaging cell line with the retroviral vector, the media from the plate of GP2-293 cells was collected into a 50 mL conical tube. The media was then filtered using a 45 μm syringe filter (Pall Corporation) in order to remove any GP2-293 cells, and 8 μg/mL polybrene was added. The virus-containing supernatant was then transferred to a 10 cm plate of QGY-7703 cells that were at 60-70% confluence. QGY-7703 cells were cultured at 37ºC in 5% CO_2 in DMEM (Dulbecco's modification of Eagle's Medium (Corning Cellgro) supplemented with 10% FBS (Atlanta Biologicals). The following day, the virus-containing media was replaced with 10 mL of DMEM + 10% FBS + 500 μg/mL G418 anti-biotic (Gibco). The G418-containing DMEM was replaced every 3 days for about 10 days until the majority of cells expressed the YFP-histone fusion protein. Presence of the fluorescent protein was checked using an Endow GFP/EGFP Bandpass filter (Chroma) in an Olympus IX50 inverted fluorescent microscope, exciting the protein at 514 nm and detecting subsequent emission at 527 nm. [Performed by Mark Roberto of the Hansen laboratory at Boston University.]

The QGY-7703 cells were also infected with a lentivirus to express the mEmerald Alpha-tubulin, selected in 5 μg/ml Blasticidin, and sorted by FACS to enrich for positive cells. [Performed by Dr. Kelly George of the Shah Laboratory at Harvard Medical School.]

siRNA Knockdown of LSF and/or LBP1a in Asynchronous QGY-7703 Cells Expressing Fluorescently Tagged H2B

Fluorescently tagged H2B-QGY7703 cells were plated on 6-well glass plates (MatTek) at $5x10^4$ cells/well. The next day, the cells were transfected with a siRNA against firefly luciferase GL3 at a 20 nM concentration or siRNA against LSF at either a 10 nM or 20 nM concentrations by using 70 μL of RNAiMax (Invitrogen) per plate with a final volume of 2.5 mL DMEM with transfection mixture. The cells were incubated at 37^OC with the transfection mixture for 48 hours, after which the mixture was removed and the cells were washed twice with 1x PBS. Fresh DMEM + 10% FBS was then added to each well. The cells were imaged by time lapse microscopy the next day (72 hours post-transfection), or two days later (96 hours post-transfection).

Double and single thymidine block synchronization of fluorescently tagged QGY-7703 cells after siRNA Knockdown

The fluorescently tagged H2B-QGY7703 cells were synchronized by using a single thymidine block. Two days after the cells were transfected with either control siRNA against luciferase or siRNA against LSF, LBP1a, or the combination of the two, the siRNA-containing media was removed and cells were washed twice with 1x PBS. The media was then replaced with 2 mL of DMEM containing 2 mM thymidine. After 18 hours, the media was removed, the cells were washed once with PBS, and 2 mL of DMEM was added to the cells. Following 6-7 hours, the DMEM was removed and replaced with 2 mL of DMEM containing 2 mM thymidine. After 16-24 hours, the media

was removed, the cells were washed twice with 1x PBS, and 2 mL of complete media was added to the cells with or without 20 μM thymidine. The cells were imaged by time lapse microscopy at 48 hours after transfection. Additionally, some experiments were executed using a single thymidine block. There, the cells were transfected with siRNA, 24 hours later 2 mM thymidine was added for 24hours. The cells were then released from the block following a 1XPBS wash and imaged.

2.16 Time lapse microscopy

Single thymidine block synchronization of QGY-7703 Cells Expressing Fluorescently Tagged H2B after siRNA knockdown

QGY-7703 cells with H2B labeled with YFP or with alpha tubulin labeled with mEmerald were plated at 250,000 cells per well in 6 well glass plates acquired from MatTek Corporation. The cells were placed in the 37°C 10% CO_2 incubator overnight. For siRNA studies, the cells were transfected on day 2 with RNAiMAX at 1:25 dilution into OptiMEM (Gibco). The siRNA was diluted in OptiMEM at appropriate concentrations and mixed 1:1 with the RNAimax/OptiMEM solution; 500 μl of the siRNA/Lipid mix was added to 2 ml of complete media. Following 10 minute incubation at room temperature, the lipid/siRNA mixture was added to the 6 well plates. The cells were placed in the 37°C 10% CO_2 incubator overnight. Twenty-four hours later the media was removed and 2 mM of sterile filtered thymidine in Complete media was added to each well. The cells were placed in the 37°C 10% CO_2 incubator overnight. Cells were washed with 1xPBS and were imaged in the CO_2 independent medium (Leibovitz's

L-15 without phenol red) on a Nikon TA10 Eclipse with a 20X objected with a heated environment (37°C).

Treatment of QGY-7703 Cells Expressing Fluorescently Tagged H2B with FQI1

QGY-7703 cells with H2B labeled with YFP or with alpha tubulin labeled with mEmerald were plated at 500,000 cells per well in 6 well glass plates acquired from MatTek Corporation. The cells were placed in the 37^{O}C 10% CO_2 incubator overnight. Vehicle control or FQI1 was added at final concentrations of 0.9, 1.8, or 3.6 μM in CO_2 independent medium (Leibovitz's L-15 without phenol red). Cells were imaged immediately after adding FQI1 in on a Nikon TA10 Eclipse with a 20X objective with a heated environment (37°C).

Measuring mitotic times

Images were acquired for cells, treated with either FQI1 or transfected with siRNAs, every four minutes at 7-10 positions per condition for at least five hours. Length of mitosis was measured from nuclear envelope breakdown to anaphase. Nuclear envelope breakdown as demonstrated by disordered condensed chromosomes was used to demarcate entry into mitosis. Anaphase was determined as the first image in which sister chromatid separation is apparent (for normal anaphases) or when a furrow begins to form over the chromosomes. The pictures were then compiled into a video at a speed of five frames per second. Imaging and photo compilation was carried out by Dr. Kelly George of the Shah Laboratory at Harvard Medical School.

2.17 Analysis of γ H2AX to assay for double stranded DNA breaks

Levels of γ-H2AX were analyzed by both flow cytometry and immunofluorescent microscopy. Immunofluorescence staining for γH2AX was performed in similar fashion to all immunofluorescence imaging previously discussed using an anti γH2AX antibody from Abcam at a 1:50 dilution. Images were gathered using the methodology described in 2.2 and 2.3. These cells analyzed following siRNA transfection of FQI1 treatment were either asynchronous or synchronized using a double thymidine block.

γH2AX staining was also measured by flow cytometry using a kit from EMD Millipore (17-344). The cells were treated with FQI1 or siRNA knockdown (2.1-2.3). Cell samples were collected and washed in 1xPBS. The cell pellets were then fixed and permeabilized with overnight incubation in a 70% ethanol solution prior to staining and detection. Histone H2A.X phosphorylated at serine 139 was detected by the addition of the anti-phosphorylated-Histone H2A.X, FITC conjugate. Cells were then analyzed by flow cytometry to quantitate the number of cells staining positive for phosphorylated Histone H2A.X.

2.18 β-Galactosidase activity to determine cellular senescence

QGY-7703 cells synchronized with a double thymidine block with either FQI1 treatment or LSF knockdown in 6 well plates were washed once with 1xPBS. The cells were then stained for β-galactosidase using the activity kit from Cell Signaling Technologies. The Senescence β-Galactosidase Staining Kit is designed to conveniently provide reagents needed to detect β-galactosidase activity at pH 6, a known characteristic of senescent cells not found in presenescent, quiescent or immortal cells. The cells were fixed using

the fixation buffer including in the Cell signaling Technology kit. The staining reagent was prepared according to the manufacturer's protocol and the pH was adjusted to 6.0 using 1 M HCl. The cells were then washed twice with 1xPBS and 1 ml of the staining solution was added to each well in 6 well plates. The plate was sealed with aluminum foil and incubated overnight at 37°C. Cell images were gathered following the overnight incubation on a phase Axiovert 40 CFL (Zeiss) microscope. The number of positive cells, as determined by blue staining, was determined in comparison to cells without blue signal. Intensity of signal was not measured.

2.19 Blood collection and analysis

C57BL6 male mice (Charles River Laboratories) were acquired at approximately 8 weeks of age. Animals were kept on normal diet and light cycling conditions. Mice were dosed intraperitoneally with FQI1, FQI2 or vehicle control (DMSO) injected into each animal at 40 µl/gram. Both the vehicle and FQI injections contained 5% DMSO. One group of animals were dosed with 40 µl/gram of Saline as an additional control. The 8 mg/kg dose was injected daily for 5 days. Blood was collected utilizing the retro-orbital eye bleed procedure 24 hours post the final dose. For this procedure, the mice were anesthetized using isoflurane. Heparin coated capillary tubes (Fisher Scientific) were inserted into the posterior corner of the mouse eye; the tube was inserted at a 45-degree angle to approximately 1 cm and rotated until the blood from the retro-orbital sinus was released. Approximately 200 µl was collected from the left eye each mouse according to the IACUC protocol for blood collection. The blood was collected either in Becton Dickinson (BD) serum separator tubes or with BD plasma tubes coated with EDTA.

Serum samples were kept at room temperature for 1 hour and then spun in a micro-centrifuge at 22 x g at room temperature for 10 minutes. Serum was transferred to 1.5 ml micro-centrifuge tubes for storage at -80°C until samples were processed. Whole blood samples were collected and held at room temperature with mixing every 5 min to ensure EDTA was properly distributed to avoid clotting. The whole blood and sera samples were analyzed using an ADVIA® 120 Hematology System from Siemens. All procedures were conducted in accordance with IACUC procedures.

CHAPTER THREE

FQI1 Treatment for short intervals causes reversible mitotic defects with minimal transcriptional consequences

(Figures 3.2, 3.3d, and 3.4a include data published in Rajasekaran et al.)

Introduction

Hepatocellular carcinoma represents approximately 70-85% of the primary liver cancers, and is one of the major causes of death worldwide (Bruix, 2011; Bruix and Sherman, 2011; Wang et al., 2002). Risk factors include, but are not limited to, viral infection, toxins, and alcohol. HCC, a disease which slowly progresses over decades, presents with both non-specific symptoms and a lack of biomarkers which often lead to late diagnosis. One third of patients diagnosed may qualify for potential curative, yet invasive treatments, including surgical resection and liver transplantation. Those who have progressed into late stage disease do not qualify for such curative treatments leaving patients with only palliative treatment options as systemic therapies are limited. Current systemic therapeutic options are subpar as Sorafenib, the only approved molecular therapy, extended patient survival, at best, only 11 months (Bruix and Sherman, 2011; Llovet et al., 2015). New molecular therapies, which have demonstrated promising anti-tumor activity in preclinical models, have yet to match (or improve upon) Sorafenib, leaving a large population with a severe unmet medical need.

The ubiquitously expressed, evolutionarily conserved transcription factor LSF is overexpressed in HCC, with increased expression positively correlating with disease severity in clinical samples (Fan et al., 2011b; Yoo et al., 2010). LSF expression, which

is at relatively low levels in hepatocytes, is necessary and sufficient for HCC tumorigenicity *in vivo* as expressing LSF induced tumorigenicity in a HCC line and expression of a dominant negative LSF inhibited both subcutaneous tumor growth and metastasis formation in xenograft mouse models. These data implicated LSF as an oncogenic transcription factor in hepatocellular carcinoma.

A small molecule inhibitor of LSF (in the Factor Quinolinone Inhibitor (FQI) family), was identified from a screen of 110,000 compounds utilizing a fluorescent polarization assay designed to detect molecules able to directly inhibit LSF DNA binding (Grant et al., 2012). FQI1 and FQI2 were identified from the screen and confirmed as inhibitors of LSF in several assays including a LSF transcriptional activation in a luciferase reporter assay and a LSF- DNA binding electrophoretic mobility shift assay (EMSA). In addition, the molecules proved capable of inhibiting LSF DNA binding to a target gene, *POL*A1, *in vivo* as ascertained by chromatin immunoprecipitation (ChIP) in a tagged-LSF inducible cell line (Grant et al., 2012). The first compound identified (FQI1) was demonstrated to be specific for LSF as it was not capable of inhibiting the DNA-binding activity of other classes of transcription factors, including E2F3, Oct1, or SP1. Further, FQI1 treatment did not impact the transcriptional activation by p53 or USF (Grant et al., 2012). These data collectively indicated strongly that LSF is specifically targeted by both FQI1 and FQI2 resulting in the inability to transcriptionally regulate their direct targets. Further, treatment of HCC cells with FQI1 and FQI2 caused loss of viability as determined by reduced mitochondrial activity and an increased level of apoptosis. *In vivo*, FQI1 and FQI2 inhibited HCC tumor growth in both a subcutaneous

HCC xenograft mouse model, and more recently, in an endogenous mouse liver model (Rajasekaran et al., 2015). Taken together, these data indicate that FQI1 or FQI2 inhibition of LSF results in hepatocellular carcinoma cell death in preclinical models suggesting that LSF small molecule inhibitors may provide therapeutic benefit to the HCC patient population.

Transcription factors are generally believed to be undruggable and few *bona fide*, specific transcription factor inhibitors have been identified to date despite a great deal of effort both in academic and industrial settings (Yan and Higgins, 2013). Given the proposed unusual mechanism of action of FQI1 and 2, confirming that their observed biological effects are specifically and solely due to inhibition of LSF, as well as identifying the mechanism of HCC death resulting from FQI1 treatment are important to provide clarity around their therapeutic potential for HCC.

Previous reports have shown that LSF is required prior to the G1/S transition for cell cycle progression (Powell et al., 2000; Saxena et al., 2010). Expression of a dominant negative mutant of LSF resulted in apoptosis during S phase, as thymidylate synthase, regulated by LSF, was not as substantially induced; this phenotype was rescued with supplementation of exogenous thymidine. The dominant negative LSF utilized for these studies, a double amino acid substitution mutant of LSF named Q234L/K236E, was unable to bind DNA (Santhekadur et al., 2012a; Shirra et al., 1994). These results suggested that LSF regulation of G1/S progression in HCC cells may be responsible for the FQI1/FQI2 anti-tumor activity.

To elucidate the molecular requirement of LSF in HCC cell survival, I evaluated the impact on cell cycle progression by FQI inhibition of LSF in QGY-7703 cells. Here, I show that treatment of synchronized HCC cells with FQI1 starting at the G1/S border results (during the subsequent mitosis) in a prometaphase arrest followed by cell death. This is evidenced by cell cycle arrest following the completion of DNA synthesis, followed by multi-nucleation and/or cell death. Accumulation of cells at prometaphase is reversible if the compound is removed from the HCC cells after a short prometaphase block, suggesting that this phenotype is not related to LSF-mediated transcription. Together, these data indicate that LSF is required for proper mitotic progression in hepatocellular carcinoma cells and that this may significantly involve non-transcriptional regulation by LSF.

Results

The LSF inhibitor FQI1 causes dose dependent inhibition of cellular division and loss of viability following Caspase 3/7 activation

To investigate whether LSF was required for HCC cell cycle progression, QGY-7703 cells were synchronized at the G1/S border and released in the presence of FQI1 or vehicle (Illustration 3.1). The half maximal concentration for growth inhibition of QGY-7703 cells was reported to be 1.3 μM (Christadore, 2013). This was consistent with the G150s generated in two human tumor cell lines ranging from 0.79 to 6.3 μM (Grant, et al 2012). The concentrations were chosen to bracket the half maximal concentration, with 3.6 μM demonstrating maximal growth inhibition (Christadore, 2013). Measurement of cell numbers following release (Figure 3.1a) revealed a dose dependent reduction in total

cells upon treatment for 10 hours with FQI1. The experimental conditions chosen should result in the cell population doubling at approximately 8 hours after release, the amount of time needed for the cells to complete both DNA synthesis and mitosis. Indeed, the control cells increased in number by 2-fold, consistent with the expected division rate. In contrast progression through cell division was inhibited in a dose dependent manner with FQI1 treatment. Specifically, at the highest FQI1 concentration of 3.6 μM, the cells still had not progressed through cell division 8 hours after release from the G1/S block. At the lower FQI1 concentrations, however, cell division was able to occur in at least a subset of the cells at 1.8 μM, and in most of them at 0.9 μM.

To determine if the lack of cell division upon FQI1 treatment was due to cell death, apoptosis and cell viability assays were conducted in parallel. Caspase 3/7 activation (which occurs early in the apoptotic pathway) was measured at 6, 24, and 48 hours post release from a G1/S block (Figure 3.1b). Enzyme activity increased in a dose dependent manner and was elevated even at 6 hours, at which point the control cells would have been predicted to complete DNA synthesis. However, cell viability was not impacted until later, after 24 h (at 24 h, treated cells still retained full viability, data not shown). FQI1 concentrations that increased caspase 3/7 activity also decreased viability at 48 h, as measured by a reduction in intracellular live cell protease activity that is lost upon cell membrane disruption (Figure 3.1c). Together, these data indicate that while cells treated with FQI1 initiate cell death pathways early following release from a G1/S block, phenotypic programmed cell death is delayed. The loss of cell viability is consistent with previous reports showing reduced mitochondrial activity by an MTT

assay, TUNEL staining and Annexin V staining (the latter two being indicative of apoptosis). TUNEL staining was documented after 48 hours of incubation with 10 μM FQI1 in asynchronous HCC cell populations (Grant, et al 2012). Annexin V staining and caspase 3 activity were assayed in asynchronous QGY-7703 cells after 24 hours of incubation with 2 μM FQI1 or FQI2 (Rajasekaran et al 2015). Because Annexin V staining measures apoptotic signaling through the flipping of phosphatidylserine in the plasma membrane to the cell surface, one of the earliest responses in the apoptotic pathway, it is not surprising that this occurred within 24 hours of incubation even in the asynchronous population.

FQI1-mediated inhibition of cellular division in HCC cells results from mitotic defects

The observation of cellular death following the inhibition of cellular division suggested that LSF was required for cell cycle progression. To determine at what point LSF was required for HCC cell cycle regulation we evaluated cell cycle progression in G1/S synchronized HCC cells released in presence of 2 or 5 μM of FQI1 or vehicle. Cell cycle progression was analyzed by cellular DNA content using flow cytometry. Because tumor cells in general, and QGY-7703 in particular, are aneuploid, DNA content as ascertained by flow cytometry does not reflect a true 2n. Given the aneuploid nature of the cells, I aligned the cell populations with non-replicated DNA at the 2n peak, with 4n representing a successful round of DNA synthesis (Figure 3.2). Utilizing this protocol, successful synchronization of the cells at the G1/S border was demonstrated by the peak of cellular DNA at 2n immediately prior to release (compare Figures 3.2a and b).

Subsequent cell cycle progression following the release (0 hours) of control cells results in a doubling of DNA content to G2/M levels at 7 hours, followed by a return to G1 levels 3 hours later (Figure 3.2c). Unexpectedly, unlike the vehicle-treated cells, the FQI1-treated cells remained at 4n DNA content at the 10-hour time point. At 17 hours post release, the 5 μM FQI1 treated cells remained arrested, except for a small population with sub-G1 DNA content, indicative of cell death. A lower concentration of FQI1 also resulted in accumulation at 4n DNA shortly after control cells had exited mitosis (10 hours), however, seven hours later when controls were still in G1 three populations were observed: a population of cells with 4n DNA content, a population with sub G1 DNA content, and a population that appears to have re-entered G1. The mixed populations observed with the lower concentrations of FQI1 are consistent with a partial inhibition of LSF activity at those doses.

The observation of both a cell proliferation defect along with an accumulation at 4n DNA content indicated that the impact of FQI1 inhibition on the cells likely occurred after completion of DNA synthesis, however, whether the cells had actually entered mitosis remained unclear. To investigate this, I measured both Cyclin A and B levels in FQI1 treated cells that had entered mitosis at 6-7 hours after G1/S (Figure 3.3). In normal cells Cyclin A and B levels change during mitosis as Cyclin Dependent Kinase 1 (CDK1) associates with different cyclins at different points to phosphorylate key targets. Cyclin A levels degrade in late prophase whereas levels of Cyclin B are maintained through mitosis until anaphase (Casimiro et al., 2012; Malumbres, 2007; Sherr and Roberts, 1995, 2004). While cyclin A gene expression at 8 hours after G1/S release was

unaltered by FQI1 treatment (Figure 3a), Cyclin A protein levels were reduced at both 0.9 and 1.8 μM relative to the controls (Figure 3b,c). This result was particularly striking as the control cells at that point had an elevation of Cyclin A protein, these results suggest that as opposed to the control cells that had successfully gone through mitosis, the treated cells remained in mitosis (Figures 3.3b and c). However, the cells treated with 5 μM FQI1 surprisingly had comparable Cyclin A levels in comparison to the control, which combined with the DNA profiling data (Figure 3.2) suggested that these cells were arrested earlier (e.g. G2 or early mitosis) than the cells treated at the lower FQI1 concentrations. To determine whether the cells had progressed at least to late G2 by 7 hours after G1/S release, Cyclin B expression was also measured. The vehicle treated, control cells show an initial increase in Cyclin B expression when the cells are about to enter mitosis (7 hours), which is then reduced at 10 hours after the G1/S release (consistent with the cellular DNA profiles) indicating mitotic exit and G1 re-entry at this time (Figure 3.3d). In contrast, the Cyclin B protein levels remained elevated at 10 and 17 hours in both of the FQI1-treated samples. Together, these data suggest that the FQI1 treated cells are arrested at in late G2/early mitosis. However, since Cyclin B RNA levels in FQI1 treated cells at 7 hours after G1/S was comparable to that of the control, the persisting, higher protein levels must result from the G2/mitotic arrest, rather than from transcriptional dysregulation (Figure 3.3e). Collectively, these data are suggestive of a G2/mitotic arrest in FQI1 treated cells where the higher concentrations result in a delay in late prophase whereas at the lower concentrations there is an arrest following mitotic entry.

To investigate further the apparent mitotic defect caused by FQI1, cells were imaged for progression through mitosis by visualizing their cellular morphology as determined by staining for alpha tubulin and DNA. Eight hours after release from the G1/S block, FQI1-treated cells revealed increased numbers of cells in prometaphase whereas the vehicle-treated cells were in final stages of mitosis or interphase (Figure 3.4a). These cells, analyzed at 63x magnification, were deemed to be arrested in prometaphase as the DNA had condensed, however, the chromosomes were not aligned as expected in metaphase. FQI1 treatment for 48 hours led to a reduced number of cells in comparison to the control (not shown). The cells remaining were multi-nucleated (Figure 3.4b). When progression of synchronized HCC cells was followed over time, those treated with 5 μM FQI1 that had entered mitosis at 6 hours after release from the G1/S block, were predominantly in prometaphase, whereas the vehicle-treated cells that had entered mitosis were predominantly in metaphase (Figure 3.4c). At later timepoints, the control cells had divided and eventually were again observed in metaphase, whereas the FQI1-treated cells were both lower in cell number and generally multi-nucleated, as indicated by the arrows at 19 hours (Figure 3.4c 16.5, 19, and 23 hours).

Higher magnification (100x) of cells treated for 7.5 to 9 hours with FQI1 and imaged for both α-tubulin and DNA revealed additional phenotypes: occasional cells with multi-asters (cells with more than two microtubule structures known as asters), and cells in prophase (defined by rounded cells with non-condensed DNA), in addition to cells in prometaphase (rounded cells with condensed DNA that had not formed a metaphase plate) (Figure 3.5a and b). Image quantitation revealed that FQI1 treatment resulted in an

increasing proportion of cells in prophase, particularly with those that display protrusions (Figure 3.5b) and correlated with increasing FQI1 concentrations at 9 hours post release (Figure 3.5d). The increase in both prophase and prometaphase cells was the most prominent phenotype of FQI treatment (Figure 3.5d, e, and f). These findings are consistent with the analysis of DNA content by flow cytometry where the FQI1 treated cells showed a cell cycle arrest at 4n levels of DNA (Figure 3.2). An additional FQI-induced phenotype was multi-aster prometaphase cells, whose proportion increased in particular at higher FQI1 concentrations and later time points, approaching 20% at 3.6 μM FQI1 (Figure 3.5g). It is noteworthy that the extent of the multi-aster prometaphase phenotype may have been underestimated due to limitations of analyzing selected time points in fixed cell populations.

Finally, multi-nucleation, a phenotype resulting when a cell exits mitosis in the absence of bipolar separation of its chromosomes, was observed following in 80% of the cells after incubation with 5 μM FQI1 (Figures 3.4b and c, 3.5c). Both the prophase and prometaphase arrest and the accumulation of cells with 4n DNA content are consistent with the maintenance of elevated levels of Cyclin B expression at 7, 10 and 17 hours after release from the G1/S block in the presence of the LSF inhibitor (Figure 3.3e) as Cyclin B expression is elevated during mitosis, but degraded prior to mitotic exit. Together, the data indicate that FQI1 treated cells are accumulating in mitosis whereas the control cells re-enter the cell cycle at G1.

Short term incubation with FQI1 does not impact transcription of key mitotic genes

Given that LSF is a transcription factor and previous studies indicated that FQI1 and FQI2 could inhibit LSF DNA-binding activity, we hypothesized that direct dysregulation of mitotic gene transcription might be the mechanism of the observed FQI1 mediated prometaphase arrest. To investigate this hypothesis, we looked a gene expression changes via qPCR across cells treated with various concentrations of FQI1 versus control cells. In particular, expression levels of both Aurora kinase B and Cdc20 (two genes that are required for prometaphase and mitotic exit) in the presence of FQI1 were comparable to levels in control cells (Figures 3.6a-c, e-g). Unexpectedly, the highest FQI1 concentration, unlike that observed at lower concentrations, was absent of phosphorylated Histone 3, a crucial event for mitotic onset. However, these findings are consistent with the increased Cyclin A expression shown in Figure 3.3c and large number of prophase cells (Figure 3.5e and f) indicating that at 8 hours the cells treated with 5 μM FQI1 are delayed from entering prometaphase. Regardless, the lack of expression changes in genes encoding mitotic regulators (Figures 3.3 and 3.6) suggested that the FQI-induced prophase/prometaphase arrest might not be the result of changes in transcription but possibly that of translation, phosphorylation or protein: protein interactions.

Short-term FQI1-mediated mitotic arrest in QGY-7703 cells is reversible

In order to independently test whether LSF transcriptional activity was involved in any of the mitotic phenotypes, a washout experiment was performed in which FQI1 treated cells were arrested and then the compound removed. If FQI1 induced cellular phenotypes by blocking transcriptional induction of key genes during cell cycle

progression (prior to mitotic entry), the phenotypes would not be reversible after a mitotic block had been established, as transcription is inhibited during mitosis and would not be able to reinitiate (Delcuve et al., 2008; Gottesfeld and Forbes, 1997; Long et al., 1998). However, if the mitotic phenotypes were reversible by washing out FQI1, it would strongly suggest that the effects were independent of the transcriptional activity of LSF and due to other mechanisms.

To this end, QGY-7703 cells synchronized at the G1/S border (Figure 3.7a) were initially released back into the cell cycle in the presence or absence of 5 μM FQI1 for 10 hours. A group treated with 5 μM FQI1 for 10 hours was washed with 1xPBS whereas all other groups were incubated further with either FQI1 or vehicle. Thirteen hours after the wash, the cell cycle distributions of the different populations were compared by DNA flow cytometry profiles (Figure 3.7b-d). As expected (Figure 3.2), the vehicle-treated cells exhibited cells throughout the cell cycle (Figure 3.7b) while the cells treated continuously with FQI1 remained in an arrested mitotic state (Figure 3.7c). Interestingly, the FQI1-treated cells that had been briefly washed 10 hours post release to remove the compound resulted in cells in all stages of the cell cycle (Figure 3.7d), clearly demonstrating reversibility of the FQI1 phenotype. Consistent with these data, phase contrast images demonstrated that the population in which FQI1 was washed out was similar to the vehicle control cells (Figure 3.7g, e), with most cells flattened and firmly attached to the surface of the plates. In contrast, cells treated with FQI1 for the duration of the study (Figure 3.7f) exhibited rounded morphology typical of a mitotic cell arrest, as described previously in this chapter.

Discussion

The finding that LSF promotes oncogenesis of HCC prompted previous preclinical studies regarding the potential utility of LSF small molecule inhibitors in treatment of HCC. These studies demonstrated that FQI1 and FQI2, which inhibit LSF DNA-binding activity, both in biochemical assays and in cellular contexts, induce HCC cell death *in vitro* and inhibit tumor growth. (Grant et al., 2012; Rajasekaran et al., 2015). Strikingly, at concentrations that significantly inhibited tumor growth, no general toxicity was evident. Based on these data, it was important to better characterize the mechanism by which FQI1 caused HCC cell death, its specificity of action, and its relationship to LSF inhibition.

LSF has long been appreciated to play a role in mammalian cell cycle, with previous studies mainly focused on G1/S transition (Powell et al., 2000; Saxena et al., 2010), however it remained unclear if cell cycle defects were the trigger by which FQI1 treatment induced cell death. To investigate this mechanism of FQI1 further, three approaches were taken: A flow cytometry based characterization of cell cycle and apoptotic effects of different concentrations of FQI1 (supplemented with investigating levels of activated caspase and selected protein markers of mitosis); a microscopy based characterization of cellular morphological effects of FQI1 treatment, and finally a compound washout experiment to investigate the mechanism of the observed FQI1 effects. Interestingly the effects of FQI1 on cell cycle arrested HCC cells at prophase and

prometaphase and occasionally caused multi-aster formation prior to cell death or the appearance of multi-nucleated cells.

FQI1 treatment of synchronized QGY 7703 cells resulted in Caspase 3/7 activation, followed by loss of viability and subG1 content of cellular DNA (Figure 3.2). These data, while consistent with previous reports, also suggested that FQI1 treatment resulted in a defect in mitosis. Specifically, the defect was most significantly in prophase and prometaphase. In addition, these data show that the loss of viability occurred well after mitotic arrest. The observations including a prometaphase arrest, elevated cyclin B levels and observations of multi-nucleated cells prior to cell death suggest that death through mitotic slippage may be occurring. The process by which cells escape mitosis when they cannot satisfy the SAC requires the ubiquitination and/or proteolysis of cyclin B and is known as mitotic "slippage" (Brito and Rieder, 2006; Brito et al., 2008; Hunt et al., 1992; Yang et al., 2009). Consistent with this notion, at 17 hours (Figure 3.3d), the cyclin B levels appear to be diminishing in the FQI1 treated cells in comparison to earlier time points. Further evaluation would be need to determine whether cyclin B degradation has triggered mitotic slippage. Slow degradation of cyclin B can occur in mitotic arrest induced by microtubule depolymerizing agents (Dai et al., 2004; Xu et al., 2010), an interesting potential parallel given the appearance of multi-asters suggests microtubule disruption in FQI1 treated cells. Elevated levels of Cyclin B in FQI1 treated G1/S synchronized cells 10 hours post release from G1/S (Figure 3.3) are consistent with the observation of a mitotic defect as Cyclin B must be degraded, or Cdk1 inactivated in some other manner, prior to mitotic exit (Guadagno and Newport, 1996; Irniger, 2002).

In Rajesekaran et al., FQI1 inhibition of LSF resulted in a prometaphase arrest (presented in Figure 6) and was associated with increased Cyclin B. Here, the data indicate that the increased expression of Cyclin B protein levels is actually a consequence, and not causative of the prometaphase arrest, as Cyclin B RNA levels were not altered as would have been anticipated if the gene were a direct target of LSF as a transcription factor. It is not surprising that Cyclin B protein levels would be elevated as the cells arrested in prometaphase. It is only once cells have reached anaphase that Cyclin B protein is degraded by the Anaphase Promoting Complex.

These results are quite distinct from those of (Powell et al., 2000) where a dominant negative version of LSF demonstrated apoptosis in S phase. The differences in phenotypes could represent disparate mechanisms of action of the agents utilized. Dominant negative LSF disrupts the ability of LSF to bind DNA and activate transcription, however, interactions with other protein cofactors may be left intact. Of course, endogenous LSF may still have been active in the dnLSF evaluation confounding the results. The small molecule on the other hand also prevents LSF DNA binding, but may interfere with other activities of LSF creating more of a null phenotype. Alternatively, a trivial explanation for the difference in phenotypes could be that separate cell lines were utilized in the experiments. Indeed, whereas dominant negative LSF expression abolished thymidylate synthase expression in the cells in which it caused S phase death, it diminished, but did not eliminate, thymidylate synthase expression in HCC cells (Yoo et al., 2010; Yoo et al., 2009). FQI1, on the other hand, may be a more robust inhibitor, in that it appears to cause similar phenotypes (accumulation of cells with

4n DNA content) in multiple cell types, including the HCC Hep3b and Huh7 cells (Rajasekaran et al., 2015). The phenotypes observed by microscopy were entirely consistent with the DNA profiling, showing rounded cells with and without condensed DNA that had not formed a metaphase plate indicative of a prophase/prometaphase arrest (Figure 3.5a, b, d and e). Also consistent was the elevated levels of Cyclin B expression at 7, 10 and 17 hours after release from the G1/S block in the presence of the LSF inhibitor (Figure 3.3a), as Cyclin B is elevated during mitosis.

Since Cyclin B RNA levels were unaffected by FQI1 treatment, I examined expression of other potential LSF targets whose dysregulation could cause prometaphase arrest. Aurora B Kinase inhibition also causes accumulation of cells in prometaphase due to incomplete kinetochore attachment, subsequently resulting in multi-nucleation and apoptosis (Kallio et al., 2002; Wang et al., 2006). Additionally, a coactivator of the Anaphase promoting complex (APC), Cdc20, is required for proteolysis of Cyclin B. However, a Cdc20 deficiency would most likely arrest the cells immediately before anaphase rather than in prometaphase. Under these conditions, in which cells were incubated with FQI1 only starting at the G1/S border, neither RNA nor protein levels of these two genes were altered. Further, phosphorylation of Histone 3 on Serine 10, which is catalyzed substantially by Aurora kinase B, was not reduced. Surprisingly, phosphorylation of Histone 3 on Serine 10 was diminished when cells were treated with 5 μM of FQI1, the same concentration at which Cyclin A protein levels are not reduced. These data indicate that at sufficiently high FQI1 concentrations, LSF may have an additional role required for mitotic progression that is crucial in prophase.

In the absence of identifying specific mitotic regulatory genes whose expression was altered by short-term FQI1/2 treatment, a general scheme was developed to test whether or not the mitotic defect was due to transcriptional regulation. Transcription mediated by RNA polymerase II does not generally occur during mitosis (Delcuve et al., 2008; Gottesfeld and Forbes, 1997; Long et al., 1998) thus expression of mitotic genes occurs during G2 and S phases, but not in mitosis. If transcriptional dysregulation were the main driver of the FQI1-mediated mitotic defect, removing FQI1 at the time of arrest, when cells are in mitosis with condensed chromosomes, would not be reversible. The cells would not recover, as LSF-mediated transcriptional events could not resume. Interestingly the results demonstrated that the mitotic defect in HCC cells was reversible upon removal of the LSF inhibitor (FQI1) within a few hours of inducing the mitotic block, allowing proper cell cycle progression to G1. In these experiments, the cells were synchronized at the G1/S border to allow specific interrogation of the impact of FQI1 incubation on different cell cycle stages, and FQI1 was added only at the time of release from this cell cycle block at G1/S. Although FQI1 has been demonstrated to inhibit LSF DNA-binding activity (Grant et al., 2012), the question remains as to whether FQI1 would be able to compete off pre-bound LSF from the DNA. If not, FQI1 may be unable to inhibit LSF-mediated gene expression under these circumstances. Overall, these data support a role for LSF, the target of FQI1, in regulating prometaphase to metaphase transition through a non-transcriptional means.

However, these results open the question of whether FQI1 has targets besides LSF. FQI1s do inhibit LSF family members, but only the close paralogs: LBP1a/b and

LBP9. FQIs do not inhibit the Grainyhead proteins (T. Grant and U. Hansen, unpublished), more distant family members to LSF. If specific knockdown of LSF by RNAi result in a similar phenotype, it would confirm the role for LSF in mitosis in HCC cells.

The elucidation of a potential mitotic role for LSF was unanticipated. Powell et al. (Powell et al., 2000) demonstrate that expression of dominant negative LSF resulted in apoptosis in S phase due to reduction of thymidylate synthase levels, however, all these experiments were performed in cells synchronized prior to S phase, defects later in the cell cycle, as in mitosis, would not have been observed. Alternatively, the non-transcriptional role uncovered by reversibility of the prometaphase arrest by FQI1 removal may suggest a regulatory role for LSF in proper mitotic progression through protein-protein interactions. It is possible that the dominant negative LSF would maintain all protein-protein interactions and not be defective in this regard.

The collective evidence supporting that FQIs specifically target LSF and LSF paralogs indicates that the anti-tumor activity observed in preclinical tumor models is likely not a result of an off target effect. FQI1 was previously identified to inhibit LSF DNA binding and shown not to inhibit transcriptional activity of other transcription factors including p53, a transcription factor predicted to be structurally similar to LSF. Further, FQIs did not impact transcriptional activation of the Grainyhead family members (Trevor Grant, Ulla Hansen, unpublished observations), transcription factors that have similar DNA binding domains but have diversified from the LSF subfamily of factors (Traylor-Knowles et al., 2010). Finally, compound structure-activity relationships (SAR)

demonstrated a linear relationship between the $G1_{50}$ and the IC_{50} generated using the LSF activity assay. This high degree of correlation indicates that FQI inhibition of LSF resulted in growth inhibition (Christadore, 2013). These data, among others, provide confidence that FQI1 and FQI2 specifically target LSF, in comparison to other transcription factors.

In summary the results in this chapter indicate that by a non-transcriptional mechanism, FQI1 inhibition induces a prophase/prometaphase arrest prior to cell death, and suggest that this may occur by interfering with an LSF protein-protein requirement for proper mitotic progression. Further work is needed to evaluate what key interactions LSF may have with proteins required for spindle formation, DNA condensation, or microtubule-kinetochore attachments, or to eliminate the alternative hypothesis, that the mitotic defect is a secondary event characteristic to the compound, rather than to LSF itself.

Figures

Illustration 3.1 FQI Incubation in Synchronized HCC Cells (Short incubation)

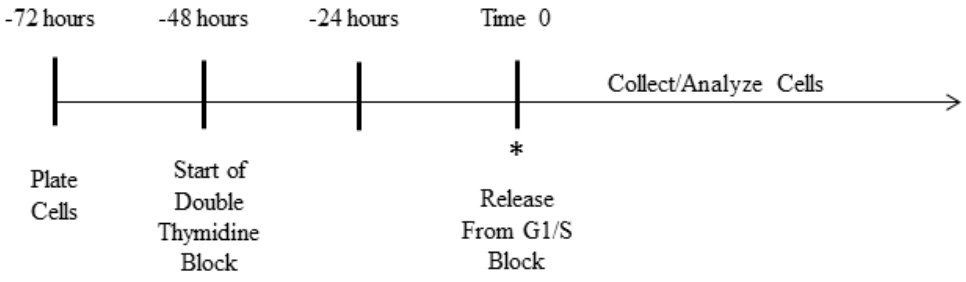

*** FQI1 or Vehicle Control Added and Maintained For Remainder of Experiment**

Figure 3.1 Treatment of QGY-7703 cells with FQI1 inhibits cell division, activates Caspase 3/7 and results in loss of cell viability in a concentration-dependent manner.

(a) QGY-7703 cells were synchronized at the G1/S border and released in presence of the indicated concentrations of FQI1. The averages of total cell counts at 0 and 10 hours after release from the G1/S block are shown. Standard deviations represent 3 independent experiments. Absence of error bars due to data being averaged from 2 independent experiments. (b) QGY-7703 cells were synchronized at the G1/S border and released in the presence of increasing amounts of FQI1, or in the presence of only vehicle or no treatment as controls. Cells were analyzed for Caspase 3/7 activity at the indicated times after release by directly measuring cleavage of a luminogenic caspase 3/7 substrate. Data are depicted as percent of the activity in the vehicle-treated cells. Dashed line represents control cells (100%). Standard deviations represent technical triplicates. Data are representative of two independent experiments. (c) Caspase 3/7 activation and cell viability were measured by a luminogenic caspase 3/7 substrate (as in b) and by cleavage by intracellular protease(s) of a fluorogenic permeant peptide (Promega Apotoxglo kit), respectively, at 48 hours post incubation with FQI1 or vehicle. Standard deviations represent technical triplicates. Loss of viability was observed at 1.8 μM and 3.6 μM FQI1, concomitantly with increased Caspase 3/7 activity. Statistical significance was determined using a Student T Test; * $P<0.05$, ** $P<0.01$, *** $P<0.001$, **** $P<0.0001$

a.

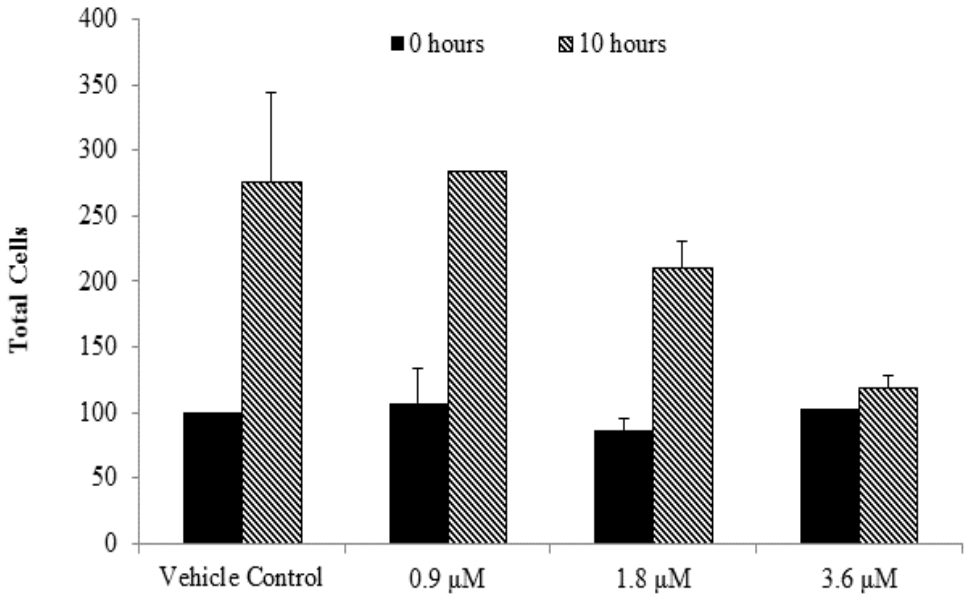
400
350
300
250
200
150
100
50
0
Total Cells
0 hours
10 hours
Vehicle Control
0.9 µM
1.8 µM
3.6 µM

b.

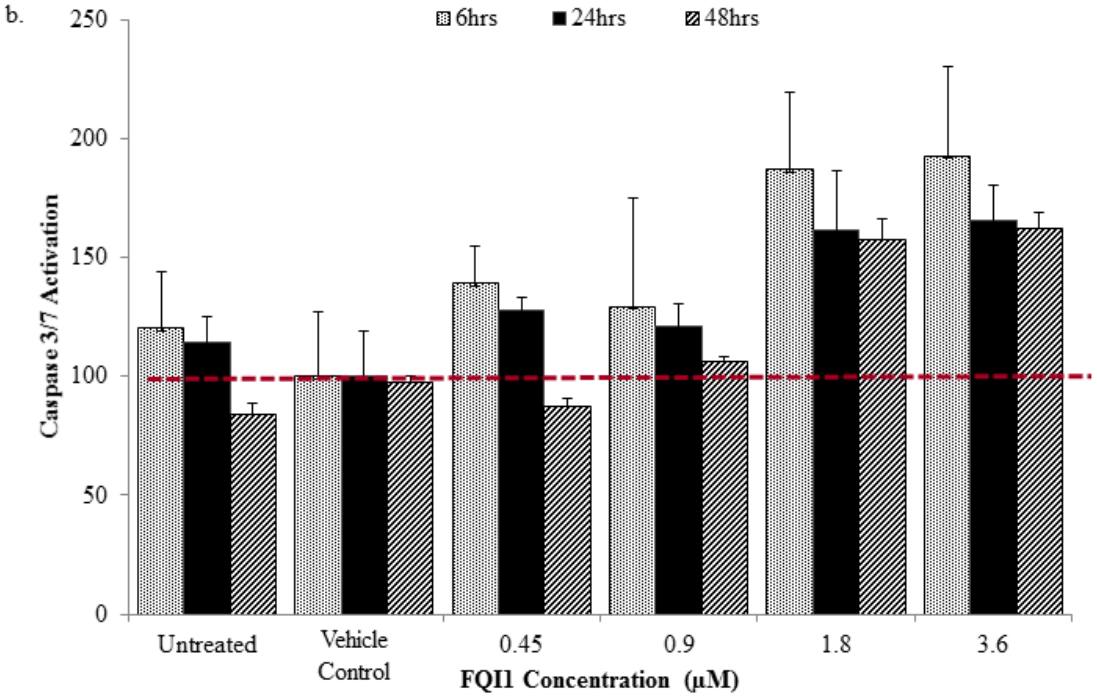
6hrs
24hrs
48hrs
Caspase 3/7 Activation
250
200
150
100
50
0
Untreated
Vehicle Control
0.45
0.9
1.8
3.6
FQI1 Concentration (µM)

c.

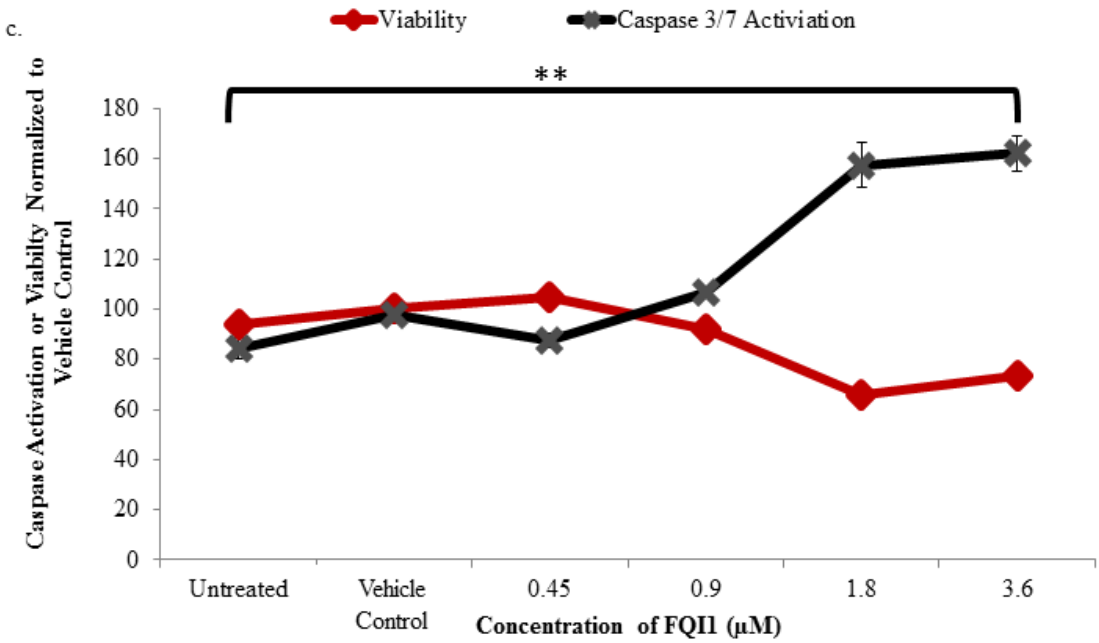
Viability
Caspase 3/7 Activiation
**
Caspase Activation or Viabilty Normalized to Vehicle Control
180
160
140
120
100
80
60
40
20
0
Untreated
Vehicle Control
0.45
0.9
1.8
3.6
Concentration of FQI1 (µM)

Figure 3.2 Treatment of synchronized QGY-7703 cells with FQI1 results in accumulations of cells with G2/M and/or subG1 DNA content.

HCC cells were synchronized at the G1/S border and released in the presence of increasing amounts of FQI1 or vehicle. Cells stained with propidium iodide were analyzed at 7, 10, and 17 hours following release to evaluate DNA content. 10,000 events were assayed per condition. The area measures the DNA content per event. (a) A parallel untreated asynchronous population of cells shows the expected distribution of cellular DNA across phases of the cell cycle. (b) Synchronized cells were collected immediately prior to the time of release, confirming appropriate synchronization at G1/S. (c) Cells released in presence of 2 or 5 μM FQI1 were analyzed at the indicated time points and directly compared with the cells treated with vehicle to evaluate cell cycle progression.

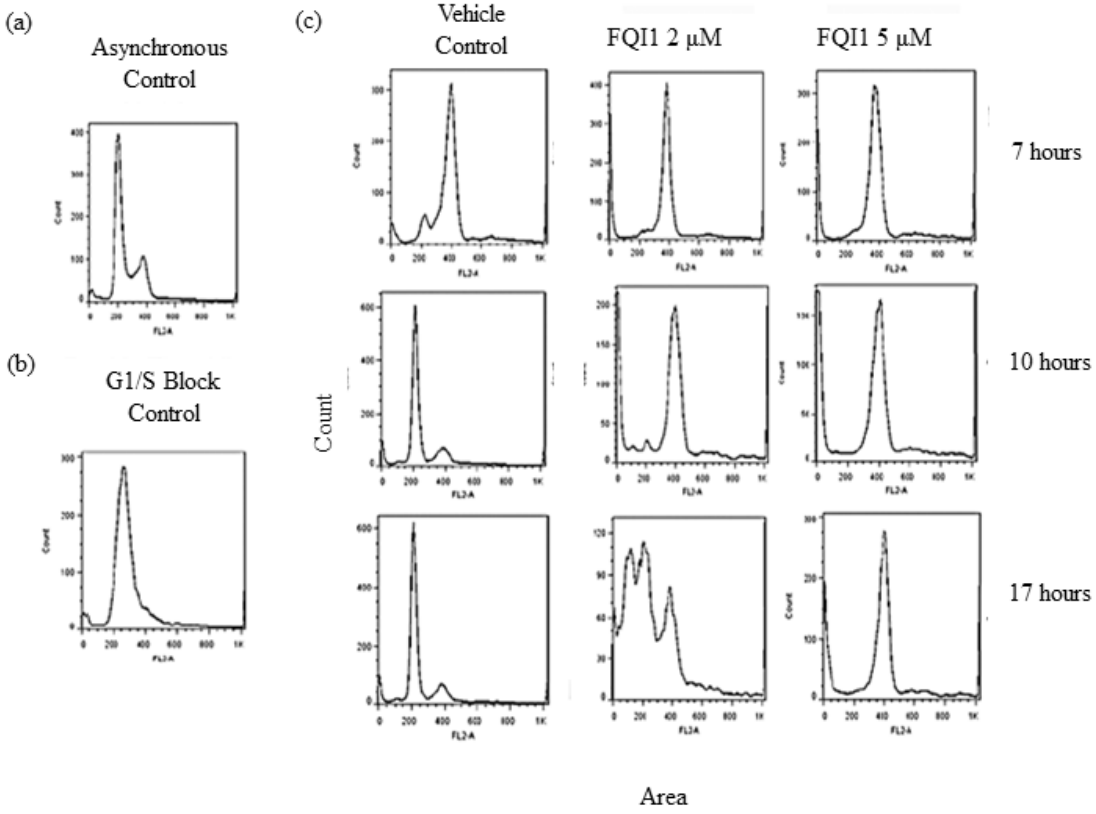
(a)
Asynchronous Control
(b)
G1/S Block Control
(c)
Vehicle Control
FQI1 2 µM
FQI1 5 µM
7 hours
10 hours
17 hours
Count
Area

Figure 3.3 Cyclin B protein expression is increased and maintained in QGY-7703 cells treated with FQI1.

Synchronized HCC cells were collected at the indicated time points after release from a G1/S block in the presence or absence of FQI1. (a) RNA was isolated for gene analysis by Taqman. *CCNA1* RNA levels were normalized to levels of *GAPDH* RNA in QGY-7703 cells released in the absence or presence of FQI1 for 7 hours. (b) Immunoblot for cyclin A1 and β-actin (as a loading control) of lysates collected at 8 hours post release from a G1/S block in presence of 0.9, 1.8 or 5 μM of FQI1 or vehicle as a control. (c) Quantitation of cyclin A1 protein expression was determined using the Odyssey Licor detection system. Data are depicted as the area of pixels determined for Cyclin A1 normalized to that for β-actin. (d) Immunoblots of cyclin B1 and β-actin from cell lysates collected at 0, 7, 10 and 17 hours after release from a G1/S block in presence of 2 or 5 μM FQI1 or vehicle. The data are representative of 3 independent experiments. (e) *CCNB1* RNA levels normalized to those of *GAPDH* in QGY-7703 cells 8 hours post G1/S release with increasing FQI1 concentrations. Data are from a single experiment. The results are representative of two independent experiments.

a.

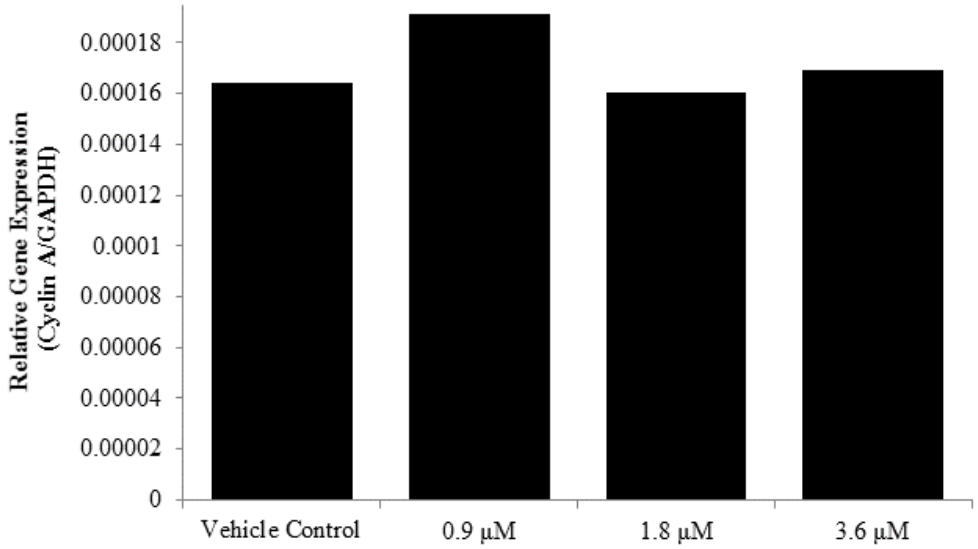
Relative Gene Expression (Cyclin A/GAPDH)
0.00018
0.00016
0.00014
0.00012
0.0001
0.00008
0.00006
0.00004
0.00002
0
Vehicle Control
0.9 µM
1.8 µM
3.6 µM

b

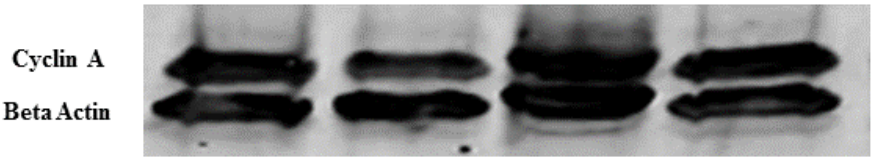
Cyclin A
Beta Actin

c.

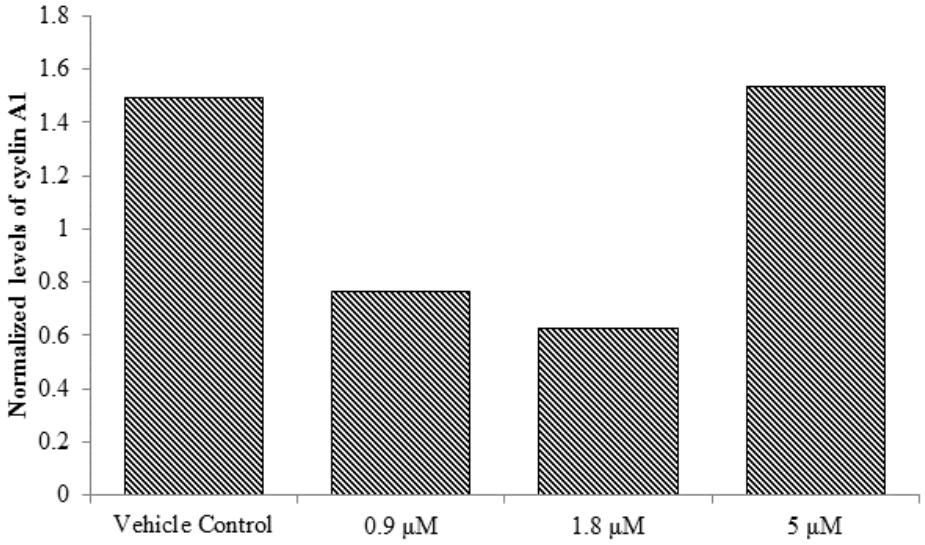
Normalized levels of cyclin A1
1.8
1.6
1.4
1.2
1
0.8
0.6
0.4
0.2
0
Vehicle Control
0.9 µM
1.8 µM
5 µM

d.

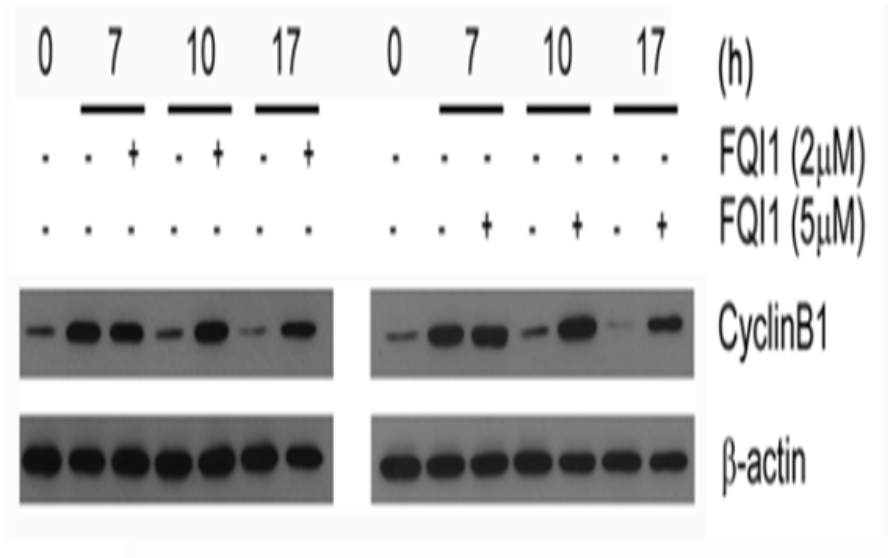
0 7 10 17 0 7 10 17 (h)
FQI1 (2μM)
FQI1 (5μM)
CyclinB1
β-actin

e.

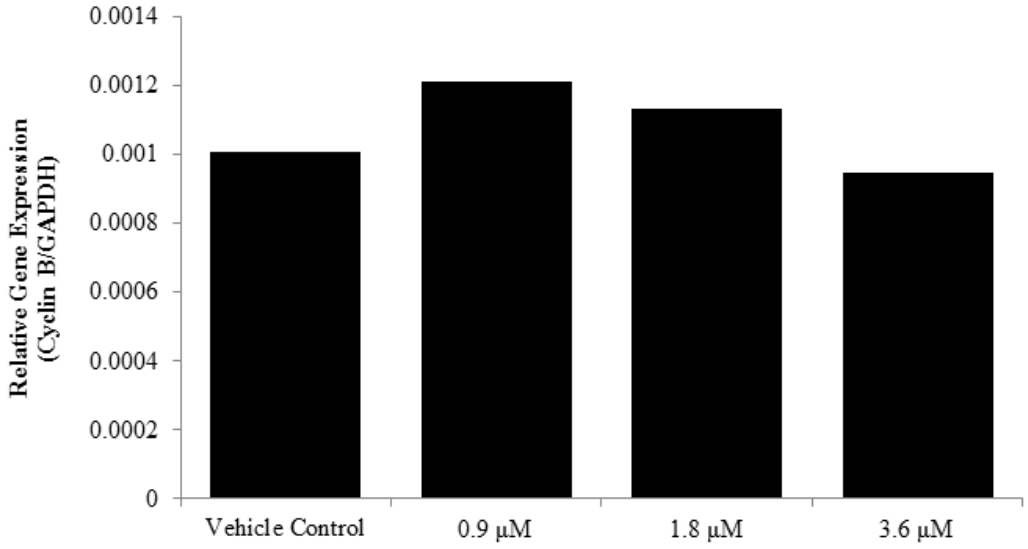
Relative Gene Expression (Cyclin B/GAPDH)
0.0014
0.0012
0.001
0.0008
0.0006
0.0004
0.0002
0
Vehicle Control
0.9 μM
1.8 μM
3.6 μM

Figure 3.4 Treatment of QGY-7703 cells with FQI1 results in prometaphase arrest and subsequent multi-nucleation.

HCC cells were synchronized at the G1/S border and released in presence of 5 μM FQI1 or vehicle. (a) Fixed HCC cells stained with DAPI and an antibody against alpha tubulin were analyzed on a Zeiss axioimager at 63x magnification. DAPI staining reveals a prometaphase arrest in the FQI1-treated QGY-7703 cells 8 hours post release from a G1/S block, as shown by the arrows. (b) Hematoxylin and Eosin staining of asynchronous QGY-7703 cells treated with 5 μM of FQI1 or vehicle for 48 hours at 63x magnification. (c) DAPI staining for synchronized cells treated with DMSO or 5 μM FQI1 and analyzed at 20x magnification. Samples were collected at 0, 3.5, 6, 8, 16.5, 19 and 23 hours post release from a G1/S block in presence of DMSO or FQI1. Insets represent individual cells in more detail. Arrows represent cells in metaphase or prometaphase, respectively, at the 6 hour time point, and multi-nucleated cells at the 19-hour time point.

a.

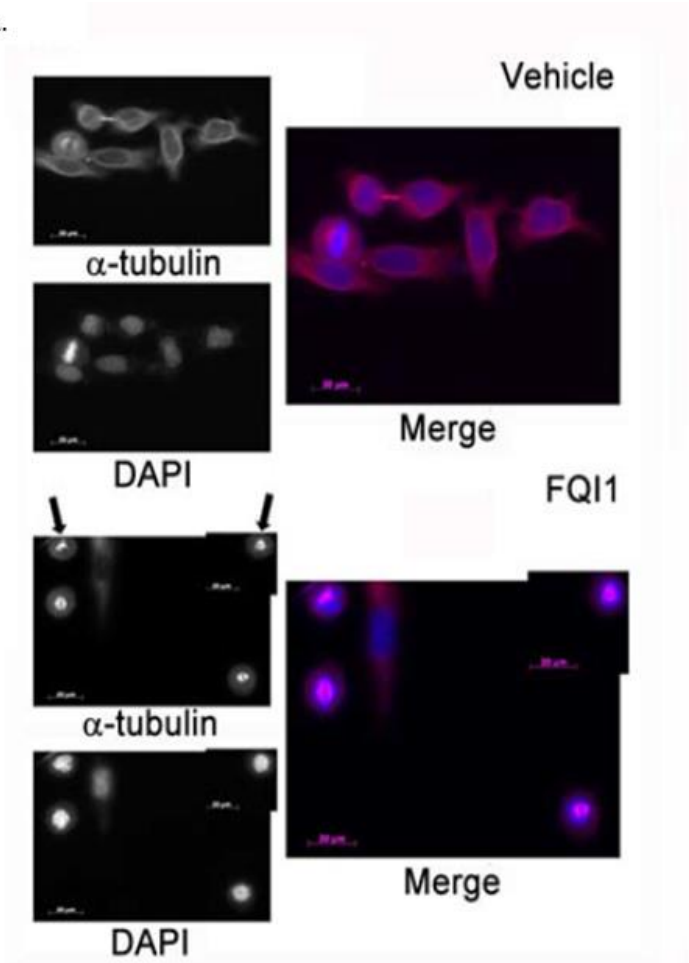
Vehicle
α-tubulin
Merge
DAPI
FQI1
α-tubulin
Merge
DAPI

b.

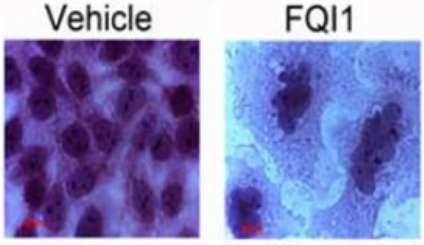
Vehicle
FQI1

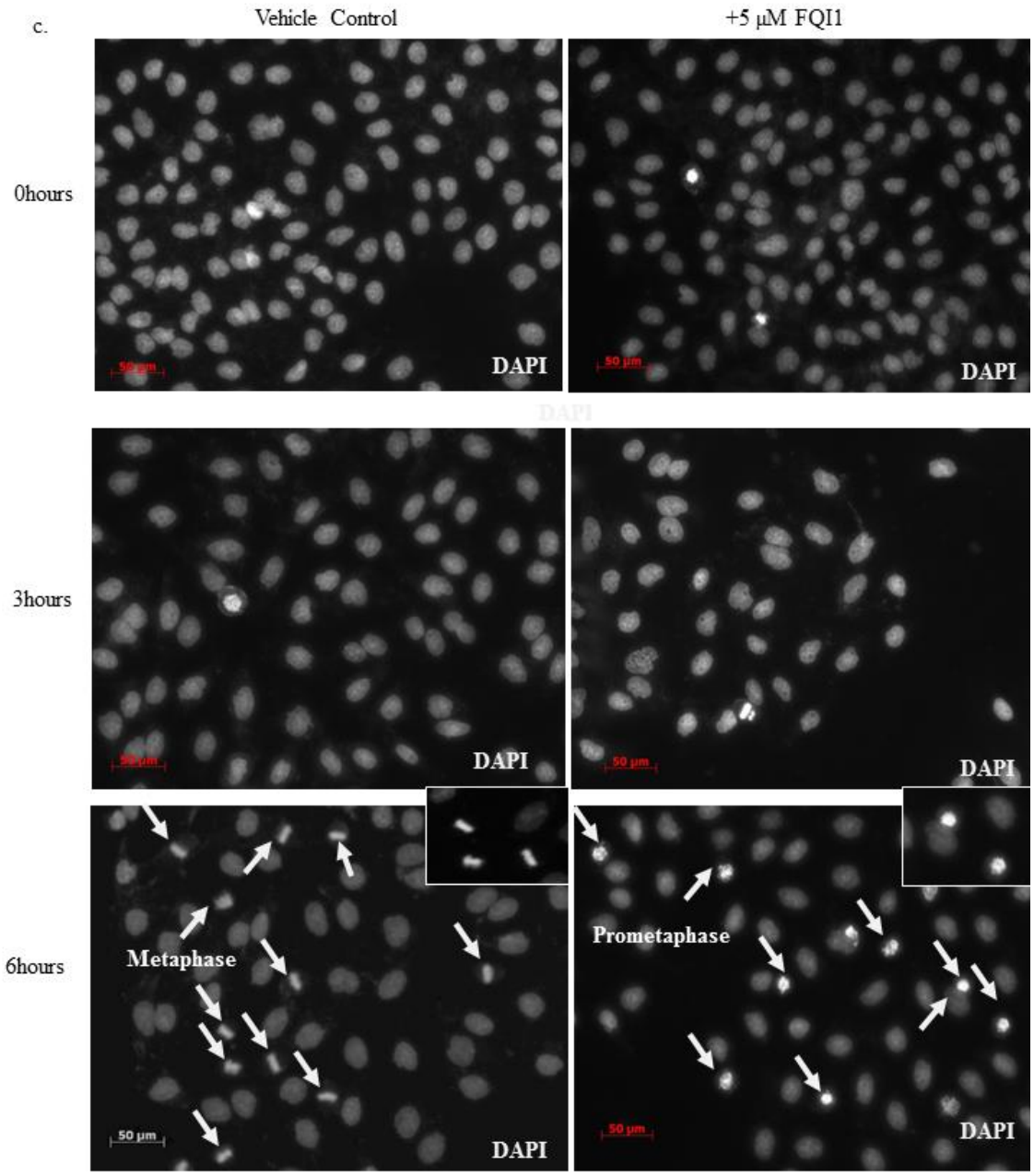
c.
Vehicle Control
+5 µM FQI1
0hours
3hours
6hours
DAPI
Metaphase
Prometaphase
50 µm

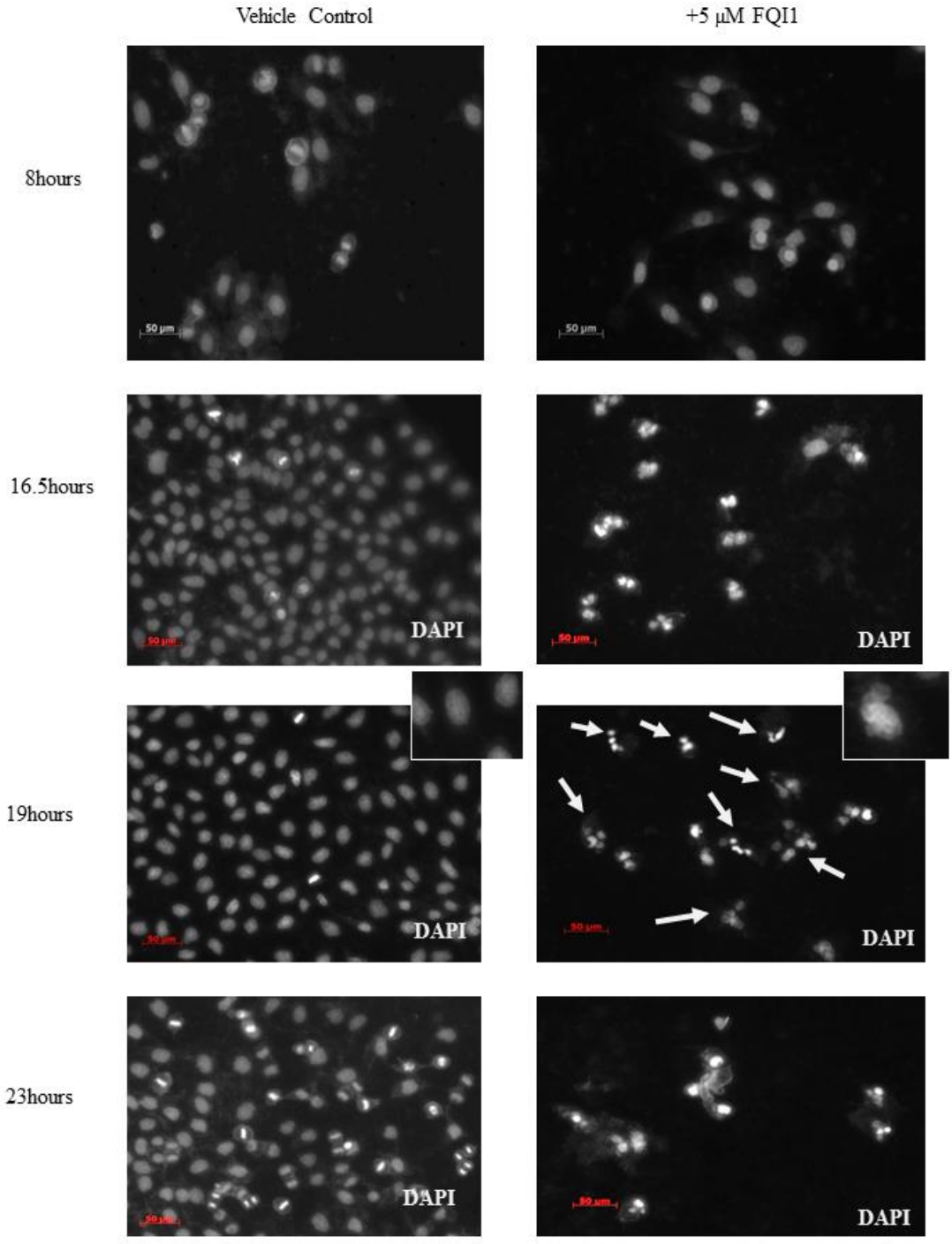
Vehicle Control
+5 μM FQI1
8hours
16.5hours
19hours
23hours
DAPI
DAPI
DAPI
DAPI
DAPI
DAPI
DAPI
DAPI

Figure 3.5 Treatment of synchronized HCC cells results in a concentration-dependent increase of cells in prometaphase as well as mitotic anomalies such as multi-asters and prophase cells with protrusions.

HCC cells were synchronized at the G1/S border and released in presence of vehicle or increasing concentrations of FQI1 or FQI2. HCC cells, fixed and stained for α-tubulin and DNA. (a, b) Representative images of cells analyzed using a Zeiss Axioimager 7.5 hours post release from the G1/S block, showing examples of (5μM) FQI1-mediated phenotypes including multi-aster (a, bottom right) and cells in prometaphase/metaphase (a, bottom left). Examples of prophase cells with and without protrusions (b, bottom right). All images were taken at 100x magnification. (c) Representative image of a multi-nucleated cell observed post treatment with 5 μM FQI1 in synchronous cells 24 hours post release. (d) Quantification from 75-100 total cells 7.5 hours post release from a G1/S block that were in interphase, prometaphase, metaphase and cytokinesis, as determined by DNA and alpha tubulin characteristics. There are no phenotypes shown for the highest concentration of FQI2 (3.7 μM), because at this time point, all cells remained in prophase. (e) Quantification from the same population of 75-100 total cells as in (d), analyzed by DNA and alpha tubulin morphologies indicating cells containing prophase cells, with and without protrusions, and multi-asters analyzed 8 hours post release from a G1/S block. (f) Quantification from 75-100 total cells analyzed by DNA and alpha tubulin morphologies indicating cells containing interphase, prophase, prometaphase, metaphase, and cytokinesis, fixed for imaging at 9 hours post release from a G1/S block. (g) Quantification from 75-100 total cells analyzed by DNA and alpha tubulin

morphologies indicating cells containing multi-asters, at 9 hours post release from a G1/S block. Data are representative of 2 quantitation experiments.

a.

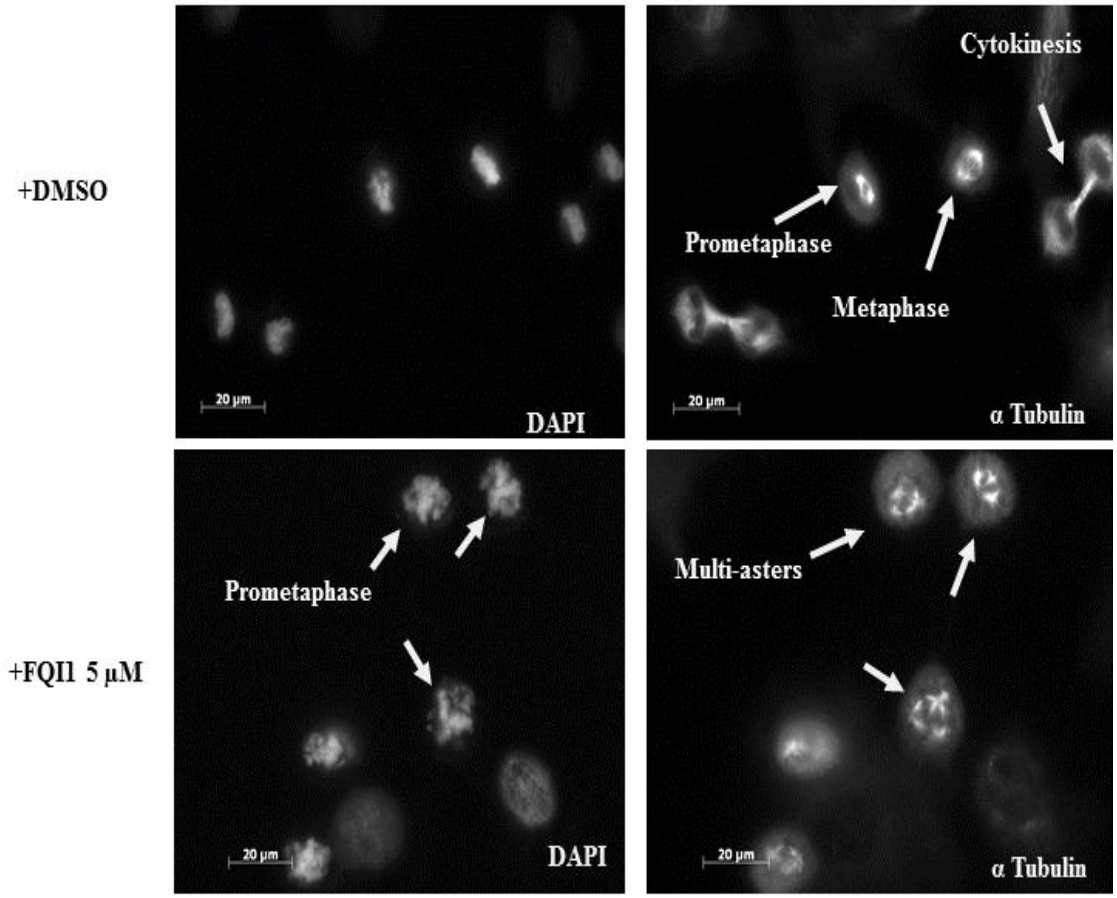
+DMSO
+FQI1 5 µM
20 µm
DAPI
Cytokinesis
Prometaphase
Metaphase
α Tubulin
Prometaphase
Multi-asters

b.

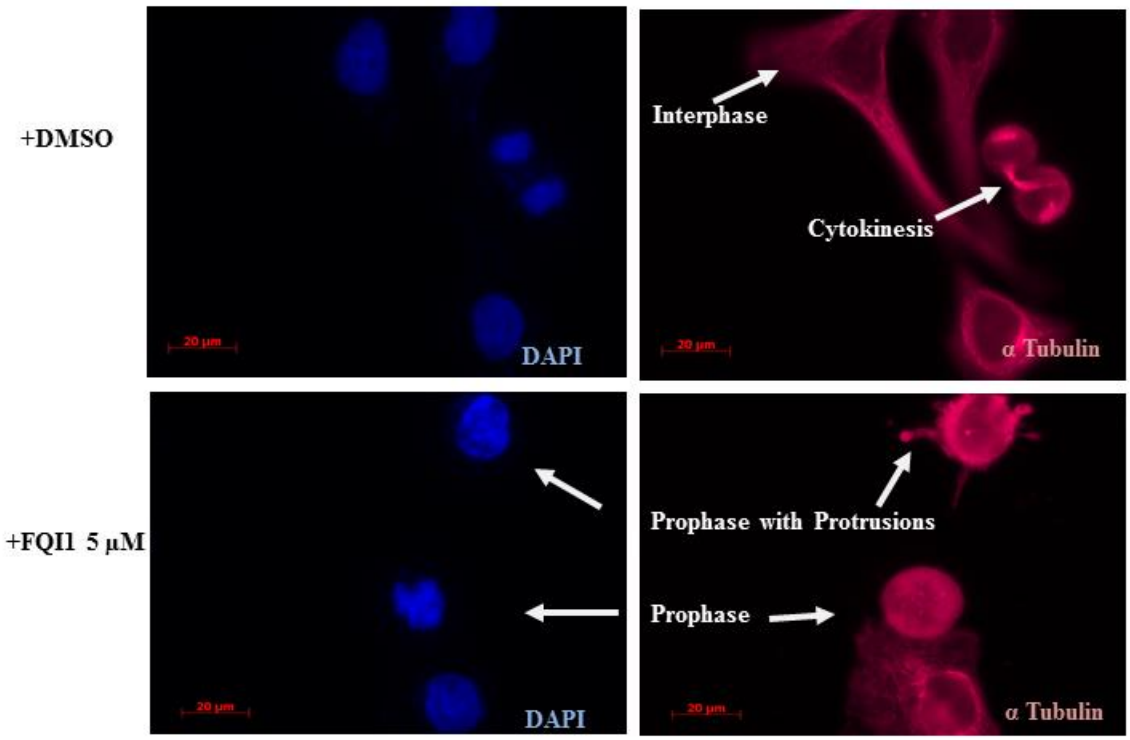
+DMSO
Interphase
Cytokinesis
20 µm
DAPI
20 µm
α Tubulin
+FQI1 5 µM
Prophase with Protrusions
Prophase
20 µm
DAPI
20 µm
α Tubulin

c.

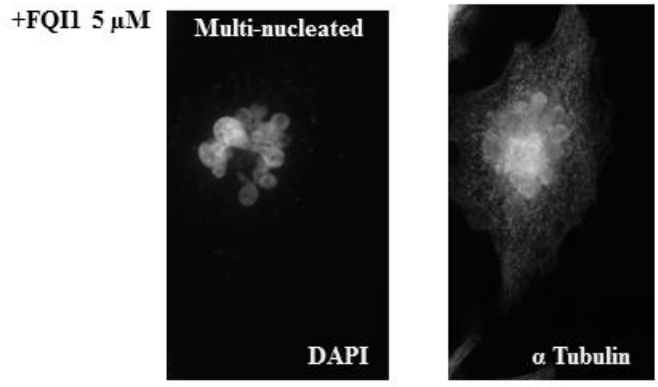
+FQI1 5 µM
Multi-nucleated
DAPI
α Tubulin

d.

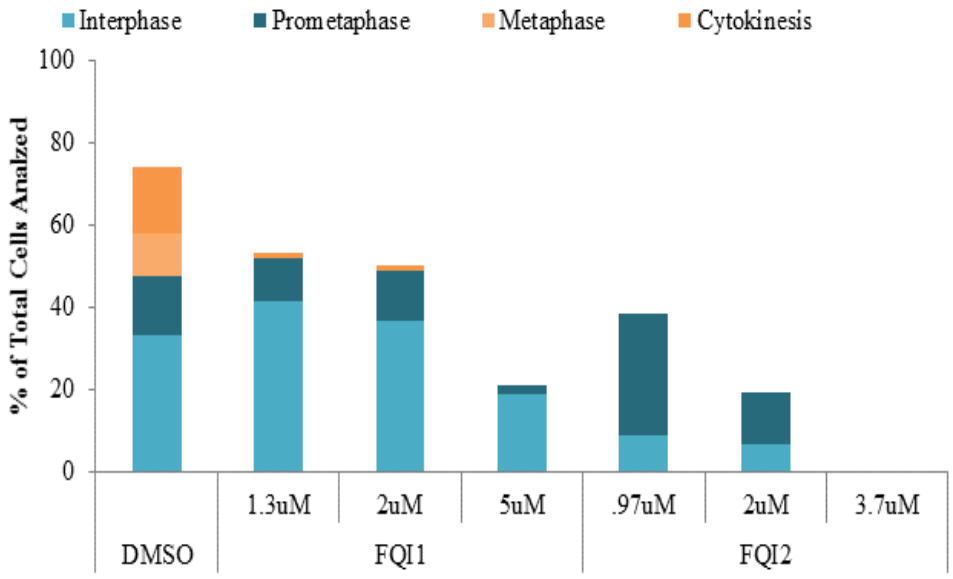
Interphase
Prometaphase
Metaphase
Cytokinesis
% of Total Cells Analzed
100
80
60
40
20
0
1.3uM
2uM
5uM
.97uM
2uM
3.7uM
DMSO
FQI1
FQI2

e.

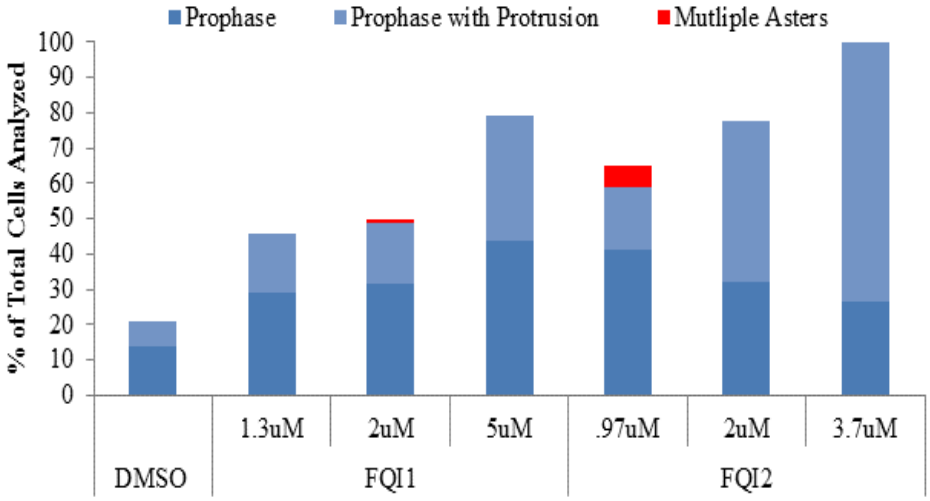
Prophase
Prophase with Protrusion
Mutliple Asters
% of Total Cells Analyzed
100
90
80
70
60
50
40
30
20
10
0
1.3uM
2uM
5uM
.97uM
2uM
3.7uM
DMSO
FQI1
FQI2

f.

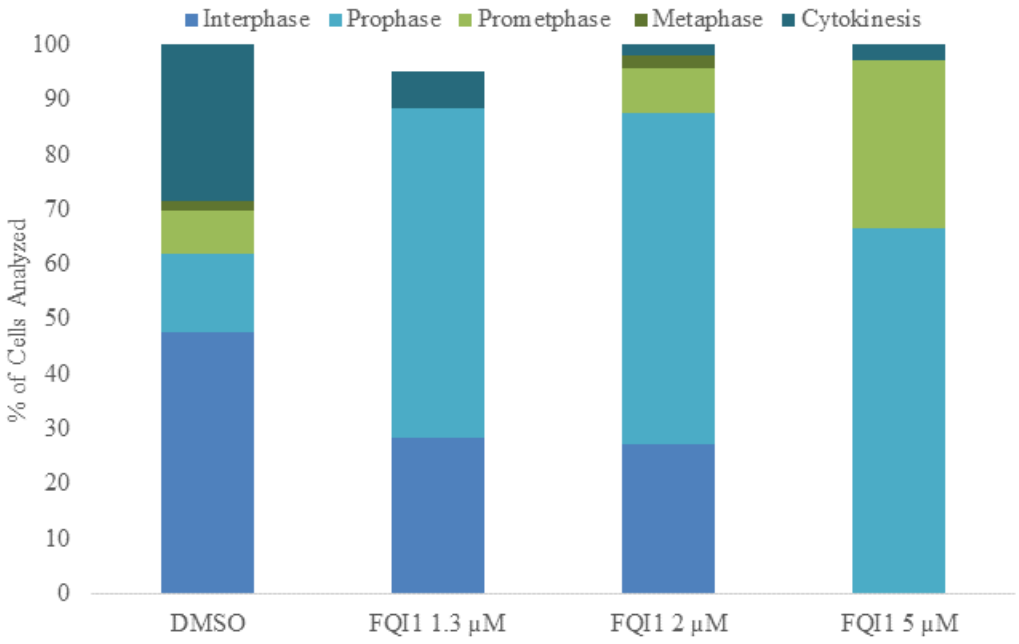
Interphase
Prophase
Prometphase
Metaphase
Cytokinesis
% of Cells Analyzed
100
90
80
70
60
50
40
30
20
10
0
DMSO
FQI1 1.3 µM
FQI1 2 µM
FQI1 5 µM

g.

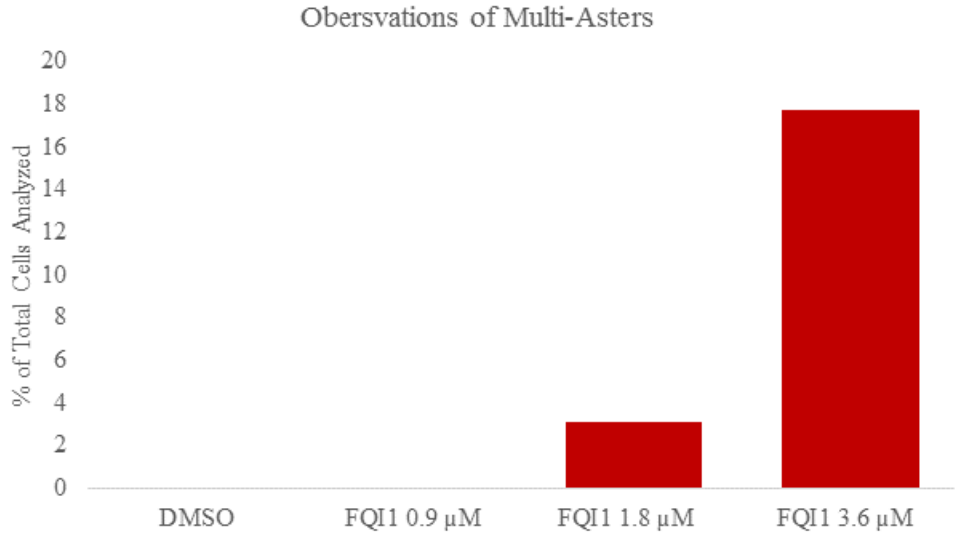
Obersvations of Multi-Asters
% of Total Cells Analyzed
20
18
16
14
12
10
8
6
4
2
0
DMSO
FQI1 0.9 µM
FQI1 1.8 µM
FQI1 3.6 µM

Figure 3.6. FQI1 addition to synchronized HCC cells at the G1/S transition does not alter subsequent expression of Aurora B Kinase or Cdc20 prior to mitosis.

Synchronized HCC cells were released from a G1/S block in the presence or absence of FQI1 at the indicated concentrations. Cell lysates were prepared 9 hours post release from the G1/S block. (a) Aurora kinase B RNA levels were determined using bDNA (Affymetrix) and normalized to those of beta actin within each lysate. Error bars represent standard deviation of two independent experiments. (b) Immunoblots of Aurora kinase B and β-actin. Data are representative of greater than 4 experiments. (c) Immunoblot measuring phosphorylation of Histone 3 Serine 10 on lysates collected 9 hours post release. (d) Protein expression was quantitated using the Odyssey Licor detection system. Data are depicted as the area of pixels determined for Aurora Kinase B normalized to the area of pixels detected for β-actin. (e) Gene expression determined using bDNA (Affymetrix) of *CDC20* RNA levels were normalized to *ACTB R*NA within each lysate. Error bars represent standard deviation of technical triplicates. Data are representative of two independent experiments. (f) Immunoblots of CDC20 and β-actin in lysates collected 9 hours post release from a G1/S block. Each lysate was probed for beta actin as a loading control. Data are representative of 3 experiments. (g) Data are depicted as the area of pixels determined for Cdc20 normalized to the area of pixels detected for the beta actin loading control.

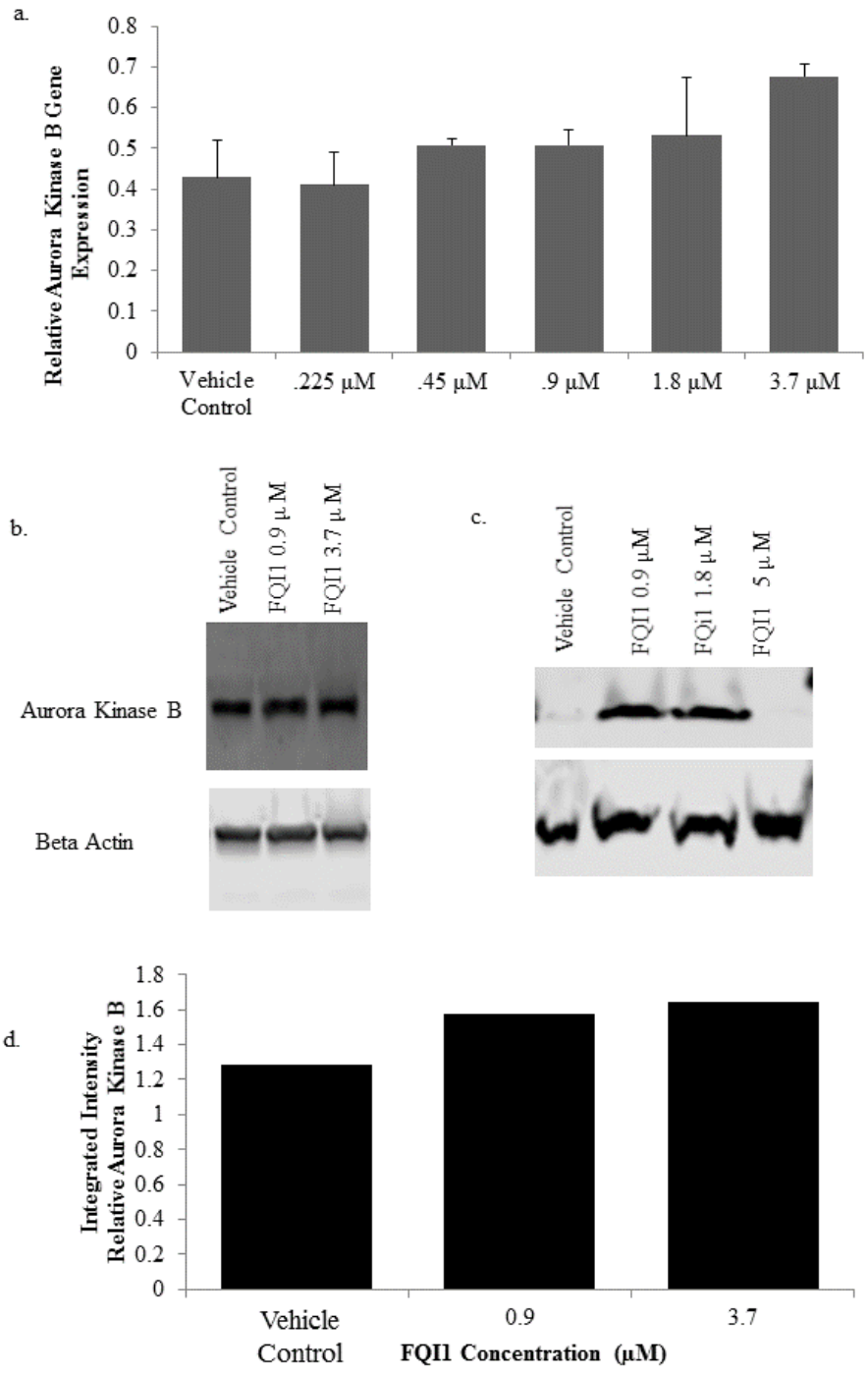
a.
Relative Aurora Kinase B Gene Expression
0.8
0.7
0.6
0.5
0.4
0.3
0.2
0.1
0
Vehicle Control
.225 µM
.45 µM
.9 µM
1.8 µM
3.7 µM
b.
Vehicle Control
FQI1 0.9 µM
FQI1 3.7 µM
Aurora Kinase B
Beta Actin
c.
Vehicle Control
FQI1 0.9 µM
FQi1 1.8 µM
FQI1 5 µM
d.
Integrated Intensity Relative Aurora Kinase B
1.8
1.6
1.4
1.2
1
0.8
0.6
0.4
0.2
0
Vehicle Control
0.9
3.7
FQI1 Concentration (µM)

e.

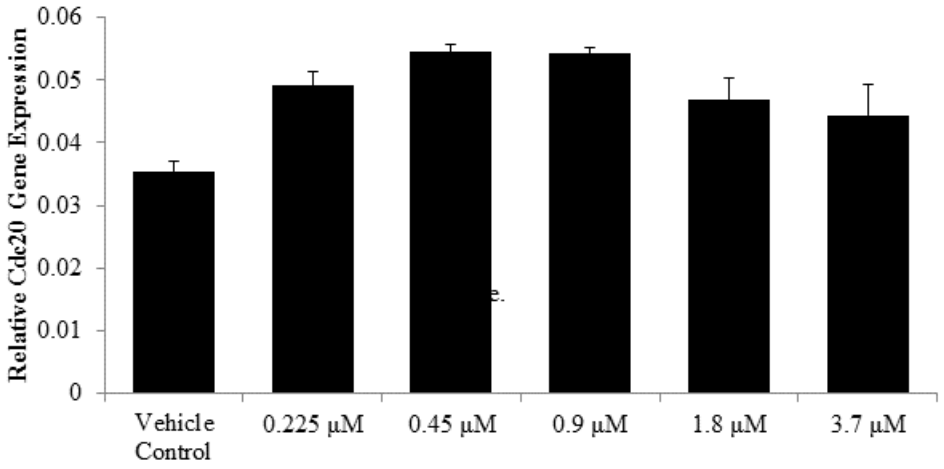
Relative Cdc20 Gene Expression
0.06
0.05
0.04
0.03
0.02
0.01
0
Vehicle Control
0.225 µM
0.45 µM
0.9 µM
1.8 µM
3.7 µM

f.

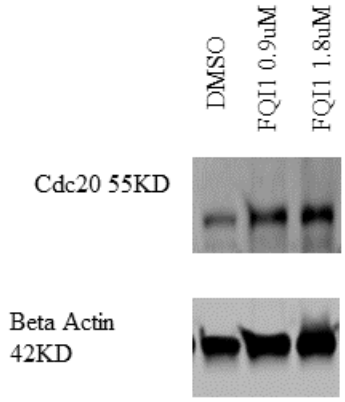
DMSO
FQI1 0.9uM
FQI1 1.8uM
Cdc20 55KD
Beta Actin
42KD

g.

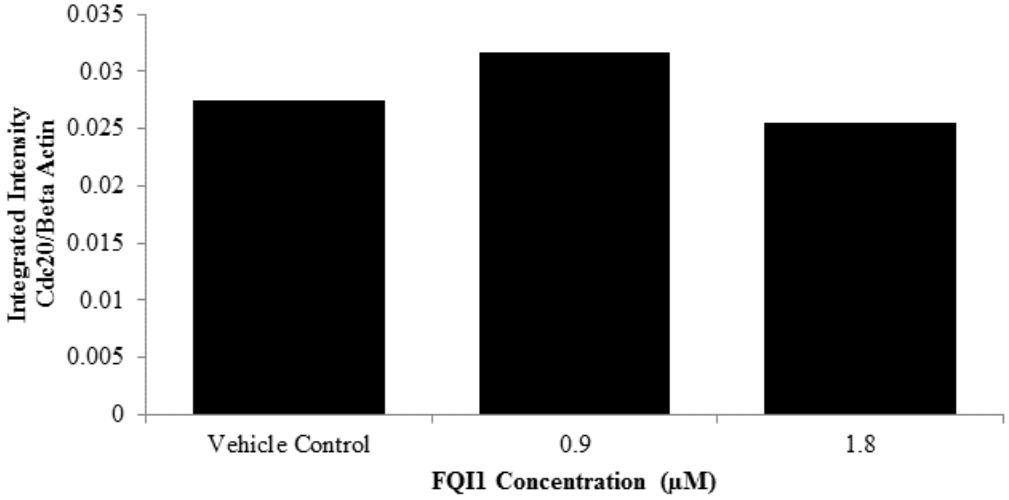
Integrated Intensity Cdc20/Beta Actin
0.035
0.03
0.025
0.02
0.015
0.01
0.005
0
Vehicle Control
0.9
1.8
FQI1 Concentration (µM)

Figure 3.7 The prophase/prometaphase arrest mediated by short-term FQI1 treatment of synchronized HCC cells is reversible.

Synchronized QGY-7703 cells were released in the presence of 5 μM of FQI from a G1/S block. Ten hours after the release, the cells were washed and then either incubated with media alone or re-incubated with media in the presence of 5 μM FQI1. Samples were collected 24 hours post release. Fixed cells were stained with propidium iodide to analyze DNA content. (a) Synchronized cells harvested immediately prior to release from the G1/S block. Cellular DNA profiles 10 hours post release for (b) vehicle control and (c) cells released with 5 μM FQI1. Cellular DNA profiles 24 hours post release for (d) cells treated throughout only with vehicle (e) cells treated throughout with 5 μM FQI1 and (f) cells treated initially with 5μM FQI1 for 10 hours, but then incubated in the absence of FQI1. Phase contrast images of QGY-7703 cells treated with (g) vehicle control, (h) 5 μM FQI1 treated cells and (i) cells treated with 5 μM FQI1 at release, washed, and incubated with complete media 10 hours post release. This is representative of two independent experiments.

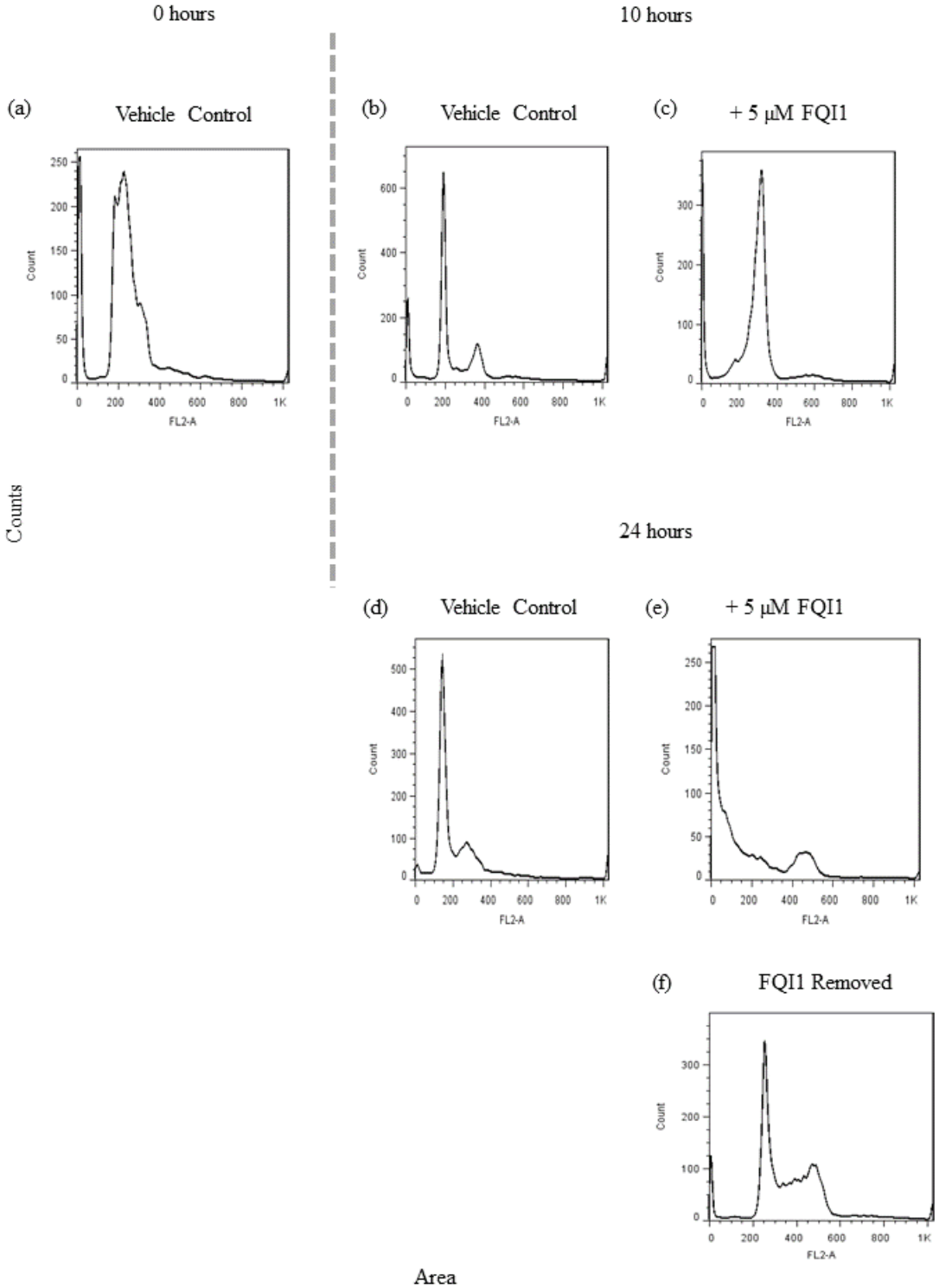
0 hours
10 hours
(a)
Vehicle Control
(b)
Vehicle Control
(c)
+ 5 μM FQI1
Counts
24 hours
(d)
Vehicle Control
(e)
+ 5 μM FQI1
(f)
FQI1 Removed
Count
FL2-A
Area

(g)

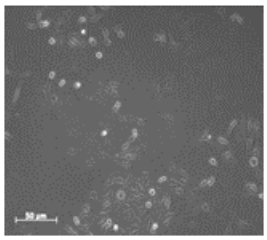

(h)

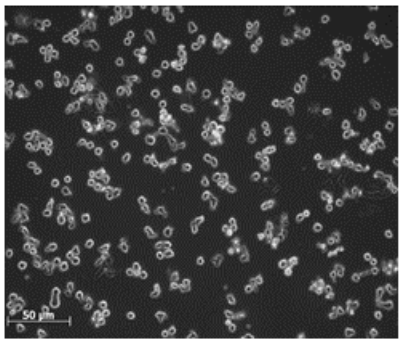

FQI1 Treatment Continued

(i)

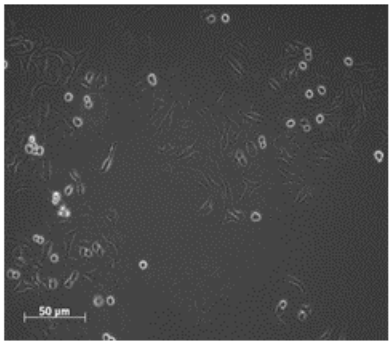

FQI1 Treatment Removed

CHAPTER FOUR

The transcription factor LSF regulates mitotic progression in hepatocellular carcinoma cells

Contributions

Kelly George generated mEmerald Tubulin QGY-7703 cells, the time lapse imaging data, and analysis for mitotic time determinations
Mark Roberto generated the YFP H2B QGY-7703 cell line

Introduction

Primary liver cancer is the fifth most common cancer worldwide and the third leading cause of cancer mortality (Bruix, 2011; Bruix and Sherman, 2011; Llovet et al., 2015; Marengo et al., 2016; Torrecilla and Llovet, 2015; Wang et al., 2002). Hepatocellular carcinoma (HCC) represents approximately 70-80% of primary liver cancer cases (Bruix, 2011; Bruix and Sherman, 2011; Llovet et al., 2015; Marengo et al., 2016; Torrecilla and Llovet, 2015). The leading risk factors, worldwide, include Hepatitis, both B and C, and alcoholism. More recently metabolic syndrome and obesity have resulted in Non-Alcoholic Steatohepatitis (NASH) development, another precursor to HCC. Today, one million individuals in the US alone are afflicted with NASH (Marengo et al., 2016), a condition for which there are no approved treatments, and therefore put large numbers of individuals at risk for developing hepatocellular carcinoma (Zoller and Tilg, 2016). Regardless of the disease etiology, each HCC case follows a lengthy disease progression with the majority of patients developing fibrosis, with a percentage of those patient's livers progressing to cirrhosis and eventually to frank

carcinoma. The factors that cause some patients to progress rapidly while others slowly or never are unknown and are currently under intense investigation. However, a major risk factor for HCC is cirrhotic liver (Bruix and Llovet, 2003; Llovet, 2006). Patients with HCC are often diagnosed in the late stages, with few meeting the requirements for invasive procedures, such as surgical resections, with the majority qualifying for mere palliative treatments (Bruix and Sherman, 2011). Further, hepatocellular carcinoma patients, in general, have not responded to standard chemotherapeutics. Sorafenib, a small kinase inhibitor shown to target vascular endothelial growth factor receptors, platelet derived growth factor receptors and Raf kinases (originally approved for renal cell carcinoma) has demonstrated modest improvement in survival rates in HCC patients suggesting that molecularly targeted therapies may be helpful in mitigating the disease (Torrecilla and Llovet, 2015). The improvement in overall survival rates with this treatment, however, is subpar and patients suffer with significant side effects leaving the hepatocellular carcinoma patient population with a large unmet medical need.

LSF was identified as an oncogene in hepatocellular carcinoma by virtue of being necessary and sufficient, in the background of a non-tumorigenic, but tumor-primed hepatocyte cell line, for HCC tumor growth in mouse xenograft models. Dominant negative LSF expression reduced tumor growth, and conversely, LSF overexpression in a non-tumorigenic HCC cell line resulted in increased tumorigenicity (Yoo et al., 2010). Small molecule inhibitors of LSF, Factor Quinolinone Inhibitors (FQIs), were identified from a compound screen in a fluorescent polarization assay where FQIs inhibited the DNA binding of purified LSF. Additionally, FQIs have no effect on the DNA binding

activity of transcription factors from multiple structural classes, including Oct1, E2F3, and Sp1 (Grant et al., 2012). Specific inhibition of LSF with these FQIs resulted in growth inhibition of HCC cells *in vitro* and *in vivo* as initially ascertained in a subcutaneous mouse xenograft HCC tumor model (Grant et al., 2012). More recently, FQIs were shown to inhibit growth and apparently cause regression in a mouse endogenous liver tumor model (Rajasekaran et al., 2015). In all cases, inhibition of HCC tumor growth was accompanied with no signs of toxicity, as assessed by liver injury markers or histopathology of tissues with rapid cell turnover, suggesting a case of oncogene addiction of HCC to LSF.

Oncogenic transcription factors are promising therapeutic targets given that they regulate tumorigenic pathways. Transcription factors, in general, have been notoriously difficult to target with small inhibitors as their DNA binding pockets are commonly small and the proteins themselves are intrinsically unstructured, a feature allowing binding site promiscuity (Dunker and Uversky, 2010; Yan and Higgins, 2013). The DNA binding pocket of LSF, however, is uncharacteristically large (Kokoszynska et al., 2008; Shirra et al., 1994). Identification of the transcription factor LSF as an oncogene in HCC and the significant inhibition of tumor growth upon LSF inhibition with no observed toxicity indicate that LSF holds great promise as an HCC therapeutic target (Grant et al., 2012; Santhekadur et al., 2012b; Yoo et al., 2010). The molecular role by which LSF is necessary for HCC survival, however, has yet to be identified. Targeting a transcription factor has been challenging, therefore clarifying the mechanism by which inhibition of

LSF leads to hepatocellular carcinoma cell death would further support the candidacy of FQIs as a molecular therapy.

Initial studies (Rajasekaran et al., 2015) revealed that short term FQI1 treatment in HCC cells caused cells to accumulate at prometaphase, suggesting that inhibition of LSF activity resulted in a mitotic defect. Furthermore, reversibility of the phenotype through FQI1 removal at the time of mitotic arrest revealed a non-transcriptional role for LSF in mitosis (Chapter 3). Previous investigations that indicated a transcriptional role for LSF in cell cycle progression during the G1/S transition were performed by overexpressing a dominant negative LSF mutant (Powell et al., 2000)(). These studies, with a very distinct type of inhibitor, did not investigate mitotic progression. Since FQI1 was initially identified based on its ability to inhibit LSF DNA-binding and transcriptional activation potential, its ability also to apparently inhibit non-transcriptional functions of LSF suggests that FQI1 treatment results in a null phenotype for LSF.

To both fully evaluate the hypothesis that LSF regulates mitosis and investigate whether or not the mitotic arrest was due to perturbation of an off target of FQI1, we interrogated LSF activity in HCC cells using RNAi technology to recapitulate the LSF null phenotype. Titrating LSF activity with either FQI1 or siRNA in HCC cells resulted in similar mitotic phenotypes, indicating that LSF is the major target of FQI1. Surprisingly, we did not fully recapitulate the persistent prometaphase arrest observed upon short-term FQI1 treatment (Chapter 3. (Rajasekaran et al., 2015)), but instead observed a similar phenotype of prometaphase/metaphase delays leading to lengthening

of times to progress through mitosis. In addition to the delay, mitotic phenotypes included defective cell division and multi-nucleation. At the mechanistic level, in contrast to the short-term FQI1 treatment, long-term inactivation of LSF by both approaches did reveal specific RNA and protein reduction of key mitotic regulators. In particular, both Aurora Kinase B, a major mitotic kinase, and Cdc20, a major component of the proteolysis complex, were downregulated upon LSF inhibition. Thus, this study also shows that LSF controls gene expression of mitotic proteins.

Results

Identification of potent and durable siRNAs targeting LSF and LBP1A expression.

To optimize transfection conditions for the HCC cells, a control siRNA targeting the luciferase transcript was synthesized with a Cy3 fluorescent tag. This allowed visual confirmation of a successful transfection. The luciferase targeting siRNA is an excellent control siRNA, as it is a non-targeting siRNA in the QGY-7703 cells in that they do not express the luciferase gene. Thus, complications from knockdown of additional targets of non-interest are eliminated. The fluorescent distribution following transfection with this tagged siRNA (Figure 4.1a) reveals efficient uptake, with approximately 90% of the cells depicted in the phase contrast image (Figure 4.1b), overlapping the fluorescent signal. The degree of background fluorescence was measured at the same exposure using LSF siRNA-transfected cells (Figure 4.1, c and d), where no fluorescent tag was included.

To identify potent molecules targeting LSF or LBP1A, multiple siRNAs targeting each were synthesized. In order to recapitulate the findings generated by the FQIs in HCC, it was imperative to also investigate the other widely-expressed LSF family member, LBP1A, since FQI1 also inhibits the activity of LBP1A (T. Grant and U. Hansen, unpublished results). Therefore, to interrogate the mechanism of FQI1 anti-tumor activity, the role of LBP1A, if any, in HCC cell proliferation must also be investigated. The siRNAs (designed using algorithms generated to reduce off target hybridization by either the sense or antisense strand) were chemically modified and included a 21/23 design (21 nucleotides on the guide strand and 23 complementary nucleotides with an overhang on the 3' end of targeting strand, a siRNA scheme previously shown to result in potent and durable knockdown (Zimmermann et al., 2006). Specifically, 24 siRNAs designed to target LSF were synthesized and screened in a two dose screening paradigm to identify potent molecules. siRNAs were transfected into both Hep3B (Figure 4.1e) and QGY-7703 (Figure 4.1f) cells at concentrations of either 2 or 10 nM. Hep3b and QGY-7703 are both HCC cell lines that overexpress LSF (Grant et al., 2012; Yoo et al., 2010), with QGY-7703 cells those utilized to create the subcutaneous xenograft model that was responsive to FQI1 treatment. Normalized *LSF* transcript levels from these transfections are depicted as the percentage of LSF RNA levels in HCC cells treated with LSF siRNA compared to the levels in cells treated with the non-targeting luciferase control siRNA. Multiple siRNAs were determined to be potent, as defined by inducing a minimum of 80 percent target knockdown at 10 nM and greater than 50 percent knockdown at 2 nM. In particular, siRNA 9 and 22, henceforth referred

to as LSF siRNA and as LSF siRNA 2 respectively, were chosen and utilized for all subsequent experiments in this chapter and the Appendix. Additionally, 8 siRNAs targeting *LBP1A* were designed and synthesized using the same design scheme, and screened at a 20 nM dose in QGY-7703 cells (Figure 4.1i). Relative gene expression levels showed significant knockdown of the LBP1A transcript; siRNA 28 was chosen for investigating the impact of LBP1A knockdown in QGY-7703 cells.

Previous reports (Hubner et al., 2010) have described an off target effect with certain siRNAs, which resulted in nonspecific reductions in MAD2 mRNA and protein levels. Given the critical importance of MAD2 in mitosis, siRNAs targeting *LSF* or *LBP1A* were transfected into HCC cells, and RNA was isolated 72 hours after the transfection to evaluate *Mad2* transcript levels. Transfection with either the siRNA targeting *LSF* or *LBP1A* (Figures 4.1g, h and j) did not reduce *Mad2* transcript levels when directly compared to cells transfected with the control siRNA, demonstrating that they were specific and effective.

Both RNAi-mediated knockdown of LSF and FQI1 treatment inhibit HCC cellular division prior to cell death

In order to investigate potential cell cycle defects in QGY-7703 cells we first evaluated cellular proliferation. QGY-7703 cells synchronized at the G1/S border (0 hours) were treated with increasing concentrations of FQI1 or siRNAs targeting LSF, as they were released into S phase. Since FQIs inhibit the activity of both LSF and LBP1A (T. Grant and U. Hansen, unpubl. results), siRNAs against both were included for

evaluation. A detailed protocol schematic is depicted in Illustration 4.2. The success of this protocol depended on durability of LSF knockdown, given the long half-life of LSF protein (Hansen et al., 2009). 20 nM LSF siRNA resulted in ~90% LSF RNA reduction at 72 hours, and 95% reduction at 96 hours (Figure 4.2a). As expected given the half-life of 24 hours, levels of LSF protein decreased more slowly than those of the transcript, with maximum decline of protein being achieved at ~48 hours after transfection (Figure 4.2c). With this degree of durability of RNA knockdown, LSF protein knockdown was able to persist through the entire course of the experiment (Figures 4.2d). The double thymidine block synchronization protocol spanned approximately 48 hours and could not be initiated on the day of siRNA transfection as the combination resulted in severe toxicity. Similarly, expression of LBP1A RNA after transfection with 20 nM LBP1A siRNA yielded 96% knockdown at 24 hours post transfection- a level of knockdown that was maintained as far out as 96 hours post transfection (Figure 4.2b). These results demonstrate potent and long-lasting knockdown of both LSF and LBP1A with the siRNAs.

To attempt to recapitulate effects of FQI1, we tested the impact of decreased protein levels of LSF, LBP1A or the combination of both. A single cell division of HCC cells treated with one or more siRNAs was monitored by arresting cells at the G1/S border and then releasing them to continue cell cycle progression. After the synchronization protocol, cell populations that had been transfected with LSF siRNA, at any concentration or in combination with LBP1A, had fewer cells. Upon release from the G1/S block, populations treated with LSF siRNA did not divide. In contrast, control cells

substantially completed the first mitosis and cellular division, as did cells treated with LBP1A siRNA. Phase contrast images of synchronized QGY-7703 cells treated with control or LSF siRNAs (Figure 4.2 h,i) are consistent with reduced total cell counts following LSF knockdown. Note that many of the LSF siRNA-treated cells are rounded up, a phenotype of mitotic cells. These data suggest that LSF alone, but not LBP1A, is necessary for timely HCC cellular division at the first mitosis following reduction in protein expression.

To determine if FQI1 treatment, which inhibits LSF activity, would mirror the reduction in cellular division observed upon loss of LSF protein, a similar synchronization experiment was performed in the presence of FQI1. QGY-7703 cells were treated with FQI1 at 0.9, 1.8, and 3.6 μM, or vehicle, for 24 hours immediately following the first thymidine block and continually thereafter, including release in the presence of FQI1 from the G1/S block at the same concentration as the initial incubation (Illustration 4.1). In previous growth inhibition assays, 1.3 μM of FQI1 resulted in half maximal growth inhibition in the QGY-7703 cell line (Christadore, 2013). Therefore, concentrations were chosen in order to flank the GI_{50} concentration. Figure 4.2g shows that with progressively increasing FQI1, there is an increasingly pronounced decline in cell division. Phase contrast images of synchronized QGY-7703 cells treated with control (Figure 4.2j) or with 1.8 μM of FQI1 (Figure 4.2k) are consistent with the reduced cell number reflected in total cell counts. Again, many cells in the FQI1 treated group are rounded up.

To determine if the LSF knockdown or FQI1 treatment resulted in cell death, the viability of the treated cells was assayed using multiple methods (Figure 4.3). Asynchronous HCC cells were treated either with FQI1 or LSF siRNA, and the Trypan Blue positive cells were counted. Trypan blue staining occurs only if the cell membrane is compromised, as in dying cells. By this measurement, 20 nM of LSF siRNA or 3.6 μM of FQI1 resulted in reduced percentage of viable cells (Figure 4.3a and 4.3b). FQI1 treatment resulted in reduced viability at the 24 hour time point whereas the cells with RNAi mediated LSF knockdown do not show signs of reduced viability until 96 hours following transfection. The differential timing in viability loss is consistent with the modalities (small molecule and siRNA) utilized to inhibit LSF as most small molecules are anticipated to interact with their targets fairly rapidly upon incubation whereas the reduction of LSF levels by siRNAs takes 48-72 hours. When cell viability was measured by mitochondrial functionality in synchronized cells, 3.6 μM of FQI1 or 20 nM of LSF siRNA resulted in approximately 40% reduction of viability or reduced cell number when assayed 24 hours post release from a G1/S block (Figure 4.3c). Reduced mitochondrial activity may simply reflect reduced cell number, rather than cell death at this time point, as the cells do not proliferate upon LSF inhibition (Figure 4.2 f and g). To determine whether cells were dying as a consequence of LSF knockdown or FQI1 treatment, and whether this immediately followed inhibition of cellular division, synchronized HCC cells incubated with various concentrations of LSF targeting siRNA or with various FQI1 concentrations were assayed for apoptosis by measuring Caspase 3/7 activity (Figure 4.3e). Both LSF knockdown and LSF small molecule inhibition (Grant et al., 2012)

resulted in induction of apoptosis by 48 hours, with caspase activity undetectable as the cells entered the first mitosis.

LSF knockdown or inhibition in QGY-7703 cells results in multiple cellular phenotypes including cell cycle delay in G2 or M and cellular senescence

To elucidate how LSF knockdown inhibited cell division, cellular DNA content was measured in synchronized QGY-7703 cells after LSF inhibition, focusing on times spanning when cells would normally progress from the G1/S transition through mitosis and re-entry into G1. Because HCC cells are generally aneuploid, the DNA content as ascertained by flow cytometry would not be a true 2n or 4n. However, for ease I aligned the cell populations with non-replicated DNA at the 2n peak, with 4n representing successful DNA synthesis.

The QGY-7703 cells were transfected with increasing amounts of LSF siRNA, from 0 to 20 nM, and compared to cells transfected with highest amount of control siRNA. All cell populations showed the expected profile of cellular DNA, predominantly at the G1/S border, after synchronization (Figure 4.4, 0 hours). Control cells were in S phase at 3.5 hours after release from the block, in G2 or mitosis at 8 hours, and back in G1 phase by 18 hours, having divided. However, with levels of LSF diminishing from RNAi activity during the course of the synchronization procedure, at the end of the double thymidine block procedure a subpopulation of all the LSF siRNA-treated cells no longer was able to progress into DNA replication, but instead was arrested with 2n DNA. The remainder of the cells continued to progress through the cell cycle. Consistent with

the viability and caspase activity assays, subG1 DNA populations (Figure 4.4), indicative of apoptosis, were observed by flow cytometry in all the LSF siRNA-treated samples, but not significantly in the control cells. These data indicate that whereas gradual LSF knockdown generates a population of cells that no longer progresses into S phase, the remaining cells do progress from G1 into mitosis, accompanied by some cell death thereafter.

Synchronized QGY 7703 cells in which LBP1A was knocked down showed no apparent difference in cell cycle progression, as compared to the control cells (Figure 4.5). These results are consistent with the analysis of cellular division (Figure 4.2f) where cell progression of cells with LBP1A knockdown was comparable to the siRNA control group.

In order to compare cell cycle phenotypes generated by LSF small molecule inhibitors with those produced by RNAi treatment, QGY-7703 cells were also treated with FQI1 during the synchronization protocol (Illustration 4.1). At the lower concentrations of 0.9 and 1.8 μM, the FQI1-treated cells were initially delayed in returning from G2/M to G1, remaining with 4n DNA content, compared to the control cells that had re-entered G1 (Figure 4.9, 8.5 h), an observation consistent with previous studies (Chapter 3, Christadore, 2010, (Rajasekaran et al., 2015)). At 16 hours, some of these FQI1-treated cells had either divided (2n DNA) or initiated cell death (subG1 DNA content). At the highest FQI1 concentration, cells also were delayed with 4n DNA content, but the entire population converted to subG1 content by 16 hours post release from the G1/S block (Figure 4.6).

The surprising inability of cells to progress into S phase after synchronization coupled with LSF inhibition led to the hypothesis that the decreasing LSF levels during the previous cell division might have caused defects leading in G1 to senescence. To test this hypothesis, β-galactosidase activity, indicative of senescent cells (Debacq-Chainiaux et al., 2009), was measured. QGY-7703 cells were synchronized as before by a double thymidine block in the presence of 0 to 3.6 μM of FQI1, LSF siRNA at 20 nM, or the appropriate controls. Cells were fixed at the time when control cells were approximately at mitotic entry and the levels of β galactosidase activity, which is indicated by blue staining upon phase contrast microscopy (Figure 4.7 a-j), were imaged. Reduction in LSF levels or inhibition of its activity resulted in significantly greater numbers of cells expressing β-galactosidase activity compared to control samples. Quantitation of the number of cells analyzed as well as the number of cells positive for β galactosidase activity with LSF knockdown resulting in 88% of β-galactosidase-positive cells compared to 24% in the control group. Increasing FQI1 treatment resulted in 47% and 72% in the 1.8 and 3.6 μM groups, respectively, whereas the vehicle control group and 0.9 μM FQI1 group had 6 and 4 percent of a positive cell population. The observed increase in β-galactosidase-positive cells with reduced LSF activity correlates with the analysis of DNA content by flow cytometry, as fewer cells continue progression through the cell cycle with increasing siRNA or FQI1 concentrations (Figures 4.4 and 4.6). Furthermore, increasing FQI1 or LSF siRNA concentration positively correlated with the percentage of β galactosidase-positive cells (Figure 4.7 k and l). These data demonstrate that reduced LSF levels or activity during previous cell cycles can predispose cells to

senescence. In contrast to data with short-term incubation of FQI1 (Chapter 3), here, when cells are incubated with FQI1 throughout the entire synchronization process there is a population that remains at 2n upon cell cycle release, albeit a minor percentage of the cells analyzed. This is especially apparent in the 3.6 μM treated group and is consistent with the observation of senescence in the FQI treated cells (Figure 4.6).

Cell cycle progression defects in QGY-7703 cells upon LSF inhibition do not result from DNA damage

LSF has previously been shown to be necessary for appropriate cell cycle progression at the G1/S transition, due to its requirement for upregulation of thymidylate synthase expression (Powell et al., 2000). Indeed, in the non-HCC cells previously examined, the requirement for LSF at this transition was eliminated by exogenous addition of low levels (20 μM) of thymidine (Powell et al., 2000). However, in HCC cells, the requirement for LSF in expressing adequate thymidylate synthase is not as severe. In particular, the enzyme levels were not abolished upon inhibition of LSF (Yoo et al., 2009). Furthermore, addition of thymidine did not affect FQI1-mediated reduction in cell viability, indicating that altered thymidylate synthase expression is not the mediator of FQI-mediated cell death (Grant et al., 2012). To determine whether reduction in thymidylate synthase expression might impact the senescent or cell cycle phenotypes, thymidine was added to synchronized cells at the time of release from the G1/S block for QGY-7703 cells treated with either LSF siRNA or FQI1. Cell cycle DNA

profiles generated from flow cytometry were indistinguishable in the presence or absence of 20 μM of thymidine (data not shown).

Nonetheless, to test directly whether S phase defects potentially caused by deficiency in LSF function might be responsible for the defects prior to G1 re-entry, DNA damage was monitored using antibodies to phosphorylated H2AX (γ-H2AX). We assayed this by two separate techniques: flow cytometry and immunofluorescence. Cells treated with LSF siRNA were imaged by fluorescent microscopy at multiple time points following release of synchronized cells from a G1/S block; cells harvested at time points representing completion of DNA synthesis (4 hours) and re-entry into G1 (16 hours) showed comparable γ-H2AX staining (Figure 4.8 a, right) to those treated with control siRNA (Figure 4.8a, left). Similarly, cells treated with FQI1 (Figure 4.8b, left) have similar profiles as compared to the control cells treated only with vehicle, exhibiting a small population with positive γ-H2AX staining (Figure 4.8b, right). At the later time point, 16 hours, it is noteworthy that both groups with reduced LSF activity do have increased γ-H2AX staining in comparison to the control cells at the same time point, but this would be long after the mitotic defects occurred, and consistent with induction of apoptosis in such cells. To confirm the results obtained by flow cytometry, a similar experiment was performed, however, the synchronized cells were then analyzed for γ-H2AX signal by immunofluorescence at 8 hours post release (Figure 4.8 c and d). A positive control was included (Figure 4.8c, bottom) where UV-irradiated HCC cells showed strong γ-H2AX staining. Both the siRNA (Figured 4.8c) and FQI1 (Figure 4.8d) treated groups had comparable levels of phosphorylated H2AX as did controls, and

dramatically reduced levels compared with the positive control (Figure 4.8c bottom). Evaluation of asynchronous HCC cells treated with either LSF siRNA (Figure 4.8e) or FQI1s (Figure 4.8f) did result in increased γ-H2AX in both cases, however, this occurred approximately 24 hours following the documented aberrant mitosis, indicating that a defective mitosis, rather than any defects during initial progression through DNA synthesis, was responsible for the DNA damage (Orth et al., 2012). Overall, these data indicate that LSF knockdown or inhibition does not induce double stranded DNA breaks prior to mitotic entry, consistent with LSF being required more directly for regulation of proper progression through G2 or M in hepatocellular carcinoma cells.

Reduced LSF Activity Results in a Prometaphase Arrest, Cell Division Defects, and Multi-Nucleation

To further investigate the consequences of mitotic delay and aberrant cell division induced by LSF inhibition, synchronized cells treated with LSF targeting siRNA or FQI1 along with their respective controls were phenotypically analyzed at time points when control cells had exited mitosis by visualizing fixed cells for LSF, α-tubulin, and DNA (Figures 4.9a, c). Both LSF loss and FQI1 treatment resulted in cells persisting in prometaphase, with those that exited from faulty mitoses leading to various phenotypes including multi-nucleation (Figure 4.9a, c). These data combined show that inhibition of LSF activity, by either method, results in persistence of mitotic cells much later than normal, with a prometaphase (Figure 4.9b, d) delay followed by aberrant cell division. Representative images gathered from immunofluorescent analyses (Figures 4.10-4.12)

show that synchronized cells with reduced LSF activity resulted in a prometaphase delay (Figure 4.10), defective cytokinesis (Figure 4.11) and multi-nucleation (Figure 4.12). These data are consistent with our previous findings indicating that high concentrations of FQI1 induce a profound prometaphase arrest in HCC cell lines (Chapter 3;(Rajasekaran et al., 2015)).

Expression of Aurora kinase B and Cdc20 is significantly down regulated upon LSF knockdown or inhibition in HCC cells

Given that inhibition of Aurora kinase B can result in prometaphase delay, cytokinesis defects, and multinucleation (Andrews, 2005; Ditchfield et al., 2003; Vader and Lens, 2008), and that ChIP-seq data in an LSF inducible system identified multiple binding sites both within the Aurora Kinase B promoter and in presumptive enhancer regions (Gene Chin, Sriharsa Pradhan, Ulla Hansen, unpublished results), I determined whether loss of LSF activity would impact expression of key mitotic regulators such as Aurora kinase B. QGY-7703 cells treated with LSF siRNA or control siRNA were analyzed for expression of multiple mitotic regulators at various time points from G1/S to M.

In order to investigate the delay in mitosis observed by immunofluorescent microscopy, expression of key drivers of mitotic entry, Cyclin A and Cyclin B, was examined first in synchronized QGY-7703 cells. Eight hours after release of cells from a G1/S block, at which time the control cells should have completed mitosis and re-entered G1, Cyclin B levels were significantly decreased by both siRNA and FQI1 treatments in

a dose dependent manner (Figure 4.13a and 4.14a, respectively). Cyclin A levels were also reduced correlating with reduced LSF activity suggesting that cells had completed late prophase and, unlike the controls, had not re-entered G1 (Figures 4.13 and 4.14). Interestingly cyclin B protein levels under this experimental design were inconsistent with those published (Rajasekaran et al., 2015) and those reported in Chapter 3 of this thesis where cyclin B protein levels remained elevated in the presence of FQI1. This difference is due to distinct experimental protocols. The studies here included incubation of HCC cells with FQI1 for an extended time, whereas in the previous experiments (Chapter 3) cells were incubated with FQI1 only after release from the G1/S block. Consistent with this interpretation, whereas Cyclin B RNA levels were not affected by the short-term incubation with FQI1 (Chapter 3 and (Rajasekaran et al., 2015)), when FQI1 treatment was extended RNA levels diminished in line with the protein levels (Figure 4.15j). However, Cyclin B RNA levels in the cells treated with LSF siRNA was comparable to those in the control at the same time point (Figure 4.15k). The apparent discrepancy between the siRNA and FQI1 results may be due to a timing difference between the two technologies utilized to deplete LSF activity where LSF knockdown, and its impact on downstream regulation may occur earlier than with the FQI1 treatment. In addition, many of the siRNA-treated cells by this protocol appear not to progress back into G2 or M upon release from G1/S, which may dilute any differences in cell cycle-dependent RNA expression.

Upon examination of Aurora kinase B expression, both LSF siRNA and FQI1 treatments reduced protein expression of Aurora Kinase B (Figures 4.13a and 4.14a,

respectively). Consistent with this observation, phosphorylation of direct targets of Aurora Kinase B, Serines 3 and 28 on Histone 3 (pH3 S10 and pH3 S28), were also reduced when either LSF levels or activity were diminished by siRNA or FQI1, respectively (Figures 4.13a and 4.14a). Because RNAseq studies in HEK293 cells implicated LSF regulation of APC/C proteins, Cdc20 was also evaluated (Gene Chin, unpublished). Cdc20 protein expression was also reduced in a dose dependent manner (Figures 4.13a and 4.14a), with decreasing LSF expression or activity resulting in decreasing Cdc20 expression.

To determine whether the changes in Aurora Kinase B and/or Cdc20 levels were potentially transcriptional in nature, the relative RNA levels of both genes were measured following LSF inhibition or knockdown. Gene expression of both *AURB* and *CDC20* was indeed down-regulated; and correlated to the degree of LSF protein decreased by RNAi knockdown (Figures 4.15 a-d) or via treatment with increasing concentrations of the LSF inhibitor, FQI1 (Figure 4.15 f,g). As expected, Cdc20 levels increased as the control cells progressed through the cell cycle with peak levels at mitosis (Inbal et al., 1999) (Figure 4.15c, g), however, cells with LSF loss had significantly reduced levels at all time points indicating that Cdc20 was no longer being transcriptionally activated during G2. Although Aurora Kinase B RNA levels normally also increase during G2 due to transcriptional activation (Kimura et al., 2004), in the untreated QGY-7703 cells Aurora Kinase B gene expression (Figures 4.15a, f) did not show a substantial increase as the cells entered mitosis. This is likely due to the constitutive overexpression of Aurora Kinase B in HCC cells (Sistayanarain et al., 2006; Tanaka et al., 2008; Yasen et al.,

2009). Nonetheless, both LSF siRNA and inhibitor led to decreased *AURKB* expression. Overall, both methods of reducing LSF activity resulted in a significant loss of expression of *CDC20* and *AURKB*.

LSF knockdown or FQI1 treatment results in increased mitotic time, due to a prometaphase/metaphase delay followed by aberrant cellular division

Given the complexity of multiple phenotypes, it was critical to analyze the phenotype and fate, cell by cell, of those that continue cell cycle progression beyond G1/S in the absence of or inhibition of LSF. QGY-7703 cells stably expressing fluorescently labeled histone H2B or α-tubulin (YFP-H2B and Emerald-α-tubulin, respectively) were generated. H2B labeled cells allowed visualization of the DNA structure and α-tubulin labeling allowed visualization of spindle formation, kinetochore attachment, and cytokinesis. Synchronized QGY-7703 YFP-H2B cells were transfected with siRNAs targeting LSF, LBP1A, both LSF and LBP1A, or a non-expressed control. For these experiments, a single thymidine block protocol was chosen for synchronization (Illustration 4.3), as the double thymidine block protocol resulted in monotonically fewer cells being released through S phase and ultimately into mitosis upon treatment with increasing amounts of LSF siRNA (Figure 4.4 and data not shown). Using a single thymidine block, a larger percentage of cells reached mitosis. Representative time lapse images of cells treated with the highest concentration (20 nM) of either LSF targeting siRNA or control highlight dramatic changes in mitotic progression. The control cells exhibit normal mitosis with progression through prometaphase, metaphase, anaphase and telophase in a timely manner (Figure 4.16a). However, the cells with diminished LSF

levels exhibit a prometaphase/metaphase delay followed by cell division defects (Figure 4.16b). Upon quantitation, the time required for each cell to progress through mitosis, measured from the start of nuclear envelope breakdown (NEB) to anaphase, was dramatically increased in the cells with reductions in LSF (Figure 4.16c). Counterintuitively, the lower concentrations of LSF siRNA resulted in longer times for mitotic progression.

LBP1A knockdown alone resulted in only a subtle increase in mitotic time. Taken together with the cell viability and DNA profiling data (Figures 4.3 b and c; 4.5) this minor increase does not significantly impact either proper HCC cellular mitotic progression or cellular division. Further, no abnormal mitotic phenotypes were observed in the time-lapse studies of cells with LBP1A knockdown. LBP1A siRNA (10 nM) added in combination with LSF siRNA (10 nM) diminished the effect on mitotic progression compared to 10 nM LSF siRNA alone (Figure 4.16c), which may relate to the lesser effect of 20 nM LBP1a siRNA alone.

Upon examining the outcomes for individual cells treated with LSF siRNA as they progressed through mitosis, major defects were observed. Most striking was an extended delay in prometaphase and/or metaphase (representative images in Figure 4.16 b, e and f). On a cell-by-cell basis, this was often followed by aberrant cellular division (Figure 4.16 b, g-j). Figure 4.16 e and f show the same cell delayed in prometaphase/metaphase with 4.16e exhibiting a prometaphase phenotype and 4.16 f exhibiting a metaphase phenotype. Figure 4.16 g represents a cell arrested in prometaphase in which the DNA condensed into a near-apoptotic state, whereas Figure

4.16i and j display a cell that, following a prolonged prometaphase/metaphase arrest, divided in a multi-polar fashion without separating into two daughter cells. Quantitation indicated a significant increase in both the prometaphase/metaphase and aberrant cellular division phenotypes over a range of degrees of LSF knockdown (Figure 4.16d). In addition, some cells remained in prometaphase-metaphase by the end of the analysis (e.g. Figure 4.16 g,h); thus it is not certain that these cells would exit mitosis at all.

Asynchronous H2B YFP QGY-7703 cells were also treated with increasing concentrations of FQI1 and imaged by time-lapse microscopy. Synchronization was not regarded as necessary in this case, as time-lapse imaging allowed the tracking of individual cells as they pass through mitosis and FQI1 addition to asynchronous cells was hypothesized to relatively rapidly interact with LSF following addition. At the highest concentration (3.6 μM), representative images show cells that apparently arrested in prometaphase with no observable transitioning to metaphase throughout the 640 minutes of imaging (Figure 4.17c). This was in stark contrast to control cells, which progressed through mitosis within the normal timespan (Figure 4.17a). Cells treated with half the maximal concentration of FQI1 (1.8 μM) were delayed in prometaphase and/or metaphase, with cells subsequently progressing through defective cellular division (Figure 4.17b). Upon quantitation, mitotic time (time from nuclear envelope breakdown (NEB) to anaphase) increased with increasing concentrations of FQI1 (Figure 4.17d). The time was indeterminable for cells treated with 3.6 μM of FQI1, as the cells never reached anaphase during the course of the experiment. Overall, phenotypes were similar to those documented with LSF siRNA treatment (compare Figure 4.16e with Figure

4.17d). By following individual cells as they progressed through mitosis, it became apparent that cells delayed progression either in prometaphase (e.g. Figure 4.17f) or metaphase (e.g. Figure 4.17g), and subsequently exited mitosis aberrantly (Figure 4.17h, i). A recurring consequence was multi-nucleation upon mitotic exit (Figure 4.17i). Lastly, Figure 4.18 d and e are representative images where upon reduced LSF activity, regardless of the method utilized, appearance of cellular protrusions was evident. As to whether loss of LSF directly leads to the membrane protrusions or whether this observation is secondary to the mitotic arrest is unknown.

Discussion

LSF, a ubiquitously expressed transcription factor, is an oncogene in human hepatocellular carcinoma (Santhekadur et al., 2012b; Yoo et al., 2010). Recent studies have shown that small molecule inhibitors directly targeting LSF inhibited HCC cell proliferation i*n vitro* and tumor growth *in vivo* (Grant et al., 2012; Rajasekaran et al., 2015). These inhibitors, FQI1 and FQI2, both resulted in significant anti-tumor activity in an endogenous liver model with no signs of toxicity at the doses required for tumor inhibition (Grant et al., 2012; Rajasekaran et al., 2015). Together, these data indicate that LSF is an exciting therapeutic candidate for HCC patients. The recent reports used Factor Quinolinone Inhibitors as a tool to inhibit LSF activity showing robust anti-tumor activity, and were consistent with earlier observations of a dominant negative LSF reducing HCC tumorigenicity (Yoo et al., 2010). However, although the data support specific targeting of the transcription factor LSF by FQIs, this result was surprising given

the generally encountered difficulties in targeting transcription factors with small molecules (Yan and Higgins, 2013).

Here, the combinatorial use of small molecule inhibitors that eliminate LSF DNA binding with RNAi technology which specifically reduces LSF synthesis was utilized to confirm FQI1 specificity. The data show that titrating LSF activity by either small inhibitors or LSF activity resulted in extensive mitotic defects prior to cell death. These data provide definitive evidence both that the FQI1-induced mitotic defects previously published are not a secondary effect of FQI1, and that LSF regulates mitosis in hepatocellular carcinoma cells.

Eliminating LSF activity inhibited HCC cellular division and resulted in the duplicated DNA remaining in one cell prior to cell death. Analysis of cell cycle progression revealed a population of cells undergoing mitotic delay prior to cell death through apoptosis, as well as a population of senescent cells. The mitotic delay, particularly in prometaphase or metaphase, was highlighted by time lapse microscopy, upon inhibition of LSF activity by the two independent approaches. Mitotic time, measured as the amount of time from NEB to anaphase, was similarly boosted upon increasing either FQI1 or LSF siRNA concentrations. Strikingly, the lower siRNA concentrations produced greater delays in mitotic progression than higher siRNA concentrations. One interpretation of this result is that LSF targets multiple mitotic components, and higher levels of LSF inhibition may be required to solidify the mechanism of prometaphase arrest.

Presence of DNA damage as cells enter mitosis can result in mitotic delay (Ganem and Pellman, 2012). However, this was ruled out by two types of controls. First, misregulation of thymidylate synthase was not the cause of the mitotic defects because supplementation of these cells with exogenous thymidine in order to circumvent a thymidylate synthase deficiency did not impact the phenotype (Grant et al., 2012). Second, staining for double stranded DNA breaks indicated that minimal, if any DNA damage occurred under these conditions prior to mitotic progression.

Key phenotypes observed in the HCC cells with LSF depletion included: cellular senescence, prometaphase/metaphase arrest, cell division defects and multi-nucleation. To identify potentially relevant LSF targets, we assayed expression of key mitotic proteins that generate similar phenotypes when inhibited, showing that levels of both Aurora kinase B and CDC20 decrease when LSF is inhibited by either siRNA or small molecule inhibitors. Notably, phenotypes previously documented for agents that inhibit Aurora Kinase B are consistent with all those described for LSF inhibition in Chapters 3 and 4 (Kim et al., 2011; Le et al., 2013; Poon, 2013; Sistayanarain et al., 2006; Vader and Lens, 2008). In addition, reduction of Cdc20 levels also results in increased mitotic times (Huang et al., 2009; Irniger, 2002). Cdc20 is required for proteolysis of key mitotic regulators, including securin, and is a prerequisite for the promotion of anaphase and mitotic exit.

When Cdc20 is depleted with siRNA, cells remain in mitotic distress for lengthy periods, and die in mitosis (Huang et al., 2009; Irniger, 2002). The increase in mitotic time with the reduced Cdc20 expression jive with a strategy that has been proposed as promising

for anti-tumor therapies (Gascoigne and Taylor, 2008, 2009; Kimura et al., 2013). Overall, that both Aurora Kinase B and Cdc20 are down regulated at the mRNA and protein levels when LSF is diminished begs the question as to whether LSF directly activates expression of these two target genes during G2. This hypothesis is being actively pursued in the Hansen laboratory.

The mitotic phenotypes prove that LSF is required for mitotic progression in HCC, and that Aurora Kinase B and Cdc20 expression are downstream from LSF. The mechanism by which LSF regulates these targets remains to be determined. However, ChIP-seq data generated in a non-HCC cell line revealed multiple LSF DNA binding sites in Aurora Kinase B regulatory regions (Gene Chin, unpublished results) raising direct regulation as a possibility. In addition, separate analyses of clinical HCC samples have shown increased LSF (Fan et al., 2011a; Gu et al., 2015; Yoo et al., 2010) and Aurora Kinase B expression, albeit independently, that positively correlate with HCC disease severity. These observations are consistent with our data that LSF regulates Aurora Kinase B expression, albeit whether the interaction is direct or indirect remains to be proven. The indirect hypothesis is that Aurora Kinase B and Cdc20 reductions are a secondary consequence of a mitotic defect initiated through another form of regulation, perhaps such as a non-transcriptional mechanism suggested from results in Chapter 3. Whether the interaction is direct or indirect, however, the observed phenotypes including cellular senescence, prometaphase/metaphase delay, aberrant cell division, multi-nucleation and cell death, are all consistent with Aurora Kinase B inhibition/knockdown (Andrews, 2005; Ditchfield et al., 2003; Vader and Lens, 2008).

The mitotic phenotypes generated by either LSF knockdown or FQI1 treatment were similar in many respects, although not identical. With FQI1 treatment, cell division defects included a unique chromosome alignment (shaped like a boomerang) and the highest FQI1 concentration resulted in a complete prometaphase arrest. In contrast, diminishment of LSF protein levels (even at siRNA concentrations as high as 20 nM) did not result in a complete arrest in mitosis, but instead mitotic slippage to aberrant cell divisions. The differences in phenotypes may simply be due to LSF RNAi knockdown not completely ablating LSF, whereas high concentrations of the small molecule inhibitor may well inhibit LSF completely. Alternatively, since FQI1 inactivates, but does not remove LSF from the cell, it may only inhibit some of LSF functions.

Finally, FQIs also inhibit LSF paralogs, including the ubiquitously expressed LBP1a (Trevor Grant and Ulla Hansen, unpublished). Therefore, to accurately recapitulate the FQI1 phenotype to confirm target specificity we perturbed LSF and LBP1a levels, both alone and in combination. Our results, however, show that LBP1A has only limited impact indicating that LBP1A is likely not involved in producing the LSF-related mitotic phenotypes. In fact, individual loss of LBP1A did not affect cellular division or induce death of the HCC cells. The one noted consequence of LBP1A knockdown, however, was a small, but statistically significant, increase in the amount of time required to progress from NEB to anaphase. This prolonged mitosis did simply not result in aberrant phenotypes or cell death.

These findings support the notion that LSF is a strong clinical candidate to treat the afflicted hepatocellular carcinoma population, a patient population increasing globally

with a strong unmet medical need. Aurora Kinase B inhibitors, initially clinical candidates with great promise, have dwindled in the clinic as off target effects and minimal efficacy have plagued the trials (Chan et al., 2012). Targeting LSF, an oncogenic transcription factor, could have greater impact on the HCC patient population. FQIs were non-toxic in preclinical tumor models and this work now implicates LSF as being upstream of a major mitotic kinase, APC/C member, Cdc20, whose knockdown in tumor cells with induced mitotic delay, has been hypothesized to having an advantage in targeting and killing tumor cells (Huang et al., 2009). Together, the interrogation of LSF by multiple means, including the two described here, has corroborated the clinical candidacy for this target, as well as revealing a previously unknown role in mitotic regulation. Targeting an oncogenic transcription factor that is necessary for hepatocellular proliferation and survival could have a significant impact on a significant disease population.

Figures

Illustration 4.1 FQI1 Treatment in Synchronized HCC Cells (Long Incubation)

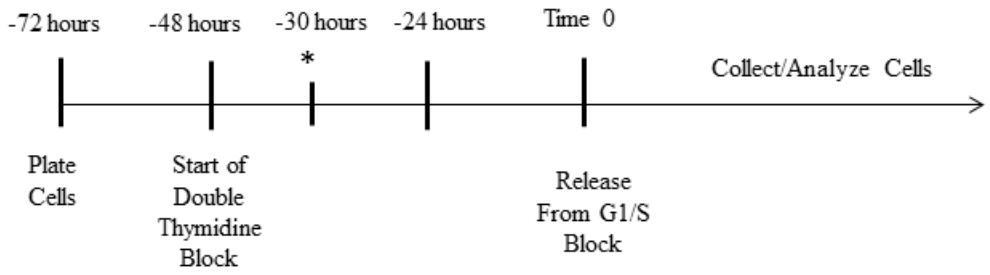

*** FQI1 or Vehicle Control Added and Maintained For Remainder of Experiment**

Illustration 4.2 siRNA Transfection in Synchronized HCC Cells-Double Thymidine Block

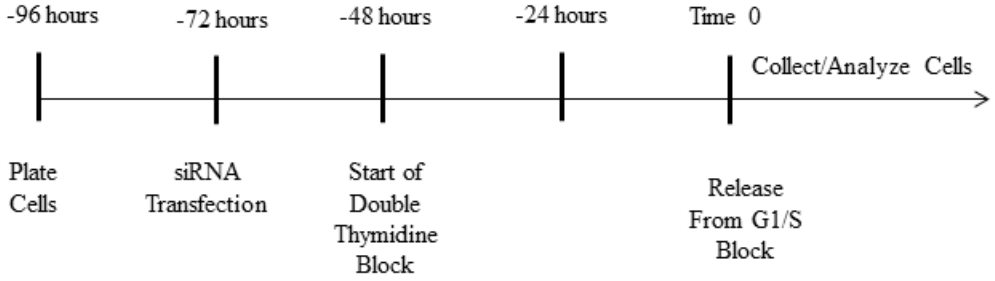

Illustration 4.3 siRNA Transfection in Synchronized HCC Cells-Single Thymidine Block

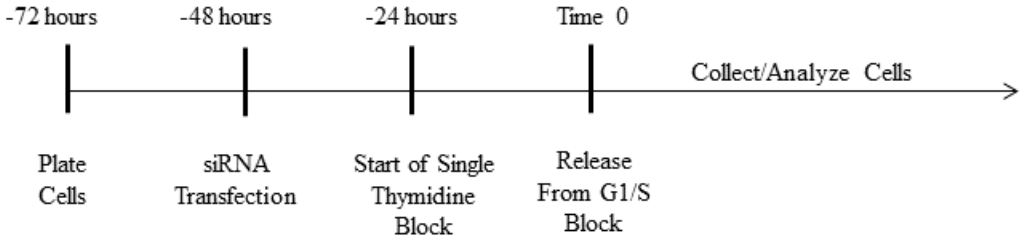

Figure 4.1 Lipid transfection of siRNA in HCC cells results in efficient knockdown of LSF and LBP1A

(a-d) QGY-7703 cells plated in 100 mm x 20 mm dishes were transfected using Invitrogen RNAimax with either 20 nM of control siRNA or *TFCP2* targeting siRNA. The Control siRNA was tagged with Cy3 to follow cellular uptake. Images were taken on a Zeiss microscope at a 40x magnification approximately 24 hours following lipid transfection. Cy3 channel images of Control siRNA-Cy3 transfected (a) or LSF siRNA transfected (c) cells, Phase contrast images of Control siRNA-Cy3 transfected (b) or LSF siRNA transfected (d) cells. Images in (a) and (c) were taken at the same length of exposure. (e,f) Twenty-four candidate siRNAs targeting *TFCP2*, the gene encoding LSF, were identified. Each siRNA was transfected using RNAimax into two different HCC cell lines - Hep3B (e) and QGY-7703 (f), at 20, 10, or 2 nM. LSF RNA harvested at 24 hours post transfection was quantified using a hybridization-based bDNA assay (Affymetrix). LSF RNA levels were normalized to those of an internal control gene, *GAPDH*, and are depicted as percentages of LSF RNA levels in the control siRNA-treated cells. (g, h) *Mad2* RNA harvested at 72 hours (g,h) and 96 hours (h) post transfection was quantified using the Taqman gene expression system. Relative gene expression was determined by normalizing *MAD2* RNA levels to those of an internal control, *GAPDH*. Mad2 gene expression was not altered following treatment with the siRNA targeting LSF. This finding was consistent across 2 independent experiments for the lead siRNA chosen. (i) Eight candidate siRNAs designed to target LBP1A were transfected into QGY-7703 cells at 20 nM. Expression at 72 hours post transfection of *UBP1*, the gene encoding LBP1A, was determined using a Taqman qPCR assay. LBP1A

RNA levels were normalized to those of *GAPDH* and are depicted as percentages of LPB1a RNA levels in the control siRNA-treated cells. (j) Relative *MAD2* RNA levels 72 hours post transfection in asynchronous QGY-7703 cells treated with control siRNA or the each of the 8 siRNAs targeting LBP1A.

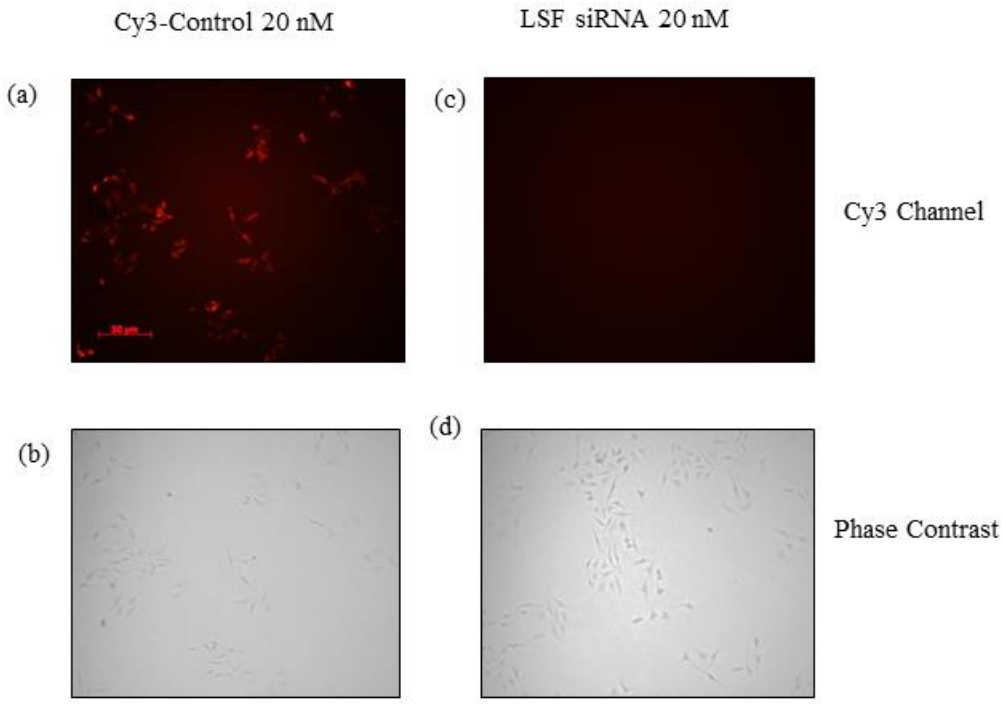
Cy3-Control 20 nM
LSF siRNA 20 nM
(a)
(c)
Cy3 Channel
(b)
(d)
Phase Contrast

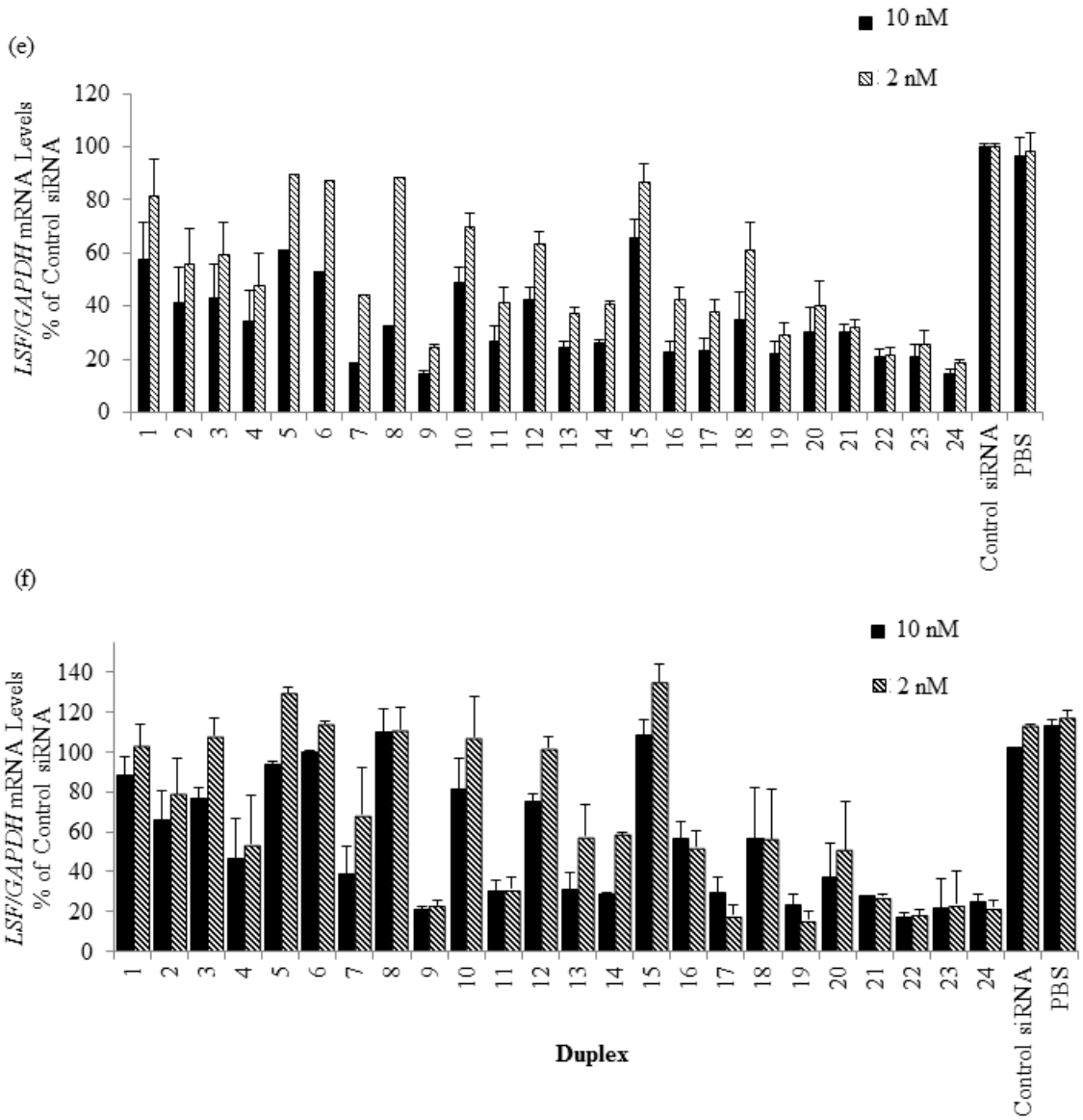
(e)
10 nM
2 nM
LSF/GAPDH mRNA Levels
% of Control siRNA
120
100
80
60
40
20
0
1
2
3
4
5
6
7
8
9
10
11
12
13
14
15
16
17
18
19
20
21
22
23
24
Control siRNA
PBS
(f)
10 nM
2 nM
LSF/GAPDH mRNA Levels
% of Control siRNA
140
120
100
80
60
40
20
0
1
2
3
4
5
6
7
8
9
10
11
12
13
14
15
16
17
18
19
20
21
22
23
24
Control siRNA
PBS
Duplex

(g)

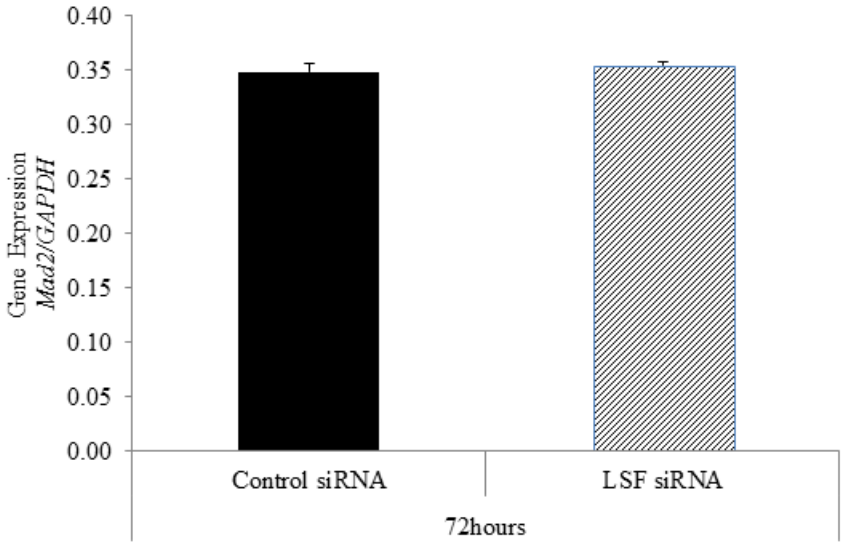
0.40
0.35
0.30
0.25
0.20
0.15
0.10
0.05
0.00
Gene Expression
Mad2/GAPDH
Control siRNA
LSF siRNA
72hours

(h)

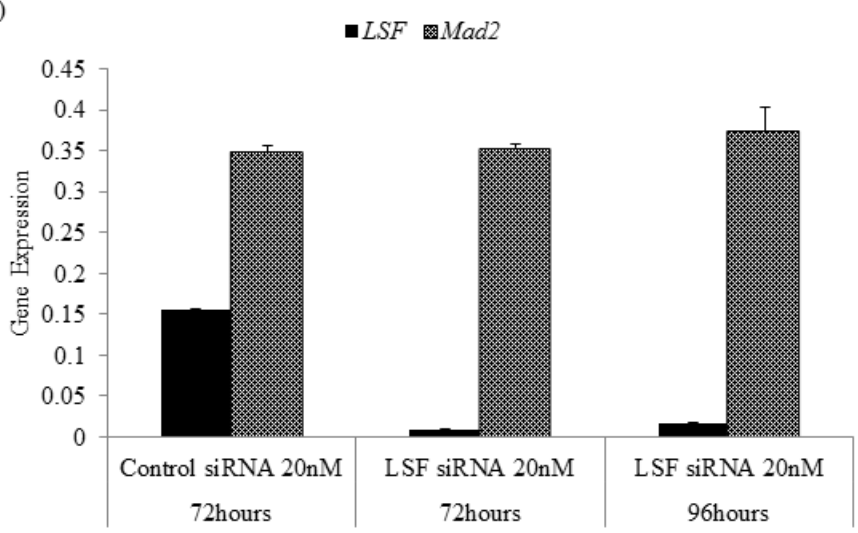
LSF
Mad2
0.45
0.4
0.35
0.3
0.25
0.2
0.15
0.1
0.05
0
Gene Expression
Control siRNA 20nM
72hours
LSF siRNA 20nM
72hours
LSF siRNA 20nM
96hours

(i)

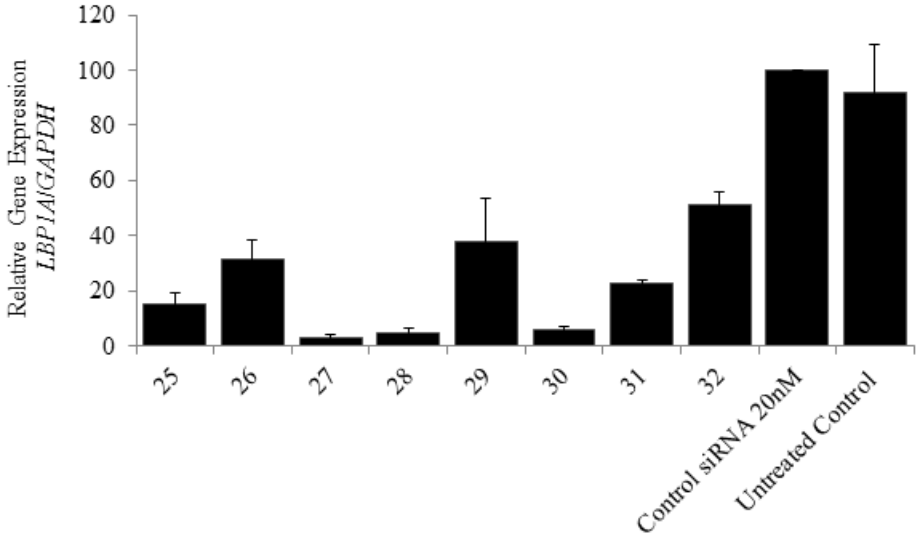
Relative Gene Expression
LBP1A/GAPDH
120
100
80
60
40
20
0
25
26
27
28
29
30
31
32
Control siRNA 20nM
Untreated Control

(j)

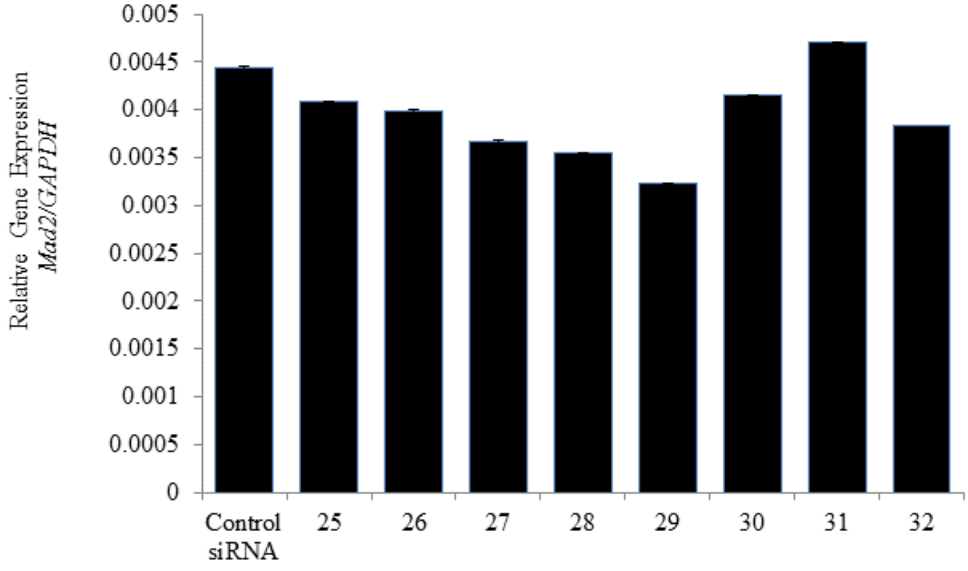
Relative Gene Expression
Mad2/GAPDH
0.005
0.0045
0.004
0.0035
0.003
0.0025
0.002
0.0015
0.001
0.0005
0
Control siRNA
25
26
27
28
29
30
31
32

Figure 4.2 Division of synchronized HCC cells is abrogated upon inhibition of LSF. siRNAs targeting LSF, LBP1A or a non-expressed target were transfected into to QGY-7703 cells at 20 nM. (a-b) LSF and LBP1A mRNA levels were detected using a Taqman gene expression assay. Remaining (a) LSF RNA and (b) LBP1A RNA levels were measured at 24, 48, 72 and 96 hours post transfection. Relative RNA levels, normalized to those of *GAPDH*, are depicted as percentages of the levels in the control siRNA-treated cells. (c-e) Representative immunoblots of LSF and beta tubulin are shown for (c) lysates collected at 24, 48 hours post transfection during cell synchronization or (d) lysates collected following synchronization and release from the final G1/S block for 0, 4 and 8 hours. (e) LBP1A protein expression measured 24, 48 and 72 hours post transfection. α-Tubulin was used as a loading control. Control siRNA was transfected at 20 nM and analyzed 24 hours post transfection. LBP1A siRNA was transfected at a 10 nM concentration. (f) siRNAs targeting LSF or both LSF and LBP1A were transfected into QGY-7703 cells at 10 or 20 nM. Cells were synchronized using a double thymidine block as depicted in Illustration 4.2 and counted at 0 or 16 hours following release from the G1/S block. (f-g) QGY-7703 cells were synchronized using Illustration 4.1 or 4.2. The total cell number had increased 1.5-fold in comparison to the total cell number measured at 0 hours. The control cells may contain less than 2-fold the number of cells at 0 hours due to cell loss during washing of the cells upon change of media for release from the G1/S block. However, such loss would have been consistent across all populations. (f) Cells treated with siRNAs targeting either control, LSF, LBP1a, or LSF and LBP1a in combination. (g) Cells were treated with vehicle control, 0.9, 1.8 or 3.6

μM FQI1 and counted at 0 and 16 hours following a release from a G1/S block. Standard deviation represented of 3 biological experiments. (h-k) Synchronized QGY 7703 cells were transfected with 20 nM Control siRNA (h) or 20 nM LSF siRNA (i) or treated with 1.8 μM FQI1 (j) or vehicle (k). Phase contrast images were taken at 96 hours post release from the G1/S block at a magnification of 20x.

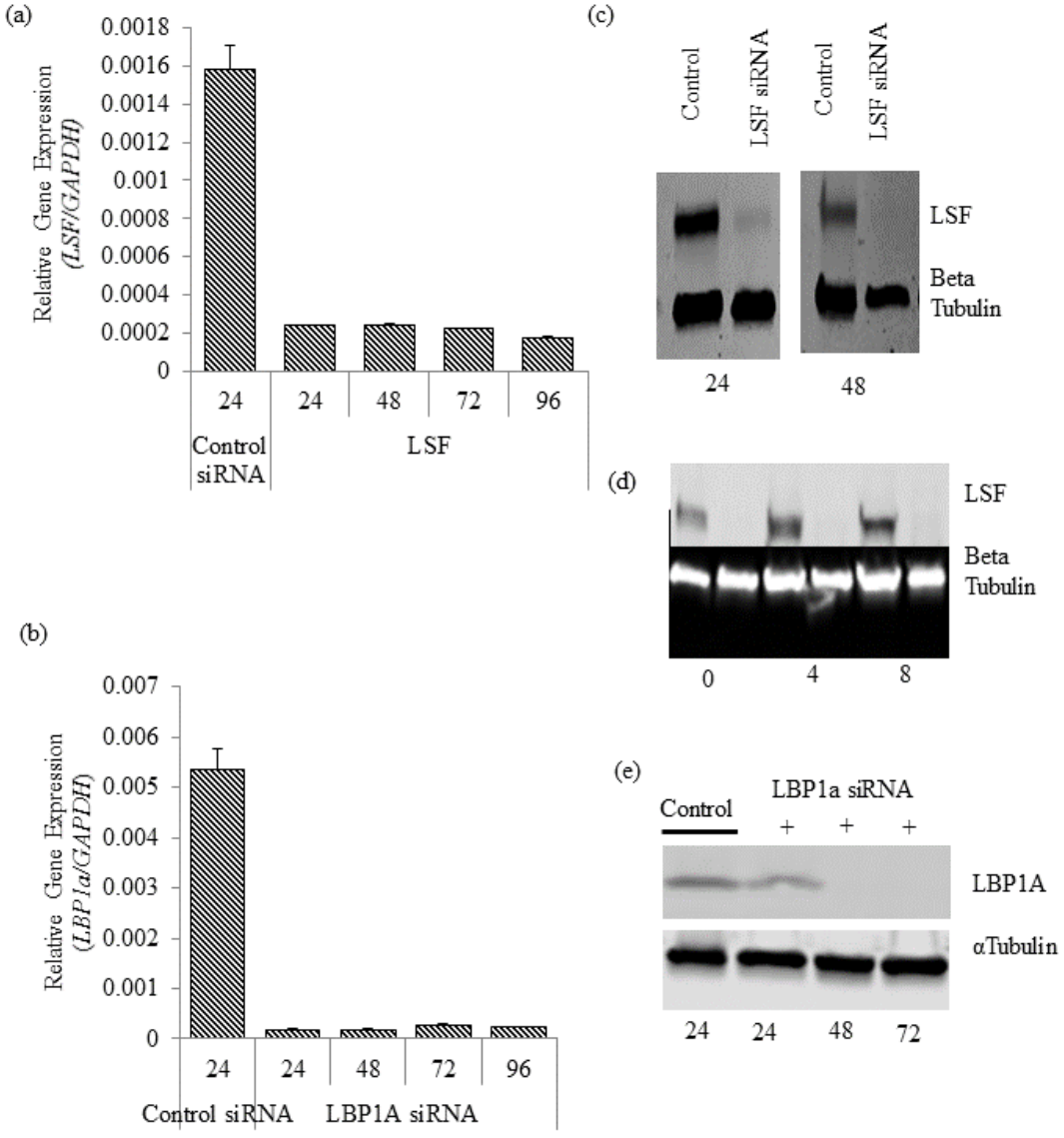
(a)
Relative Gene Expression (LSF/GAPDH)
0.0018
0.0016
0.0014
0.0012
0.001
0.0008
0.0006
0.0004
0.0002
0
24
24
48
72
96
Control siRNA
LSF
(b)
Relative Gene Expression (LBP1a/GAPDH)
0.007
0.006
0.005
0.004
0.003
0.002
0.001
0
24
24
48
72
96
Control siRNA
LBP1A siRNA
(c)
Control
LSF siRNA
Control
LSF siRNA
LSF
Beta Tubulin
24
48
(d)
LSF
Beta Tubulin
0
4
8
(e)
Control
LBP1a siRNA
+
+
+
LBP1A
αTubulin
24
24
48
72

(f)

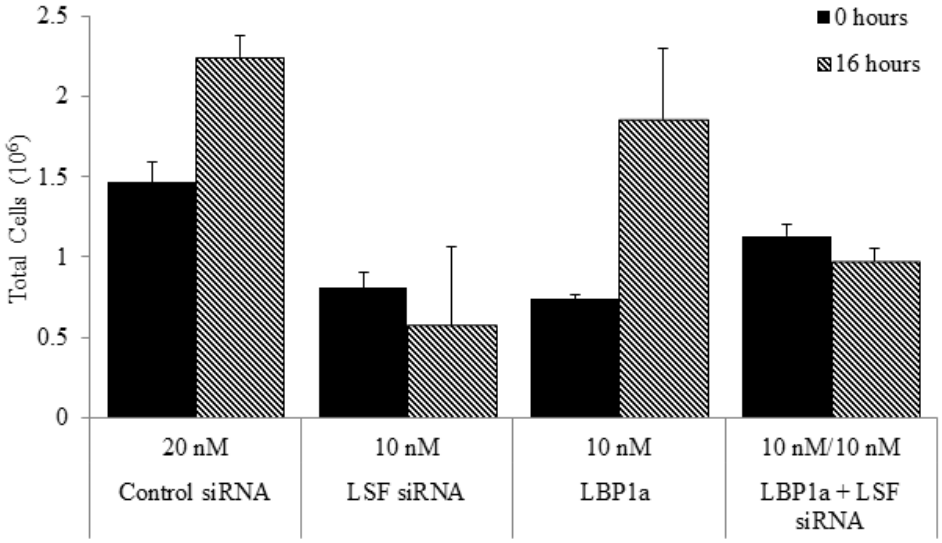
0 hours
16 hours
Total Cells (10^6)
2.5
2
1.5
1
0.5
0
20 nM Control siRNA
10 nM LSF siRNA
10 nM LBP1a
10 nM/10 nM LBP1a + LSF siRNA

(g)

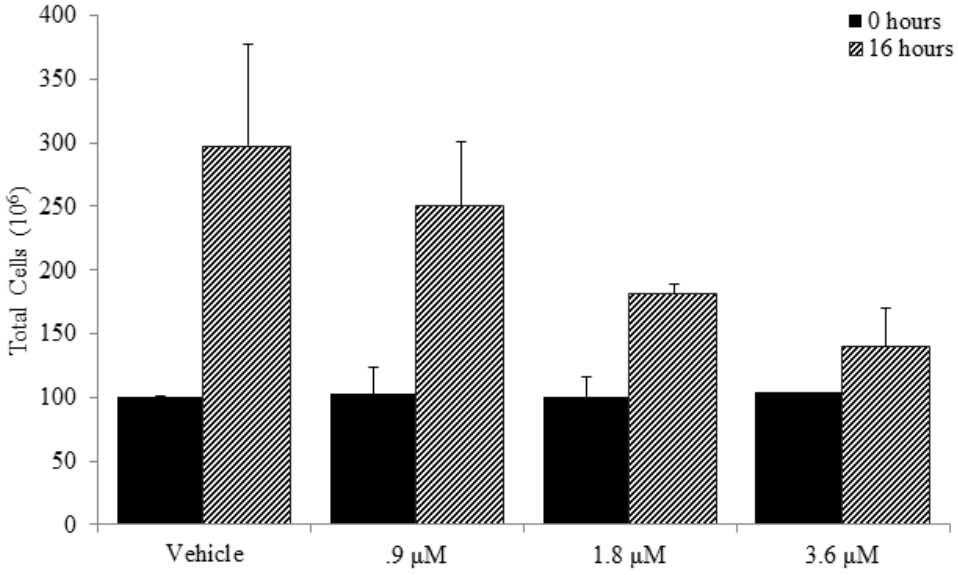
0 hours
16 hours
Total Cells (10^6)
400
350
300
250
200
150
100
50
0
Vehicle
.9 µM
1.8 µM
3.6 µM

(h)

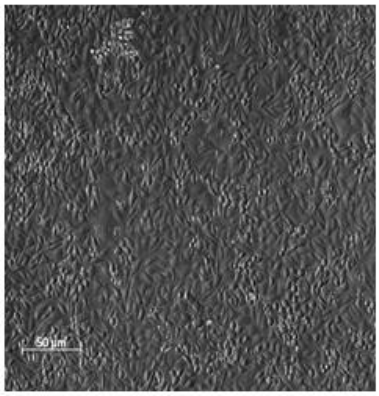

Control siRNA 20 nM

(i)

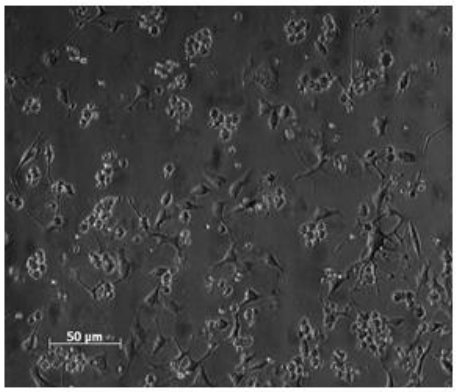

LSF siRNA 20 nM

(j)

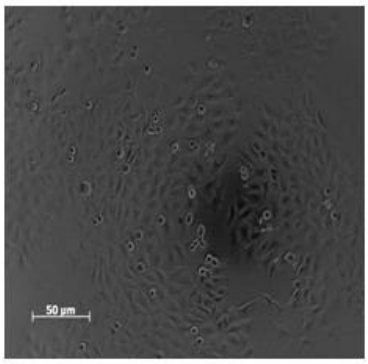

Vehicle Control

(k)

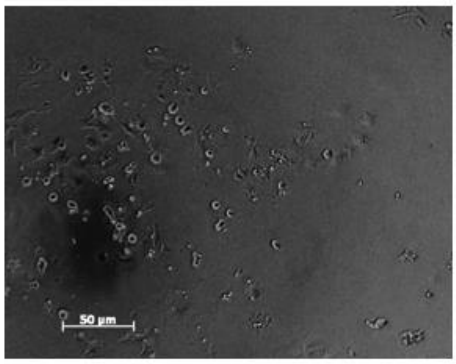

FQI1 1.8 µM

Figure 4.3 LSF knockdown and FQI1 treatment in HCC cells results in reduced cell number and induction of caspase activity

(a-b) Asynchronous QGY-7703 cells were (a) transfected with siRNA targeting either LSF or a control, or (b) treated with 3.6 μM of FQI1 or vehicle. The cells were analyzed at 24, 48, 72, 96, and 120 hours post treatment for cell viability/number by Trypan blue staining. Fifty individual fields were quantitated for the number of trypan blue positive cells; which is depicted as a percentage of the cell count for those 50 fields. Data represent 3 independent experiments. (c) Viability, as determined by cell permeability (Trypan Blue), of asynchronous QGY 7703 cells treated with 20 nM of control siRNA or siRNAs targeting either LSF or LBP1A. Data were generated 120 hours post transfection and include 3 independent experiments. (d) QGY-7703 cells were transfected with control siRNA targeting either LSF or a control, or treated with 3.6 μM of FQI1 or vehicle. The cells were synchronized at the G1/S border and released. Cells were analyzed 48 hours after release for cell viability using cell titer blue (Promega). Standard error bars were derived from 3 independent experiments. (e) Synchronized QGY-7703 cells were analyzed for caspase activation at 8 and 48 hours post release in presence of 20 nM of LSF or 3.6 μM of FQI1. Compiled data from all three time points depicted as percent of the vehicle control. Standard deviation derived from two independent experiments. Statistical significance was determined using a Student T Test; * $P<0.05$, ** $P<0.01$, *** $P<0.001$, **** $P<0.0001$

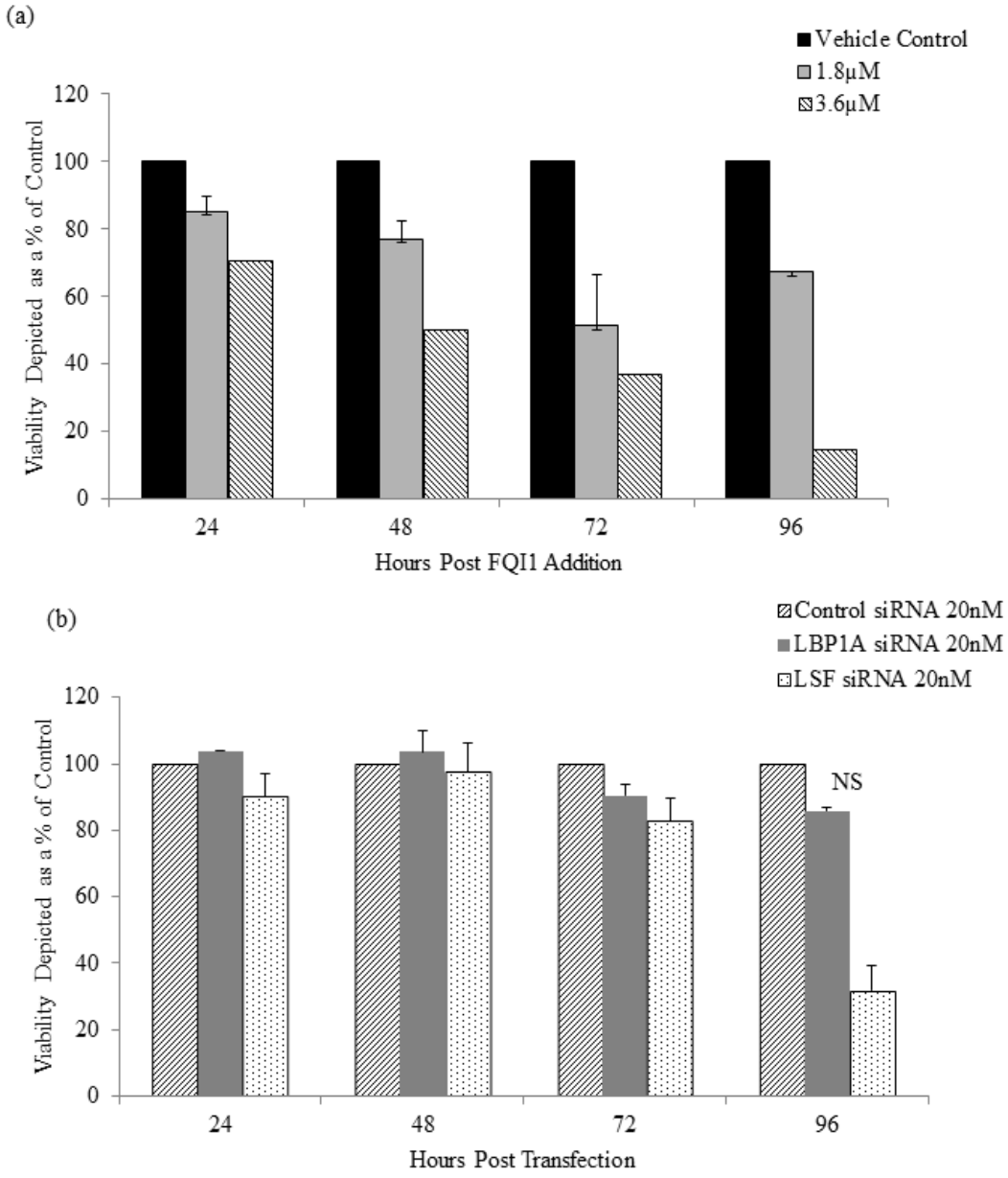
(a)
Vehicle Control
1.8µM
3.6µM
Viability Depicted as a % of Control
120
100
80
60
40
20
0
24
48
72
96
Hours Post FQI1 Addition
(b)
Control siRNA 20nM
LBP1A siRNA 20nM
LSF siRNA 20nM
Viability Depicted as a % of Control
120
100
80
60
40
20
0
NS
24
48
72
96
Hours Post Transfection

(c)

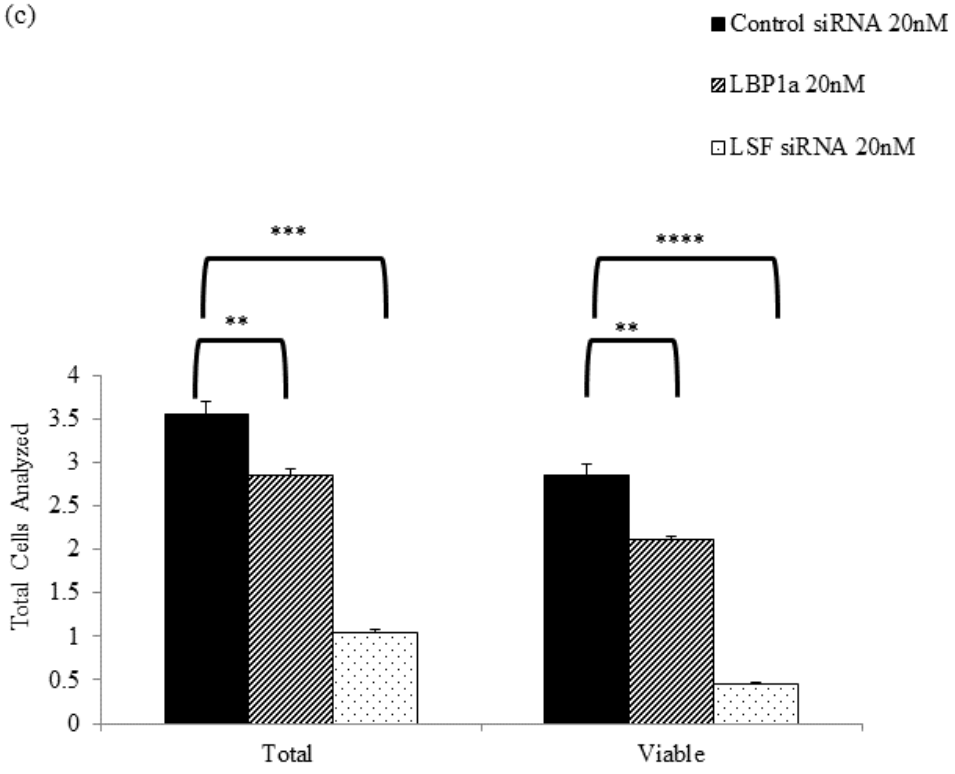
Control siRNA 20nM
LBP1a 20nM
LSF siRNA 20nM
***
****
**
**
Total Cells Analyzed
4
3.5
3
2.5
2
1.5
1
0.5
0
Total
Viable

(d)

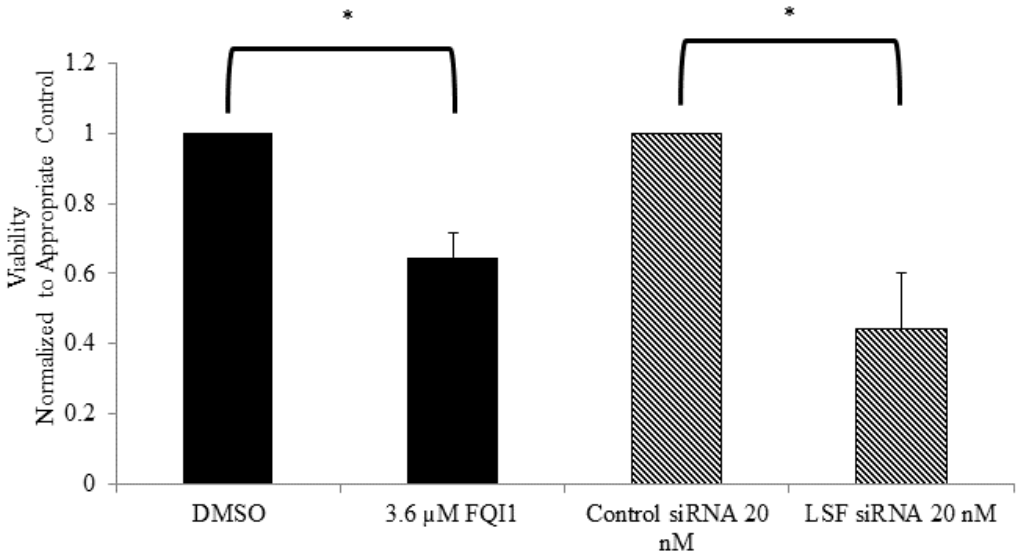
*
*
1.2
1
0.8
0.6
0.4
0.2
0
Viability Normalized to Appropriate Control
DMSO
3.6 µM FQI1
Control siRNA 20 nM
LSF siRNA 20 nM

(e)

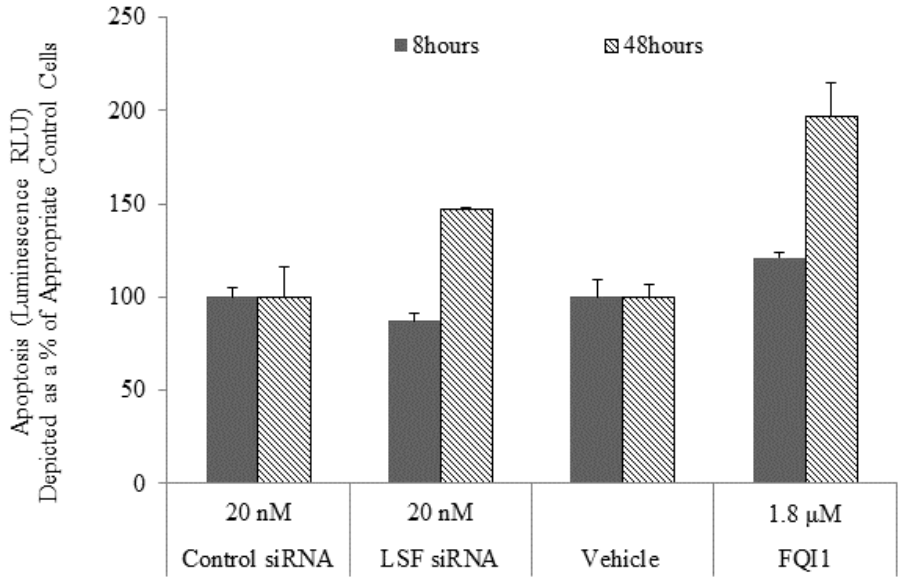
250
200
150
100
50
0
8hours
48hours
Apoptosis (Luminescence RLU) Depicted as a % of Appropriate Control Cells
20 nM Control siRNA
20 nM LSF siRNA
Vehicle
1.8 µM FQI1

Figure 4.4 Synchronization of HCC cells after LSF knockdown reveals two distinct phenotypes: a static 2n DNA population and a population progressing from 2n to 4n DNA content transitioning to a subG1 population.

QGY-7703 cells were synchronized at the G1/S border post transfection with 20 nM control siRNA or 5, 10, or 20 nM LSF siRNA (Illustration 4.2). At 0, 3.5, 8 and 18 hours after release from the block, cells were fixed and stained with propidium iodide for analysis of DNA content by flow cytometry. Data are representative of greater than 4 experiments.

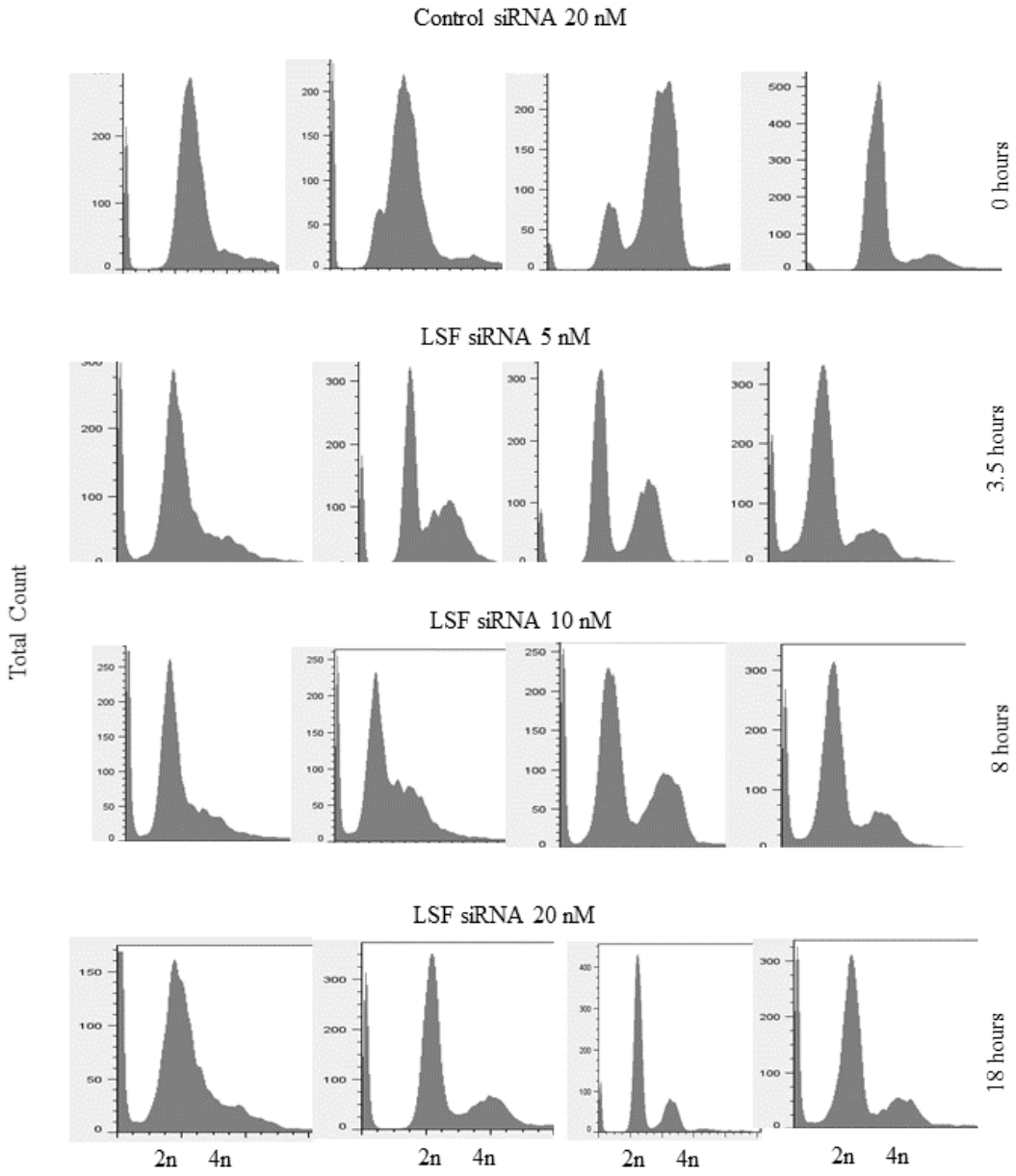
Control siRNA 20 nM
LSF siRNA 5 nM
LSF siRNA 10 nM
LSF siRNA 20 nM
0 hours
3.5 hours
8 hours
18 hours
Total Count
2n
4n
FL2 Area

Figure 4.5 Synchronization of HCC cells after LBP1A knockdown does not impact cell cycle progression.

QGY-7703 cells were synchronized at the G1/S border 24 hours post transfection with LBP1A or control siRNA at 20 nM (Illustration 4.2). At 0, 4, and 8 hours post release, cells were fixed and stained with propidium iodide for analysis of DNA content by flow cytometry. (a) Untreated cells were synchronized and analyzed at 0 hours. Synchronized HCC cells transfected with (b) control siRNA or (c) siRNA targeting LBPA1a. Data are representative of 3 independent experiments.

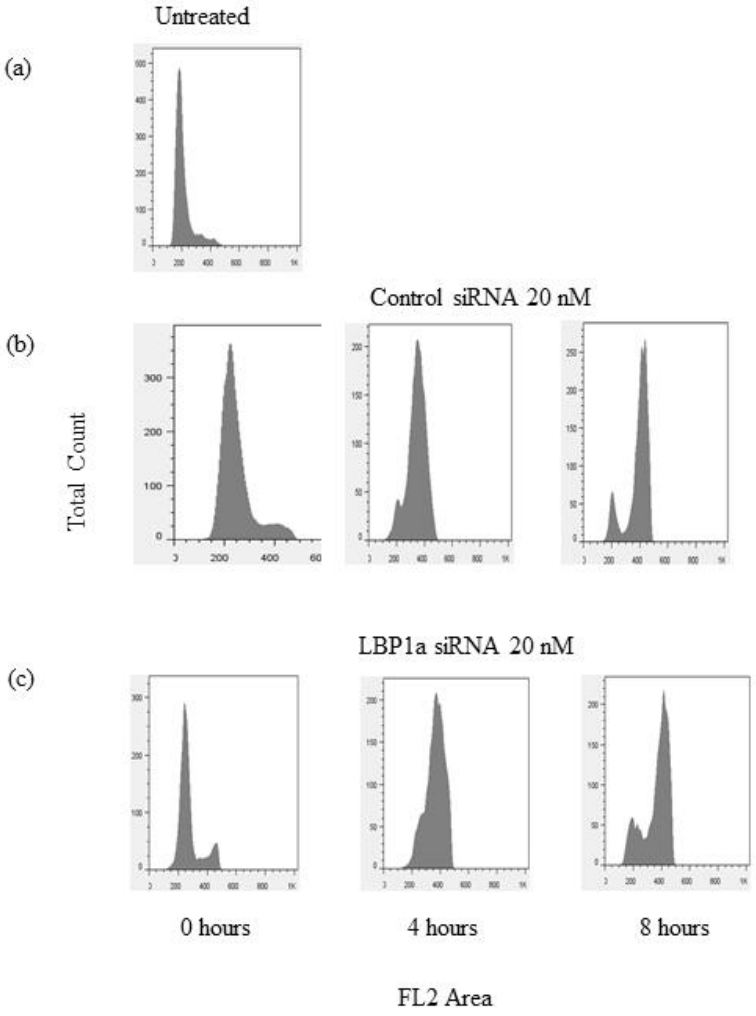
Untreated
(a)
Control siRNA 20 nM
(b)
Total Count
LBP1a siRNA 20 nM
(c)
0 hours
4 hours
8 hours
FL2 Area

Figure 4.6 Synchronized HCC cells treated with FQI1 reveal a G1/S population, and accumulation at 4n

FQI1-treated QGY-7703 cells were synchronized at the G1/S border using a double thymidine block (Illustration 4.1). Cells were incubated with 0.9, 1.8, or 3.6 μM of FQI1 or vehicle. At 0, 4.5, 5.5, 8.5, and 16 hours post release from the G1/S block, cells were fixed and stained with propidium iodide for analysis of DNA content by flow cytometry. These data are representative of at least 3 independent experiments.

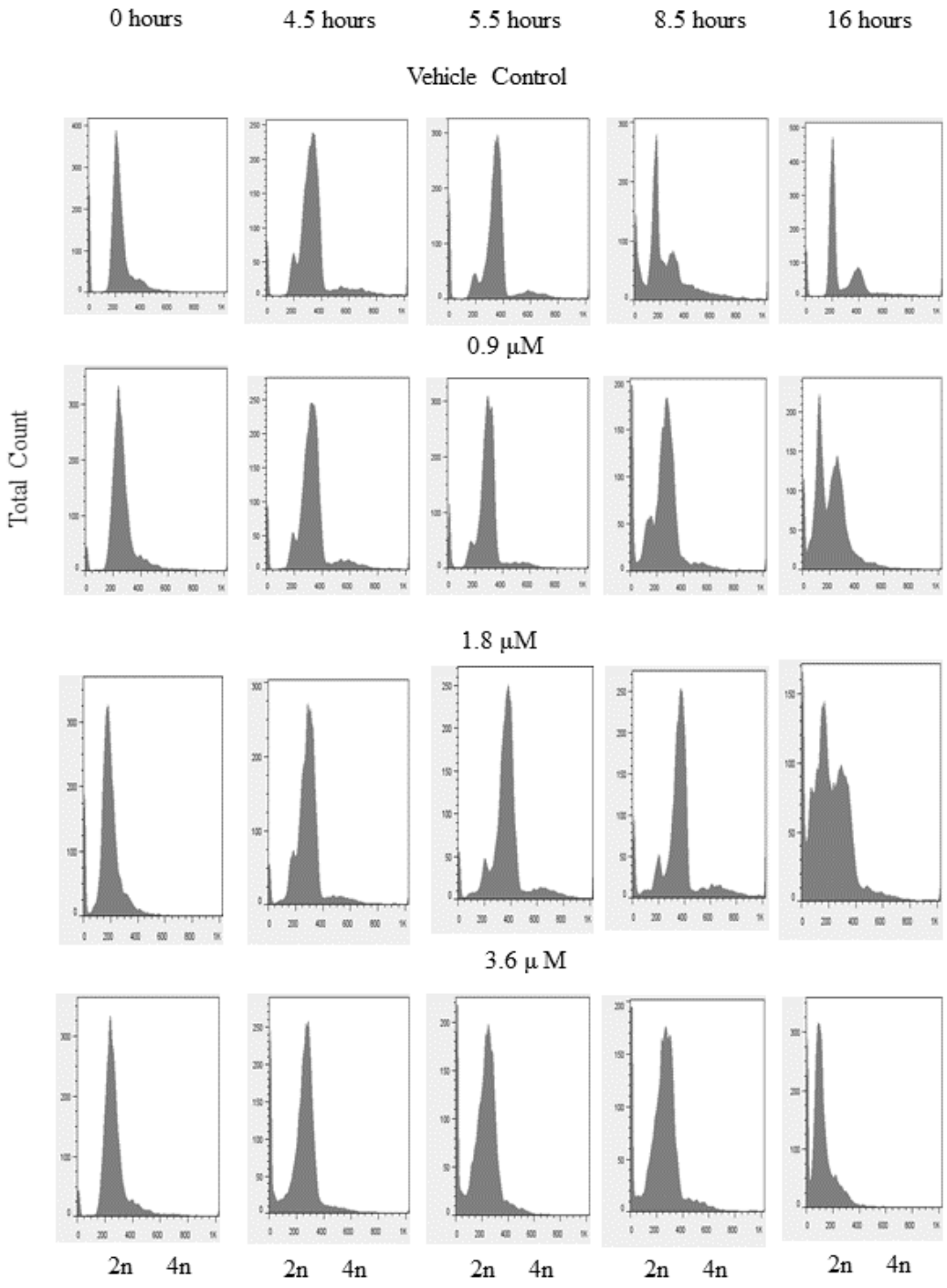
0 hours
4.5 hours
5.5 hours
8.5 hours
16 hours
Vehicle Control
0.9 µM
1.8 µM
3.6 µ M
Total Count
2n 4n
2n 4n
2n 4n
2n 4n
2n 4n
FL2 Area

Figure 4.7 LSF removal or inhibition in synchronized HCC cells results in cellular senescence

FQI1-treated QGY-7703 cells were synchronized at the G1/S border using a double thymidine block. Cells were incubated with 0.9, 1.8, or 3.6 μM of FQI1 or vehicle (Illustration 4.1), or with Control or LSF siRNA (Illustration 4.2), and then fixed and stained for β-galactosidase activity at 8 h after release from the G1/S block. Phase contrast images were taken at 20x magnification. Representative images are shown for cells treated with (a) 20 nM Control siRNA, (b) 20 nM LSF siRNA, (c) Vehicle (DMSO) or (d, e and f) 0.9, 1.8, and 3.6 μM of FQI1, respectively. Images in (a-f) are representative of 3 independent experiments. (g-j) Representative images are shown from three independent experiments evaluating LSF siRNA at dose levels including 5, 10, and 20 nM in comparison to control siRNA at 20 nM. (k,l) The correlation of increasing FQI1 concentrations or increasing siRNA concentrations with the number β-galactosidase positive cells is depicted as a percentage of the control for each individual experiment. 75 cells were analyzed per condition. Statistical significance was determined using a Student T Test; * $P<0.05$, ** $P<0.01$, *** $P<0.001$, **** $P<0.0001$

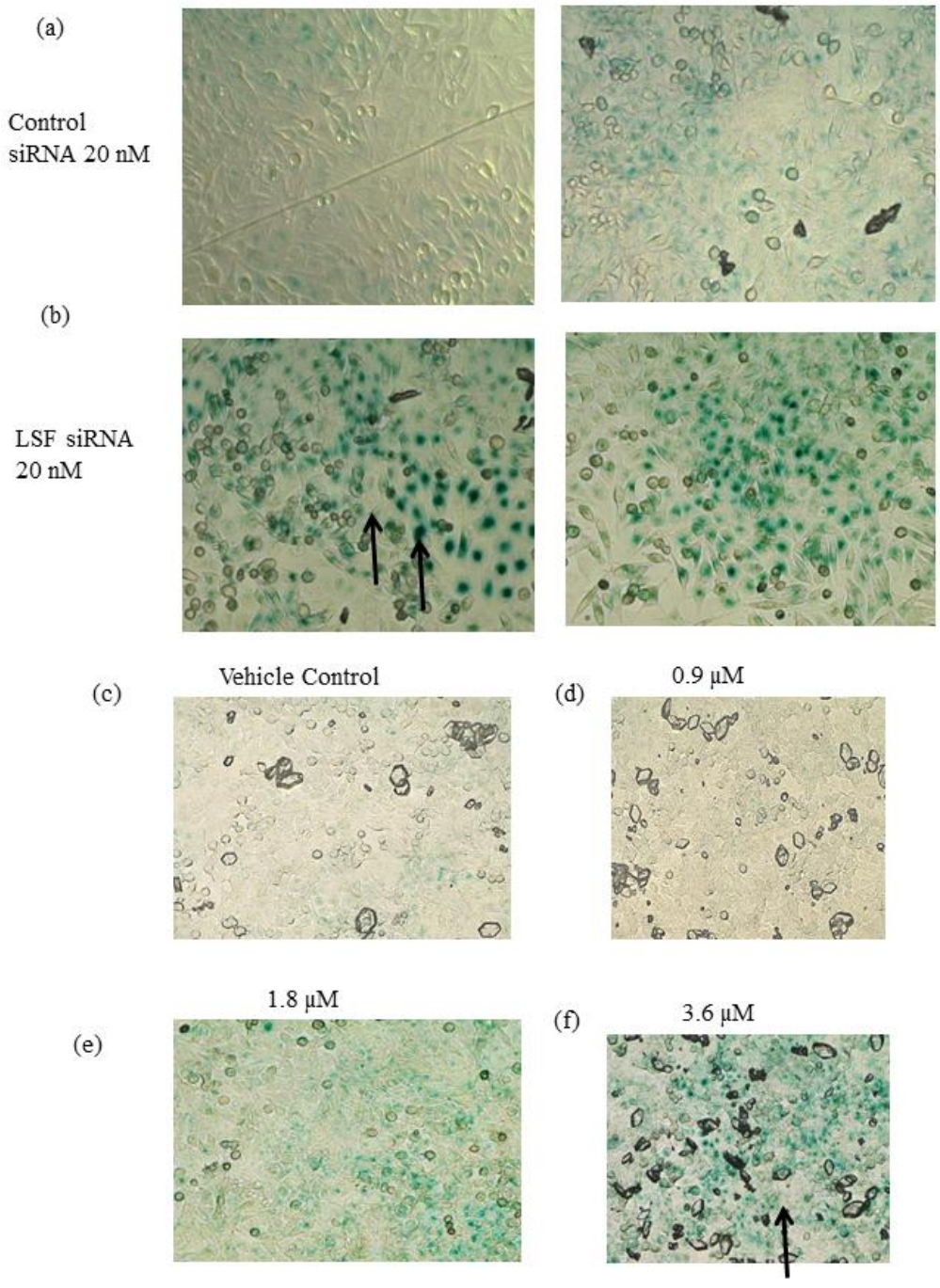
(a)
Control
siRNA 20 nM
(b)
LSF siRNA
20 nM
(c)
Vehicle Control
(d)
0.9 µM
(e)
1.8 µM
(f)
3.6 µM

(g) Control siRNA 20 nM

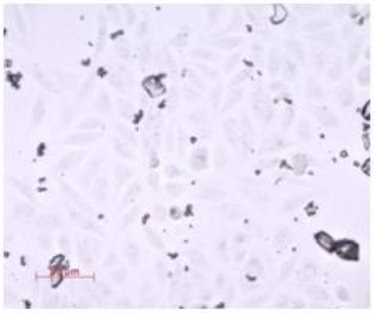

(h) LSF siRNA 5 nM

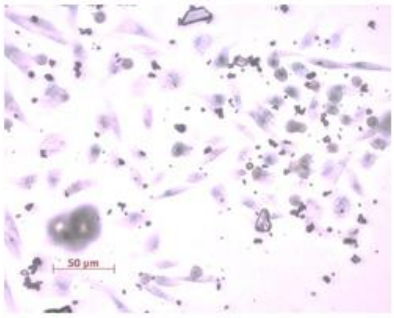

(i) LSF siRNA 10 nM

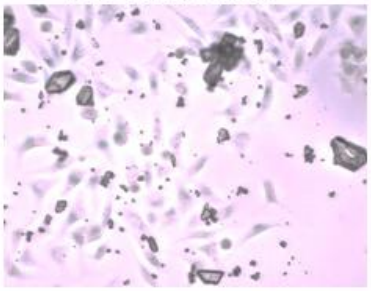

(j) LSF siRNA 20 nM

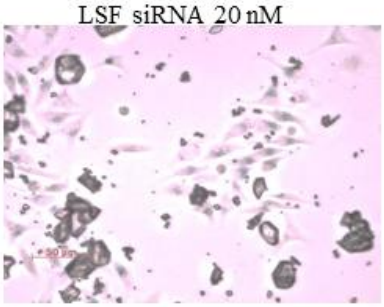

(k)

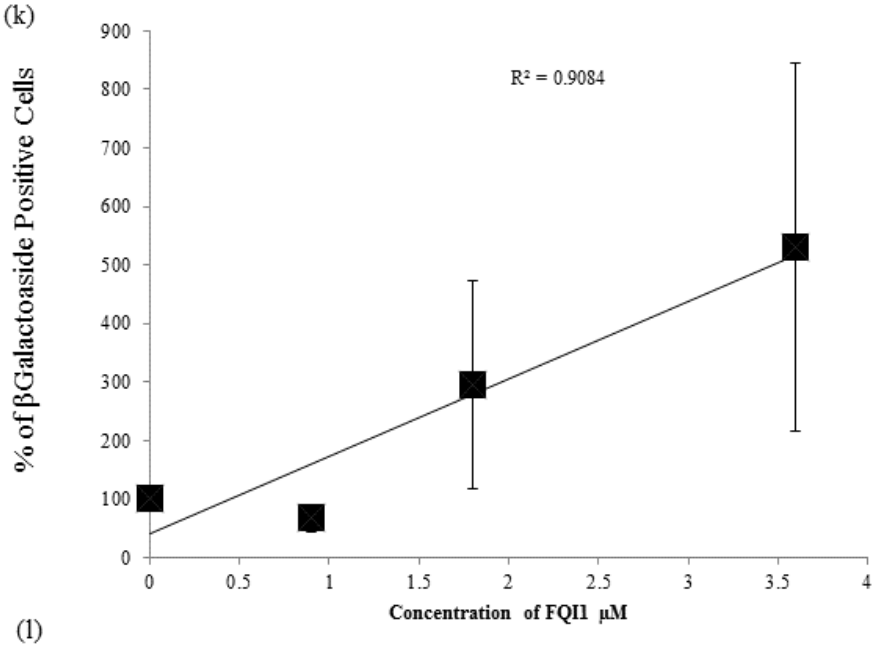
% of βGalactoaside Positive Cells
R² = 0.9084
900
800
700
600
500
400
300
200
100
0
0
0.5
1
1.5
2
2.5
3
3.5
4
Concentration of FQI1 µM

(l)

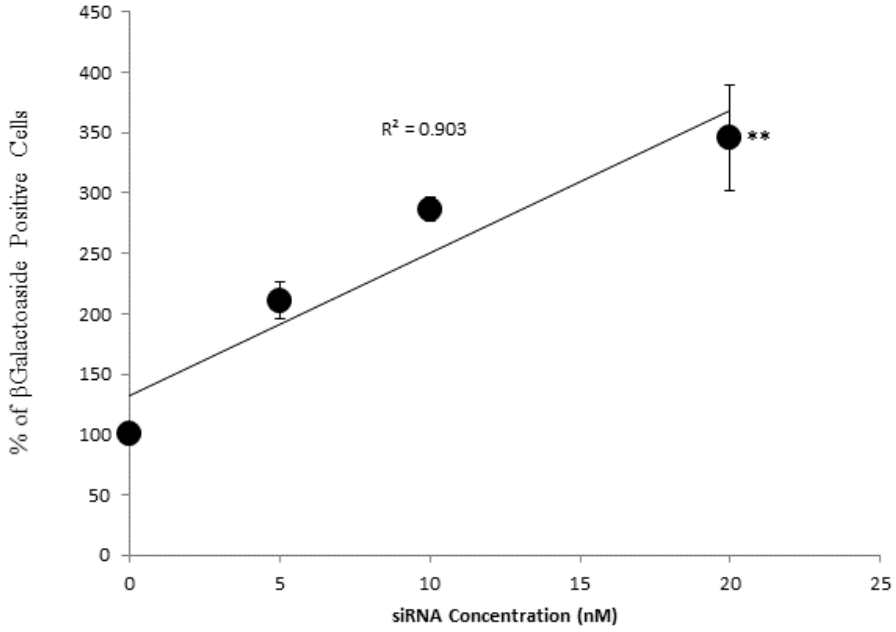
% of βGalactoaside Positive Cells
R² = 0.903
**
450
400
350
300
250
200
150
100
50
0
0
5
10
15
20
25
siRNA Concentration (nM)

Figure 4.8 γ-H2AX levels remain minimal prior to mitosis in synchronized QGY-7703 cells treated with either LSF knockdown or FQI1 treatment.

(a) QGY-7703 cells were treated with LSF siRNA or control siRNA at 20 nM and synchronized with a single thymidine block, as indicated in Illustration 4.3. Cells were collected at 4 and 16 hours post release from the G1/S block, fixed, and probed with an anti γ-H2AX antibody directly conjugated Alexa 488 to measure double stranded DNA breaks. In addition, the cellular DNA was stained with propidium iodide. Data were analyzed by flow cytometry. (b) QGY-7703 cells were synchronized with a single thymidine block at the G1/S border following incubation with 1.8 μM FQI1 or vehicle and then released. γ-H2AX staining in FQI1 treated cells versus vehicle was analyzed as in (a) at 4 and 16 hours post release from the G1/S block. The percentage of cells in the indicated gate is shown in each panel at the top. (c,d) Cells treated as in (a) and (b), respectively, were stained with anti-γ-H2AX antibody but analyzed by immunofluorescence at 63x magnification 8 hours post release from a G1/S block. All images were taken at the same exposure. Representative images are displayed in (c) for control siRNA (left) and LSF siRNA (right), and an ultra-violet treated control (bottom left) and in (d) for vehicle (left) and 1.8 μM FQI1 treated cells (right). (e) Asynchronous QGY-7703 cells treated with LSF siRNA or control were collected at 24 and 48 hours post treatment and stained for anti-γ-H2AX. (f) Asynchronous cells treated with 0.9, 1.8 or 3.6 μM of FQI1 were collected at 24 and 48 hours post treatment and stained for anti-γ-H2AX. Representative images are shown for each time point.

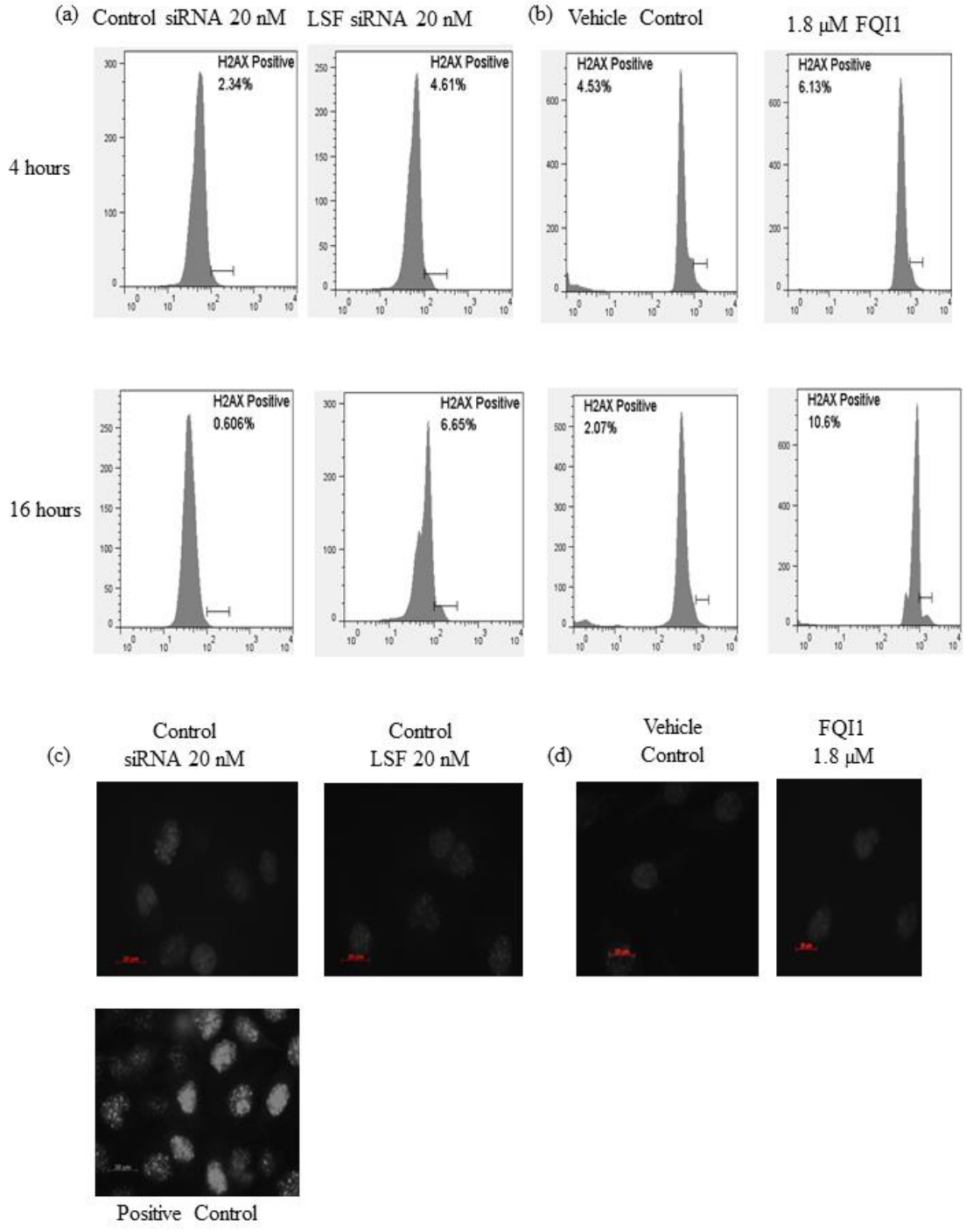
(a) Control siRNA 20 nM
LSF siRNA 20 nM
(b) Vehicle Control
1.8 μM FQI1
4 hours
16 hours
H2AX Positive
2.34%
H2AX Positive
4.61%
H2AX Positive
4.53%
H2AX Positive
6.13%
H2AX Positive
0.606%
H2AX Positive
6.65%
H2AX Positive
2.07%
H2AX Positive
10.6%
(c)
Control
siRNA 20 nM
Control
LSF 20 nM
(d)
Vehicle
Control
FQI1
1.8 μM
Positive Control

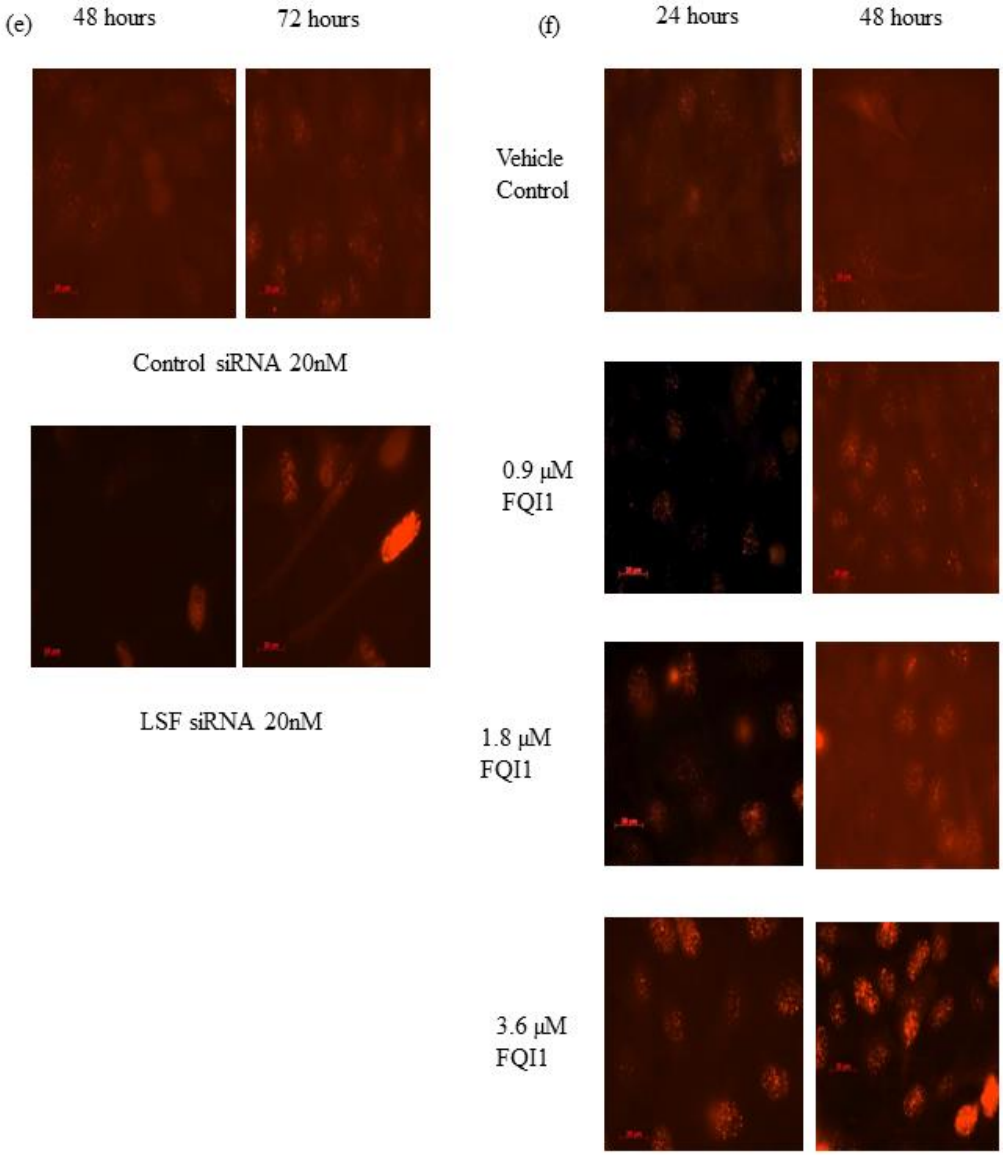
(e)
48 hours
72 hours
Control siRNA 20nM
LSF siRNA 20nM
(f)
24 hours
48 hours
Vehicle Control
0.9 µM FQI1
1.8 µM FQI1
3.6 µM FQI1

Figure 4.9 Immunofluorescent analysis of synchronized HCC cells with LSF knockdown or FQI1 treatment reveal multi-nucleation and cell division defects

(a,b) QGY 7703 cells were synchronized at the G1/S border following transfection with LSF or control siRNA at 20 nM, and then released to progress through the cell cycle, as depicted in the schematic at the top. Cells were fixed and probed with an anti-LSF (red) and anti-alpha tubulin (green) antibody and stained with DAPI (blue) at multiple time points to analyze mitotic figures. Images were analyzed at 16 hours post release at 63x magnification. 89-102 individual cells were analyzed within each group. (a) Representative images 16 hours post release revealing cells still in prometaphase/metaphase, aberrant cell division and multi-nucleation in cells with LSF knockdown as well as examples of normal mitotic figures in the control siRNA group including metaphase and telophase at earlier time points. (b) Quantitation of mitotic cells as well as observations of apoptosis determined by fragmented nuclei and multi-nucleation. 100 individual cells were analyzed within each group at 16 hours post release. (c,d) QGY 7703 cells were synchronized at the G1/S border following incubation with vehicle control or FQI1 at concentrations of 1.8 or 3.6 μM and then released (Illustration 4.1). QGY 7703 cells were fixed and probed with an anti-LSF antibody, anti-α-tubulin antibody and then stained with DAPI to analyze mitotic figures. Images were analyzed at 16 hours post release at 63x magnification. 100 individual cells were analyzed within each group. (c) Representative images 16 hours post release revealing signs of aberrant cytokinesis, and multi-nucleation in the FQI1 treated cells. (d) Quantitation of cellular phenotypes. 98-107 individual cells were analyzed within each group.

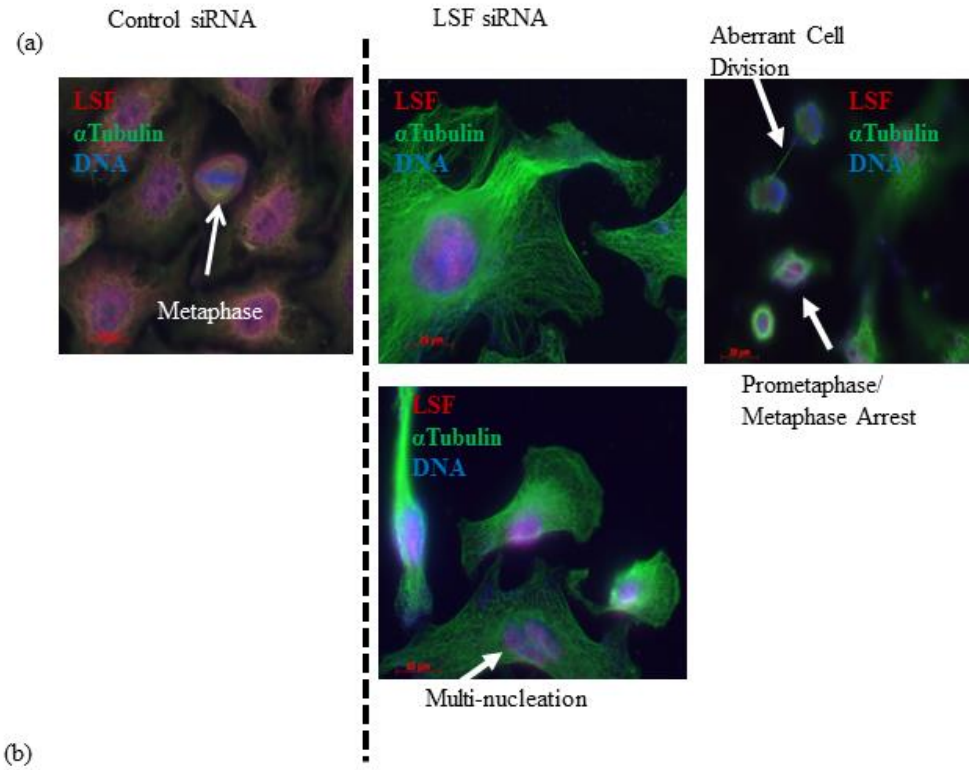
(a)
Control siRNA
LSF siRNA
Aberrant Cell Division
LSF
αTubulin
DNA
Metaphase
Prometaphase/ Metaphase Arrest
Multi-nucleation
(b)
Interphase
Cytokinesis
Prometaphase/Metaphase Arrest
Aberrant Cytokinesis
Multi-nucleation
Percentage of Cells Analyzed
100
90
80
70
60
50
40
30
20
10
0
20nM
Control siRNA
20nM
LSF siRNA

(c)

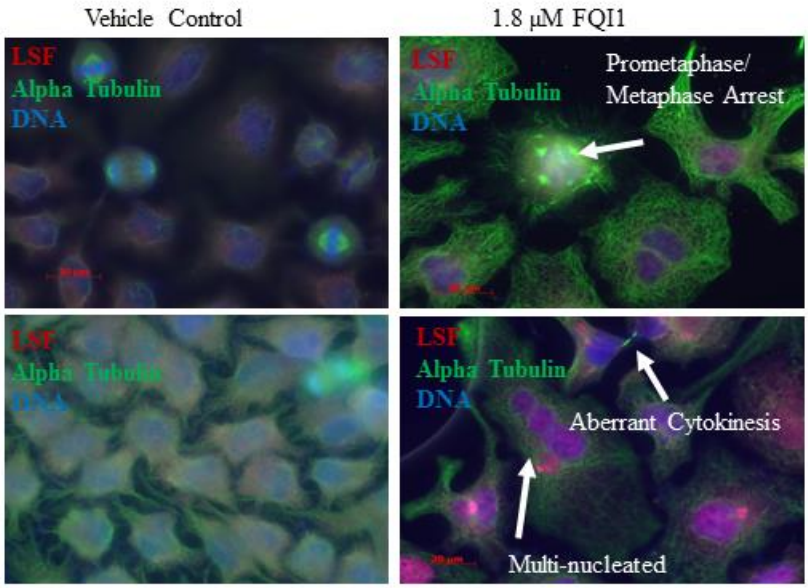
Vehicle Control
1.8 μM FQI1
LSF
Alpha Tubulin
DNA
Prometaphase/
Metaphase Arrest
Aberrant Cytokinesis
Multi-nucleated

(d)

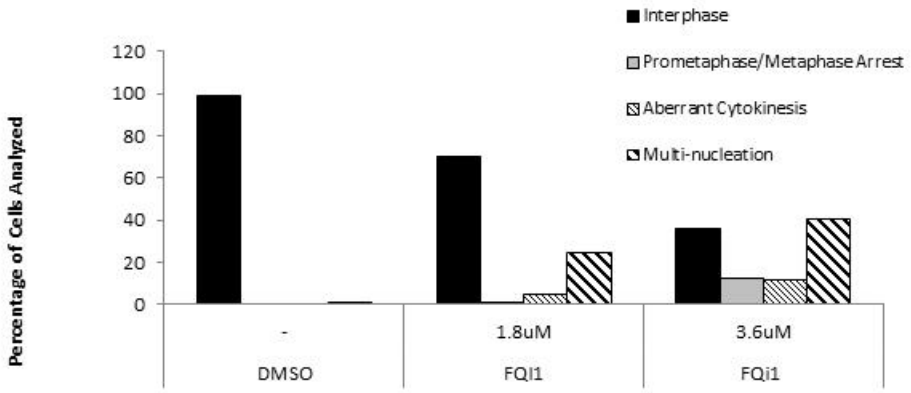
Interphase
Prometaphase/Metaphase Arrest
Aberrant Cytokinesis
Multi-nucleation
Percentage of Cells Analyzed
120
100
80
60
40
20
0
-
DMSO
1.8uM
FQI1
3.6uM
FQi1

Figure 4.10 Immunofluorescent analysis of FQI1 and siRNA treated HCC cells reveals prometaphase/metaphase arrest

Synchronized HCC cells were treated with either 20 nM of LSF siRNA or 1.8 μM FQI1. Cells were collected 8 hours post release from the final G1/S block and stained for α-tubulin and DNA. DNA is shown in FQI1 treated or LSF siRNA treated cells on bottom (b,d), Alpha-Tubulin staining shown on top (a,c). Representative images of a prometaphase-metaphase delay are shown.

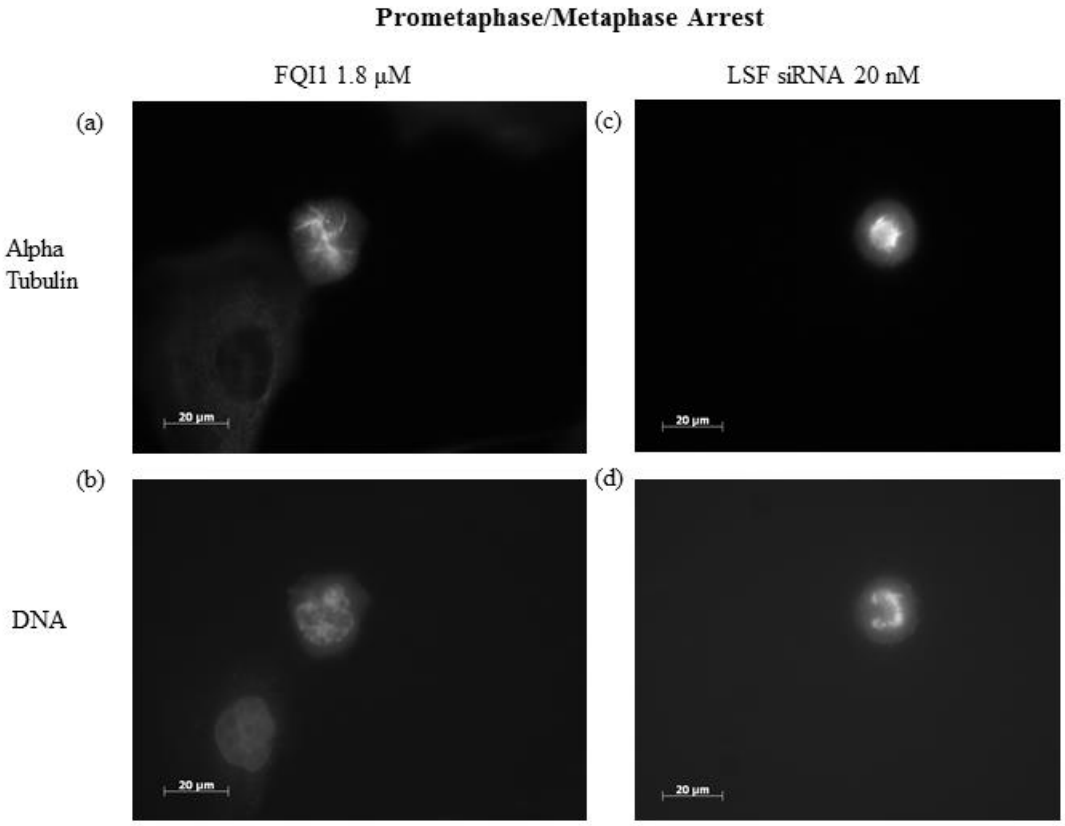

Figure 4.11 Immunofluorescent analysis of FQI1 and siRNA treated HCC cells reveal aberrant cell division

Synchronized HCC cells were treated with either 20 nM of LSF siRNA or 1.8 μM of FQI1. Cells were harvested 16 hours post release and stained for α-tubulin and DNA. DNA is shown in FQI1 treated or LSF siRNA treated cells on the right (b,d,f), α--tubulin staining is shown on the left (a,c,e). Representative images of cells exhibiting an aberrant cell division are shown.

Aberrant Cell Division

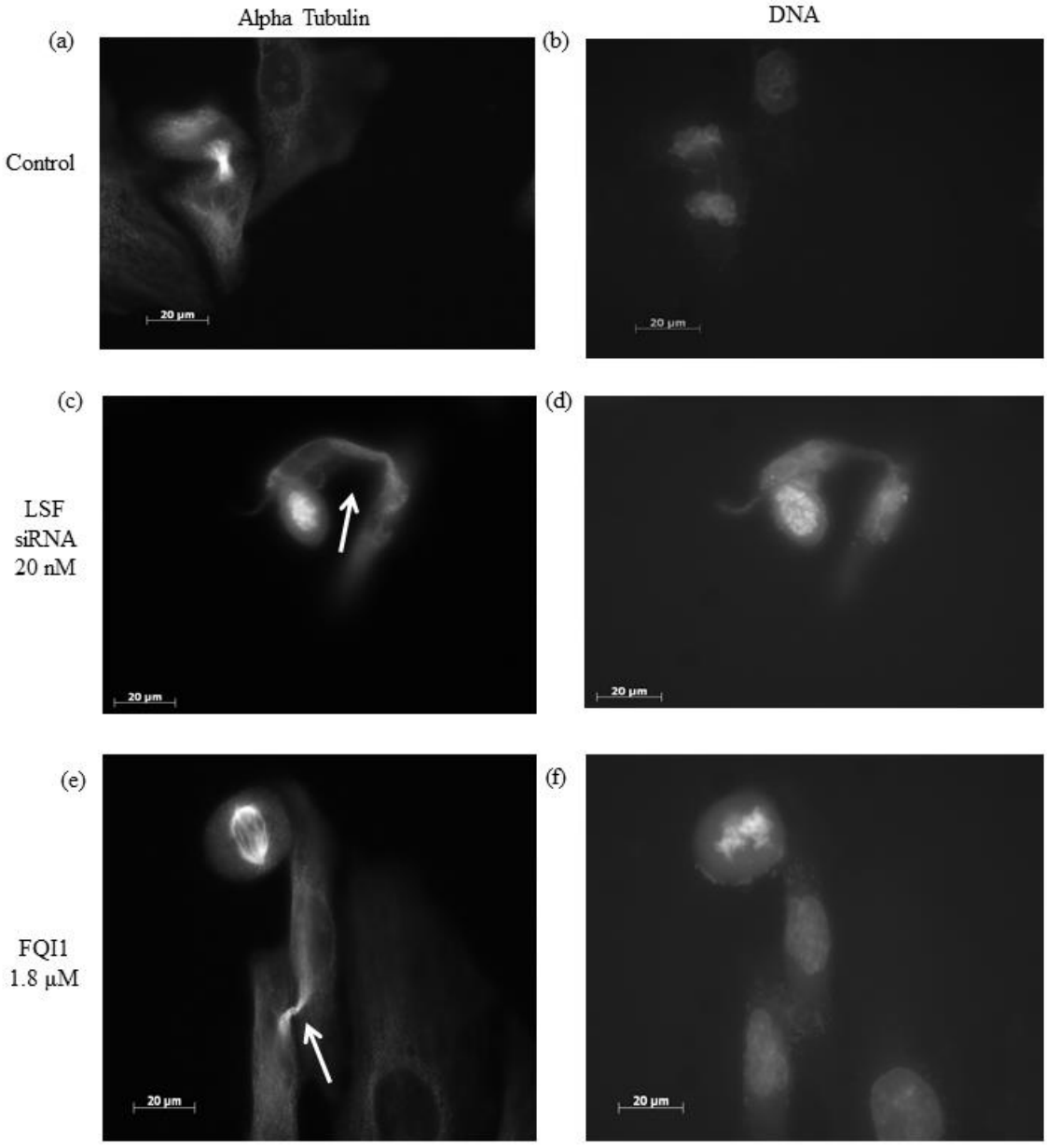

Figure 4.12 Immunofluorescent analysis of FQI1 and siRNA treated HCC cells reveals multinucleated cells

Synchronized HCC cells were treated with either 20 nM of LSF siRNA or 1.8 μM of FQI1. Cells were harvested 16 hours post release and stained for α-tubulin and DNA. DNA is shown in FQI1 treated or LSF siRNA treated cells on bottom (b,d), alpha-tubulin staining shown on top (a,c). Representative images of multinucleated cells are shown.

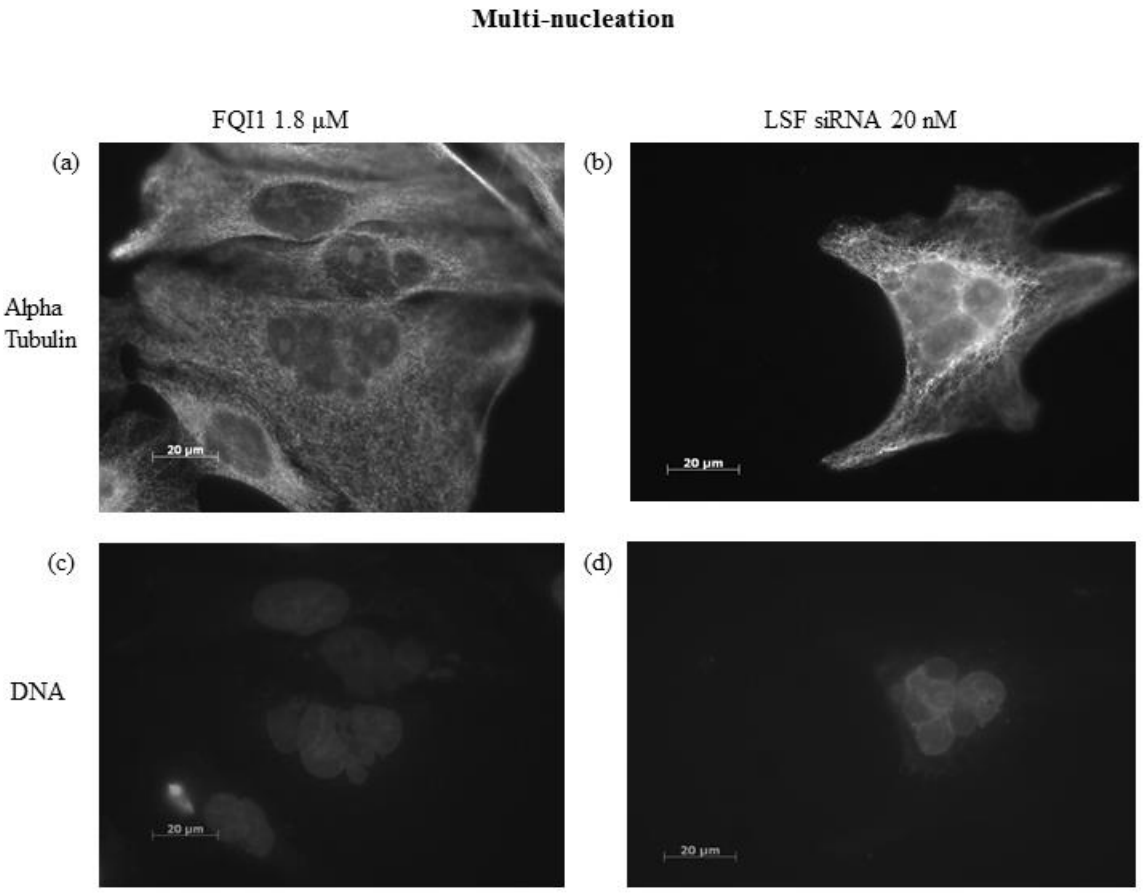

Figure 4.13 Protein expression of Aurora Kinase B, Cdc20, and Cyclin B is decreased in synchronized HCC cells upon reduction of LSF protein levels

QGY-7703 cells transfected with siRNA were synchronized and harvested 8 hours post release from a G1/S block. Cell lysates were probed for a variety of proteins involved in mitosis. (a) Immunoblot images of lysates collected 9 hours post release from a G1/S block for LSF, Cyclin A, Cyclin B, Cdc20, Aurora Kinase B, pH3 Ser10, and pH3 Ser28. Beta actin levels were used to control for differential loading. Quantitation of the levels of (b) Aurora Kinase B and (c) Cdc20 normalized to beta actin levels. Data are representative from 3 independent studies. Statistical significance was determined using a Student T Test; * $P<0.05$, ** $P<0.01$, *** $P<0.001$, **** $P<0.0001$

(a)

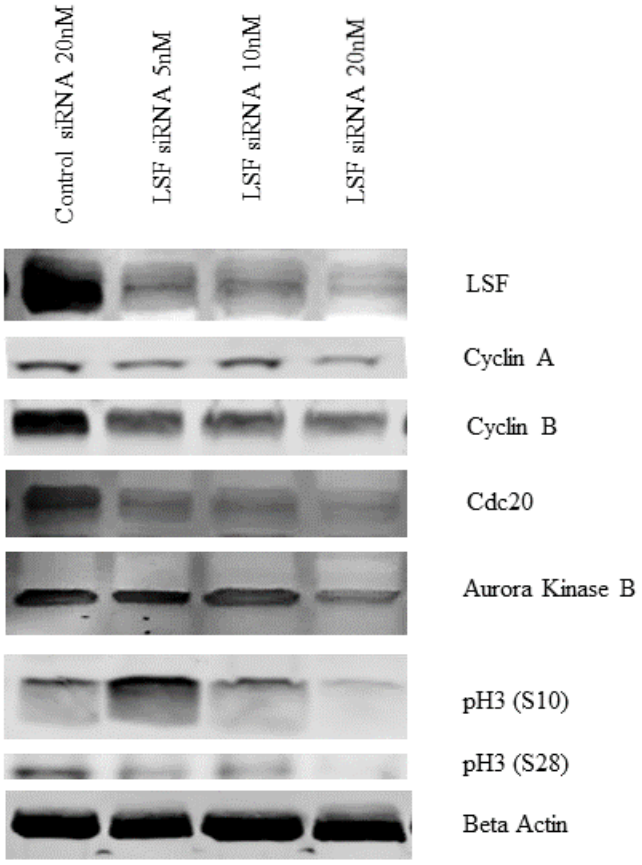
Control siRNA 20nM
LSF siRNA 5nM
LSF siRNA 10nM
LSF siRNA 20nM
LSF
Cyclin A
Cyclin B
Cdc20
Aurora Kinase B
pH3 (S10)
pH3 (S28)
Beta Actin

(b)

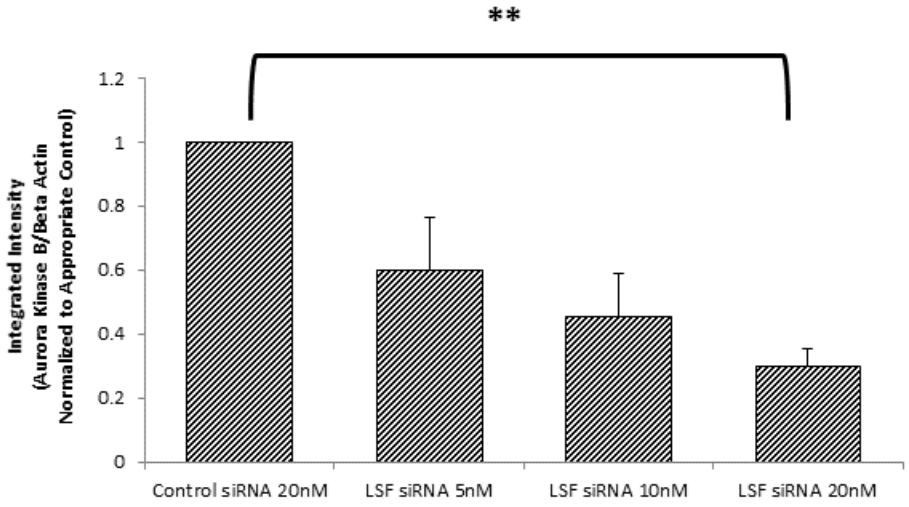
**
Integrated Intensity
(Aurora Kinase B/Beta Actin
Normalized to Appropriate Control)
1.2
1
0.8
0.6
0.4
0.2
0
Control siRNA 20nM
LSF siRNA 5nM
LSF siRNA 10nM
LSF siRNA 20nM

(c)

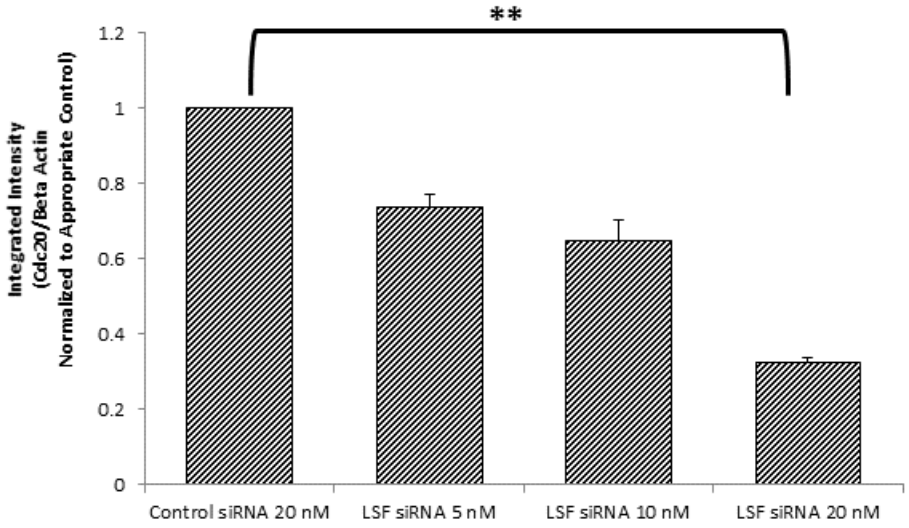
**
Integrated Intensity
(Cdc20/Beta Actin
Normalized to Appropriate Control)
1.2
1
0.8
0.6
0.4
0.2
0
Control siRNA 20 nM
LSF siRNA 5 nM
LSF siRNA 10 nM
LSF siRNA 20 nM

Figure 4.14 Protein expression of Aurora Kinase B, Cdc20, and Cyclin B are significantly reduced in synchronized HCC cells treated with FQI1

FQI1 treated QGY 7703 cells were synchronized at the G1/S border using a double thymidine block. Cells were incubated with 0.9, 1.8, or 3.6 μM of FQI1 or vehicle control. Lysates were probed for proteins of interest. (a) Western blot images for lysates collected 9 hours post release from a G1/S block for LSF, Cyclin A, Cyclin B, Cdc20, Aurora Kinase B, and pH3 S10. Beta actin levels were used to control for differential loading. Quantitation of the levels of (b) Cdc20 and (c) Cyclin B, (d) Aurora B Kinase, (e) Phosphorylated Histone 3 Serine 10 normalized to Beta Actin levels. Data are representative of 2-4 independent experiments. Standard error calculated where data were averaged from 3 independent studies. Statistical significance was determined using a Student T Test; * $P<0.05$, ** $P<0.01$, *** $P<0.001$, **** $P<0.0001$

(a)

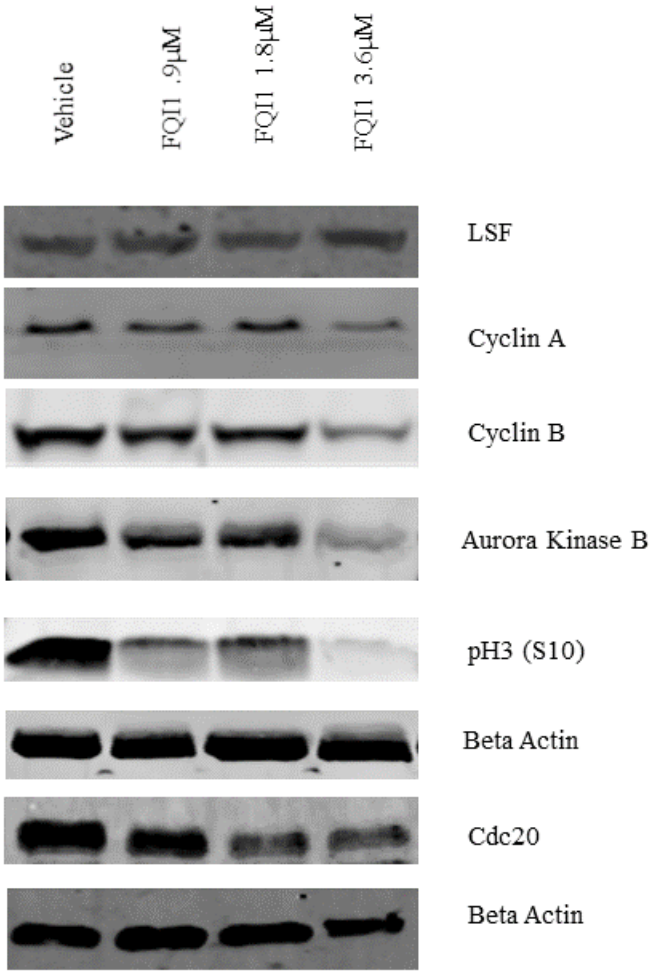
Vehicle
FQI1 .9μM
FQI1 1.8μM
FQI1 3.6μM
LSF
Cyclin A
Cyclin B
Aurora Kinase B
pH3 (S10)
Beta Actin
Cdc20
Beta Actin

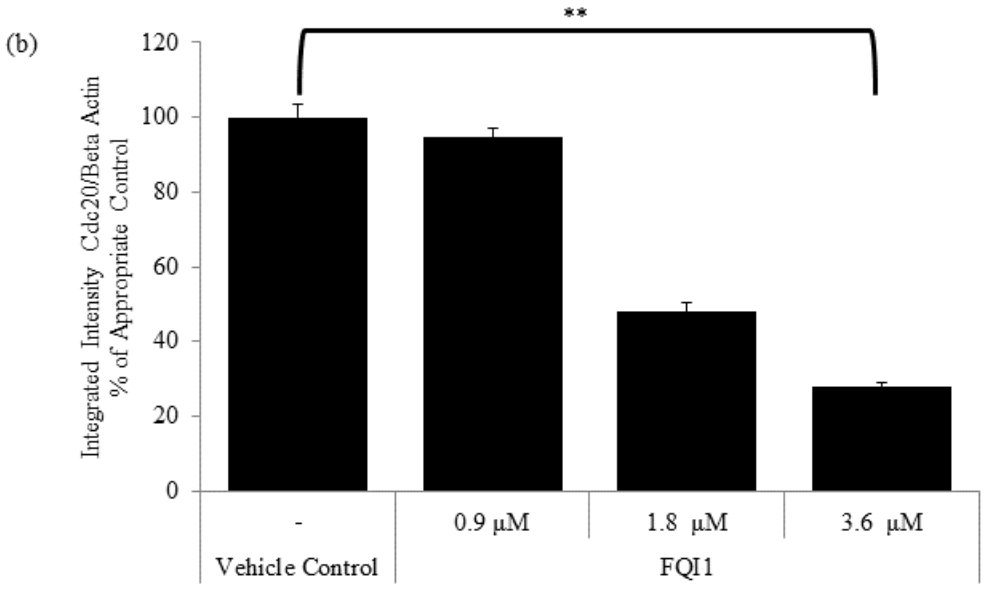
(b)
**
120
100
80
60
40
20
0
Integrated Intensity Cdc20/Beta Actin
% of Appropriate Control
-
0.9 µM
1.8 µM
3.6 µM
Vehicle Control
FQI1

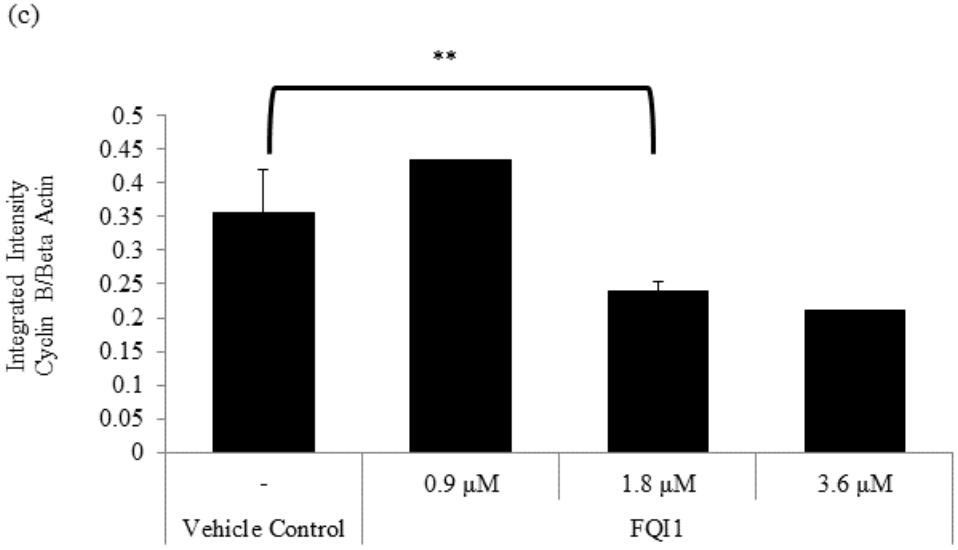
(c)
**
0.5
0.45
0.4
0.35
0.3
0.25
0.2
0.15
0.1
0.05
0
Integrated Intensity
Cyclin B/Beta Actin
-
0.9 µM
1.8 µM
3.6 µM
Vehicle Control
FQI1

(d)

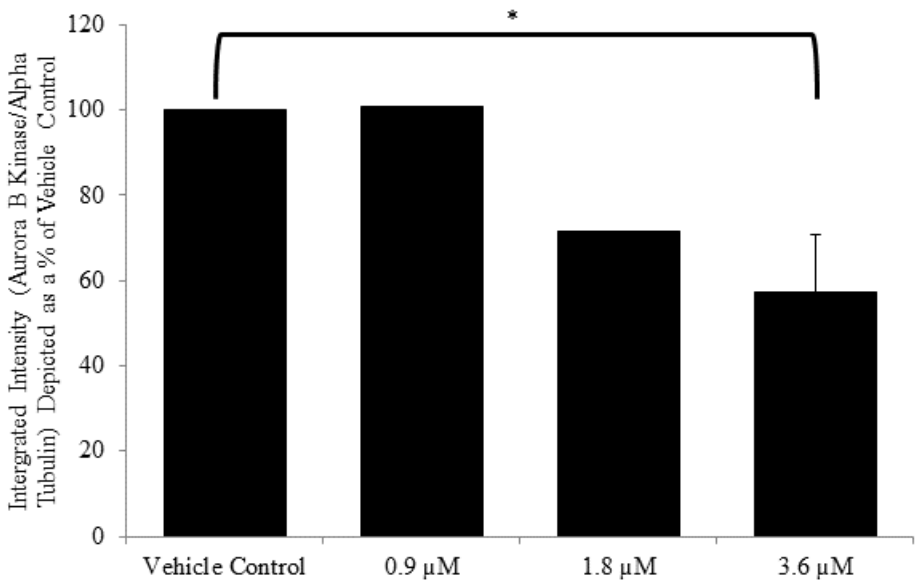
*
120
100
80
60
40
20
0
Intergrated Intensity (Aurora B Kinase/Alpha Tubulin) Depicted as a % of Vehicle Control
Vehicle Control
0.9 µM
1.8 µM
3.6 µM

(e)

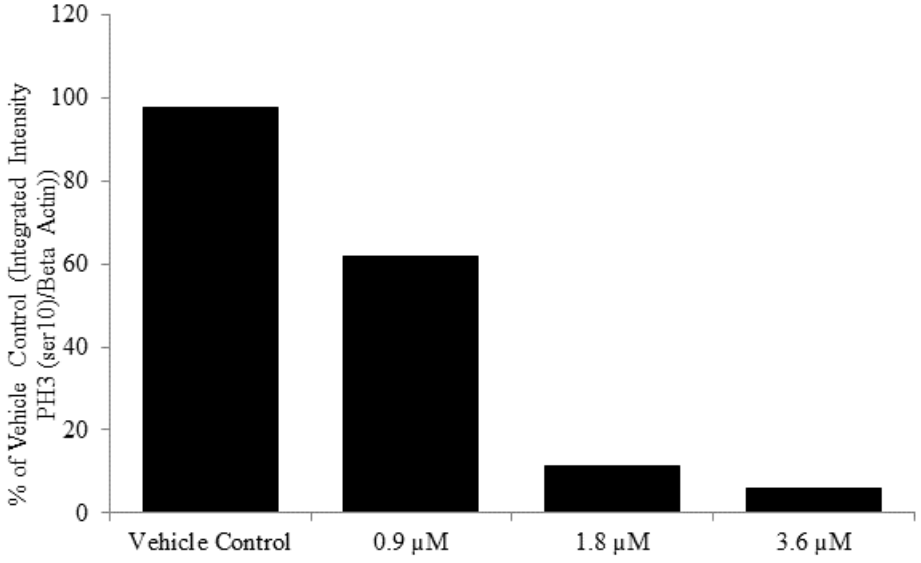
120
100
80
60
40
20
0
% of Vehicle Control (Integrated Intensity PH3 (ser10)/Beta Actin))
Vehicle Control
0.9 µM
1.8 µM
3.6 µM

Figure 4.15 Aurora Kinase B and Cdc20 gene expression is reduced in HCC cells upon inactivating LSF with either LSF siRNA or FQI1

(a-d) QGY-7703 cells transfected with siRNA were synchronized and released as indicated in Illustration 4.2. Cells were harvested between 0 and 8 hours post release from a G1/S block. RNA was isolated for gene expression analysis by qPCR using Taqman probes. The relative levels of gene expression were determined by normalizing RNA levels to those of GAPDH as an internal control. (a) Aurora Kinase B gene expression measured at 0, 4, and 8 hours post release from a G1/S block. Standard error is based on 4 biological replicates for the 8 hour time point. (b) Aurora Kinase B expression normalized to siRNA control 8 hours post release from a G1/S block following treatment with 5, 10, 20 nM of LSF siRNA, 10 nM LBP1A or 10 nM of both LSF and LBP1A siRNA. (c) Cdc20 gene expression was determined on samples treated with the various siRNAs alone or in combination 0, 4, 6 and 8 hours post release from the G1/S block. Standard error is based 4 biological replicates for the 8 hour time point (d) Cdc20 expression determined on samples treated with siRNA targeting a control, LSF, LBP1A or a combination at 8 hours post release from a G1/S block. Concentrations were 20 nM for the control siRNA, 5, 10, or 20 nM for LSF siRNA, or a combination of with 10 nM of LBP1A siRNA and 10 nM of LSF siRNA. Standard error is based on 2 biological experiments for the 0 and 4 hour time points, and 4 biological experiments for the 8 hour analysis. (e-g) FQI1-treated QGY-7703 cells were synchronized at the G1/S border using a double thymidine block, according to Illustration 4.1. Cells were incubated with either 1.8 μM of FQI1 or vehicle starting at the release from the first G1/S block and maintained throughout the remainder of the time course. Samples were harvested at 0, 4,

and 8 hours post release from the final G1/S block and RNA for gene expression was analyzed by qPCR using Taqman probes. Relative levels of gene expression were determined by normalizing RNA levels to those of GAPDH as an internal control. RNA levels are depicted for (e) LSF, (f) Aurora Kinase B (g) Cdc20 following incubation with either 1.8 μM FQI1 or vehicle. Standard error of the mean was derived from 4 independent experiments. Gene expression for Cyclin A (h,i) or Cyclin B (j,k) was determined at 8 hours post release from the G1/S block for samples treated either with 0.9, 1.8 or 3.6 μM FQI1 vs vehicle control (h,j), or with 20 nM control siRNA or 20 nM LSF siRNA (i,k). SEM derive from 2 independent experiments. Statistical significance was determined using a Student T Test; * $P<0.05$, ** $P<0.01$, *** $P<0.001$, **** $P<0.0001$

(a)

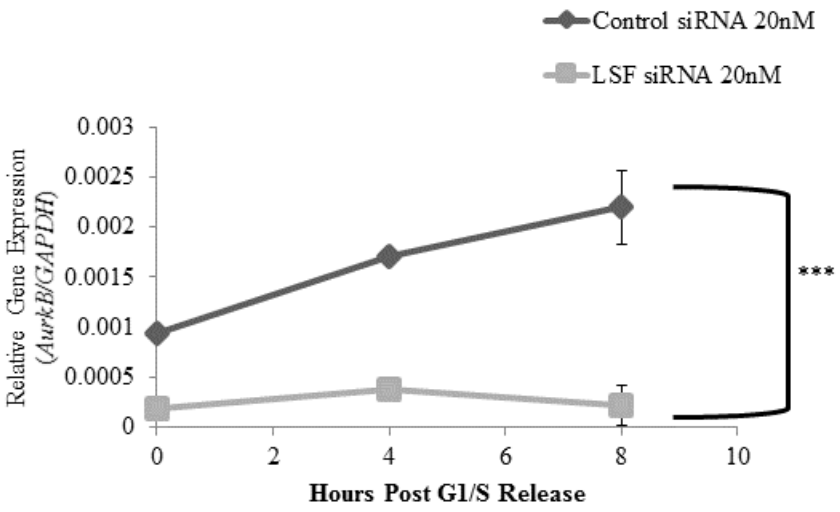
Control siRNA 20nM
LSF siRNA 20nM
Relative Gene Expression (AurkB/GAPDH)
0.003
0.0025
0.002
0.0015
0.001
0.0005
0
0
2
4
6
8
10
Hours Post G1/S Release
***

(b)

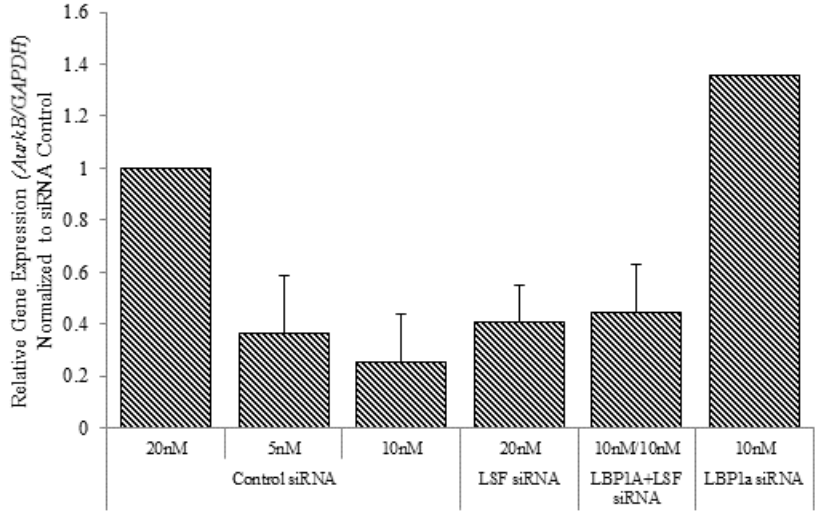
Relative Gene Expression (AurkB/GAPDH) Normalized to siRNA Control
1.6
1.4
1.2
1
0.8
0.6
0.4
0.2
0
20nM
5nM
10nM
Control siRNA
20nM
LSF siRNA
10nM/10nM
LBP1A+LSF siRNA
10nM
LBP1a siRNA

(c)

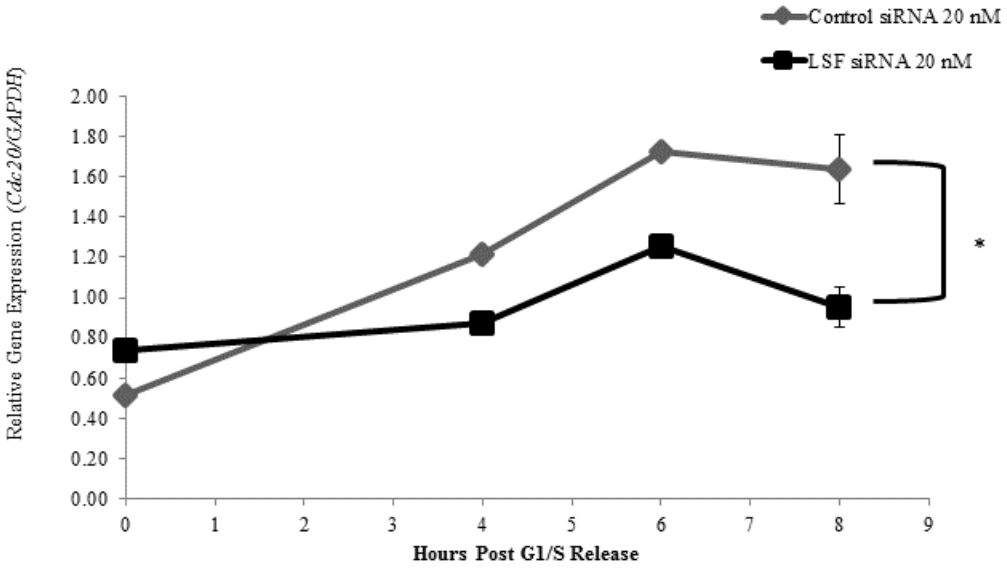
Control siRNA 20 nM
LSF siRNA 20 nM
Relative Gene Expression (Cdc20/GAPDH)
2.00
1.80
1.60
1.40
1.20
1.00
0.80
0.60
0.40
0.20
0.00
0
1
2
3
4
5
6
7
8
9
Hours Post G1/S Release
*

(d)

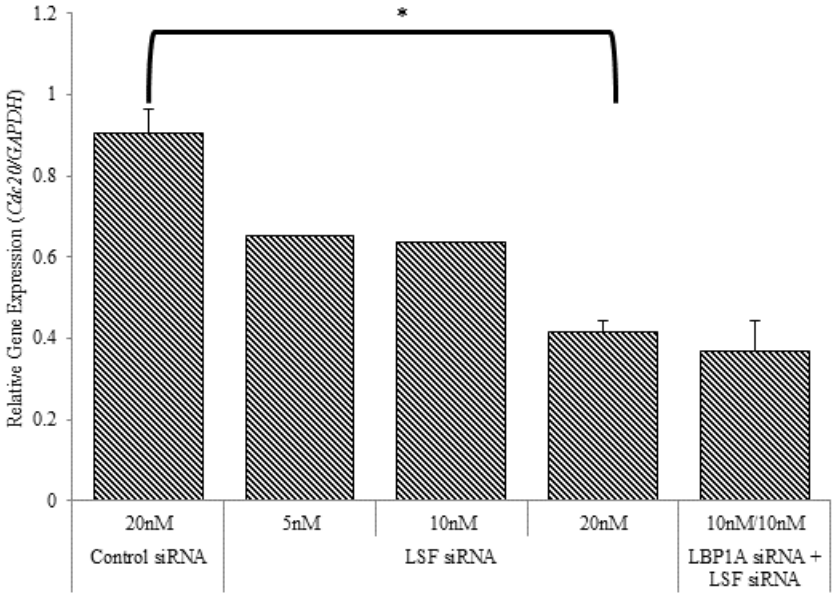
Relative Gene Expression (Cdc20/GAPDH)
1.2
1
0.8
0.6
0.4
0.2
0
*
20nM
Control siRNA
5nM
10nM
20nM
LSF siRNA
10nM/10nM
LBP1A siRNA + LSF siRNA

Figure 4.2

(e)

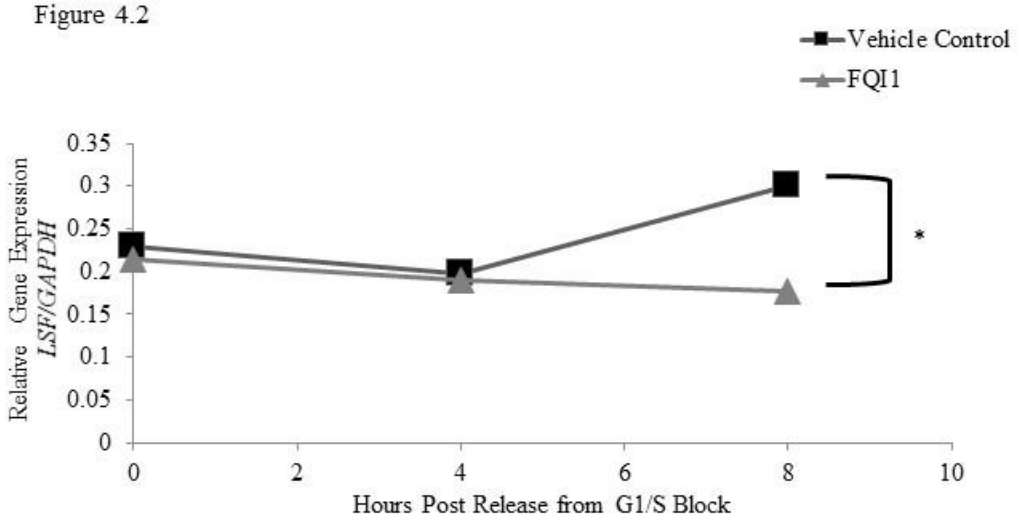

(f)

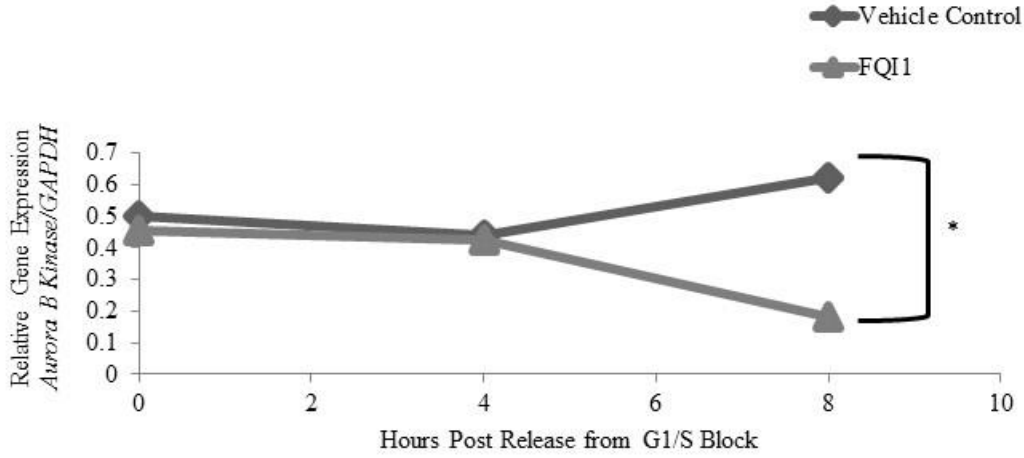

(g)

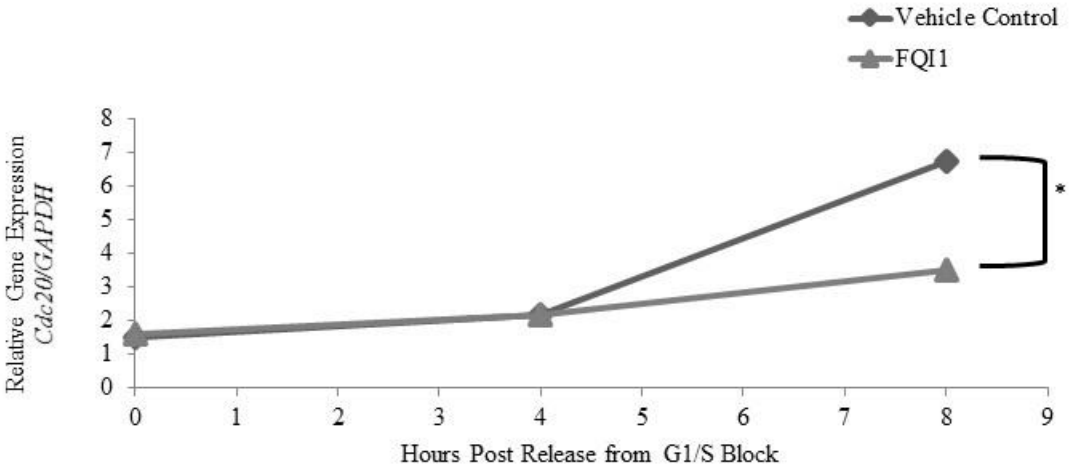

(h)

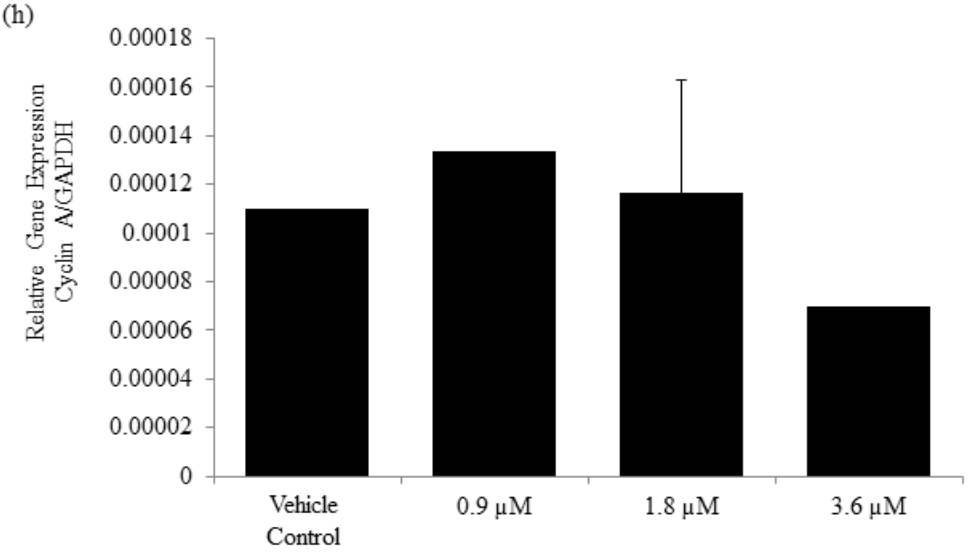
Relative Gene Expression
Cyclin A/GAPDH
0.00018
0.00016
0.00014
0.00012
0.0001
0.00008
0.00006
0.00004
0.00002
0
Vehicle Control
0.9 µM
1.8 µM
3.6 µM

(i)

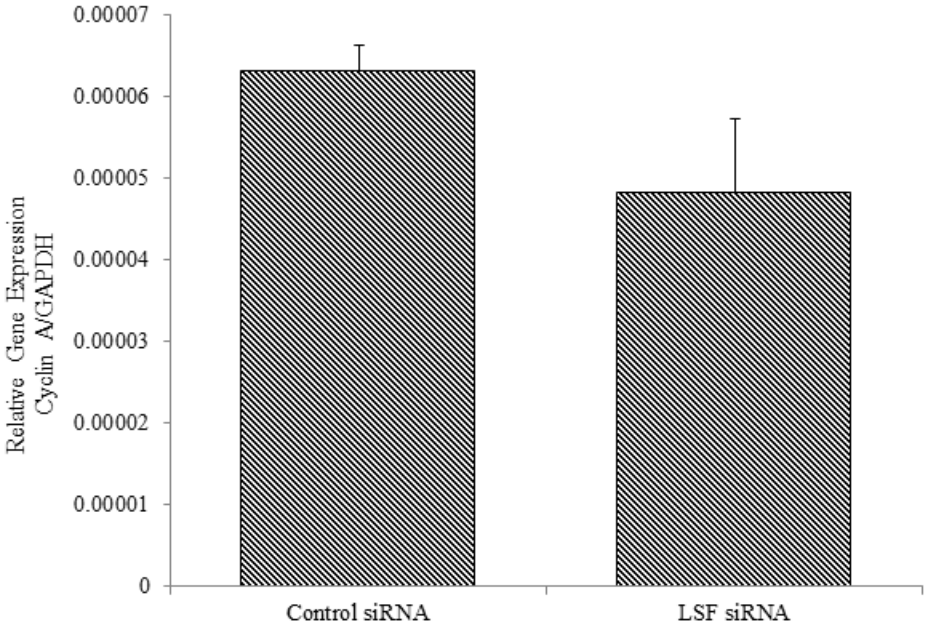
Relative Gene Expression
Cyclin A/GAPDH
0.00007
0.00006
0.00005
0.00004
0.00003
0.00002
0.00001
0
Control siRNA
LSF siRNA

(j)

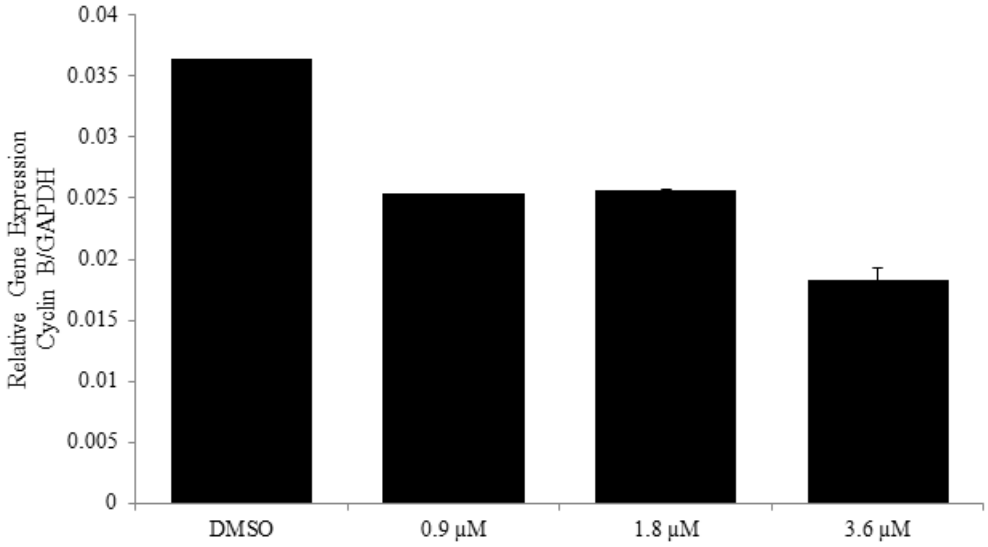
Relative Gene Expression
Cyclin B/GAPDH
0.04
0.035
0.03
0.025
0.02
0.015
0.01
0.005
0
DMSO
0.9 µM
1.8 µM
3.6 µM

(k)

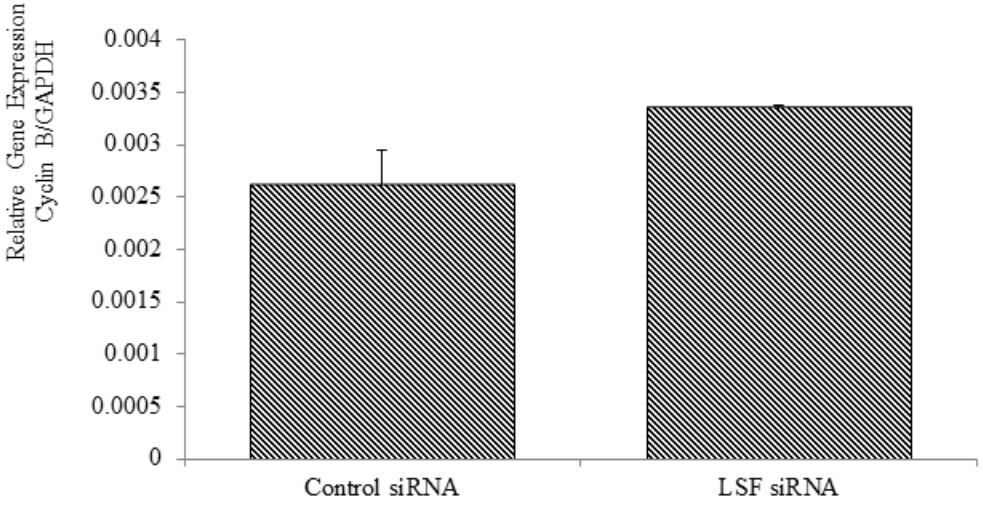
Relative Gene Expression
Cyclin B/GAPDH
0.004
0.0035
0.003
0.0025
0.002
0.0015
0.001
0.0005
0
Control siRNA
LSF siRNA

Figure 4.16 LSF knockdowns in synchronized HCC cells results in increased mitotic time with prometaphase/metaphase delay and cell division defects

Synchronized QGY-7703 cells expressing YFP-labeled H2B were analyzed utilizing time lapse microscopy. Cells were transfected with 20 nM of either control siRNA, or siRNA targeting LSF, LBP1A, or LSF and LBP1A in combination. Cells were treated with a single thymidine block and released prior to imaging (Illustration 4.3). (a-b) Representative images of cells treated with control siRNA (a) or with LSF siRNA (b) are pictured. Numbers represent minutes from nuclear envelope breakdown. (c) Quantitation of mitotic time determined on 100 cells following nuclear envelope breakdown treated with control siRNA or siRNAs targeting LSF or LBP1A separately or in combination. Standard error is depicted based on the number of cells analyzed in a single experiment. (d) Quantitation of cellular events including numbers of cells entering mitosis, exhibiting delay in prometaphase/metaphase, and defects in cell division at the indicated concentrations of transfected LSF siRNA. The controls had neither of the indicated defects among the cells counted. Approximately 120-140 cells were analyzed per condition. Statistical significance was determined using a Student T Test; * $P<0.05$, ** $P<0.01$, *** $P<0.001$, **** $P<0.0001$. (e-i) Representative images of individual cells to demonstrate mitotic phenotypes in cells transfected with 5 nM LSF siRNA: (e-f) prometaphase/metaphase delay, (g-h) cells that never divided within the time course (16 hours) of the experiment, and (i-j) cells undergoing aberrant cell division.

(a)

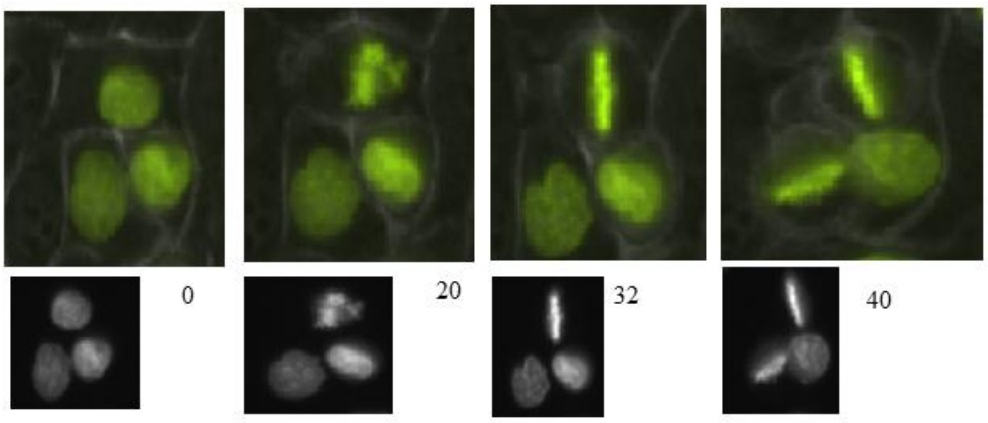

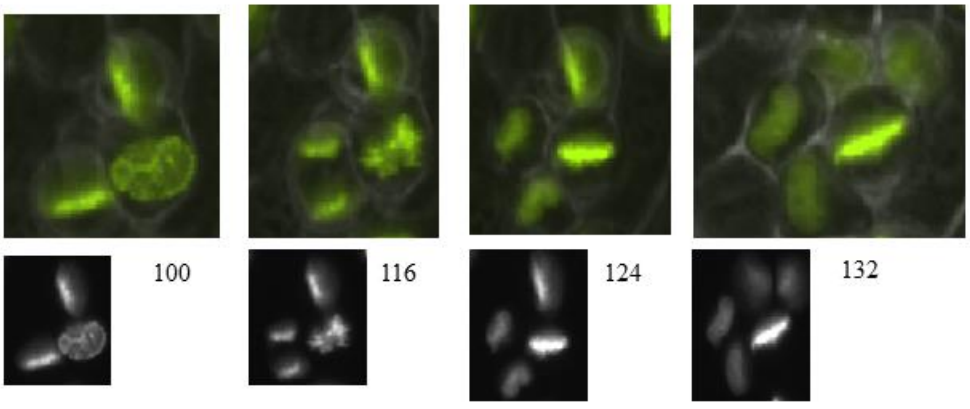

(b)

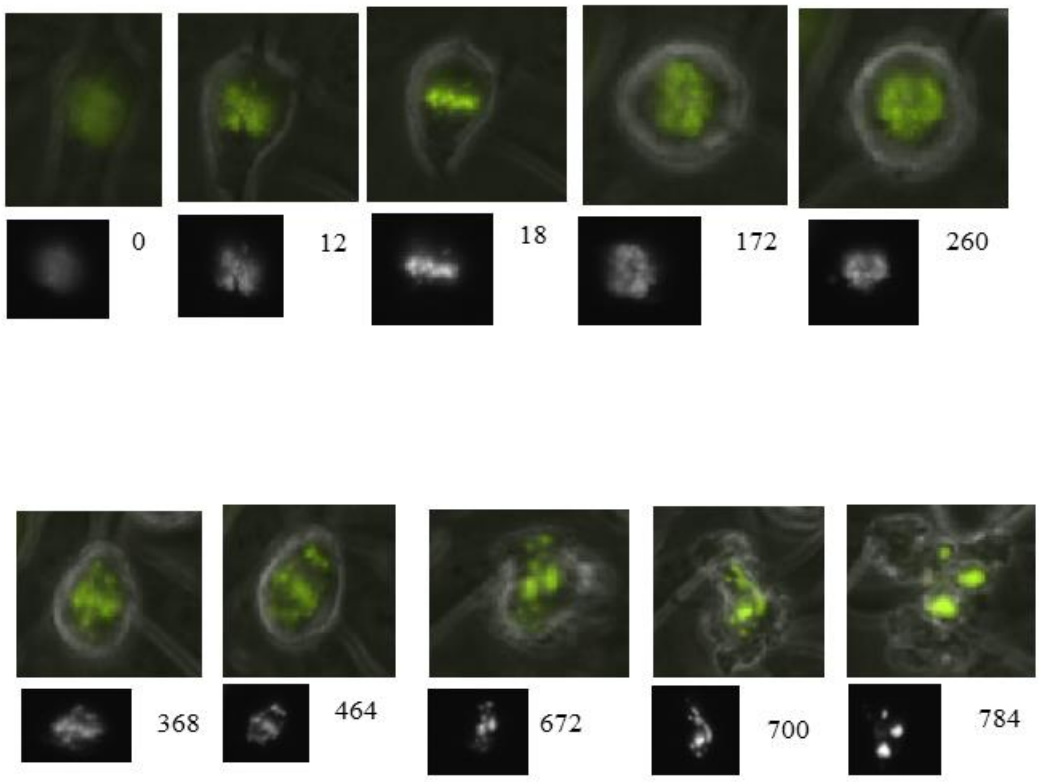

(c)

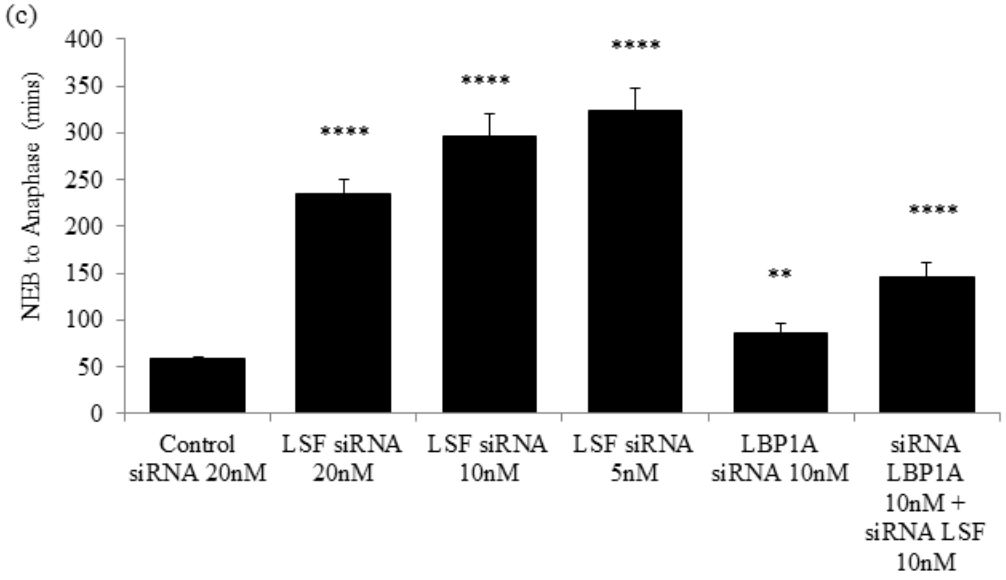
NEB to Anaphase (mins)
400
350
300
250
200
150
100
50
0
****
****
****
**
****
Control siRNA 20nM
LSF siRNA 20nM
LSF siRNA 10nM
LSF siRNA 5nM
LBP1A siRNA 10nM
siRNA LBP1A 10nM + siRNA LSF 10nM

(d)

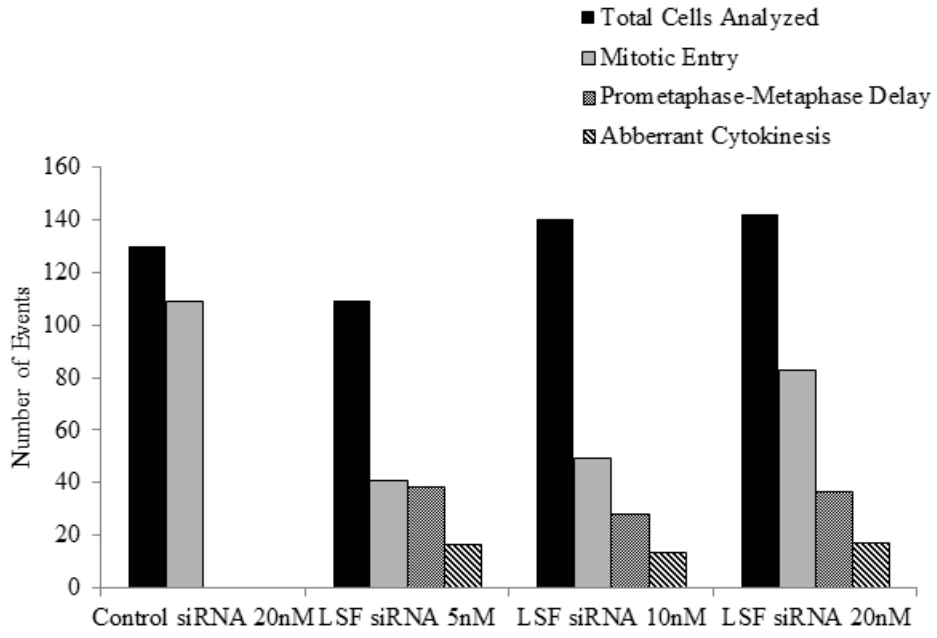
Total Cells Analyzed
Mitotic Entry
Prometaphase-Metaphase Delay
Abberrant Cytokinesis
Number of Events
160
140
120
100
80
60
40
20
0
Control siRNA 20nM
LSF siRNA 5nM
LSF siRNA 10nM
LSF siRNA 20nM

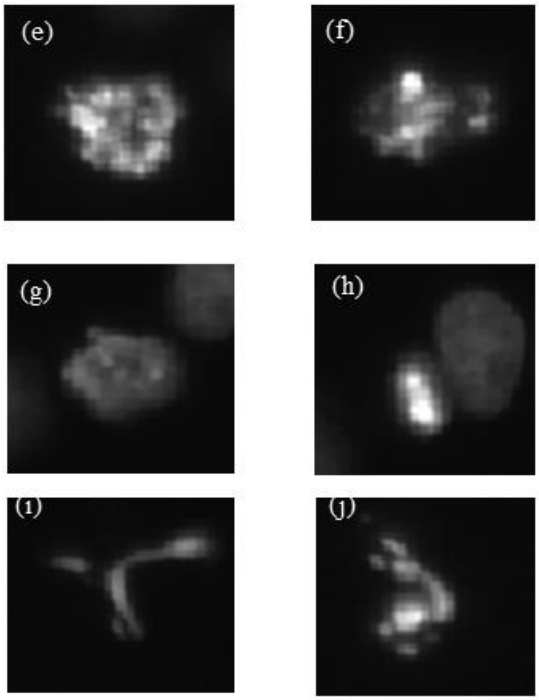
(e)
(f)
(g)
(h)
(i)
(j)

Figure 4.17 FQI1 treatment of HCC cells causes a dose dependent increase in mitotic time, prometaphase/metaphase delay and cell division defects

Asynchronous QGY-7703 cells expressing YFP-labeled H2B were analyzed utilizing time lapse microscopy after treatment with increasing concentrations of FQI1. Representative images of cells treated with (a) vehicle, (b) 1.8 μM FQI1 or (c) 3.6 μM FQI1. Numbers represent minutes from nuclear envelope breakdown. (d) Quantitation of mitotic time determined on 101 cells following nuclear envelope breakdown treated with 0.9 μM or 1.8 μM FQI1 or vehicle. Standard error is depicted based on the number of cells analyzed in a single experiment. Cells treated with 3.6 μM were not included as those entering mitosis did not reach anaphase during the overnight imaging period. (e) Quantitation of cellular events including number of cells entering mitosis, delayed in prometaphase/metaphase, and exhibiting cell division defects. 120-140 events were analyzed per condition. Statistical significance was determined using a Student T Test; * $P<0.05$, ** $P<0.01$, *** $P<0.001$, **** $P<0.0001$. (f-i) Representative images of prometaphase/metaphase delay and cell division defects, taken of cells treated with 1.8 μM FQI1. (f-g) Cells delayed in prometaphase/metaphase; (h-i) cells undergoing aberrant cellular division are the same as those in (f-g), although at later times.

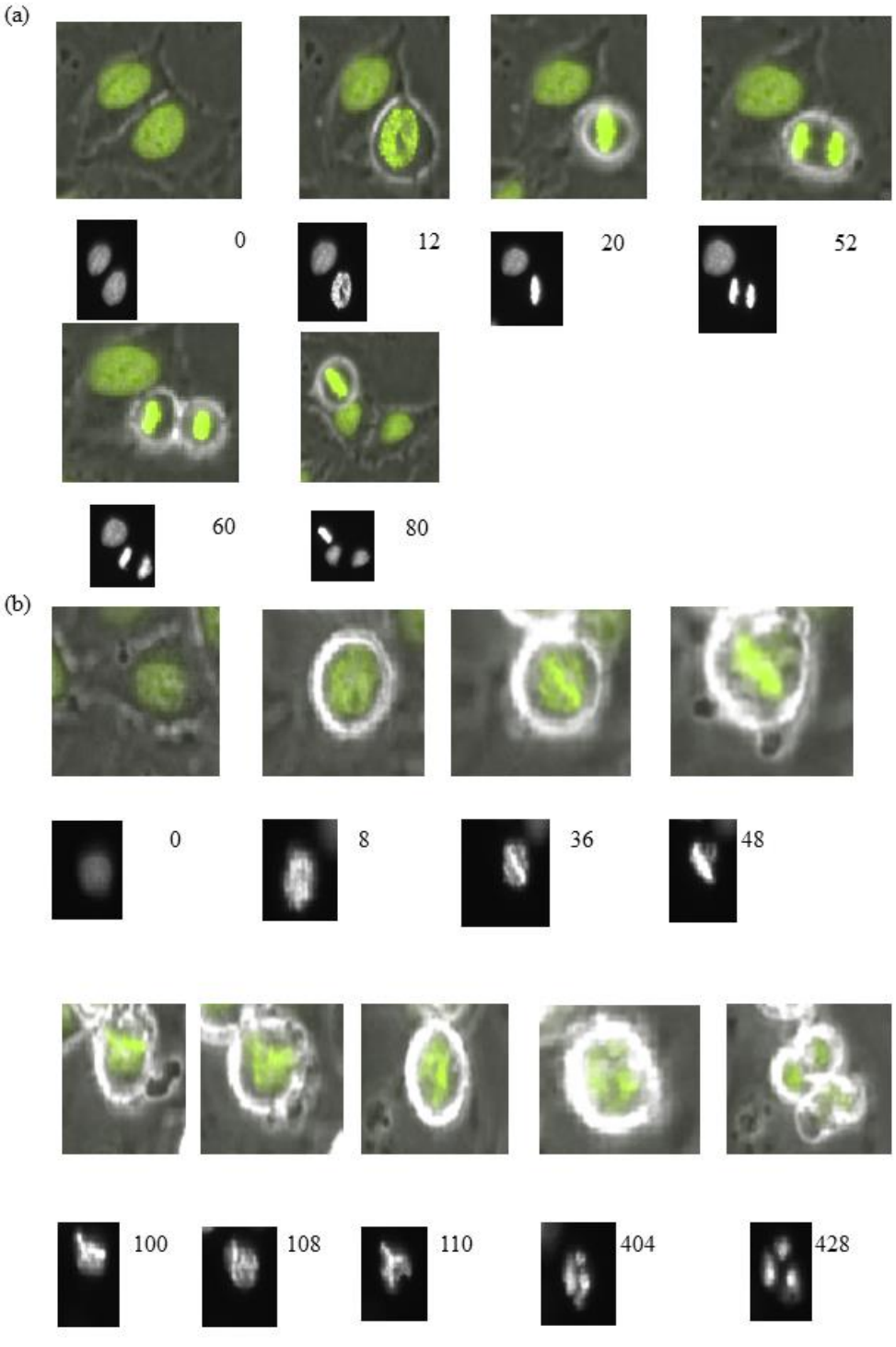
(a)
0
12
20
52
60
80
(b)
0
8
36
48
100
108
110
404
428

(c)

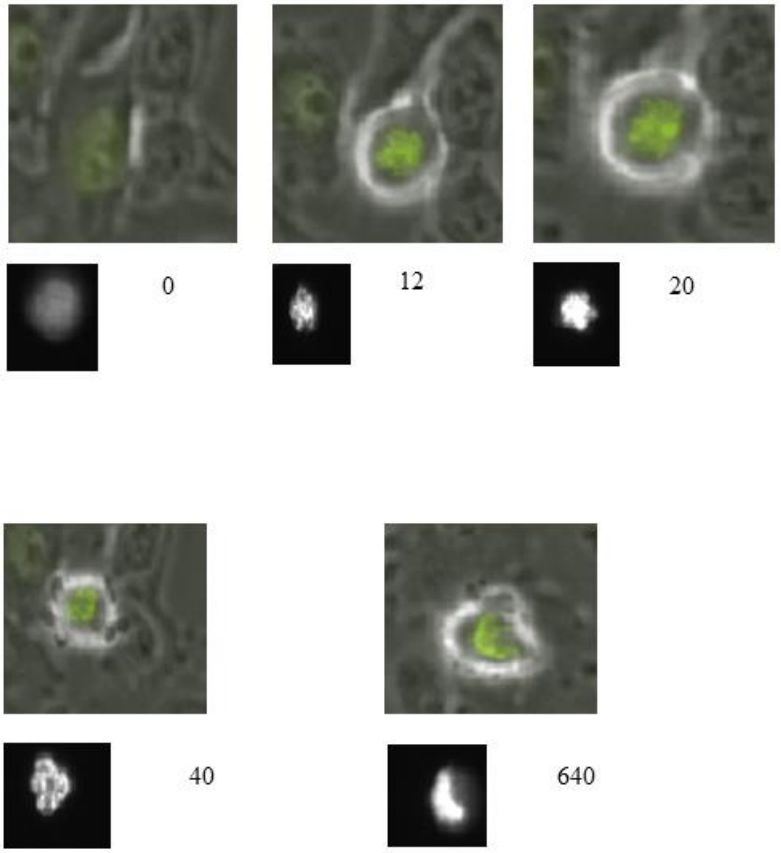

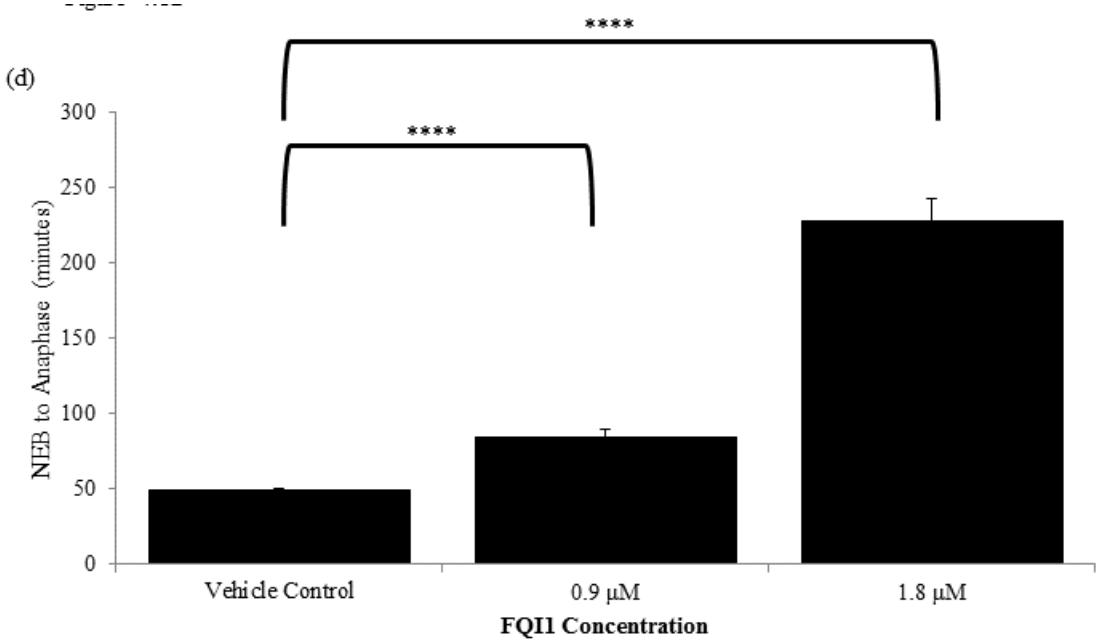
(d)
****
****
300
250
200
150
100
50
0
NEB to Anaphase (minutes)
Vehicle Control
0.9 µM
1.8 µM
FQI1 Concentration

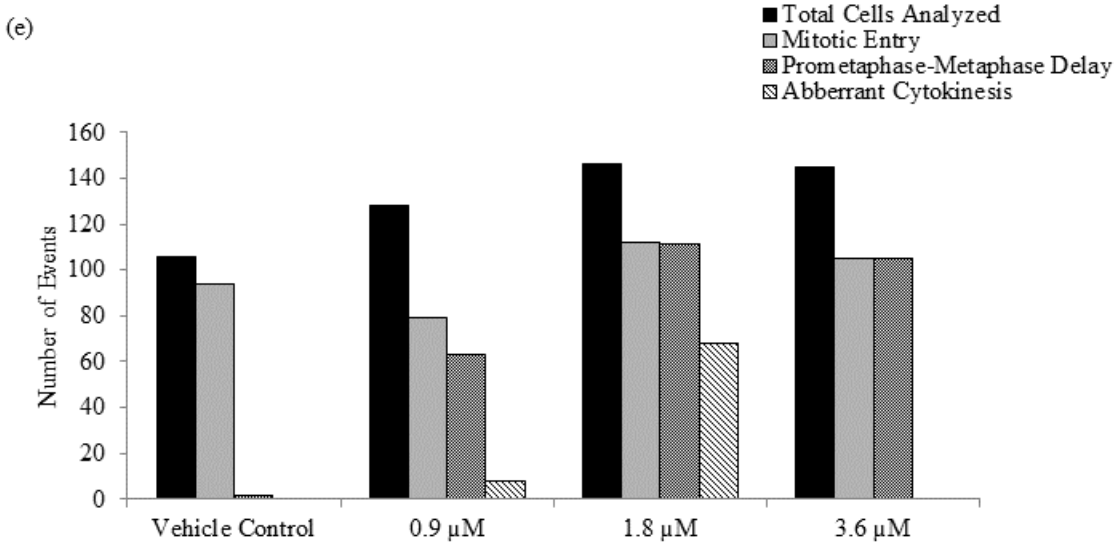
(e)
Total Cells Analyzed
Mitotic Entry
Prometaphase-Metaphase Delay
Abberrant Cytokinesis
160
140
120
100
80
60
40
20
0
Number of Events
Vehicle Control
0.9 µM
1.8 µM
3.6 µM

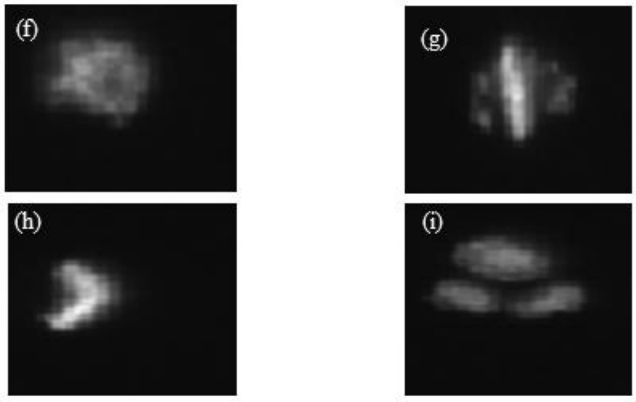
(f)
(g)
(h)
(i)

Figure 4.18 HCC cells delayed in prometaphase/metaphase upon LSF inhibition or knockdown often exhibit cellular protrusions

(a,b) Asynchronous HCC cells expressing mEmerald labeled α-tubulin were analyzed phenotypically utilizing time lapse microscopy following treatment with 3.6μM of FQI1 or vehicle. Representative images of QGY-7703 cells labeled with mEmerald α-tubulin treated with vehicle control (a) or 1.8 μM FQI1 (b) or (c) 3.6 μM FQI1. The numbers represent the time in minutes from nuclear envelope breakdown. (d) Synchronized HCC cells were treated with either 20 nM of LSF siRNA (Illustration 4.3) or 1.8 μM of FQI1 (Illustration 4.1). Cells were collected 8 hours after release from the final G1/S block and fixed for IF analysis with an anti-α-tubulin antibody and stained with DAPI. Anti-α-tubulin staining is shown in vehicle control (d), FQI1-treated (e), or LSF siRNA-treated (f) cells. Arrows indicate the cytoskeletal protrusions. siRNA control images were identical to those in vehicle control (d) (data not shown).

(a)

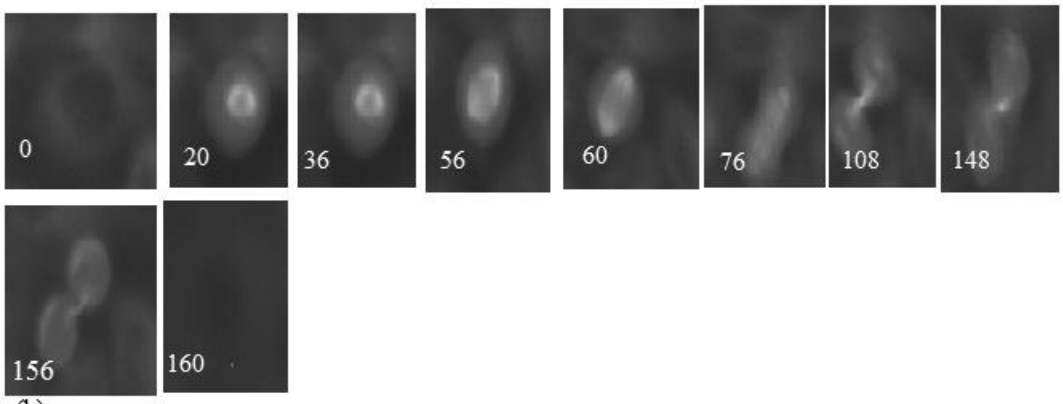
0
20
36
56
60
76
108
148
156
160

(b)

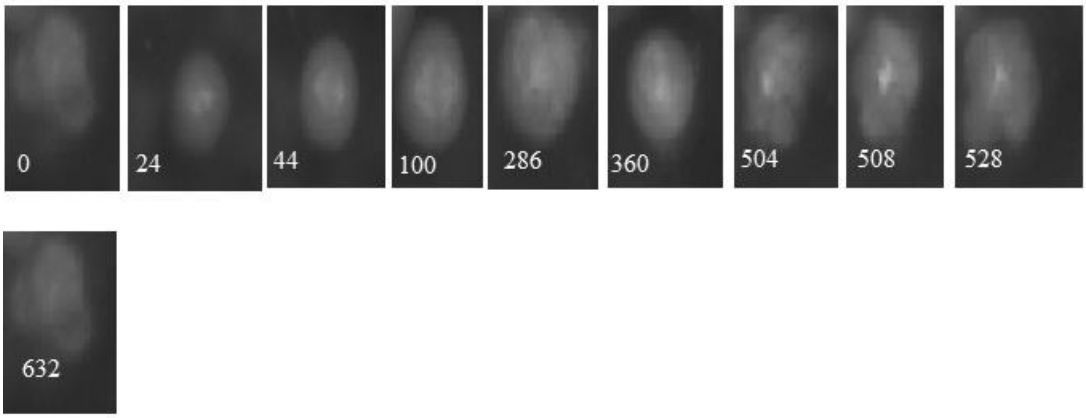
0
24
44
100
286
360
504
508
528
632

(c)

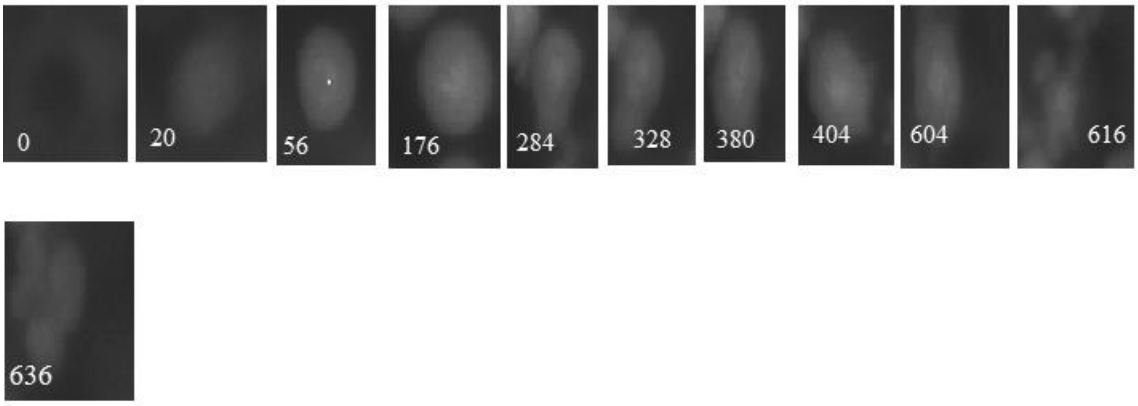
0
20
56
176
284
328
380
404
604
616
636

Control

(d)

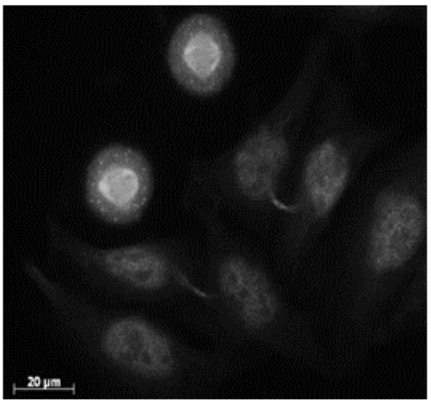

FQI1 1.8 µM

(e)

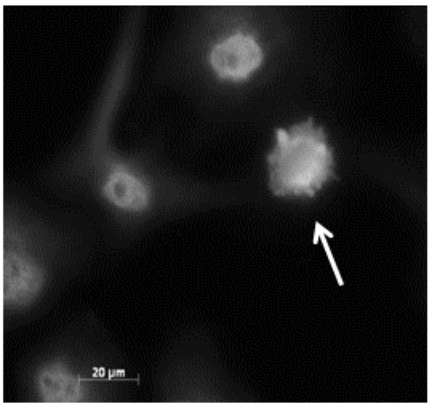

LSF siRNA 20 nM

(f)

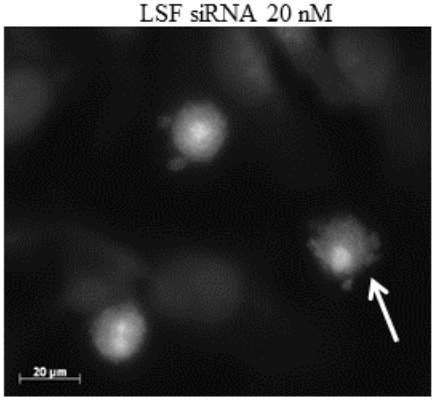

CHAPTER FIVE

LSF inhibition by FQI1 does not impact primary mouse hepatocytes ex vivo nor does FQI1 or FQI2 treatment in wild type mice reduce circulating rapidly dividing cell populations.

Introduction

Current treatments for those afflicted with Hepatocellular carcinoma (HCC) are subpar with the majority of patients qualifying for only palliative treatments (Bruix and Sherman, 2011; Farazi and DePinho, 2006; Torrecilla and Llovet, 2015). A minority of patients do qualify for invasive therapies including surgical resection or a liver transplant. Currently, Sorafenib, a tyrosine kinase and Raf inhibitor initially approved for renal cell carcinoma, is the only approved molecular therapy for HCC. Sorafenib has been shown to be efficacious in a subset of HCC patients where 71 patients had stable disease versus 67 in the placebo control, with only 2 patients showing complete response to 1 observed in the control group (Llovet et al., 2008). Further, the improvement in survival rates was subpar leaving the afflicted population with a significant unmet need (Llovet et al., 2008). Following the improvement observed with Sorafenib, a large number of molecularly targeted therapies were tested in clinical trials (Torrecilla and Llovet, 2015; Villanueva and Llovet, 2011). These drugs include both new agents and agents that have proven effective in other types of cancer, including inhibitors of angiogenesis, oncogenic signaling pathways, and histone deacetylases (Torrecilla and Llovet, 2015; Villanueva and Llovet, 2011).

Chemotherapeutics have long been a mainstay of therapy for a broad range of cancer types. The majority of chemotherapeutics demonstrate a robust ability to kill rapidly dividing cancer cells, however they also target rapidly dividing non- tumor cell populations. These normal cell populations include epithelial cells in both the intestine and hair follicles, resulting in two or the more notorious side effects experienced by cancer patients (diarrhea and hair loss). Approaches to specifically target cancer cells are ongoing with efforts to identify cancer specific receptors or to eliminate the uptake by non-carcinogenic cells of cancer therapeutics. Once a cancer cell population is successfully targeted by a drug, regardless of whether it targets one or multiple proteins, that tumor cell population could potentially escape rendering the therapy ineffective (Bergmann-Leitner et al., 2003; Khong and Restifo, 2002). Targeting of an oncogenic transcription factor would be advantageous as it might be possible with this approach to target an entire oncogenic pathway.

In the last decade, certain molecular targets were identified and hypothesized to be cases of oncogene addiction (Pagliarini et al., 2015; Weinstein and Joe, 2008; Weinstein and Joe, 2006). These cases involve the dependence of oncogenic cell proliferation and survival on a single target or pathway, which once removed, completely incapacitated the tumor cell, inducing cell death. Most importantly, the removal of this protein or pathway did not impact the healthy, non-tumor cell populations (Weinstein and Joe, 2008). The concept of therapies targeting an oncogene to which cells have become addicted has been tested in clinical trials, however, the results have been mixed with some therapies having a positive effect and others having no effect at all (Torti and Trusolino, 2011). The lack

of translation in those patients could potentially be due to heterogeneity in the molecular signature. None of these therapies however have targeted transcription factors or whole pathways. The inhibition of an oncogenic transcription factor to which HCC tumor cells are addicted is a new approach that could provide a promising therapeutic option HCC, a disease with very high unmet medical need.

We have shown that small molecular inhibitors of LSF, FQI1 and FQI2, inhibit human hepatocellular tumor growth in a subcutaneous xenograft mouse model (Grant et al., 2012). Animals receiving efficacious doses of FQI1 or FQI2 (that substantially reduced tumor growth), resulted in no detectable elevations in markers of liver toxicity. Specifically, there were no elevations in alanine aminotransferase (ALT), aspartate aminotransferase (AST), or albumin (ALB) following total doses of 10 or 20 mg/kg over a 1-week period. Furthermore, histopathological analysis of various tissues, including those with rapidly dividing cell populations (such as the epithelial lining of the small intestine) did not reveal any observable toxicity one week following treatments (Grant et al., 2012). More recently, FQI1 and FQI2 administration to an endogenous liver cancer mouse model also resulted in significant tumor inhibition (Rajasekaran et al., 2015). In that study, there were no gross signs of toxicity in mice dosed with either compound using a 4 mg/kg dose for each of the five dosing treatments. The significant inhibition of tumors *in vivo* combined with the lack of toxicity observed in non-tumor cell populations led to a proposal of oncogene addiction (Grant et al., 2012; Shlomai, 2012).

As discussed above, a case of oncogene addiction would indicate that LSF is not absolutely required for cell survival in non-tumorigenic cells and therefore that LSF inhibition would not impact the healthy cell populations. FQI inhibition of LSF would result in a significant advantage in the hepatocellular carcinoma (HCC) patient population compared to the currently approved therapeutics that not only target the rapidly dividing cancer cell, but could negatively impact rapidly dividing non tumor cells in the body. Sorafenib for instance causes lymphopenia, neutropenia, and thrombocytopenia as well as diarrhea, nausea, hand-foot skin reaction and fatigue, all hallmarks of chemotherapeutics that impact normal cells (Bruix and Sherman, 2011).

In Chapters 3 and 4, I demonstrated that inhibition by FQI1 and FQI2 in hepatocellular carcinoma cells resulted in reduced cell viability following significant mitotic defects. Here, I show that FQI1 treatment of primary mouse hepatocytes *ex vivo* did not result in any observable toxicity. Additionally, I show that intraperitoneal dosing of FQI1 or FQI2 administered at dose levels 2 to 4 times those required to inhibit tumor growth (Grant et al., 2012; Rajasekaran et al., 2015), did not result in reduction in non-tumor cell populations analyzed at a time point where toxicity is typically observed (Scott Barros-Alnylam Pharmaceutical Toxicology Expert, Personal comm.).

Results

LSF inhibition is without consequence in primary mouse hepatocytes

To determine whether LSF inhibition would result in cell death in normal, non-carcinogenic and non-dividing hepatocytes, mouse hepatocytes were isolated from C57BL6 mice using a rapid two step isolation method and plated for maintenance in culture (Chapter 2). The protocol generated a pure population of hepatocytes (Severgnini et al., 2012). Following confirmation of a successful isolation, with the adherent cells showing expected cellular morphology (Figures 5.1a and c), cells were incubated with 5 μM of FQI1 or vehicle. Cells were collected 24, 48, or 72 hours after FQI1 treatment, and stained with both DAPI and Phalloidin allowing visualization of DNA and actin filaments to evaluate cellular morphology. Representative images of vehicle-treated cells (top) and 5 μM FQI1-treated cells (bottom) are comparable in cell morphology with no discernible differences (Figure 5.1b). In a separate study a distinct batch of primary mouse hepatocytes were treated with vehicle or 5 μM FQI1 for 48 hours, and then stained with hematoxylin and eosin. Representative images (Figure 5.1d) of the vehicle control (top) and FQI1 treated cells (bottom) confirm the initial observations that there are no discernible differences between the treated or control cells.

FQI1 or FQI2 treatment in mice does not result in weight loss, elevation of liver enzyme levels or reduction in circulating whole blood cell populations.

LSF inhibition results in mitotic defects followed by cell death in rapidly dividing HCC cells (Chapters 3 and 4); however, in tumor bearing animals dosed with FQI1 or FQI2 there was no elevation in liver enzyme levels or cytotoxicity of tissues analyzed by

H&E staining (Grant et al., 2012). This result was surprising given the small inhibitors generally have exposure to tissues (including those with dividing cells) outside of HCC tumor cells. It is also unusual for a chemotherapeutic that targets dividing tumor cells to have no impact on normal and dividing cell populations. Therefore, I asked whether FQI1 or FQI2 in *vivo* is toxic to the rapidly dividing cell populations (assayed via FACS) or normal liver cells (assayed by measuring liver enzyme elevations) in peripheral blood. Furthermore, I specifically tested early timepoints (24 hours after the final compound dose), as previous studies had tested later timepoints at which it was theoretically possible that compound effects were missed due to are resolution of any defects. Animals were treated with 2 to 4 times the therapeutic dose levels (Grant et al., 2012; Rajasekaran et al., 2015) reported to treat HCC xenograft animals or the mice with endogenous liver cancer. Specifically, C57BL/6 male mice were dosed intraperitoneally (i.p.) with 8 mg/kg of compound, vehicle or saline daily for five consecutive days with four animals per group. Male mice were used as in the previous studies, because HCC occurs with higher frequency in males, both in mice and humans. Body weights were recorded prior to the treatment regimen and at end of the study. No significant difference in weight was observed when comparing mice before and after FQI1 or FQI2 exposure, in comparison to controls (Figure 5.2).

Serum was collected 24 hours after the final dose (Table 5.1). Albumin levels were unchanged in treated versus the controls indicating that liver protein levels were not elevated significantly in treated animals. There was no statistical difference between the FQI treated animals and the vehicle control group as measured by the Student T Test. As

another measurement of whether any of the liver protein levels in the blood were abnormal, the data were compared to the reference standards generated for C57BL/6 males. The values in all groups were comparable to or lower than those observed in non-treated C57BL6 males at a similar age range (http://www.criver.com/products-services/basic-research/find-a-model/c57bl-6n-mouse). These data confirm that there is no liver toxicity.

Whole blood was also analyzed from each animal 24 hours after the final dose of controls or compound, in order to assay for alterations in rapidly dividing blood cell populations. All whole blood cell populations following both FQI1 and FQI2 treatments were similar overall as comparable to those of the vehicle control (Table 5.2). Further, the data were comparable to the reference standards generated for C57BL/6 males (http://www.criver.com/products-services/basic-research/find-a-model/c57bl-6n-mouse), indicating that this dosing regimen did not result in any statistically significant abnormal findings.

Discussion

The robust inhibition of HCC tumor growth *in vivo* with either FQI1 or FQI2, combined with the apparent lack of toxicity from previous studies, suggested that the tumor cells could be addicted to LSF. To properly investigate whether FQI1 or FQI2 would harm non-tumor cells, the compounds were analyzed in mouse primary hepatocytes ex vivo and in untreated C57BL/6 mice *in vivo*.

Evaluation of the cellular morphology of primary mouse hepatocytes *ex vivo* with FQI1 revealed no obvious signs of toxicity consistent with previous observations. Specifically, liver enzymes were not elevated and histopathological analysis was unremarkable *in vivo* with subcutaneous xenograft models (Grant et al., 2012). The lack of toxicity of FQI1 on mouse hepatocytes *in vivo* is promising given that FQI1 and FQI2 caused cell death of hepatocellular carcinoma cells. One obvious difference between HCC cells and primary isolated hepatocytes, however, is that the isolated mouse hepatocytes are not capable of cell division. Previous studies have documented roles for LSF during cell cycle progression, both at the G1/S transition and in mitosis (Chapter 3 and 4)(Powell et al., 2000). Thus, one interpretation would be that LSF activity is only critical for dividing cells. Nonetheless, it is promising that LSF inhibition does not impact non-dividing primary hepatocytes but could potentially benefit HCC patients as the rapidly dividing tumor cells are LSF dependent. A therapy that does not impact normal hepatocytes in HCC patients is important as their liver function is already compromised, often by non-tumor disease such as cirrhosis, and keeping whatever normal hepatocytes they have left is key to both the toxic profile of the therapy but also the ability of the liver to possibly regenerate. One area for further investigation is to determine what role (if any) LSF or its family members play in liver regeneration.

The *in vivo* examination of the impact of FQI1 and FQI2, at 2-4 times therapeutically relevant dose levels, on various mouse cell populations (Figures 5.2 and Tables 5.1 and 5.2) are consistent with previous reports with no loss of body weight or significant elevation of key liver injury markers. Here, I evaluated the cell populations

24 hours after the final dose levels eliminating the possibility that the liver could recover at late time points. Further, for the first time I show that FQI1 and FQI2 doses *in vivo* do not significantly impact various hematopoietic cells populations (summarized in Illustration 5.1). Whether FQI1 or FQI2 do not impact these populations because LSF is not required in these cells types or because insufficient drug levels have permeated these cells populations to result in impairment cannot be determined from these studies. However, these data are consistent with the proposed model of LSF in HCC being a case of oncogene addiction.

Illustration 5.1

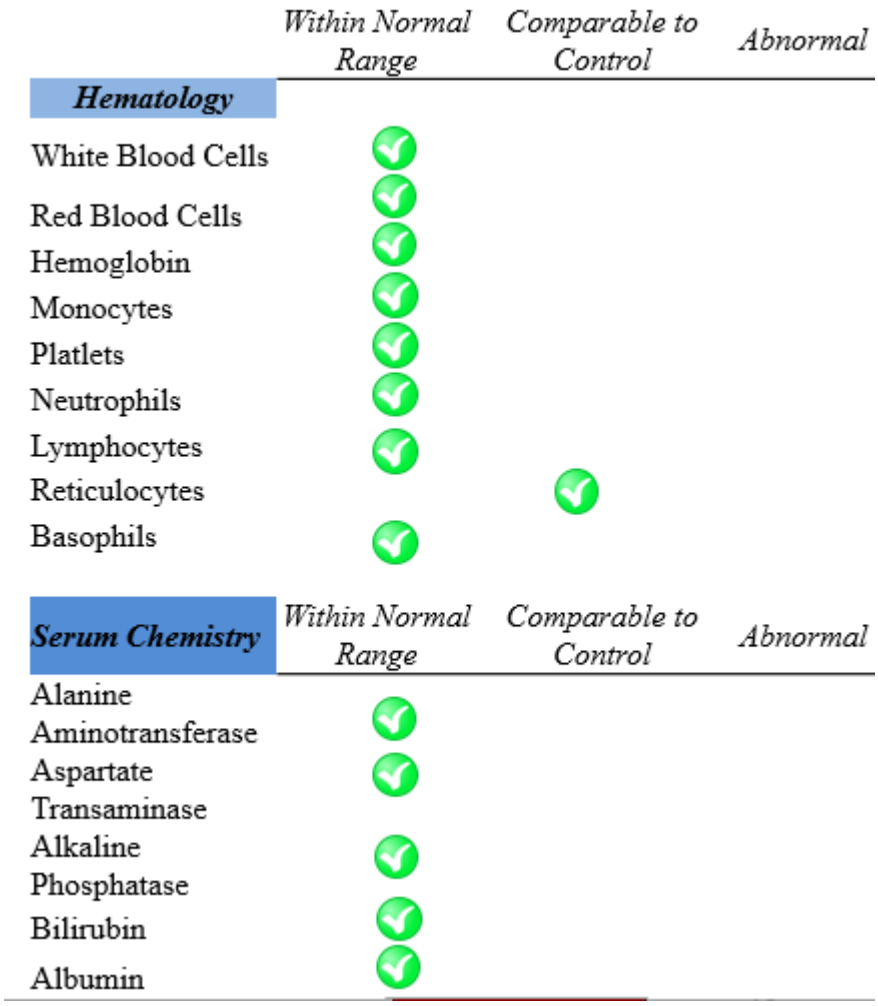

Hematology	*Within Normal Range*	*Comparable to Control*	*Abnormal*
White Blood Cells	✓		
Red Blood Cells	✓		
Hemoglobin	✓		
Monocytes	✓		
Platlets	✓		
Neutrophils	✓		
Lymphocytes	✓		
Reticulocytes		✓	
Basophils	✓		

Serum Chemistry	*Within Normal Range*	*Comparable to Control*	*Abnormal*
Alanine Aminotransferase	✓		
Aspartate Transaminase	✓		
Alkaline Phosphatase	✓		
Bilirubin	✓		
Albumin	✓		

In summary, these data support the notion that the LSF requirement in HCC cells is a case of oncogene addiction. LSF inhibition via treatment with FQI1 and 2 specifically inhibits HCC tumor growth without compromising normal hepatocytes or other rapidly dividing cell populations such as blood cells in mouse models (as assayed at early or later time points). Consistent with the tumor model data in vivo, isolated primary hepatocytes also appear to be unaffected by treatment with LSF inhibitors.

Taken together the data support further investigation of LSF as a target for the treatment of HCC and the FQI family of compounds in particular.

Figures

Figure 5.1. LSF inhibition by FQI1 is without consequence in primary mouse hepatocytes

Primary mouse hepatocytes were isolated from wild type C57BL6 mice acquired from Charles River Laboratories. Hepatocytes were isolated, plated, and treated with 5 μM FQI1 or vehicle. Cells were analyzed for morphology 24, 48, and 72 hours post incubation with FQI1 treatment. Representative images above were taken following fluorescent staining with DAPI and Phalloidin (a,b) or following fixation and staining with Hematoxylin and Eosin (H&E) (c,d). Images were gathered using a Zeiss axioimager at 63x magnification. (a) Representative image of the cells 4 hours post plating. (b) Representative images of cells collected and fixed at approximately 24, 48 or 72 hours post incubation with vehicle (top) or with 5 μM FQI1 (bottom). H&E stained isolated primary mouse hepatocytes with successful plating 4 hours post isolation (c) or treated with (d) vehicle control (top) and with 5 μM FQI1 (bottom) for 48 hours.

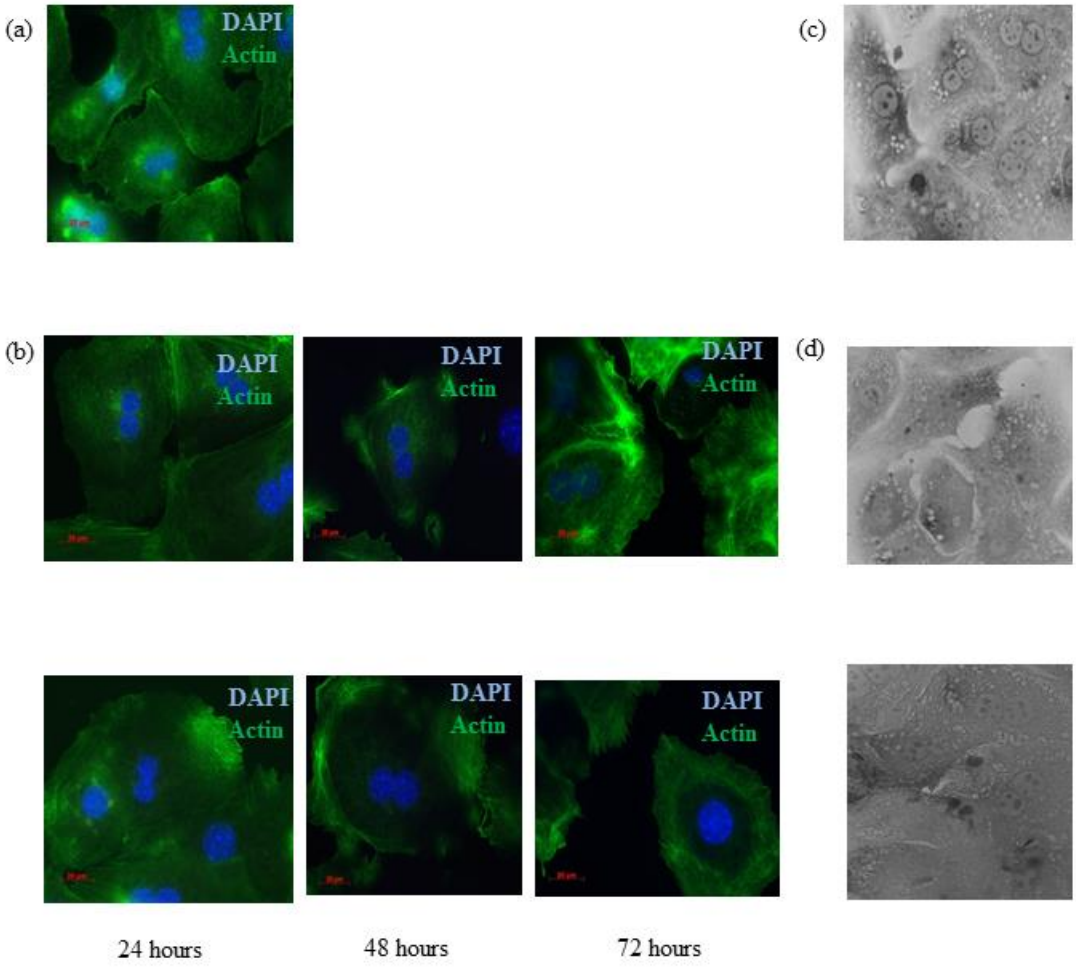
(a)
DAPI
Actin
(c)
(b)
DAPI
Actin
DAPI
Actin
DAPI
Actin
(d)
DAPI
Actin
DAPI
Actin
DAPI
Actin
24 hours
48 hours
72 hours

Figure 5.2. Mice retain expected body weight upon treatment with FQI1 or FQI2 at doses that exceed efficacious levels

C57BL/6 male mice were dosed intraperitoneally (i.p.) daily for 5 consecutive days at 8 mg/kg of FQI1 or FQI2, or vehicle (DMSO), or physiological saline. Body weights were taken prior to the first dose and 24 hours following the final dose. n=5 per group. Standard error of the mean is depicted. These data are representative of two independent experiments.

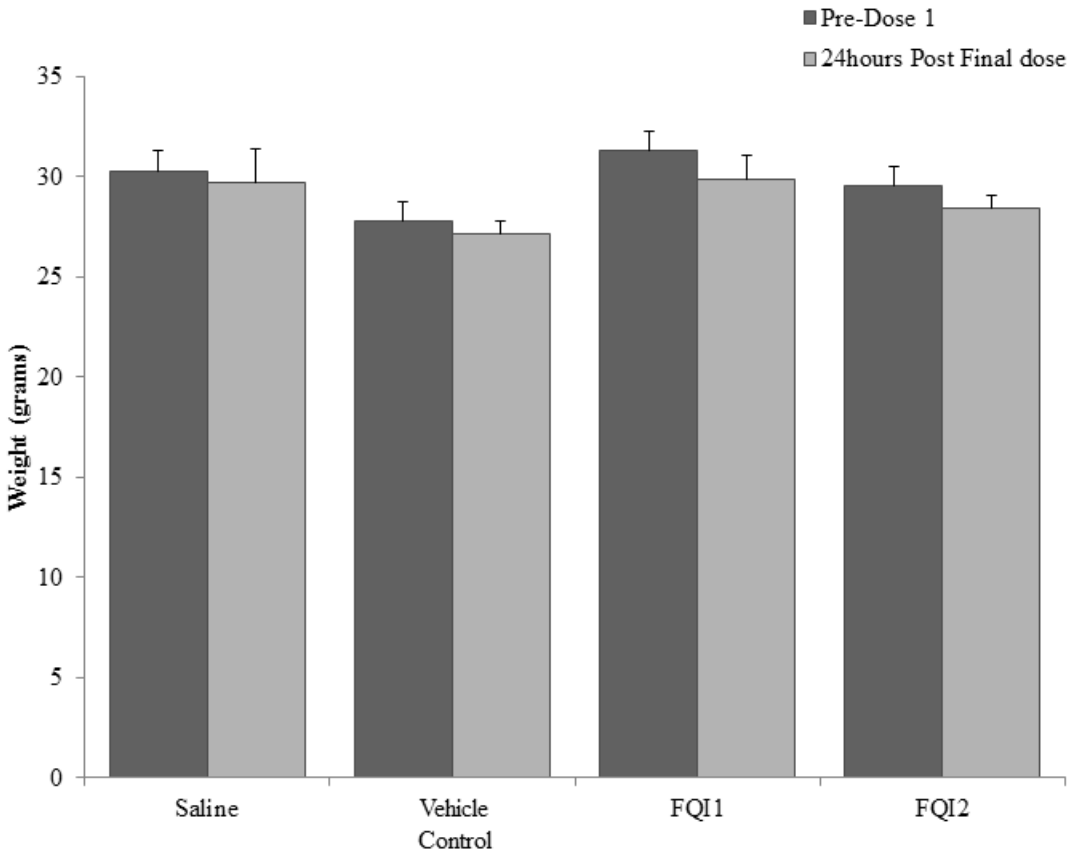

Table 5.1. Mice treated with higher than efficacious levels of FQI1 or FQI2 have comparable liver function readouts in comparison to controls, assayed shortly after dosing.

These data are representative of two independent experiments in which n=4 per group. The reference intervals (last row) were generated by Charles River Laboratories (http://www.criver.com/products-services/basic-research/find-a-model/c57bl-6n-mouse) on at least 123 C57BL6 male mice at 8-10 weeks of age using a Drew Scientific HemaVet analyzer.

	Albumin		Alkaline Phosphatase		Alanine Transaminase		Aspartate Transaminase		Bilirubin	
	g/dL		U/L		U/L		U/L		mg/dL	
	Average	*St Error*	*Average*	*St Error*	*Average*	*St Error*	*Average*	*St Error*	*Average*	*St Error*
Vehicle	2.8	± 0.05	68.8	± 1.65	30.6	± 3.6	54.0	10.7	0.1	± 0.01
FQI1	2.7	± 0.04	63.5	± 4.43	25.6	± 2.1	70.5	4.7	0.1	± 0.01
FQI2	2.7	± 0.09	57.4	± 4.55	23.3	± 2.5	38.2	2.7	0.1	± 0.00
Saline	2.8	± 0.03	71.5	± 8.41	26.7	± 3.6	56.2	4.5	0.1	± 0.02
Reference Intervals	**2.8-3.8**		**111-275**		**28-129**		**46-392**		**.2-.6**	

Table 5.2. Higher than efficacious treatments with FQI1 or FQI2 in C57BL6 male mice do not alter blood cell distributions or levels in comparison to levels in controls. .

Data are representative of two independent experiments in which n=4 per group. Abbreviations include: Red blood cells (RBC), Hemoglobin (HGB), Hematocrit (HCT), Mean Corpuscular Volume (MCV), Mean Corpuscular Hemoglobin (MCH), Mean Corpuscular Hemoglobin Concentration (MCHC), Platelets (PLT), White Blood Cells (WBC), Neutrophil (NEUT), Neutrophil count (NEUT ABS), Lymphocyte (LYM), Lymphocyte count (LYM ABS), Monocyte (MONO), Monocyte Count (MONO ABS), Eosinophil (EOS), Eosinophil Count (EOS ABS), Basophil (BASO), Basophil count (BASO ABS), Large Unstained Cells (LUC), Large Unstained Cell Count (LUC ABS), Reticulocyte (RETIC), Reticulocyte count (Retic ABS). The reference intervals (last row) were generated by Charles River Laboratories (http://www.criver.com/products-services/basic-research/find-a-model/c57bl-6n-mouse)on at least 123 C57BL6 male mice, 8-10 weeks of ageusing a Drew Scientific HemaVet analyzer.

(a)

	RBC ($x10^6$ cells/µL)		HGB (g/dL)		HCT %		MCV (fL)		MCH (pg)	
	Average	*St Error*	*Average*	*St Error*	*Average*	*St Error*	*Average*	*St Error*	*Average*	*St Error*
Vehicle	10.3	± 0.18	14.4	± 0.2	52.1	± 0.9	50.4	± 0.3	13.9	± 0.1
FQI1	10.5	± 0.11	14.7	± 0.1	53.7	± 0.7	51.1	± 0.2	14.0	± 0.2
FQI2	10.4	± 0.25	14.3	± 0.3	51.5	± 1.2	49.7	± 0.3	13.8	± 0.1
Saline	10.7	± 0.27	14.5	± 0.3	54.6	± 1.1	51.2	± 0.6	13.7	± 0.2
Reference Intervals	**7.14-12.20**		**10.8-19.8**		**37.3-62.0**		**42.7-56.0**		**11.7-16.3**	

(b)

	MCHC (g/dL)		PLT ($x10^3$ cells/µL)	
	Average	*St Error*	*Average*	*St Error*
Vehicle	27.7	± 0.3	994	± 40
FQI1	27.4	± 0.2	915	± 47
FQI2	27.7	± 0.3	980	± 63
Saline	26.6	± 0.2	841	± 54
Reference Intervals	**24.6-34.9**		**841-2159**	

(c)

	WBC (x10³ cells/µL)			NEUT %			NEUT ABS (x10³ cells/µL)			LYM %		
	Average		*St Error*	*Average*		*St Error*	*Average*		*St Error*	*Average*		*St Error*
Vehicle	8	±	0.42	11.6	±	1.2	0.9	±	0.06	78.9	±	1.4
FQI1	9	±	0.45	11.3	±	1.8	1.0	±	0.21	79.8	±	2.0
FQI2	9	±	1.05	13.8	±	2.5	1.2	±	0.30	76.6	±	2.6
Saline	9	±	0.49	8.8	±	1.0	0.8	±	0.09	82.6	±	0.6
Reference Intervals	**4.45-13.96**			**7.36-28.59**			**.53-3.09**			**61.26-87.18**		

(d)

	LYM ABS (x10³ cells/µL)			MONO %			MONO ABS (x10³ cells/µL)		
	Average		*St Error*	*Average*		*St Error*	*Average*		*St Error*
Vehicle	6.5	±	0.46	2.8	±	0.2	0.2	±	0.01
FQI1	6.9	±	0.20	2.6	±	0.2	0.2	±	0.03
FQI2	6.9	±	0.87	2.6	±	0.5	0.2	±	0.06
Saline	7.8	±	0.39	3.0	±	0.3	0.3	±	0.02
Reference Intervals	**3.24-11.15**			**2.18-11.02**			**.15-94**		

(e)

	EOS %			EOS ABS (x10³ cells/µL)			BASO %			BASO ABS (x10³ cells/µL)		
	Average	*St Error*		*Average*	*St Error*		*Average*	*St Error*		*Average*	*St Error*	
Vehicle	4.9	±	0.34	0.4	±	0.03	1.4	±	0.0	0.1	±	0.00
FQI1	4.6	±	0.30	0.4	±	0.04	1.3	±	0.0	0.1	±	0.01
FQI2	5.1	±	0.58	0.5	±	0.07	1.4	±	0.1	0.1	±	0.02
Saline	3.8	±	0.77	0.4	±	0.08	1.4	±	0.1	0.1	±	0.01
Reference Intervals	**0.13-4.42**			**0.01-.42**			**0.01-1.24**			**0.0-0.13**		

(f)

	LUC%**			LUC ABS** (x10³ cells/µL)			RETIC %			Retic ABS (x10⁹ calls/L)		
	Average	*St Error*		*Average*	*St Error*		*Average*	*St Error*		*Average*	*St Error*	
Vehicle	0.5	±	0.1	0.0	±	0.01	3.3	±	0.18	343	±	15
FQI1	0.4	±	0.1	0.0	±	0.01	3.0	±	0.16	318	±	15
FQI2	0.6	±	0.1	0.1	±	0.01	3.2	±	0.18	335	±	14
Saline	0.6	±	0.0	0.1	±	0.00	2.7	±	0.29	289	±	23
Reference Intervals	**NA**			**NA**			**NA**			**NA**		

CHAPTER SIX DISCUSSION

In this body of work, I have investigated the role of LSF in Hepatocellular Carcinoma. I utilized two approaches to understand the requirement for LSF in HCC and why inhibition of LSF activity significantly reduced tumor growth in preclinical models, as well as to generate additional evidence that the FQI anti-tumor effect was specific to LSF inhibition.

I demonstrated that short incubations with FQIs revealed a non-transcriptional based, mitotic interruption resulting in cell death. The major phenotype was prometaphase arrest, followed by multi-nucleation which suggested interruption in proper kinetochore-microtubule attachment, an event that can result in mitotic arrest (Hauf et al., 2007; Hauf et al., 2003). However, levels of proteins involved in microtubule-kinetochore attachment and mitotic exit, Aurora Kinase B and Cdc20, were unchanged, as were their RNAs. To rule out that FQI1 impacted Aurora B kinase activity rather than expression, phosphorylation of the Aurora Kinase B target Histone 3 was evaluated and confirmed as comparable to the control. I also found that the upregulation of Cyclin B protein expression, as documented in Rajesekaran et al (2015), was due solely to mitotic arrest as Cyclin B RNA levels were unperturbed in the FQI treated cells. Furthermore, to confirm that the prometaphase arrest was not due to transcriptional misregulation of LSF target genes, FQI1 was removed after the arrest, resulting in phenotype reversal. Since transcription of protein-encoding genes (with the possible exception of cyclin B) is not believed to occur following mitotic entry, the release from prometaphase arrest must therefore be due to an alternative mechanism.

Utilization of RNAi interference to ablate LSF expression as well as a "long-term FQI incubation protocol" revealed a second mitotic requirement for LSF, implicating involvement of mitotic regulators Aurora kinase B and Cdc20. Both investigative approaches revealed consistent phenotypes upon the reduction of LSF activity, including prometaphase delay and subsequent cell death and senescence. Furthermore, the loss of LSF activity lengthened passage through mitosis, as determined with time lapse microscopy.

Cellular senescence, prometaphase/metaphase delay, aberrant cell division, and multi-nucleation are also all phenotypes previously reported using various methods to eliminate Aurora Kinase B expression and/or activity (Andrews, 2005; Carmena et al., 2012; Ditchfield et al., 2003; Hauf et al., 2007; Hauf et al., 2003; Huck et al., 2010; Kim et al., 2011; Sistayanarain et al., 2006; Vader and Lens, 2008). The connection between LSF and Aurora kinase B was supported in that direct substrates of Aurora Kinase B were no longer modified, consistent with observed loss of Aurora Kinase B expression and/or activity.

The deduction that short incubation with FQI1 apparently impeded microtubule attachment to kinetochores, as indicated by the prometaphase arrest, is intriguing. Microtubule-kinetochore attachment requires a multitude of proteins, and is the primary process transitioning cells from prometaphase to metaphase. Aurora Kinase B is a key regulator of this process, so it was notable that prometaphase arrest occurred under these conditions without decreasing levels of the kinase. Phosphorylation of Histone H3 on Serine 10 was also not reduced in the cells treated with FQI1 for short periods, however,

this particular Histone H3 Serine is redundantly targeted by other mitotic kinases. Therefore, phosphorylation of other Aurora Kinase B targets should be tested in the context of the short incubation protocol. Regardless, additional work is required to understand how loss of LSF activity might impact microtubule-kinetochore attachments through a non-transcriptional type of regulation.

Regarding longer times of inhibition, whether LSF directly regulates Aurora kinase B or Cdc20 is unknown and should be examined further. ChIP-seq against LSF in HCC cell lines treated with and without FQI1 would be informative as would an evaluation of Aurora Kinase B isoform regulation in circumstances of reduced LSF activity. The latter is of specific interest as upregulation of specific Aurora Kinase B isoforms has been described in HCC patients, an observation which positively correlated with poor prognosis (Yasen et al., 2009).

Finally, I have demonstrated that FQI1 and FQI2 are non-toxic to either freshly isolated primary mouse hepatocytes or in wild type non-tumor bearing mice following consecutive doses of FQIs at levels 2 to 4 times those required for therapeutic benefit in pre-clinical models. Analysis in non-dividing primary mouse hepatocytes did not result in observable toxicity, consistent with the lack of elevated liver enzyme levels detected in the anti-tumor analysis of FQIs assayed in a subcutaneous mouse xenograft model. For the first time, the studies reported here evaluated the impact of FQI1 or FQI2 on hematopoietic cell populations that divide rapidly, and could therefore be susceptible to an anti-mitotic therapy. The results indicated that neither FQI`1or 2 have a significant impact on hematopoietic populations. Whether the lack of observed toxicity is because

the FQI compounds were not exposed to or did not penetrate these cells types *in vivo* remains unknown. Proper pharmacokinetic and exposure studies need to be completed. However, these data are consistent with the accumulating evidence that FQI inhibition of LSF activity in non-immortalized or non-tumor cell populations is non-toxic, lending additional support to the argument that LSF may in fact be the Achilles heel of hepatocellular carcinoma (Shlomai, 2012). The anti-tumor activity of LSF should also be evaluated in other cancer types to determine whether inhibiting LSF could provide a therapeutic benefit and the impact of LSF knockdown in HCC should strongly be considered for further preclinical and possibly clinical evaluation.

LSF has been shown to be an oncogenic transcription factor in HCC, whose activity does not appear to be required for immediate survival of normal cells (Grant et al., 2012; Porta-de-la-Riva et al., 2011; Rajasekaran et al., 2015; Santhekadur et al., 2012a; Santhekadur et al., 2012b). I report here that LSF is a mitotic regulator for HCC cellular progression. LSF has also been reported to regulate fibronectin in Snail induced EMT. As to whether inhibition of LSF activity would inhibit EMT would be worth further investigation given that EMT is the precursor to metastasis. A more important question is whether inhibition of LSF would inhibit metastasis. It has been shown that expression of dnLSF did reduce wide spread tumor formation in an artificial metastasis model *in vivo* (Yoo et al., 2010). However, whether this is due to the inhibiting tumor cell proliferation, inhibition of EMT, or a combination was untested. This concept should be evaluated as this would have enormous implications for LSF as a molecular target for a HCC therapy.

Identifying potent molecular therapies can be complex and often trials fail due to an improper design. The SHARP trial (designed in 2004 to determine the impact of Sorafenib on HCC survival rates) evaluated the compound across various etiologies and ethnicities with great success as it reported survival rates to be in the range of 7-11 months, rates greater than those observed in earlier clinical evaluations (Torrecilla and Llovet, 2015). The increased success was attributed to improved strategies regarding clinical trial design for the HCC patient population. While the data were not stunning, the SHARP trial generated information allowing better future study designs for molecular therapies to be evaluated in the HCC populations. Unfortunately, a number of recent molecularly targeted therapies (Sunitinib, Brivanib, Erlotinib, Lifnifanib, Everolimus), have failed to show a survival benefit (Torrecilla and Llovet, 2015). One hypothesis set forth to explain the failures was that Sorafenib's "success" was most likely due to a balance of targeting cancer cells and the microenvironment, a feature absent from the new molecular candidates. Regardless, alternative molecular therapies have failed, even with new information on how to properly evaluate efficacy bringing no new relief to this population with an unmet need.

LSF remains unique among potential HCC clinical targets in that the data generated here suggest LSF-mediated mitotic regulation both potentially through non transcriptional interactions impacting microtubule-kinetochore attachment and through expression of a major mitotic kinase and mitotic proteolysis member. The inhibition of LSF does not appear to impact non-dividing cells as shown with primary mouse hepatocytes and *in vivo* studies. These data, combined with previous reports, support the

anti-tumor activity specific to HCC cells as a case of oncogene addiction (Weinstein and Joe, 2008). Current suggestions to design the ideal HCC molecular target include proposals to target oncogenic transcription factors, microtubule regulators (Komlodi-Pasztor et al., 2011), proteolysis members, and those that enhance EMT (Sekyrova et al., 2012; Torrecilla and Llovet, 2015). These are all criteria for which LSF may qualify and therefore generate further excitement around the clinical candidacy for LSF. Given the high unmet need in HCC with worldwide primary liver cancer rates on the rise, as well as, very limited available safe and effective therapies, the possibility that targeting LSF in HCC could represent a major breakthrough is exciting. Further experiments to validate LSF as a target and uncover its full mechanism of action as well as optimization of the FQI family of compounds for possible application in clinical studies are clearly warranted.

APPENDIX I

siRNAs Targeting LSF, with off target reduction of Mad2, result in HCC cell death following decreased mitotic time and reduced expression of both Aurora B kinase and Cdc20.

Introduction

The ability to robustly knockdown a gene of interest in molecular biology has enabled acquisition of significant insight in recent years. Information generated utilizing specific gene silencing has provided mechanistic insights into the functionality of proteins of interest that, prior to this technological advance, may have once been deemed out of reach. This is particularly true in the case of transcription factors, which have been notoriously difficult to target utilizing small molecular inhibitors due to the smaller size of their DNA binding domains coupled with their intrinsic structural instability, a trait allowing their promiscuity, enabling binding to various proteins resulting in diverse functionality (Yan and Higgins, 2013). However, as with all technologies, proper investigational practices must be followed in order to rule out any nonspecific events. Identifying siRNAs capable of specific and robust gene silencing can be a rigorous exercise. Generating siRNA sequences that are proficient at accessing the target site is a requirement as the structure of native mRNA or co-factor association could inhibit access and impact silencing capabilities. Direct hybridization to off-target sequences also must be minimized by using algorithms to reduce the probability of this occurring. Finally, rescue experiments should be executed, when feasible, to confirm the restoration of the observed phenotype.

However, as reported in Hubner et al 2010, results may be misleading if the phenotype is inadvertently rescued by another mechanism (Hubner et al., 2010). Mitotic Arrest Deficient 2 (Mad2) is a key member of the spindle assembly checkpoint (SAC) required for proper chromosome segregation (Ditchfield et al., 2003). Mad2 is required for cells to transit from metaphase to anaphase. Even minimal levels of Mad2 knockdown can result in cell death and multi-nucleation as cells with an inactivated checkpoint and an inappropriate spindle attachment inappropriately enter anaphase. The Hubner et al. report showed that transfection of certain siRNAs resulted in non-specific reduction of Mad2 expression impacting both its gene expression (mRNA) and protein levels (Hubner et al., 2010). Furthermore, the Mad2 knockdown was not a consequence of direct hybridization of the siRNAs to the Mad2 transcript, based on homology predictions, but rather of an upstream event in the Mad2 pathway. This target or mechanism has yet to be identified. The reduction of Mad2 levels occurred with multiple, but not all siRNAs suggesting that this observation was a sequence, not target, dependent event that resulted in the initial misinterpretation of the role of Plk1-interacting checkpoint helicase (PICH) regulating the spindle assembly checkpoint (SAC) (Hubner et al., 2010; Llovet et al., 2015). To investigate the phenotype of LSF knockdown in hepatocellular carcinoma, multiple siRNAs were designed to specifically target LSF messenger RNA. A single siRNA (LSF siRNA2) was observed to have off-target effects on Mad2. LSF siRNA2 was identified as a potent siRNA for reducing LSF expression (Figure 4.1e and f). However, additional assessment revealed that Mad2 was also nonspecifically reduced,

albeit with different kinetics (a slower rate and to a lesser extent) when compared to the predicted target (LSF) of the siRNA, but nevertheless had an impact on the phenotypes observed in the experiments. In particular, knockdown of LSF with siRNA 2 resulted in decreased amount of time to transit mitosis, followed by HCC cell death including apoptosis and multi-nucleation. These phenotypes are consistent with Mad2 reduction (Michel et al., 2004a; Michel et al., 2004b). LSF siRNA 2 treatment also resulted in dose dependent reduction of Aurora B Kinase and Cdc20 protein and RNA. A comparison of cellular consequences of siRNAs specific for only LSF (LSF siRNA) versus LSF plus Mad2 reductions (LSF siRNA2) therefore showed overlapping but not identical phenotypes. Both siRNAs caused reduction of Aurora kinase B, reduction of Cdc20, multi-nucleation, and apoptosis, however only the specific knockdown of LSF alone resulted in an increase in mitotic time (Chapter 4).

Results

Treatment with LSF siRNA 2 results in cell death following mitotic exit

A potent siRNA targeting LSF, (duplex 9) LSF 2, was identified from the screen described in chapter 4. HCC cells with LSF knockdown with LSF siRNA 2 revealed cell death following progression through the cell cycle. By phase contrast imaging, the cell number was reduced following transfection with LSF siRNA 2 compared to with control siRNA (Figure A1.1). Further, cellular DNA profiles of HCC cells treated with LSF siRNA 2 revealed an increasing amount of cells with sub-G1 DNA content in comparison to control (Figure A1.2a). Aurora Kinase B and Cdc20 levels were evaluated, as FQI1

inhibition of LSF (Chapter 3) generated phenotypes that were similar to those previously reported upon inhibition of AurkB or Cdc20. To determine if Aurora kinase B or Cdc20 levels were altered, both RNA and protein expression were evaluated in synchronized cells treated with LSF siRNA 2. The data revealed dose dependent reduction of both targets (Figure A1.3). To confirm loss of the mitotic kinase activity, phosphorylation of substrates of Aurora Kinase B, on serine 10 and serine 28 of Histone 3, were also examined. Modification on both of these targets was reduced, concomitant with increasing siRNA levels and consistent with the observed reduction in AurkB (Figure A1.3).

Due to the reduction in key mitotic proteins Aurora Kinase B and Cdc20, mitotic progression was assessed following treatment with LSF siRNA 2 or control. Mitotic phenotypes were analyzed by cellular morphology of the DNA (with DAPI) and mitotic spindles (with antibody against alpha tubulin). The analysis revealed an increased number of apoptotic cells as identified by fragmented nuclei, decreased numbers of cells in prometaphase and metaphase, and an increased number of multi-nucleated cells in comparison to the controls at various time points (Figure A1.4, Tables A1.1 and A1.2). For this analysis, 91 to 100 cells were analyzed per condition. The off center phenotype was one in which the condensed DNA was not located in the center of the cell as is typically observed prior to microtubule attachment from either spindle pole. These data collectively suggested a reduced number of cells in mitosis following LSF knockdown with LSF siRNA 2 as well as incidents of multi-nucleation. To more fully understand the

mitotic impact of LSF siRNA 2 treatment in HCC treated cells, live cell imaging was performed with QGY-7703 cells expressing mEmerald-tagged histone H2B, following transfection with either control siRNA or LSF siRNA 2. The LSF siRNA 2-treated cells reached nuclear envelope breakdown (NEB) earlier than those treated with control siRNA as determined by the time lapse analysis. Additionally, the LSF siRNA2 treated cells exhibited a significant reduction in mitotic time as measured from NEB to anaphase (Figure A1.5) with most cells traversing this in 16-24 minutes from NEB to anaphase, as compared to 24-36 minutes for the control siRNA treated cells. Spending less time to passage through mitosis is consistent with a reduced number of cells at a given time point in prometaphase or metaphase, and increased numbers of cells at a given point exhibiting cytokinesis in the cells treated with LSF siRNA 2. Consistent with these data were the DNA profiles of synchronized cells at various time points after release from the final G1/S block (Figure A1.6) where the LSF siRNA treated cells appear to progress rapidly from 2n DNA content to subG1 content. Combined with the time lapse results, we conclude that the cells progress rapidly through the cell cycle prior to cell death.

A potent siRNA targeting LSF also reduces Mad2 gene expression, albeit, with slower kinetics than those observed with the siRNA direct target

Given the impact of LSF on mitosis, which was previously undescribed, when using siRNA to reduce LSF levels and determine its biological role, it was essential to take into account that some siRNAs can cause off target effects on Mad2 expression (Hubner et al., 2010). To determine whether the potent LSF siRNA2 exhibited similar

same off target effects, Mad2 gene expression was measured in HCC cells treated with LSF siRNA 2 or control siRNA. Mad2 RNA levels were indeed reduced after treatment with this LSF siRNA (Figure A1.7). Mad2 gene expression was reduced to approximately 50 percent of the control levels at the time when maximal LSF protein reduction was predicted to have occurred, 72 hours post transfection (Figure A1.3c).

Discussion

Previous reports have shown that certain siRNA sequences can non-specifically reduce Mad2 transcript and protein levels through an unknown mechanism (Hubner et al., 2010). Transfection with the specific LSF siRNA 2, unlike transfection with the LSF siRNA used in Chapter 4, revealed an approximately 50% reduction in MAD2 RNA expression. A search using the National Center for Biotechnology Information (NCBI) revealed that the neither the sense nor antisense strand of LSF siRNA 2 duplex showed significant homology with the Mad2 mRNA, suggesting that the siRNA itself was unlikely to directly hybridize to the Mad2 RNA sequence. As shown in asynchronous cells, Mad2 gene reduction occurs at a slower rate than that observed for the intended target of LSF siRNA 2, consistent with the notion that the non-specific event is not hybridization based but occurring upstream in the Mad2 pathway. These data suggest that to confirm the impact of a particular siRNA on Mad2 regulation, the appropriate test is to measure gene expression levels in comparison to the controls as a semi-quantitative western blot may not reveal the subtle reduction in Mad2 expression. Preferably, proper controls when examining cellular phenotypes would include an siRNA previously

confirmed not to result in this phenotype or an addition of an untreated cell population. It is worth noting that the Mad2 reduction with this LSF siRNA was observed in both asynchronous and synchronous populations. Finally, since the Mad2 off target effect occurred with slower kinetics compared to the LSF knockdown, confirmation of siRNA specificity requires evaluation of Mad2 expression at time points at least 72 hours following RNAi transfection.

The evaluation of LSF knockdown in hepatocellular carcinoma cells, using LSF targeting siRNAs with and without a non-specific Mad2 reduction, generated both overlapping and distinct phenotypes. The identification of the Mad2 reduction for LSF siRNA2 induced a re-screen of candidate LSF siRNAs to identify sequences that did not impact Mad2 gene expression. The data generated with the LSF siRNA utilized in experiments in Chapter 4 largely resulted in observations consistent with those from LSF siRNA2, with the exception of the length of time to progress through mitosis. In addition, pure LSF knockdown resulted an observation of cellular senescence. The increased mitotic time is consistent with the results obtained with the LSF small inhibitor (Chapter 4), indicating that loss of LSF function is responsible for the lengthening of mitosis. LSF knockdown in both contexts resulted in HCC cell death along with multi-nucleation, and reduction in both Aurora B kinase and Cdc20 expression. I hypothesize that the reduced mitotic time observed here was solely due to the incapacitation of the Spindle Assembly Checkpoint (SAC) due to nonspecific reduction of Mad2 levels. Importantly, the phenotypes described in Chapter 4, generated with the LSF siRNA that did not inadvertently reduce Mad2 levels, were consistent with the phenotypes generated

with small molecular inhibitors of LSF. Together, these data implicate LSF as a mitotic regulator and confirm the reduction of Aurora B Kinase and Cdc20 as an observation related to LSF mitotic regulation in HCC cells.

These findings support the requirement for screening siRNAs for nonspecific knockdown of Mad2 and doing so at multiple time points as the off target event could result in improper interpretation of data. This is especially true when investigating mitotic proteins or when one needs to identify siRNAs that have no toxic consequence.

Figures

Illustration A1.1

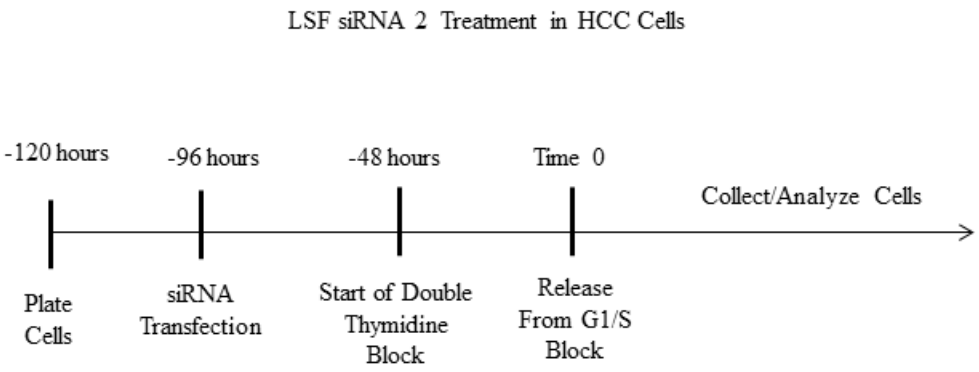

Illustration A1.2

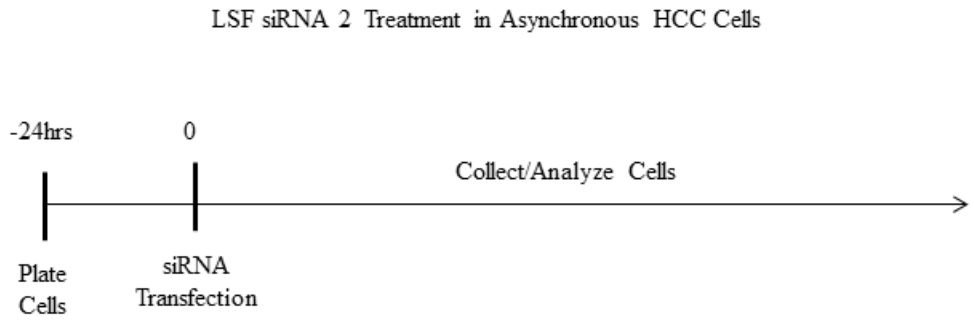

Figure A1.1 Phase contrast imaging of LSF siRNA 2-treated QGY-7703 cells suggests reduction in cell proliferation.

QGY-7703 cells were transfected with either (a) 20 nM Control siRNA or (b) 20 nM LSF siRNA 2 prior to imaging according to illustration A1.1. Cells were synchronized using a double thymidine block. 72 hours post release from the G1/S block phase contrast images were taken at a magnification of 20x. Images are representative of greater than five experiments.

(a) Control siRNA 20 nM

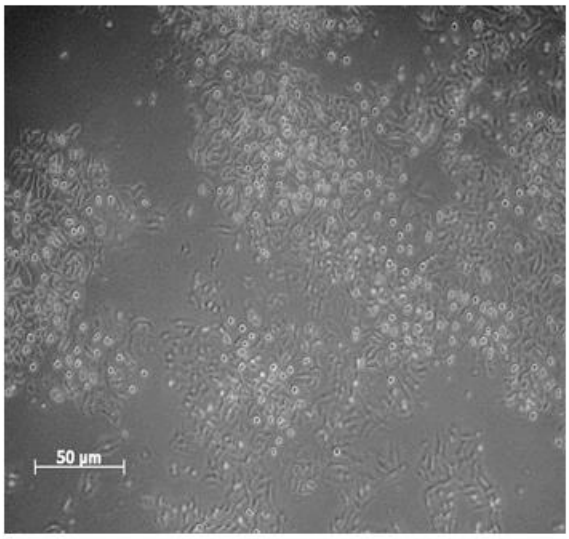

LSF siRNA 20 nM

(b)

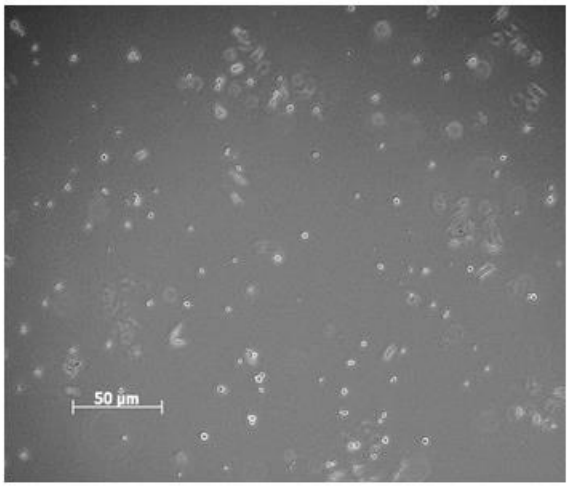

Figure A1.2 Treatment of asynchronous HCC cells with LSF siRNA2 reveals an increase in cells with sub-G1 DNA content

HCC cells were treated with LSF siRNA 2 or control siRNA at concentrations of 10 or 20 nM. QGY-7703 cells, fixed and stained with propidium iodide, were analyzed at 24, 48, 72 and 96 hours post release on a FACS Calibur to analyze DNA content. Cells transfected with control siRNA were analyzed at 0 hrs to determine instrument settings. Synchronized HCC cells transfected with control siRNA or LSF siRNA 2 were directly compared to evaluate cell cycle progression. These results are representative of 3 independent experiments.

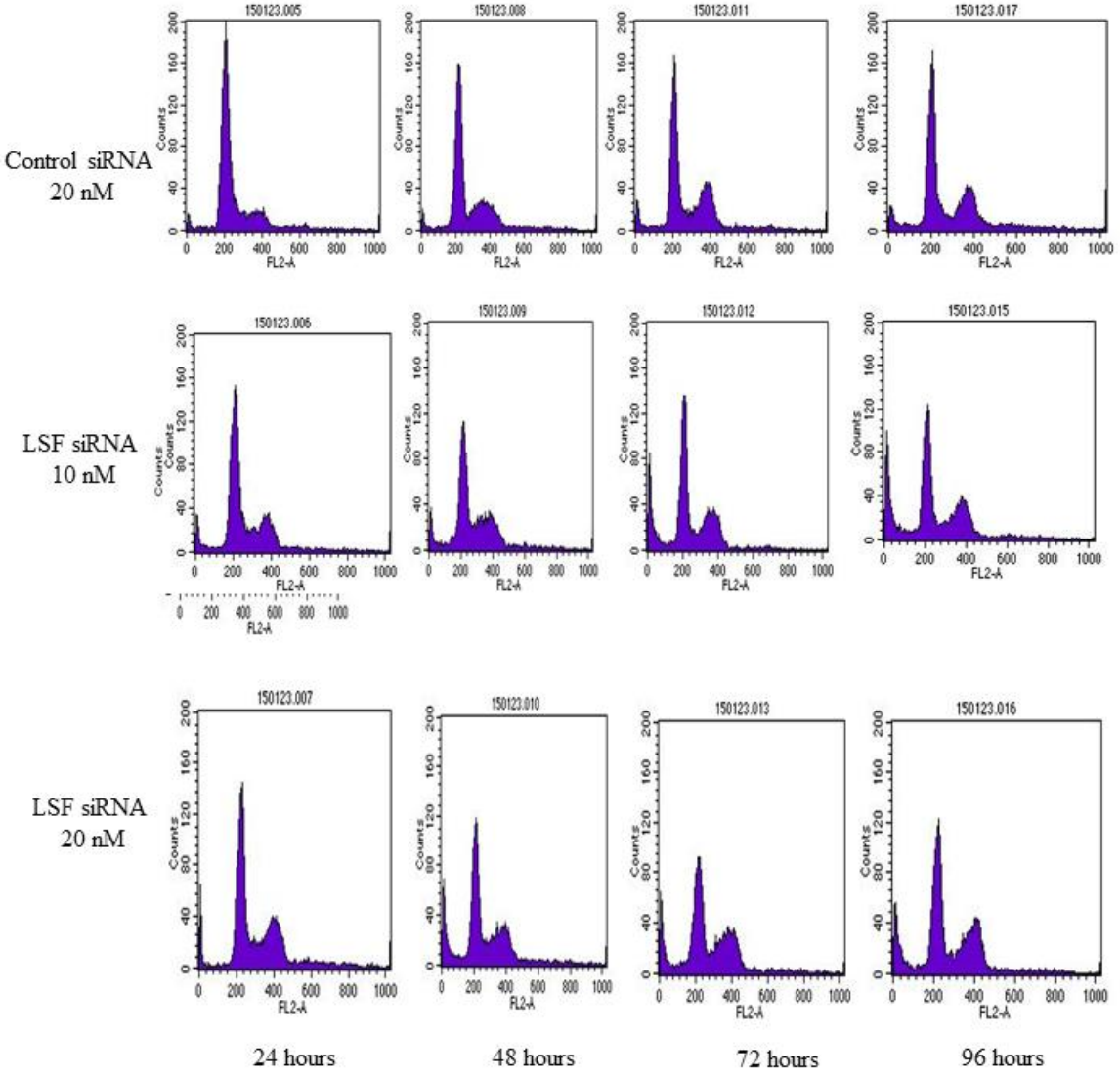
Control siRNA
20 nM
LSF siRNA
10 nM
LSF siRNA
20 nM
150123.005
150123.008
150123.011
150123.017
150123.006
150123.009
150123.012
150123.015
150123.007
150123.010
150123.013
150123.016
Counts
FL2-A
24 hours
48 hours
72 hours
96 hours

Figure A1.3. Aurora Kinase B and Cdc20 expression is significantly reduced upon LSF knockdown

Synchronized, LSF siRNA-transfected HCC cells were lysed at various time points following G1/S release. (a) Immunoblots of the indicated proteins and protein modifications from cells at 0, 4, and 9 hours after release from the G1/S block. Levels of Beta Actin were used for normalization. Numbers depicted below each band represent percentage of protein relative to the level in the siRNA control sample. Protein expression or phosphorylation was quantitated using the Odyssey Licor detection system where integrated intensity for the target protein or phosphorylation was normalized to the beta actin control. Data are depicted as the area of pixels determined for (b) LSF (c) Aurora Kinase B (d) Cdc20 (e) Phosphorylated Histone Serine 3 and (f) Phosphorylated Histone Serine 28 normalized to the area of pixels detected for beta actin. Results are representative of 3 independent experiments. mRNA expression is depicted for (g) Aurora kinase B and (h) Cdc20, with each target gene normalized to Beta Actin. Data are representative of two independent experiments.

(a)

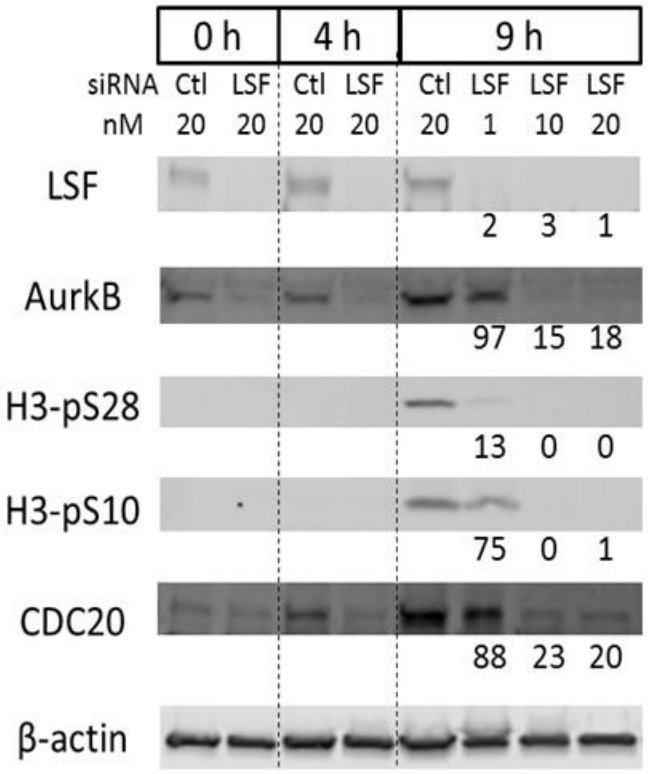
0 h
4 h
9 h
siRNA Ctl LSF Ctl LSF Ctl LSF LSF LSF
nM 20 20 20 20 20 1 10 20
LSF
2 3 1
AurkB
97 15 18
H3-pS28
13 0 0
H3-pS10
75 0 1
CDC20
88 23 20
β-actin

(b)

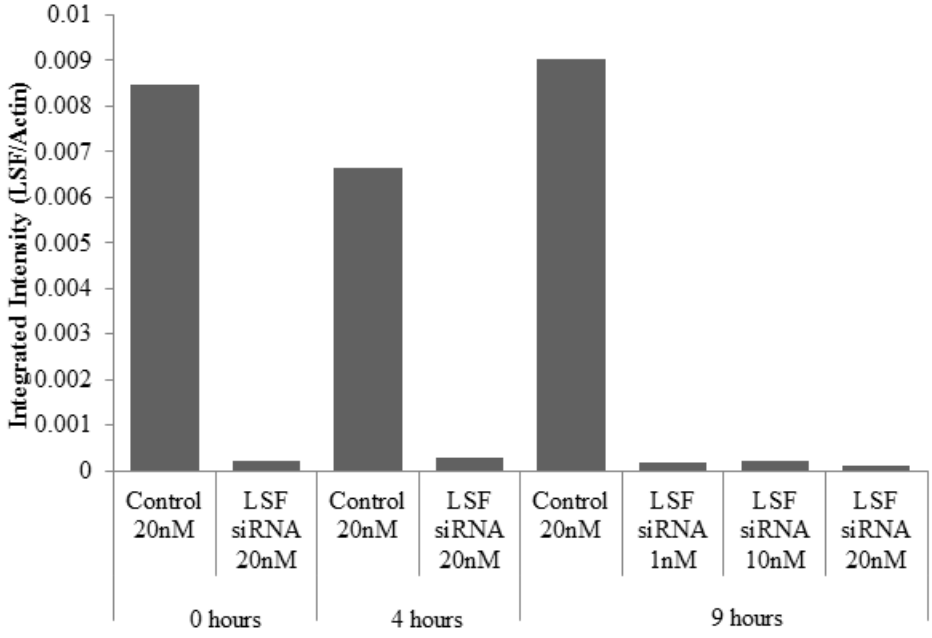
Integrated Intensity (LSF/Actin)
0.01
0.009
0.008
0.007
0.006
0.005
0.004
0.003
0.002
0.001
0
Control 20nM
LSF siRNA 20nM
Control 20nM
LSF siRNA 20nM
Control 20nM
LSF siRNA 1nM
LSF siRNA 10nM
LSF siRNA 20nM
0 hours
4 hours
9 hours

(c)

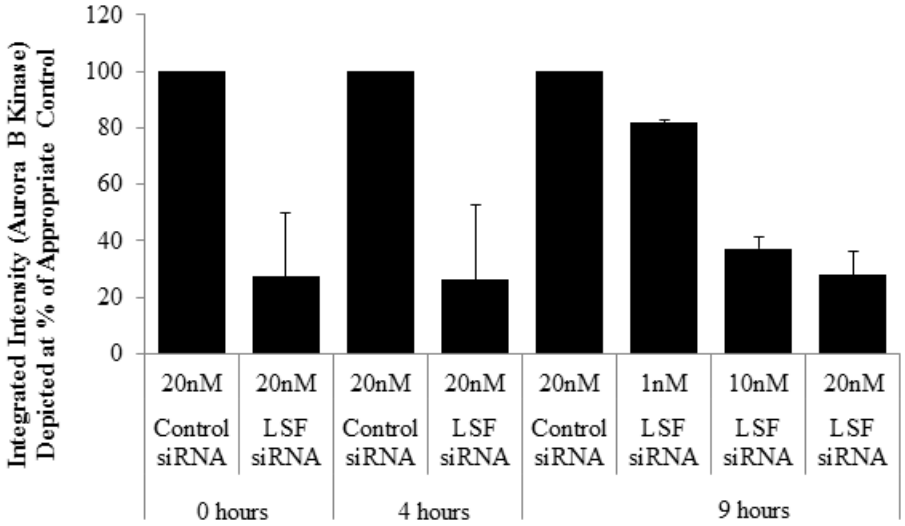
Integrated Intensity (Aurora B Kinase)
Depicted at % of Appropriate Control
120
100
80
60
40
20
0
20nM Control siRNA
20nM LSF siRNA
20nM Control siRNA
20nM LSF siRNA
20nM Control siRNA
1nM LSF siRNA
10nM LSF siRNA
20nM LSF siRNA
0 hours
4 hours
9 hours

(d)

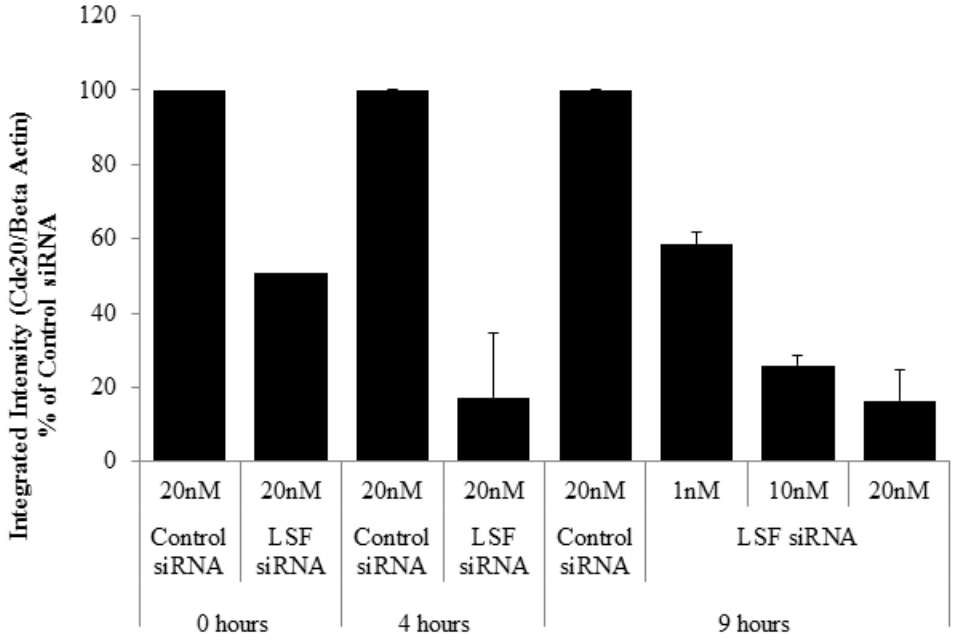
Integrated Intensity (Cdc20/Beta Actin)
% of Control siRNA
120
100
80
60
40
20
0
20nM Control siRNA
20nM LSF siRNA
20nM Control siRNA
20nM LSF siRNA
20nM Control siRNA
1nM
10nM
20nM
LSF siRNA
0 hours
4 hours
9 hours

(e)

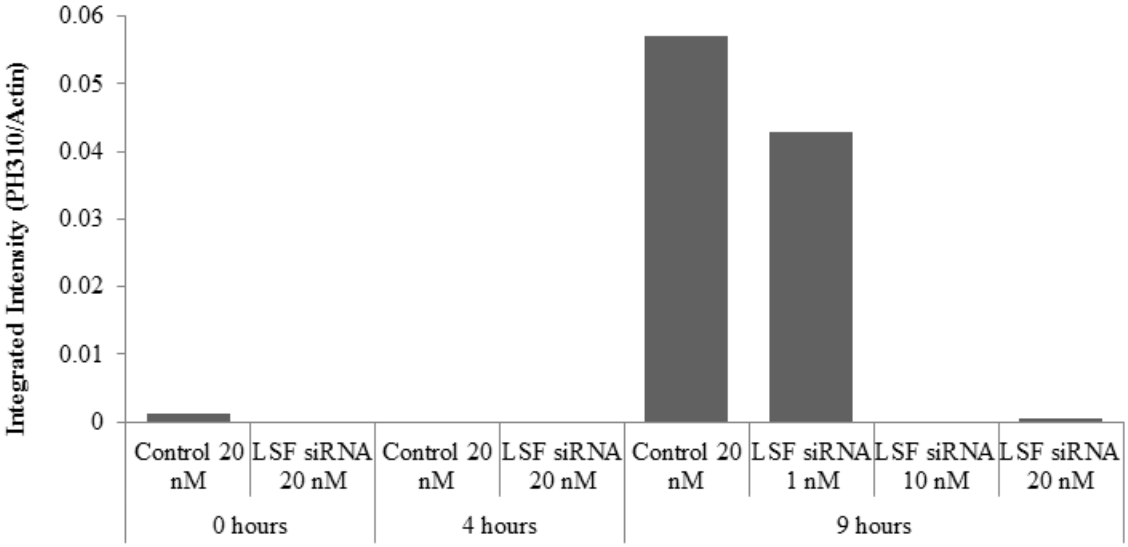
Integrated Intensity (PH310/Actin)
0.06
0.05
0.04
0.03
0.02
0.01
0
Control 20 nM
LSF siRNA 20 nM
Control 20 nM
LSF siRNA 20 nM
Control 20 nM
LSF siRNA 1 nM
LSF siRNA 10 nM
LSF siRNA 20 nM
0 hours
4 hours
9 hours

(f)

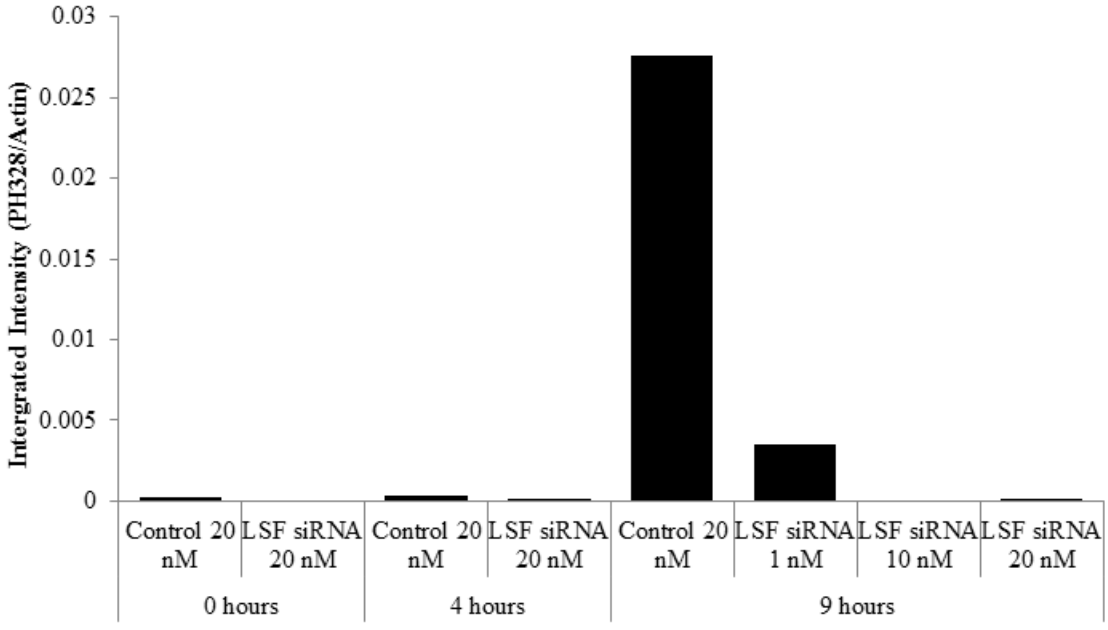
Intergrated Intensity (PH328/Actin)
0.03
0.025
0.02
0.015
0.01
0.005
0
Control 20 nM
LSF siRNA 20 nM
Control 20 nM
LSF siRNA 20 nM
Control 20 nM
LSF siRNA 1 nM
LSF siRNA 10 nM
LSF siRNA 20 nM
0 hours
4 hours
9 hours

(g)

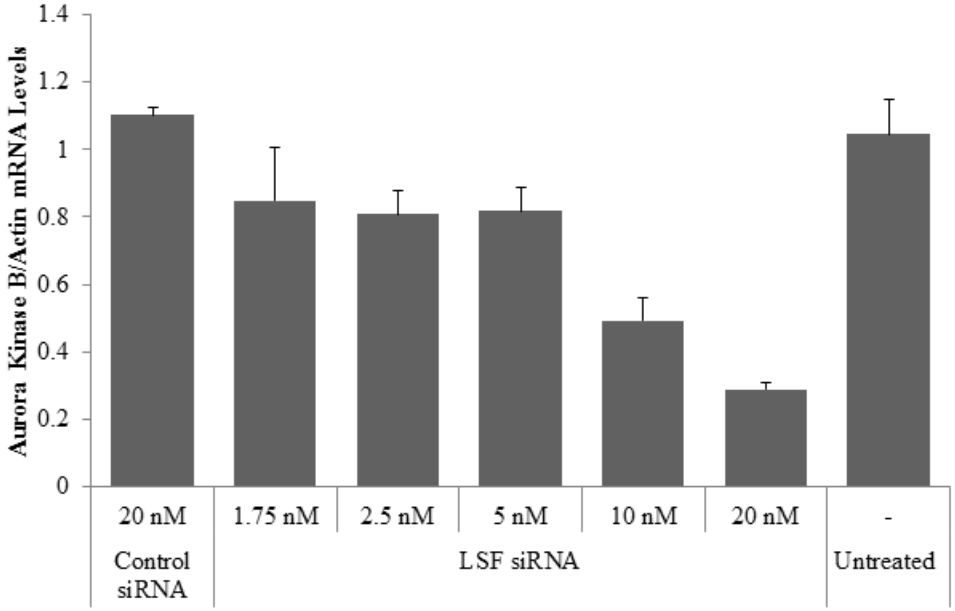
Aurora Kinase B/Actin mRNA Levels
1.4
1.2
1
0.8
0.6
0.4
0.2
0
20 nM
1.75 nM
2.5 nM
5 nM
10 nM
20 nM
-
Control siRNA
LSF siRNA
Untreated

(h)

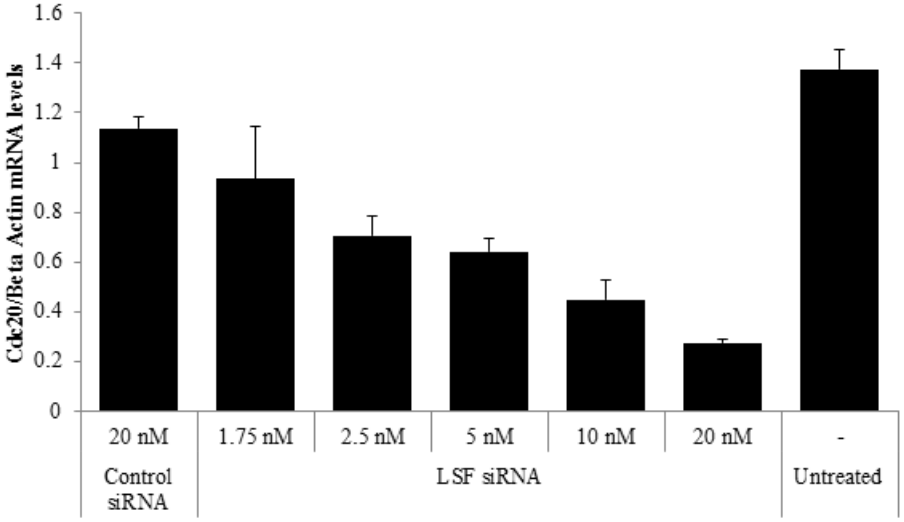
Cdc20/Beta Actin mRNA levels
1.6
1.4
1.2
1
0.8
0.6
0.4
0.2
0
20 nM
1.75 nM
2.5 nM
5 nM
10 nM
20 nM
-
Control siRNA
LSF siRNA
Untreated

Figure A1.4 Immunofluorescent analysis of synchronized QGY-7703 cells after LSF knockdown with LSF siRNA 2 reveals fewer cells in mitosis as well as observations of both multi-nucleated and apoptotic cells

QGY-7703 cells were transfected with 20 nM of either LSF or control siRNA, and then synchronized at the G1/S border. At 0, 5, 9 and 21 hours after release from G1/S, QGY-7703 cells were fixed and stained with anti-alpha tubulin antibody and with DAPI. Images were analyzed on a Zeiss Axioimager at a 63x magnification. Approximately 100 individual cells were analyzed within each group. Representative images 9 hours after release from G1/S of the cells treated with control siRNA (left panels) or LSF siRNA (right panels). Control cells show normal mitotic phenotypes, including examples of metaphase and cytokinesis. LSF siRNA-treated cells show various defects, including cells with fragmented nuclei and multi-nucleation.

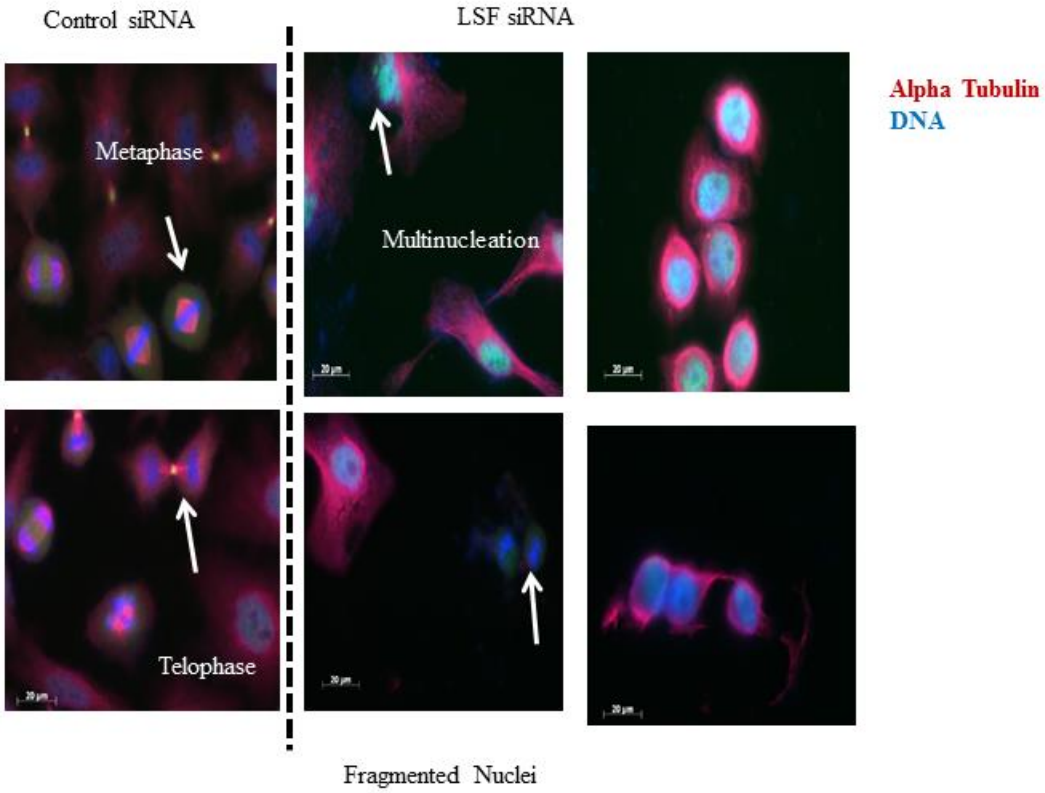
Control siRNA
LSF siRNA
Metaphase
Multinucleation
Telophase
Alpha Tubulin
DNA
Fragmented Nuclei

Figure A1.5 HCC cells expressing mEmerald-tagged histone H2B were analyzed by time lapse microscopy upon treatment with either LSF siRNA2 or control siRNA.

Synchronized cells, using a double thymidine block, were imaged every 4 minutes at 63x magnification. Time from nuclear envelope breakdown to anaphase was determined for 56-100 cells per sample treated with 20 nM of either LSF siRNA 2 or Control siRNA. The results here include multiple samples, 2 controls receiving the non-specific siRNA and 2 groups receiving LSF siRNA 2. One experiment received 20 µM exogenous thymidine at the release from the G1/S block. Because addition of thymidine did not affect the outcome, the error bars are standard deviations of the averages from the samples, plus or minus thymidine addition.

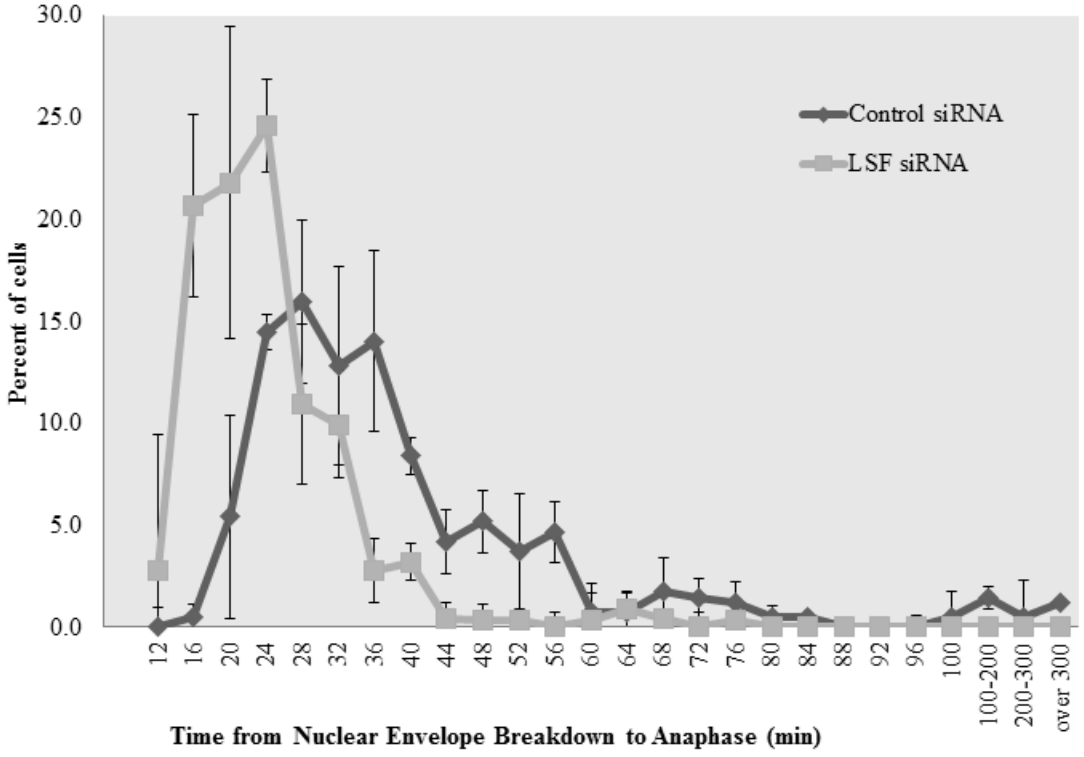

Figure A1.6 Synchronized HCC cells with LSF and Mad2 knockdown results in increasing numbers of cells with sub-G1 DNA content over time

QGY-7703 cells were synchronized at the G1/S border post transfection with 20 nM control siRNA or 20 nM LSF siRNA (Illustration 5.1). At 0, 3.5, 9 and 21 and 27 hours after release from the G1/S block, cells were fixed and stained with propidium iodide for analysis of DNA content by flow cytometry. Data are representative of greater than 4 experiments.

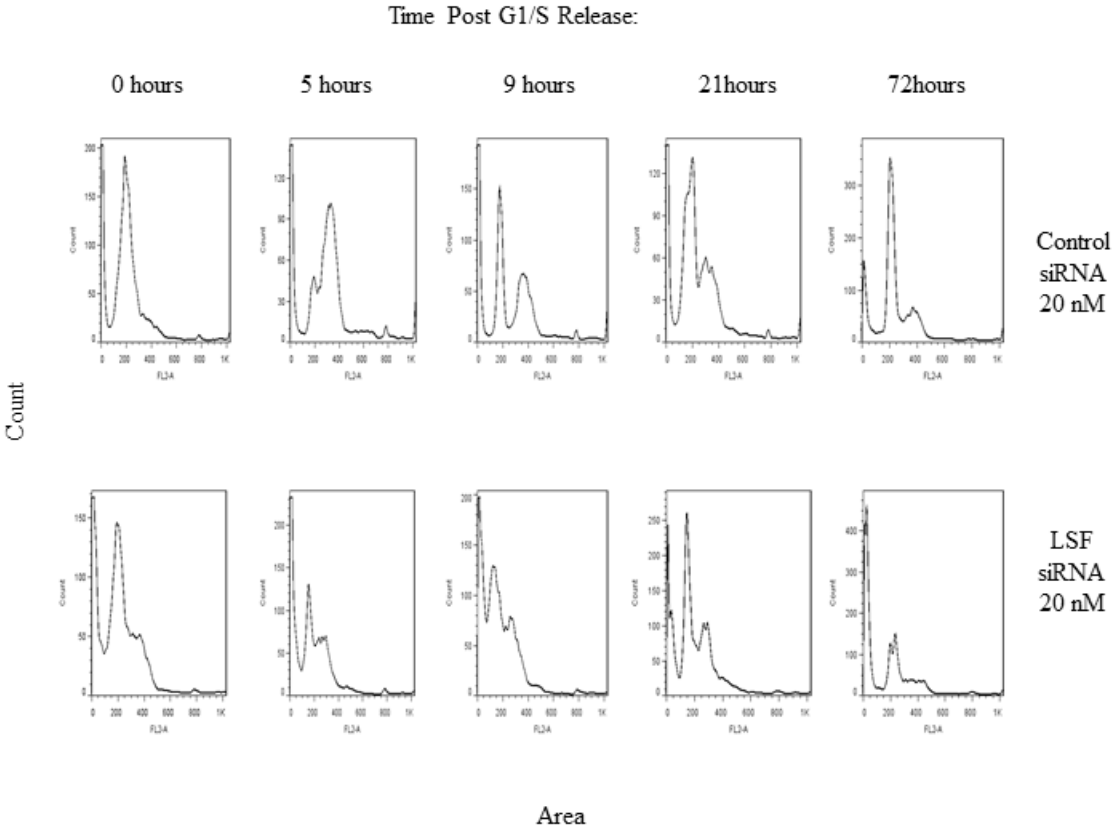

Figure A1.7 Mad2 RNA levels are reduced in LSF siRNA 2 treated cells

LSF and Mad2 RNA levels from cells treated with either LSF siRNA 2 or Control siRNA. For asynchronous cells, samples were analyzed at 24, 48 or 72 hours post transfection. For examination in synchronous cells, the protocol in Illustration in A1.1 was used. RNA was isolated at 4 and 8 hours after the final release from G1/S. Standard error represents averages from two independent experiments. These data are consistent across 3 independent experiments, with the third experiment having slightly different time points.

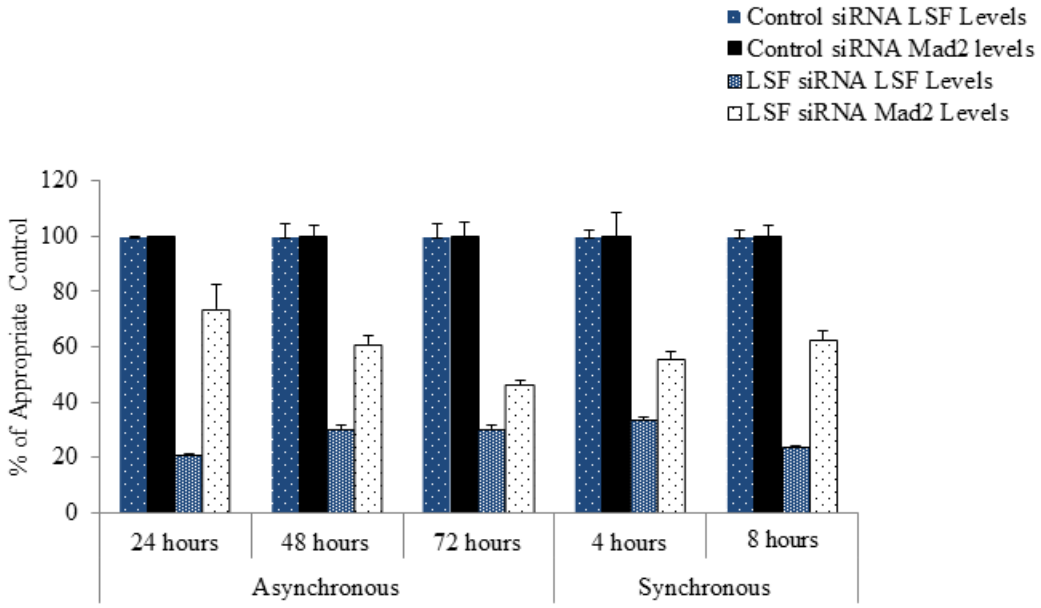

Table AI.1. Immunofluorescence of synchronized QGY 7703 cells after LSF knockdown reveals fewer cells in mitosis.

	Control siRNA 20nM			LSF siRNA 20nM		
	5 hours	9 hours	21 hours	5 hours	9 hours	21 hours
Interphase	98.5	30.4	70.3	69.0	61.5	67.4
Prometaphase	0.7	6.6	6.6	1.1	1.0	0.0
Metaphase	0.7	23.8	7.7	0.0	1.0	0.0
Cytokinesis	0.0	39.2	15.4	5.7	4.2	7.0

Table AI.2. Immunofluorescence of synchronized QGY 7703 cells after LSF knockdown reveals multi-nucleated and apoptotic cells.

	Control siRNA 20nM			LSF siRNA 20nM		
	5 hours	9 hours	21 hours	5 hours	9 hours	21 hours
Off Center	0.0	0.0	0.0	1.1	0.0	7.0
Apoptotic	0.0	0.0	0.0	19.5	32.3	9.3
Multinucleated	0.0	0.0	0.0	3.4	0.0	9.3

BIBLIOGRAPHY

Andrews, P.D. (2005). Aurora kinases: shining lights on the therapeutic horizon? Oncogene *24*, 5005-5015.

Bavetsias, V., and Linardopoulos, S. (2015). Aurora Kinase Inhibitors: Current Status and Outlook. Frontiers Oncology *5*, 278.

Bergmann-Leitner, E.S., Duncan, E.H., and Leitner, W.W. (2003). Identification and targeting of tumor escape mechanisms: a new hope for cancer therapy? Current Pharmaceutical Design *9*, 2009-2023.

Bertoli, C., and de Bruin, R.A. (2014). Turning cell cycle entry on its head. Elife *3*, e03475.

Bertoli, C., Skotheim, J.M., and de Bruin, R.A. (2013). Control of cell cycle transcription during G1 and S phases. Nature Reviews in Molecular Cell Biology *14*, 518-528.

Boveia, V., and Schutz-Geschwender, A. (2015). Quantitative Analysis of Signal Transduction with In-Cell Western Immunofluorescence Assays. Methods in Molecular Biology *1314*, 115-130.

Brito, D.A., and Rieder, C.L. (2006). Mitotic checkpoint slippage in humans occurs via cyclin B destruction in the presence of an active checkpoint. Current Biology *16*, 1194-1200.

Brito, D.A., Yang, Z., and Rieder, C.L. (2008). Microtubules do not promote mitotic slippage when the spindle assembly checkpoint cannot be satisfied. Journal of Cell Biology *182*, 623-629.

Bruix, J. (2011). Liver cancer: still a long way to go. Hepatology *54*, 1-2.
Bruix, J., and Llovet, J.M. (2003). HCC surveillance: who is the target population? Hepatology *37*, 507-509.

Bruix, J., and Sherman, M. (2011). Management of hepatocellular carcinoma: an update. Hepatology *53*, 1020-1022.

Carmena, M., Wheelock, M., Funabiki, H., and Earnshaw, W.C. (2012). The chromosomal passenger complex (CPC): from easy rider to the godfather of mitosis. Nature Reviews in Molecular Cell Biology *13*, 789-803.

Casimiro, M.C., Crosariol, M., Loro, E., Li, Z., and Pestell, R.G. (2012). Cyclins and cell cycle control in cancer and disease. Genes Cancer *3*, 649-657.

Chan, K.S., Koh, C.G., and Li, H.Y. (2012). Mitosis-targeted anti-cancer therapies: where they stand. Cell Death and Disease *3*, e411.

Christadore, L.M. (2013). Discovery of a small molecule dihydroquinolinone inhibitor with potent antiproliferative and antitumor activity results in catastrophic cell division (Boston University).

Dai, W., Wang, Q., Liu, T., Swamy, M., Fang, Y., Xie, S., Mahmood, R., Yang, Y.M., Xu, M., and Rao, C.V. (2004). Slippage of mitotic arrest and enhanced tumor development in mice with BubR1 haploinsufficiency. Cancer Research *64*, 440-445.

Debacq-Chainiaux, F., Erusalimsky, J.D., Campisi, J., and Toussaint, O. (2009). Protocols to detect senescence-associated beta-galactosidase (SA-βgal) activity, a biomarker of senescent cells in culture and in vivo. Nature Protocols *4*, 1798-1806.

Delcuve, G.P., He, S., and Davie, J.R. (2008). Mitotic partitioning of transcription factors. Journal of Cellular Biochemistry *105*, 1-8.

Ditchfield, C., Johnson, V.L., Tighe, A., Ellston, R., Haworth, C., Johnson, T., Mortlock, A., Keen, N., and Taylor, S.S. (2003). Aurora B couples chromosome alignment with anaphase by targeting BubR1, Mad2, and Cenp-E to kinetochores. Journal of Cell Biology *161*, 267-280.

Dunker, A.K., and Uversky, V.N. (2010). Drugs for 'protein clouds': targeting intrinsically disordered transcription factors. Current Opinion Pharmacology *10*, 782-788.

El-Serag, H.B., and Kanwal, F. (2014). Epidemiology of hepatocellular carcinoma in the United States: where are we? Where do we go? Hepatology *60*, 1767-1775.

Fan, R.-H., Li, J., Wu, N., and Chen, P.-S. (2011a). Late SV40 factor: a key mediator of Notch signaling in human hepatocarcinogenesis. World Journal of Gastroenterology *17*, 3420-3430.

Fan, R.H., Li, J., Wu, N., and Chen, P.S. (2011b). Late SV40 factor: a key mediator of Notch signaling in human hepatocarcinogenesis. World Journal of Gastroenterology *17*, 3420-3430.

Farazi, P.A., and DePinho, R.A. (2006). Hepatocellular carcinoma pathogenesis: from genes to environment. Nature Reviews Cancer *6*, 674-687.

Fernando, N.T., Koch, M., Rothrock, C., Gollogly, L.K., D'Amore, P.A., Ryeom, S., and Yoon, S.S. (2008). Tumor escape from endogenous, extracellular matrix-associated angiogenesis inhibitors by up-regulation of multiple proangiogenic factors. Clinical Cancer Research *14*, 1529-1539.

Foley, E.A., and Kapoor, T.M. (2013). Microtubule attachment and spindle assembly checkpoint signalling at the kinetochore. Nat Rev Mol Cell Biol *14*, 25-37. Ganem, N.J., and Pellman, D. (2012). Linking abnormal mitosis to the acquisition of DNA damage. Journal of Cell Biology *199*, 871-881.

Gascoigne, K.E., and Taylor, S.S. (2008). Cancer cells display profound intra- and interline variation following prolonged exposure to antimitotic drugs. Cancer Cell *14*, 111-122.

Gascoigne, K.E., and Taylor, S.S. (2009). How do anti-mitotic drugs kill cancer cells? Journal of Cell Science *122*, 2579-2585.

Gottesfeld, J.M., and Forbes, D.J. (1997). Mitotic repression of the transcriptional machinery. Trends in Biochemical Science *22*, 197-202.

Grant, T.J., Bishop, J.A., Christadore, L.M., Barot, G., Chin, H.G., Woodson, S., Kavouris, J., Siddiq, A., Gredler, R., Shen, X.N., *et al.* (2012). Antiproliferative small-molecule inhibitors of transcription factor LSF reveal oncogene addiction to LSF in hepatocellular carcinoma. Proceedings of the National Academy of Science U S A *109*, 4503-4508.

Gu, Y.J., Li, H.D., Zhao, L., Zhao, S., He, W.B., Rui, L., Su, C., Zheng, H.C., and Su, R.J. (2015). GRP78 confers the resistance to 5-FU by activating the c-Src/LSF/TS axis in hepatocellular carcinoma. Oncotarget *6*, 33658-33674.

Guadagno, T.M., and Newport, J.W. (1996). Cdk2 kinase is required for entry into mitosis as a positive regulator of Cdc2-cyclin B kinase activity. Cell *84*, 73-82.

Guttinger, S., Laurell, E., and Kutay, U. (2009). Orchestrating nuclear envelope disassembly and reassembly during mitosis. Nature Reviews in Molecular Cell Biology *10*, 178-191.

Hansen, U., Owens, L., and Saxena, U.H. (2009). Transcription factors LSF and E2Fs: tandem cyclists driving G0 to S? Cell Cycle *8*, 2146-2151.

Hardwick, K.G., and Shah, J.V. (2010). Spindle checkpoint silencing: ensuring rapid and concerted anaphase onset. F1000 Biology Reports *2*, 55.

Hauf, S., Biswas, A., Langegger, M., Kawashima, S.A., Tsukahara, T., and Watanabe, Y. (2007). Aurora controls sister kinetochore mono-orientation and homolog bi-orientation in meiosis-I. EMBO Journal *26*, 4475-4486.

Hauf, S., Cole, R.W., LaTerra, S., Zimmer, C., Schnapp, G., Walter, R., Heckel, A., van Meel, J., Rieder, C.L., and Peters, J.M. (2003). The small molecule Hesperadin reveals a role for Aurora B in correcting kinetochore-microtubule attachment and in maintaining the spindle assembly checkpoint. Journal of Cell Biology *161*, 281-294.

Huang, H.C., Shi, J., Orth, J.D., and Mitchison, T.J. (2009). Evidence that mitotic exit is a better cancer therapeutic target than spindle assembly. Cancer Cell *16*, 347-358.

Huang, H.C., Sundseth, R., and Hansen, U. (1990). Transcription factor LSF binds two variant bipartite sites within the SV40 late promoter. Genes and Development *4*, 287-298.

Hubner, N.C., Wang, L.H., Kaulich, M., Descombes, P., Poser, I., and Nigg, E.A. (2010). Re-examination of siRNA specificity questions role of PICH and Tao1 in the spindle checkpoint and identifies Mad2 as a sensitive target for small RNAs. Chromosoma *119*, 149-165.

Huck, J.J., Zhang, M., McDonald, A., Bowman, D., Hoar, K.M., Stringer, B., Ecsedy, J., Manfredi, M.G., and Hyer, M.L. (2010). MLN8054, an inhibitor of Aurora A kinase, induces senescence in human tumor cells both in vitro and in vivo. Molecular Cancer Research *8*, 373-384.

Hunt, T., Luca, F.C., and Ruderman, J.V. (1992). The requirements for protein synthesis and degradation, and the control of destruction of cyclins A and B in the meiotic and mitotic cell cycles of the clam embryo. Journal of Cell Biology *116*, 707-724.

Inbal, N., Listovsky, T., and Brandeis, M. (1999). The mammalian Fizzy and Fizzy-related genes are regulated at the transcriptional and post-transcriptional levels. FEBS Letters *463*, 350-354.

Irniger, S. (2002). Cyclin destruction in mitosis: a crucial task of Cdc20. FEBS Letter *532*, 7-11.

Jemal, A., Bray, F., Center, M.M., Ferlay, J., Ward, E., and Forman, D. (2011). Global cancer statistics. CA: A Cancer Journal for Clinicians *61*, 69-90.

Kallio, M.J., McCleland, M.L., Stukenberg, P.T., and Gorbsky, G.J. (2002). Inhibition of aurora B kinase blocks chromosome segregation, overrides the spindle checkpoint, and perturbs microtubule dynamics in mitosis. Current Biology *12*, 900-905.

Khong, H.T., and Restifo, N.P. (2002). Natural selection of tumor variants in the generation of "tumor escape" phenotypes. Nature Immunology *3*, 999-1005.

Kim, H.J., Cho, J.H., Quan, H., and Kim, J.R. (2011). Down-regulation of Aurora B kinase induces cellular senescence in human fibroblasts and endothelial cells through a p53-dependent pathway. FEBS Letter *585*, 3569-3576.

Kim, J.U., Shariff, M.I., Crossey, M.M., Gomez-Romero, M., Holmes, E., Cox, I.J., Fye, H.K., Njie, R., and Taylor-Robinson, S.D. (2016). Hepatocellular carcinoma: Review of disease and tumor biomarkers. World Journal of Hepatology *8*, 471-484.

Kimura, M., Uchida, C., Takano, Y., Kitagawa, M., and Okano, Y. (2004). Cell cycle-dependent regulation of the human aurora B promoter. Biochemical and Biophysical Research Communication *316*, 930-936.

Kimura, M., Yoshioka, T., Saio, M., Banno, Y., Nagaoka, H., and Okano, Y. (2013). Mitotic catastrophe and cell death induced by depletion of centrosomal proteins. Cell Death and Disease *4*, e603.

Kokoszynska, K., Ostrowski, J., Rychlewski, L., and Wyrwicz, L.S. (2008). The fold recognition of CP2 transcription factors gives new insights into the function and evolution of tumor suppressor protein p53. Cell Cycle *7*, 2907-2915.

Komlodi-Pasztor, E., Sackett, D., Wilkerson, J., and Fojo, T. (2011). Mitosis is not a key target of microtubule agents in patient tumors. Nature Reviews Clinical Oncology *8*, 244-250.

Le, L.T., Vu, H.L., Nguyen, C.H., and Molla, A. (2013). Basal aurora kinase B activity is sufficient for histone H3 phosphorylation in prophase. Biology Open *2*, 379-386.

Lim, S., and Kaldis, P. (2013). Cdks, cyclins and CKIs: roles beyond cell cycle regulation. Development *140*, 3079-3093.

Llovet, J.M. (2006). Expanding HCC criteria for liver transplant: the urgent need for prospective, robust data. Liver Transplant *12*, 1741-1743.

Llovet, J.M., Ricci, S., Mazzaferro, V., Hilgard, P., Gane, E., Blanc, J.F., de Oliveira, A.C., Santoro, A., Raoul, J.L., Forner, A., *et al.* (2008). Sorafenib in advanced hepatocellular carcinoma. New England Journal of Medicine *359*, 378-390.

Llovet, J.M., Villanueva, A., Lachenmayer, A., and Finn, R.S. (2015). Advances in targeted therapies for hepatocellular carcinoma in the genomic era. Nature Reviews in Clinical Oncology *12*, 436.

Long, J.J., Leresche, A., Kriwacki, R.W., and Gottesfeld, J.M. (1998). Repression of TFIIH transcriptional activity and TFIIH-associated cdk7 kinase activity at mitosis. Molecular Cell Biology *18*, 1467-1476.

Loong, H.H., and Yeo, W. (2014). Microtubule-targeting agents in oncology and therapeutic potential in hepatocellular carcinoma. Onco Targets Ther *7*, 575-585. Malumbres, M. (2007). Cyclins and related kinases in cancer cells. Journal of BUON *12 Suppl 1*, S45-52.

Marengo, A., Rosso, C., and Bugianesi, E. (2016). Liver Cancer: Connections with Obesity, Fatty Liver, and Cirrhosis. Annual Reviews Medicine *67*, 103-117.

Marquardt, J.U., Galle, P.R., and Teufel, A. (2012). [Hepatocellular carcinoma: molecular pathogenesis and novel targets for therapy]. Deutsche medizinische Wochenschrift *137*, 855-860.

Michel, L., Benezra, R., and Diaz-Rodriguez, E. (2004a). MAD2 dependent mitotic checkpoint defects in tumorigenesis and tumor cell death: a double edged sword. Cell Cycle *3*, 990-992.

Michel, L., Diaz-Rodriguez, E., Narayan, G., Hernando, E., Murty, V.V., and Benezra, R. (2004b). Complete loss of the tumor suppressor MAD2 causes premature cyclin B degradation and mitotic failure in human somatic cells. Proceedings of the National Academy of Science U S A *101*, 4459-4464.

Mitchison, T.J. (2012). The proliferation rate paradox in antimitotic chemotherapy. Molecular Biology Cell *23*, 1-6.

Niles, A.L., Moravec, R.A., Eric Hesselberth, P., Scurria, M.A., Daily, W.J., and Riss, T.L. (2007). A homogeneous assay to measure live and dead cells in the same sample by detecting different protease markers. Analytical Biochemistry *366*, 197-206.

Orth, J.D., Loewer, A., Lahav, G., and Mitchison, T.J. (2012). Prolonged mitotic arrest triggers partial activation of apoptosis, resulting in DNA damage and p53 induction. Molecular Biololgy Cell *23*, 567-576.

Pagliarini, R., Shao, W., and Sellers, W.R. (2015). Oncogene addiction: pathways of therapeutic response, resistance, and road maps toward a cure. EMBO Report *16*, 280-296.

Perz, J.F., Armstrong, G.L., Farrington, L.A., Hutin, Y.J., and Bell, B.P. (2006). The contributions of hepatitis B virus and hepatitis C virus infections to cirrhosis and primary liver cancer worldwide. Journal of Hepatology *45*, 529-538.

Poon, R.Y. (2013). Aurora B: hooking up with cyclin-dependent kinases. Cell Cycle *12*, 1019-1020.

Porta-de-la-Riva, M., Stanisavljevic, J., Curto, J., Franci, C., Diaz, V.M., Garcia de Herreros, A., and Baulida, J. (2011). TFCP2c/LSF/LBP-1c is required for Snail1-induced fibronectin gene expression. Biochemical Journal *435*, 563-568.

Powell, C.M., Rudge, T.L., Zhu, Q., Johnson, L.F., and Hansen, U. (2000). Inhibition of the mammalian transcription factor LSF induces S-phase-dependent apoptosis by downregulating thymidylate synthase expression. EMBO Journal *19*, 4665-4675.

Rajasekaran, D., Siddiq, A., Willoughby, J.L., Biagi, J.M., Christadore, L.M., Yunes, S.A., Gredler, R., Jariwala, N., Robertson, C.L., Akiel, M.A., *et al.* (2015). Small molecule inhibitors of Late SV40 Factor (LSF) abrogate hepatocellular carcinoma (HCC): Evaluation using an endogenous HCC model. Oncotarget *6*, 26266-26277.

Santhekadur, P.K., Gredler, R., Chen, D., Siddiq, A., Shen, X.N., Das, S.K., Emdad, L., Fisher, P.B., and Sarkar, D. (2012a). Late SV40 factor (LSF) enhances angiogenesis by transcriptionally up-regulating matrix metalloproteinase-9 (MMP-9). Journal of Bioloical Chemistry *287*, 3425-3432.

Santhekadur, P.K., Rajasekaran, D., Siddiq, A., Gredler, R., Chen, D., Schaus, S.E., Hansen, U., Fisher, P.B., and Sarkar, D. (2012b). The transcription factor LSF: a novel oncogene for hepatocellular carcinoma. American Journal of Cancer Research *2*, 269-285.

Sasai, K., Katayama, H., Stenoien, D.L., Fujii, S., Honda, R., Kimura, M., Okano, Y., Tatsuka, M., Suzuki, F., Nigg, E.A., *et al.* (2004). Aurora-C kinase is a novel chromosomal passenger protein that can complement Aurora-B kinase function in mitotic cells. Cell Motility and the Cytoskeleton *59*, 249-263.

Saxena, U.H., Owens, L., Graham, J.R., Cooper, G.M., and Hansen, U. (2010). Prolyl isomerase Pin1 regulates transcription factor LSF (TFCP2) by facilitating dephosphorylation at two serine-proline motifs. Journal of Biological Chemistry *285*, 31139-31147.

Saxena, U.H., Powell, C.M., Fecko, J.K., Cacioppo, R., Chou, H.S., Cooper, G.M., and Hansen, U. (2009). Phosphorylation by cyclin C/cyclin-dependent kinase 2 following mitogenic stimulation of murine fibroblasts inhibits transcriptional activity of LSF during G1 progression. Molecular Cellular Biology *29*, 2335-2345.

Sekyrova, P., Ostblom, J., and Andang, M. (2012). Blebbing as a physical force in cancer EMT - parallels with mitosis. Seminars in Cancer Biology *22*, 369-373.

Severgnini, M., Sherman, J., Sehgal, A., Jayaprakash, N.K., Aubin, J., Wang, G., Zhang, L., Peng, C.G., Yucius, K., Butler, J., *et al.* (2012). A rapid two-step method for isolation of functional primary mouse hepatocytes: cell characterization and asialoglycoprotein receptor based assay development. Cytotechnology *64*, 187-195.

Sherr, C.J., and Roberts, J.M. (1995). Inhibitors of mammalian G1 cyclin-dependent kinases. Genes and Devevelopment *9*, 1149-1163.

Sherr, C.J., and Roberts, J.M. (2004). Living with or without cyclins and cyclin-dependent kinases. Genes and Development *18*, 2699-2711.

Shirra, M.K., Zhu, Q., Huang, H.C., Pallas, D., and Hansen, U. (1994). One exon of the human LSF gene includes conserved regions involved in novel DNA-binding and dimerization motifs. Molecular Cell Biology *14*, 5076-5087.

Shlomai, A. (2012). Targeting late SV40 factor: is the achilles heel of hepatocarcinogenesis revealed? World Journal of Gastroenterology *18*, 6709-6711.

Sistayanarain, A., Tsuneyama, K., Zheng, H., Takahashi, H., Nomoto, K., Cheng, C., Murai, Y., Tanaka, A., and Takano, Y. (2006). Expression of Aurora-B kinase and phosphorylated histone H3 in hepatocellular carcinoma. Anticancer Research *26*, 3585-3593.

Slattery, S.D., Mancini, M.A., Brinkley, B.R., and Hall, R.M. (2009). Aurora-C kinase supports mitotic progression in the absence of Aurora-B. Cell Cycle *8*, 2984-2994.

Tanaka, S., Arii, S., Yasen, M., Mogushi, K., Su, N.T., Zhao, C., Imoto, I., Eishi, Y., Inazawa, J., Miki, Y., *et al.* (2008). Aurora kinase B is a predictive factor for the aggressive recurrence of hepatocellular carcinoma after curative hepatectomy. British Journal of Surgery *95*, 611-619.

Torrecilla, S., and Llovet, J.M. (2015). New molecular therapies for hepatocellular carcinoma. Clinics and Research in Hepatology and Gastroenterology *39 Suppl 1*, S80-85.

Torti, D., and Trusolino, L. (2011). Oncogene addiction as a foundational rationale for targeted anti-cancer therapy: promises and perils. EMBO Molecular Medicine *3*, 623-636.

Traylor-Knowles, N., Hansen, U., Dubuc, T.Q., Martindale, M.Q., Kaufman, L., and Finnerty, J.R. (2010). The evolutionary diversification of LSF and Grainyhead transcription factors preceded the radiation of basal animal lineages. BMC Evolutionary Biology *10*, 101.

Vader, G., and Lens, S.M. (2008). The Aurora kinase family in cell division and cancer. Biochimica et Biophysica Acta *1786*, 60-72.

Veljkovic, J., and Hansen, U. (2004). Lineage-specific and ubiquitous biological roles of the mammalian transcription factor LSF. Gene *343*, 23-40.

Venook, A.P., Papandreou, C., Furuse, J., and de Guevara, L.L. (2010). The incidence and epidemiology of hepatocellular carcinoma: a global and regional perspective. Oncologist *15 Suppl 4*, 5-13.

Villanueva, A., and Llovet, J.M. (2011). Targeted therapies for hepatocellular carcinoma. Gastroenterology *140*, 1410-1426.

Wang, L., Zhang, J., Wan, L., Zhou, X., Wang, Z., and Wei, W. (2015). Targeting Cdc20 as a novel cancer therapeutic strategy. Pharmacol Ther *151*, 141-151.
Wang, X.W., Hussain, S.P., Huo, T.I., Wu, C.G., Forgues, M., Hofseth, L.J., Brechot, C., and Harris, C.C. (2002). Molecular pathogenesis of human hepatocellular carcinoma. Toxicology *181-182*, 43-47.

Wang, Y., Toppari, J., Parvinen, M., and Kallio, M.J. (2006). Inhibition of Aurora kinases perturbs chromosome alignment and spindle checkpoint signaling in rat spermatocytes. Experimental Cell Research *312*, 3459-3470.

Wang, Z., Wan, L., Zhong, J., Inuzuka, H., Liu, P., Sarkar, F.H., and Wei, W. (2013). Cdc20: a potential novel therapeutic target for cancer treatment. Current Pharmacetical Design *19*, 3210-3214.

Weinstein, B. (2008). Relevance of the concept of oncogene addiction to hormonal carcinogenesis and molecular targeting in cancer prevention and therapy. Advances in Experimental Medical Biology *617*, 3-13.

Weinstein, I.B., and Joe, A. (2008). Oncogene addiction. Cancer Research *68*, 3077-3080; discussion 3080.

Weinstein, I.B., and Joe, A.K. (2006). Mechanisms of disease: Oncogene addiction--a rationale for molecular targeting in cancer therapy. Nature Clinical Practice Oncology *3*, 448-457.

Worns, M.A., and Galle, P.R. (2014). HCC therapies--lessons learned. Nature Review Gastroenterol Hepatology *11*, 447-452.

Wu, W.J., Hu, K.S., Wang, D.S., Zeng, Z.L., Zhang, D.S., Chen, D.L., Bai, L., and Xu, R.H. (2013). CDC20 overexpression predicts a poor prognosis for patients with colorectal cancer. Journal of Translational Medicine *11*, 142.

Xu, F.L., Rbaibi, Y., Kiselyov, K., Lazo, J.S., Wipf, P., and Saunders, W.S. (2010). Mitotic slippage in non-cancer cells induced by a microtubule disruptor, disorazole C1. BMC Chemical Biology *10*, 1.

Yan, C., and Higgins, P.J. (2013). Drugging the undruggable: transcription therapy for cancer. Biochimica et Biophysica Acta *1835*, 76-85.

Yang, Z., Kenny, A.E., Brito, D.A., and Rieder, C.L. (2009). Cells satisfy the mitotic checkpoint in Taxol, and do so faster in concentrations that stabilize syntelic attachments. Journal of Cell Biology *186*, 675-684.

Yasen, M., Mizushima, H., Mogushi, K., Obulhasim, G., Miyaguchi, K., Inoue, K., Nakahara, I., Ohta, T., Aihara, A., Tanaka, S., *et al.* (2009). Expression of Aurora B and alternative variant forms in hepatocellular carcinoma and adjacent tissue. Cancer Science *100*, 472-480.

Yoo, B.K., Emdad, L., Gredler, R., Fuller, C., Dumur, C.I., Jones, K.H., Jackson-Cook, C., Su, Z.Z., Chen, D., Saxena, U.H., *et al.* (2010). Transcription factor Late SV40 Factor (LSF) functions as an oncogene in hepatocellular carcinoma. Proceedings of the National Academy of Science U S A *107*, 8357-8362.

Yoo, B.K., Gredler, R., Vozhilla, N., Su, Z.Z., Chen, D., Forcier, T., Shah, K., Saxena, U., Hansen, U., Fisher, P.B., *et al.* (2009). Identification of genes conferring resistance to 5-fluorouracil. Proceedings of the National Academy of Science U S A *106*, 12938-12943.

Zhou, W.C., Zhang, Q.B., and Qiao, L. (2014). Pathogenesis of liver cirrhosis. World Journal of Gastroenterology *20*, 7312-7324.

Zimmermann, T.S., Lee, A.C., Akinc, A., Bramlage, B., Bumcrot, D., Fedoruk, M.N., Harborth, J., Heyes, J.A., Jeffs, L.B., John, M., *et al.* (2006). RNAi-mediated gene silencing in non-human primates. Nature *441*, 111-114.

Zoller, H., and Tilg, H. (2016). Nonalcoholic fatty liver disease and hepatocellular carcinoma. Metabolism.

CURRICULUM VITAE

9 Englewood Road, Winchester, MA 01890 (617)680-0634

Jennifer Lynn Sherman Willoughby

Profile

Molecular Biologist with experience in oncology and RNAi drug development for orphan and cardio metabolic diseases. Extensive experience in both *in vivo* and *in vitro assay* development and screening.

Experience

February 2006-Current — Alnylam Pharmaceuticals — 300 3rd Street Cambridge MA 02129

Principal Associate Scientist

In vivo/in vitro biologist responsible for improving conjugate potency as well as vetting potential targets/indications that Alnylam RNAi technology could potential impact.

Responsible for *in vivo* screening of RNAi compounds in various mammalian systems to characterize potency of siRNA compounds with an array of delivery systems.

August 2003-February 2006 — Children's' Hospital Boston — 300 Longwood Avenue, Boston MA 02115

Senior Research Technician

In vitro/in vivo biologist responsible for genotyping various mouse colonies to in efforts to identify genes that increased angiogenesis as ascertained by vascular response to VEGF in vivo.

Assisted with evaluation of anti-tumor screening models in rodent xenograft models

Education

2010-2016 — Boston University — 24 Cummington Mall, Boston Ma, 02215

Molecular and Cell Biology Doctoral Candidate

1999-2003 — Roger Williams University — 1 Old Ferry Road, Bristol, RI 02809

Bachelors of Science, Biology

Posters

9 Englewood Road, Winchester, MA 01890 (617)680-0634

Jennifer Lynn Sherman Willoughby

Activity of Enhanced Stabilization Chemistry (ESC)-GalNAc-siRNA Conjugates via Lung Delivery Using Microsprayer®.
Vasant Jadhav[1], Jennifer LS Willoughby[1], Svetlana Morskaya[1], Stuart Milestein[1], Martin Maier[1], Muthiah Manoharan[1], Laura Sepp-Lorenzino[1] and Rachel Meyers[1] (2013)

Subcutaneous Administration of a TTR Targeting siRNA-GalNAc$_3$ Conjugate Results in Sustained Knockdown of Transthyretin in Mice
Jennifer Sherman[1], Shannon Fishman[1], Susete Costelha[2], Amy Chan[1], Xuemei Zhang[1], Valerie Clausen[1], Husain Attarwala[1], Julia Hettinger[1], Scott Barros[1], Ligang Zhang[1], Gang Wang[1], Rajeev Kallanthottathil[1], Maria Saraiva[2], Renta Hutabarat[1], and Tracy Zimmermann[1,] Jayaprakash Narayannair[1] (2012)

Pharmacokinetics, Pharmacodynamics, Bioavailability and Biodistribution of a N-Acetylgalactoseamine (GalNAc) Conjugated siRNA Targeting the Mouse TTR Gene
Xuemei Zhang, Valerie A. Clausen, Husain Attarwala, Qianfan Wang, Sue Panesar, Jennifer Sherman, Kallanthottathil G Rajeev, K. Narayannair Jayaprakash, Ligang Zhang, Klaus Charisse, Tracy Zimmermann, Renta M. Hutabarat (2012)

Hepatocyte Specific Targeting and Delivery of siRNA-Carbohydrate Conjugates (2013)
Kallanthottathil G. Rajeev, K. Narayanannair Jayaprakash, Gang Wang, Ligang Zhang, Chang Geng Peng, Jennifer Sherman, Mariano Severgnini, Amy Chan, Justin Aubin, Klaus Charisse, Renta Hutabarat, Martin Maier, Kenneth Koblan, Kevin Fitzgerald, Dinah W.Y. Sah, Muthiah Manoharan, and Tracy S. Zimmermann

A Region of SJL/J Chromosome 7 Confers Impaired Angiogenesis on C57BL/6J Mice
Rohan, RM , Rogers, MS, Boyartchuk, V , Yuan, J , Birsner, A , Sampson, D , Yin, Huali , Sherman, J , Dietrich, WF , D'Amato, RJ

The albino allele of tyrosinase inhibits VEGF-induced angiogenesis.

9 Englewood Road, Winchester, MA 01890 (617)680-0634

Jennifer Lynn Sherman Willoughby

Rogers, MS, Sherman, J, Birsner, A, D'Amato, RJ

A Hey2 enhancer polymorphism alters VEGF-induced angiogenesis.
Rogers, MS, Sherman, J, Birsner, A, Chin, MT, D'Amato, RJ

Publications

Butler, J. S., A. Chan, et al. (2016). "Preclinical evaluation of RNAi as a treatment for transthyretin-mediated amyloidosis." Amyloid 23(2): 109-118.

ATTR amyloidosis is a systemic, debilitating and fatal disease caused by transthyretin (TTR) amyloid accumulation. RNA interference (RNAi) is a clinically validated technology that may be a promising approach to the treatment of ATTR amyloidosis. The vast majority of TTR, the soluble precursor of TTR amyloid, is expressed and synthesized in the liver. RNAi technology enables robust hepatic gene silencing, the goal of which would be to reduce systemic levels of TTR and mitigate many of the clinical manifestations of ATTR that arise from hepatic TTR expression. To test this hypothesis, TTR-targeting siRNAs were evaluated in a murine model of hereditary ATTR amyloidosis. RNAi-mediated silencing of hepatic TTR expression inhibited TTR deposition and facilitated regression of existing TTR deposits in pathologically relevant tissues. Further, the extent of deposit regression correlated with the level of RNAi-mediated knockdown. In comparison to the TTR stabilizer, tafamidis, RNAi-mediated TTR knockdown led to greater regression of TTR deposits across a broader range of affected tissues. Together, the data presented herein support the therapeutic hypothesis behind TTR lowering and highlight the potential of RNAi in the treatment of patients afflicted with ATTR amyloidosis.

Parmar, R., J. L. Willoughby, et al. (2016). "5'-(E)-Vinylphosphonate: A Stable Phosphate Mimic Can Improve the RNAi Activity of siRNA-GalNAc Conjugates." Chembiochem.

Small interfering RNA (siRNA)-mediated silencing requires siRNA loading into the RNA-induced silencing complex (RISC). Presence of 5'-phosphate (5'-P) is reported to be critical for efficient RISC loading of the antisense strand (AS) by anchoring it to the mid-domain of the Argonaute2 (Ago2) protein. Phosphorylation of exogenous duplex siRNAs is thought to be accomplished by cytosolic Clp1 kinase. However, although extensive chemical modifications are essential for siRNA-GalNAc conjugate activity, they can significantly impair Clp1 kinase activity. Here, we further elucidated the effect of 5'-P on the activity of siRNA-GalNAc conjugates. Our results demonstrate that a subset of sequences benefit from the presence of exogenous 5'-P. For those that do, incorporation of 5'-(E)-vinylphosphonate (5'-VP), a metabolically stable phosphate

mimic, results in up to 20-fold improved in vitro potency and up to a threefold benefit in in vivo activity by promoting Ago2 loading and enhancing metabolic stability.

Rajasekaran, D., A. Siddiq, et al. (2015). "Small molecule inhibitors of Late SV40 Factor (LSF) abrogate hepatocellular carcinoma (HCC): Evaluation using an endogenous HCC model." Oncotarget 6(28): 26266-26277.

Hepatocellular carcinoma (HCC) is a lethal malignancy with high mortality and poor prognosis. Oncogenic transcription factor Late SV40 Factor (LSF) plays an important role in promoting HCC. A small molecule inhibitor of LSF, Factor Quinolinone Inhibitor 1 (FQI1), significantly inhibited human HCC xenografts in nude mice without harming normal cells. Here we evaluated the efficacy of FQI1 and another inhibitor, FQI2, in inhibiting endogenous hepatocarcinogenesis. HCC was induced in a transgenic mouse with hepatocyte-specific overexpression of c-myc (Alb/c-myc) by injecting N-nitrosodiethylamine (DEN) followed by FQI1 or FQI2 treatment after tumor development. LSF inhibitors markedly decreased tumor burden in Alb/c-myc mice with a corresponding decrease in proliferation and angiogenesis. Interestingly, in vitro treatment of human HCC cells with LSF inhibitors resulted in mitotic arrest with an accompanying increase in CyclinB1. Inhibition of CyclinB1 induction by Cycloheximide or CDK1 activity by Roscovitine significantly prevented FQI-induced mitotic arrest. A significant induction of apoptosis was also observed upon treatment with FQI. These effects of LSF inhibition, mitotic arrest and induction of apoptosis by FQI1s provide multiple avenues by which these inhibitors eliminate HCC cells. LSF inhibitors might be highly potent and effective therapeutics for HCC either alone or in combination with currently existing therapies.

Matsuda, S., K. Keiser, et al. (2015). "siRNA conjugates carrying sequentially assembled trivalent N-acetylgalactosamine linked through nucleosides elicit robust gene silencing in vivo in hepatocytes." ACS Chemical Biology 10(5): 1181-1187.

Asialoglycoprotein receptor (ASGPR) mediated delivery of triantennary N-acetylgalactosamine (GalNAc) conjugated short interfering RNAs (siRNAs) to hepatocytes is a promising paradigm for RNAi therapeutics. Robust and durable gene silencing upon subcutaneous administration at therapeutically acceptable dose levels resulted in the advancement of GalNAc-conjugated oligonucleotide-based drugs into preclinical and clinical developments. To systematically evaluate the effect of display and positioning of the GalNAc moiety within the siRNA duplex on ASGPR binding and RNAi activity, nucleotides carrying monovalent GalNAc were designed. Evaluation of clustered and dispersed incorporation of GalNAc units to the sense (S) strand indicated that sugar proximity is critical for ASGPR recognition, and location of the clustered ligand impacts the intrinsic potency of the siRNA. An array of nucleosidic GalNAc monomers resembling a trivalent ligand at or near the 3' end of the S strand retained in vitro and in vivo siRNA activity, similar to the parent conjugate design. This work demonstrates the utility of simple, nucleotide-based, cost-effective siRNA-GalNAc conjugation strategies.

Rajeev, K. G., J. K. Nair, et al. (2015). "Hepatocyte-specific delivery of siRNAs conjugated to novel non-nucleosidic trivalent N-acetylgalactosamine elicits robust gene silencing in vivo." Chembiochem 16(6): 903-908.

We recently demonstrated that siRNAs conjugated to triantennary N-acetylgalactosamine (GalNAc) induce robust RNAi-mediated gene silencing in the liver, owing to uptake mediated by the asialoglycoprotein receptor (ASGPR). Novel monovalent GalNAc units, based on a non-nucleosidic linker, were developed to yield simplified trivalent GalNAc-conjugated oligonucleotides under solid-phase synthesis conditions. Synthesis of oligonucleotide conjugates using monovalent GalNAc building blocks required fewer synthetic steps compared to the previously optimized triantennary GalNAc construct. The redesigned trivalent GalNAc ligand maintained optimal valency, spatial orientation, and distance between the sugar moieties for proper recognition by ASGPR. siRNA conjugates were synthesized by sequential covalent attachment of the trivalent GalNAc to the 3'-end of the sense strand and resulted in a conjugate with in vitro and in vivo potency similar to that of the parent trivalent GalNAc conjugate design.

Nair, J. K., J. L. Willoughby, et al. (2014). "Multivalent N-acetylgalactosamine-conjugated siRNA localizes in hepatocytes and elicits robust RNAi-mediated gene silencing." Journal of American Chemical Society 136(49): 16958-16961.

Conjugation of small interfering RNA (siRNA) to an asialoglycoprotein receptor ligand derived from N-acetylgalactosamine (GalNAc) facilitates targeted delivery of the siRNA to hepatocytes in vitro and in vivo. The ligands derived from GalNAc are compatible with solid-phase oligonucleotide synthesis and deprotection conditions, with synthesis yields comparable to those of standard oligonucleotides. Subcutaneous (SC) administration of siRNA-GalNAc conjugates resulted in robust RNAi-mediated gene silencing in liver. Refinement of the siRNA chemistry achieved a 5-fold improvement in efficacy over the parent design in vivo with a median effective dose (ED50) of 1 mg/kg following a single dose. This enabled the SC administration of siRNA-GalNAc conjugates at therapeutically relevant doses and, importantly, at dose volumes of </=1 mL. Chronic weekly dosing resulted in sustained dose-dependent gene silencing for over 9 months with no adverse effects in rodents. The optimally chemically modified siRNA-GalNAc conjugates are hepatotropic and long-acting and have the potential to treat a wide range of diseases involving liver-expressed genes.

Conforto, T. L., Y. Zhang, et al. (2012). "Impact of CUX2 on the female mouse liver transcriptome: activation of female-biased genes and repression of male-biased genes." Molecular Cell Biology 32(22): 4611-4627.

The growth hormone-regulated transcription factors STAT5 and BCL6 coordinately regulate sex differences in mouse liver, primarily through effects in male liver, where male-biased genes are upregulated and many female-biased genes are actively repressed. Here we investigated whether CUX2, a highly female-specific liver transcription factor, contributes to an analogous regulatory network in female liver. Adenoviral overexpression of CUX2 in male liver induced 36% of female-biased genes and repressed 35% of male-biased genes. In female liver, CUX2 small interfering RNA

(siRNA) preferentially induced genes repressed by adenovirus expressing CUX2 (adeno-CUX2) in male liver, and it preferentially repressed genes induced by adeno-CUX2 in male liver. CUX2 binding in female liver chromatin was enriched at sites of male-biased DNase hypersensitivity and at genomic regions showing male-enriched STAT5 binding. CUX2 binding was also enriched near genes repressed by adeno-CUX2 in male liver or induced by CUX2 siRNA in female liver but not at genes induced by adeno-CUX2, indicating that CUX2 binding is preferentially associated with gene repression. Nevertheless, direct CUX2 binding was seen at several highly female-specific genes that were positively regulated by CUX2, including A1bg, Cyp2b9, Cyp3a44, Tox, and Trim24. CUX2 expression and chromatin binding were high in immature male liver, where repression of adult male-biased genes and expression of adult female-biased genes are common, suggesting that the downregulation of CUX2 in male liver at puberty contributes to the developmental changes establishing adult patterns of sex-specific gene expression.

Grant, T. J., J. A. Bishop, et al. (2012). "Antiproliferative small-molecule inhibitors of transcription factor LSF reveal oncogene addiction to LSF in hepatocellular carcinoma." Proceedings of the National Academy of Science U S A 109(12): 4503-4508.

Hepatocellular carcinoma (HCC) is the fifth most common cancer worldwide. Despite the prevalence of HCC, there is no effective, systemic treatment. The transcription factor LSF is a promising protein target for chemotherapy; it is highly expressed in HCC patient samples and cell lines, and promotes oncogenesis in rodent xenograft models of HCC. Here, we identify small molecules that effectively inhibit LSF cellular activity. The lead compound, factor quinolinone inhibitor 1 (FQI1), inhibits LSF DNA-binding activity both in vitro, as determined by electrophoretic mobility shift assays, and in cells, as determined by ChIP. Consistent with such inhibition, FQI1 eliminates transcriptional stimulation of LSF-dependent reporter constructs. FQI1 also exhibits antiproliferative activity in multiple cell lines. In LSF-overexpressing cells, including HCC cells, cell death is rapidly induced; however, primary or immortalized hepatocytes are unaffected by treatment with FQI1. The highly concordant structure-activity relationship of a panel of 23 quinolinones strongly suggests that the growth inhibitory activity is due to a single biological target or family. Coupled with the striking agreement between the concentrations required for antiproliferative activity (GI(50)s) and for inhibition of LSF transactivation (IC(50)s), we conclude that LSF is the specific biological target of FQIs. Based on these in vitro results, we tested the efficacy of FQI1 in inhibiting HCC tumor growth in a mouse xenograft model. As a single agent, tumor growth was dramatically inhibited with no observable general tissue cytotoxicity. These findings support the further development of LSF inhibitors for cancer chemotherapy.

Nakayama, T., J. S. Butler, et al. (2012). "Harnessing a physiologic mechanism for siRNA delivery with mimetic lipoprotein particles." Mol Ther 20(8): 1582-1589.

Therapeutics based on RNA interference (RNAi) have emerged as a potential new class of drugs for treating human disease by silencing the target messenger RNA (mRNA), thereby reducing levels of the corresponding pathogenic protein. The major

challenge for RNAi therapeutics is the development of safe delivery vehicles for small interfering RNAs (siRNAs). We previously showed that cholesterol-conjugated siRNAs (chol-siRNA) associate with plasma lipoprotein particles and distribute primarily to the liver after systemic administration to mice. We further demonstrated enhancement of silencing by administration of chol-siRNA pre-associated with isolated high-density lipoprotein (HDL) or low-density lipoprotein (LDL). In this study, we investigated mimetic lipoprotein particle prepared from recombinant apolipoprotein A1 (apoA) and apolipoprotein E3 (apoE) as a delivery vehicle for chol-siRNAs. We show that apoE-containing particle (E-lip) is highly effective in functional delivery of chol-siRNA to mouse liver. E-lip delivery was found to be considerably more potent than apoA-containing particle (A-lip). Furthermore, E-lip-mediated delivery was not significantly affected by high endogenous levels of plasma LDL. These results demonstrate that E-lip has substantial potential as delivery vehicles for lipophilic conjugates of siRNAs.

Severgnini, M., J. Sherman, et al. (2012). "A rapid two-step method for isolation of functional primary mouse hepatocytes: cell characterization and asialoglycoprotein receptor based assay development." Cytotechnology 64(2): 187-195.

Primary mouse hepatocytes are an important tool in the biomedical research field for the assessment of hepatocyte function. Several methods for hepatocyte isolation have been published; however, many of these methods require extensive handling and can therefore compromise the viability and function of the isolated cells. Since one advantage of utilizing freshly isolated cells is to maintain an environment in which the cells are more comparable to their in vivo state, it is important to have robust methods that produce cells with high viability, good purity and that function in a similar manner to that in their in vivo state. Here we describe a modified two-step method for the rapid isolation and characterization of mouse primary hepatocytes that results in high yields of viable cells. The asialoglycoprotein receptor (ASGPR), which is one of the most abundant cell surface receptors on hepatocytes, was used to monitor the function of the isolated hepatocytes by demonstrating specific binding of its ligand using a newly developed flow cytometry based ligand-receptor binding assay. Also, an in vitro screening method for siRNA drug candidates was successfully developed utilizing freshly isolated hepatocytes with minimum culture time.

Nguyen, D. N., S. C. Chen, et al. (2009). "Drug delivery-mediated control of RNA immunostimulation." Mol Ther 17(9): 1555-1562.

RNA interference (RNAi) has generated significant interest as a strategy to suppress viral infection, but in some cases antiviral activity of unmodified short-interfering RNA (siRNA) has been attributed to activation of innate immune responses. We hypothesized that immunostimulation by unmodified siRNA could mediate both RNAi as well as innate immune stimulation depending on the mode of drug delivery. We investigated the potential of immunostimulatory RNAs (siRNAs) to suppress influenza A virus in vivo in the mouse lung. Lipidoid 98N12-5(1) formulated with unmodified siRNA targeting the influenza nucleoprotein gene exhibited antiviral activity. Formulations were

optimized to increase antiviral activity, but the antiviral activity of lipidoid-delivered siRNA did not depend on sequence homology to the influenza genome as siRNA directed against unrelated targets also suppressed influenza replication in vivo. This activity was primarily attributed to enhancement of innate immune stimulation by lipidoid-mediated delivery, which indicates increased toll-like receptor (TLR) activation by siRNA. Certain chemical modifications to the siRNA backbone, which block TLR7/8 activation but retain in vitro RNAi activity, prevented siRNA-mediated antiviral activity despite enhanced lipidoid-mediated delivery. Here, we demonstrate that innate immune activation caused by unmodified siRNA can have therapeutically relevant effects, and that these non-RNAi effects can be controlled through chemical modifications and drug delivery.